Optical Transitions and Electrical Properties in Plasma Polymerized Thin Films of 2-(Diethylamino)ethyl methacrylate

DOCTOR OF PHILOSOPHY

Tamanna Afroze

Roll: P10071402P

Session: October 2007

BOLD ???

DEPARTMENT OF PHYSICS
BANGLADESH UNIVERSITY OF ENGINEERING AND TECHNOLOGY (BUET)
DHAKA-1000, BANGLADESH
2013

Ph. D.
Thesis

TAMANNA AFROZE

BUET

Optical Transitions and Electrical Properties in Plasma Polymerized Thin Films of 2-(Diethylamino)ethyl methacrylate

A dissertation submitted to the Department of Physics BangladeshUniversity of Engineering and Technology in partial fulfillment of the requirements for the degree of DOCTOR OF PHILOSOPHY (Ph. D.)

by

Tamanna Afroze

Roll: P10071402P

Session: October 2007

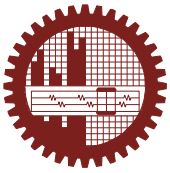

DEPARTMENT OF PHYSICS
BANGLADESH UNIVERSITY OF ENGINEERING AND TECHNOLOGY (BUET)
DHAKA-1000, BANGLADESH
2013

Paper presented from this work :

- Tamanna Afroze, A. H. Bhuiyan, 'Structural and optical properties of plasma polymerized 2-(Diethylamino)ethyl methacrylate thin films', **International Conference** On Women in Science, Engineering and Technology: Local and Global Perspective (ICWSET-2011), (held on 2 – 4 February, 2012) Organized by Bangladesh Association of Women Scientists (BAWS) & National Chapter (Bangladesh), OWSDW (Organization for Women in Science for Developing World) Venue : NNAC Senate Bhavan, University of Dhaka
- Tamanna Afroze, A. H. Bhuiyan, 'Effect of heat treatment on the structural and optical characteristics of plasma deposited thin films of 2-(diethylamino)ethylmethacrylate' presented at 'The 22nd Bangladesh Science Conference Theme: The Role of Scientist and Technologist to Achive the MDG' (held on 27-29 September, 2012), organized by Bangladesh Association for the Advancement of Science (BAAS) and Bangladesh Council of Scientific and Industrial Research (BCSIR), Venue : BCSIR Auditorium, Dhaka
- Tamanna Afroze, A. H. Bhuiyan, 'Direct Current Conduction Mechanism in the Thin Films of Plasma Polymerized 2-(diethylamino)ethylmethacrylate' presented at 'National conference on Physics for Technology Development' (held on 27-28 December, 2012), organized by Bangladesh Physical Society, Venue : Atomic Energy Center, Dhaka.
- Tamanna Afroze, A. H. Bhuiyan, 'Structural properties of Plasma Polymerized thin films of 2-(diethylamino)ethylmethacrylate' presented at **International** BOSE Conference, (held on 4 February, 2013) organized by Bose Centre for Advanced Study and Research in Natural Sciences, Venue: Nabab Nawab Ali Chowdhury Senate Bhaban, University of Dhaka.

Publications from this work :

1. Tamanna Afroze and A. H. Bhuiyan, 'Effect of heat treatment on the structural and optical characteristics of plasma deposited 2-(diethylamino)ethyl methacrylate thin films by a capacitively coupled glow discharge plasma system', Accepted in Physica Scripta (IOP Science) 88(4), 045502, (2013).

2. Tamanna Afroze, A. H. Bhuiyan, 'Structural and optical properties of plasma polymerized 2-(Diethylamino)ethyl methacrylate thin films', Institute of Science and Technology (IST) Journal on Business and Technology, Special Issue on ICWSET-2012 (held on Feb 2-4, 2012), 5(1) , 93-98, (2012).

3. Tamanna Afroze and A. H. Bhuiyan, **'**Electrical Conduction Mechanism in the Thin Films of Plasma Polymerized 2-(diethylamino)ethyl methacrylate', submitted in Journal of Physics and Chemistry of Solids (2013).

CANDIDATE'S DECLARATION

It is hereby declared that this thesis or any part of it has not been submitted elsewhere for the award of any degree or diploma.

Signature of the candidate

(Tamanna Afroze)

Dedicated

To

My Parents

&

Parents-in-law

Contents

List of Chapters

Chapter 1: Introduction

Chapter 2: Background on Polymers and Plasma polymerization

Chapter 3: Theoretical Aspects

Chapter 4: Experimental Techniques

Chapter 5 : Results and discussions

Chapter 6: Conclusions

List of Figures

Page no.

Chapter 2: Background on Polymers and Plasma polymerization

Chapter 3: Theoretical Aspects

Chapter 4: Experimental Techniques

Chapter 5: Results and Discussion

List of Tables

Abbreviations and symbols

A	Area
ABS	Absorbance
AC	Alternating Current
AFM	Atomic Force Microscopy
Al	Aluminium
B	Tauc Parameter
CC/cc	Capacitively Coupled
Cr-Al	Chromel -Alumel
DC	Direct Current
DEAEMA	2-(Diethylamino)ethyl methacrylate
DTA	Differential thermal analysis
EDX	Energy Dispersive X-ray
E_{gd}	Direct transition energy gap
E_{gi}	Indirect transition energy gap
E_u	Urbach Energy
ΔE	Activation energy
FL	Fermi Level
FTIR	Fourier Transform Infrared
I	Current
I	Intensity of Radiation
IR	Infrared
J	Current density
LB	Langmuir-Blodgett
MHz	MegaHertz
MMA	Methyl methacrylate
PECVD	Plasma Enhanced Chemical Vapour Deposition.
PVD	Physical Vapour Deposition.
PF	Poole-Frenkel
PPDEAEMA	Plasma Polymerized 2- (Diethylamino)ethyl methacrylate
PPDP	Plasma Polymerized Diphenyl

PPm-X	Plasma Polymerized m-Xylene
PMMA	Poly Methyl methacrylate
PPMMA	Plasma Polymerized Methyl methacrylate
RF/rf	Radio Frequency
SCLC	Space Charge Limited Conduction
UV	Ultra- Violet
SEM	Scanning Electron Microscopy
TGA	Thermogravimetric Analysis
$\tan\delta$	Dielectric loss tangent
α	Absorption coefficient
d	Sample Thickness
ε'	Dielectric constant
ε''	Dielectric loss
ε_0	Permittivity of free space
k	Boltzmann Constant
k	Extinction Co-efficient
λ	Wavelength
μ	Mobility of charge carrier
θ	Trapping factor
σ_{dc}	DC electrical conductivity
σ_{ac}	AC electrical conductivity

Acknowledgements

I would like to take the opportunity to express my sincere gratitude, indebtedness and profound respect to my supervisor Professor Dr. Md. Abu Hashan Bhuiyan, Department of Physics, Bangladesh University of Engineering & Technology (BUET), Dhaka, for his constant encouragement, indispensable guidance, close supervision and generous help throughout the long period of my research work.

I am thankful to the Head, Professor Dr. Md Mostak Hossain, Department of Physics, BUET, for providing the research facilities available in the Department during the research work. I would like to thank to the other respectable members of the Doctoral Committee Prof. Dr. A. K. M. Akther Hossain, Associate Prof. Dr. Md. Forhad Mina, Department of Physics, BUET and Prof. Dr. A. B. M. Obaidul Islam, Department of Physics, University of Dhaka for their valuable discussion and suggestions.

I am also thankful to Prof. Dr.Mominul Huq (Rtd.), Prof. Dr.Nazma Zaman (Rtd.), Prof. Dr.Jiban Podder, Prof. Dr. Md. Feroz Alam Khan, Ms. Fahima Khanam, Dr. Afia Begum, Dr. Md. Rafi Uddin, Dr. Nasreen akter, Dr. Md. Abdul Basit, Md. Jellur Rahman, Md. Raqibul Islam, Md. Samir Ullah and all the other teachers of the Department of Physics, BUET for their inspiration and constructive suggestions throughout the period of research.

I acknowledge the financial support offered by the authority of BUET. I am also thankful to The Govt. of Peoples Republic of Bangladesh for providing me financial assistance through Prime Minister's Scholarship for Ph. D work.

I am grateful to the authority of Ahsanullah University of Science and Technology (AUST) for permitting me to perform research at BUET. I would like to thank Professor, Dr. M. Shahabuddin, Head, Department of Arts and Sciences of AUST for his continuous inspiration to complete the work. Many thanks to my colleagues, specially to Dr. Md. Hamidur Rahman Khan, Dr. S. M. Abdul Karim, Ms. Humaira Farzana, Ms. Ruba Rummana, Mr. Md. Iftekhar Arafath and Mr. Mohammad Abdur Rashid for their support and inspiration.

I am thankful to Dr. M. A. Gafur, Senior Engineer, PP & PDC and the authority of Bangladesh Council for Scientific and Industrial Research, Dhaka, for providing me the opportunity to do the FTIR, UV-visible Spectroscopy and DTA/TGA analyses.

I am also thankful to authority of The Atomic Energy Center, Dhaka for providing me the facility to perform SEM and EDAX measurements.

Many thanks go to the thin films research group members of the Department of Physics, BUET, past and present for their suggestion and assistance. Special thanks to Dr. Hasina Akther, Dr. Rama Bijoy Sarker, Dr. Sunirmal Majumder, Mr. Masud Reza, Dr. Rummana Matin, Ms. Happy Dey and other postgraduate students for their various supports.

I would like to express my sincere gratitude to Dr. Faruque-Uz-Zaman Chowdhury, Professor, Department of Physics, Chittagong University of Engineering and Technology, Chittagong and Dr. Kh. Selima Begum for their constant encouragement.

Thanks goes to all the staff members of this Department specially Mr. Md. Idris Munshi, Mr. Liakot Ali, Mr. Swapan Kumar Das for their co-operation.

I would like to appreciate my family and friends for their unconditional support, interest and understanding throughout the years of my research work and studies. Special gratitude for my parents, brothers, parents-in-law and sisters-in-law for their multifaceted support. I would like to express my indebtedness to my husband for his continuous support and inspiration. I must convey thanks to my loving son Ronggon and adorable daughter Afsara for their patience and sacrifice during this period.

Finally all praise to Almighty Allah for blessed me with strength, courage and patience to complete the work.

Abstract

Plasma polymerized (PP) thin films of different thicknesses were prepared through glow discharge of 2-(diethylamino)ethyl methacrylate (DEAEMA) using a capacitively coupled reactor at room temperature. The scanning electron micrographs of as deposited, heat treated and iodine doped PPDEAEMA thin films are found uniform and pinhole free. The energy dispersive x-ray analyses reveal the presence of C, N, O in as deposited, heat treated PPDEAEMA thin films and the presence of iodine along with C, N, O in iodine doped samples. The thermogravimetric analysis and differential thermal analysis indicate that heat treated PPDEAEMA is more stable in comparison to as deposited samples. The Fourier transform infrared spectroscopic investigations indicate that the material is a simple carbonyl compound and the chemical structure of DEAEMA retains to some extent in the PPDEAEMA. The spectral analysis also indicates the presence of CH and CH_2 groups in both monomer DEAEMA and as deposited PPDEAEMA and the presence of CH_3 only in DEAEMA. The presence of C=O, and C=C are very prominent in all the spectra of as deposited, heat treated and iodine doped PPDEAEMA.

The absorption coefficient, allowed direct transition, E_{qd}, allowed indirect transition, E_{qi}, energy gaps; Urbach energy, extinction coefficient and steepness parameter of as deposited, heat treated (at 373, 473 and 573 K for an hour) and iodine doped PPDEAEMA thin films were determined. The variation of energy gap with thickness and heat temperature are also discussed. The E_{qd} and E_{qi} decrease with the increase in film thickness for as deposited PPDEAEMA thin films of different thicknesses. The E_{qd} and E_{qi} values decrease as the heat treatment temperature increases. The E_{qd} decreases due to iodine doping.

Current density–voltage (*J-V*) characteristics were studied over the temperature range from 298 to 423 K for PPDEAEMA thin films of thicknesses 100, 200, 250 and 300 nm in aluminum/ PPDEAEMA /aluminum sandwich configuration. *J-V* curves reveal that in the low voltage region, the conduction current obeys Ohm's law while in the high voltage region the behavior attributed to be space charge limited conduction in PPDEAEMA thin films. The carrier mobility, the free carrier density and the trap density are found to be about 9.48×10^{-19} to 2.78×10^{-18} m^{-2} $V^{-1}s^{-1}$; 1.78×10^{23} to 2.10×10^{22} m^{-3} and 6.88×10^{23} to 1.58×10^{24} m^{-3} respectively for different thicknesses and temperatures at room temperature. The activation energies were estimated to be about 0.12 to 0.20 eV and 0.16 to 0.28 eV for 2 V and 30 V of PPDEAEMA thin films of different thicknesses. These small values of the activation energies suggest the existence of the shallow traps levels in PPDEAEMA thin

films. The conductivity of the iodine doped PPDEAEMA thin films increases as compared to as deposited PPDEAEMA thin films.

AC conductivity increases sharply as the frequency increases but at very high frequency (near about 10^5 Hz) it becomes almost stable and it increases a little with the increase of temperature. It is found that the activation energy of PPDEAEMA thin films is very low about 0.02 eV. Dielectric constant decreases slightly upto 10^4 Hz with the increase of frequency and above this frequency it start to decrease rapidly. Dielectric constant decreases slightly as the temperature increases from 298 to 348 K and above this temperature the decrease is quite higher. Dielectric loss increases with increasing frequency with loss peaks found at higher frequency which is shifted towards lower frequency as the thickness of the films increases. Dielectric loss increases as the temperature increases from 298 to 398 K. From the Cole Cole plot the values of β are found 0.77-0.91 which are smaller than the value (unity) of the Debye model with a single relaxation, indicating the presence of distribution of relaxation time in PPDEAEMA thin films. Both the ac conductivity and dielectric constant increases due to iodine doping.

1.1 Introduction

A tremendous advancement has taken place in the development of organic polymers in recent years due to their interesting physical, chemical, electrical etc. properties. One of the exciting and promising developments in material science today is the synthesis of high-performance polymer films by efficient physical techniques for advanced technology application. Plasma polymerization is an excellent tool, which can be used to deposit thin polymer films from a variety of organic compounds [1-3]. Systematic investigation of plasma polymerization started in 1960s. In plasma polymerization the neutral species entering the reactor produce reactive fragments as energy is transferred by the electrons at a low temperature and low pressure plasma environment. The substrate molecules are activated by exposure to the plasma environment and chemical bonds are formed with the reactive fragments. Controllability and reproducibility of the surface composition of plasma deposited thin films are important to obtain very high performance. The structure and properties of plasma polymer films depend on plasma polymerization parameters, especially the discharge power, monomer flow rate, substrate temperature and steady state pressure in the reactor chamber. The high quality, homogeneous, chemically inert, highly adhering, pinhole-free and cross-linked plasma polymer films have potential applications in optical devices, thin film lenses, biomedical, membrane separation, aerospace and automotive fields, photovoltaic membranes, microelectronics and various devices like ultra large-scale integration, very large scale integration, light emitting diodes, sensors, super capacitors, rechargeable batteries, as intermetallic devices in integrated circuits and in other electronic circuits as insulating and dielectric materials [4-8]. Besides good chemical and thermal stability, plasma polymers are usually characterized by high electrical resistance. Many researchers have been devoted to enhance the conductivity of plasma polymers by doping using suitable dopants since doping of plasma polymers modifies the properties and offers many more interesting applications.

Therefore, it is of interest to develop plasma polymer thin films of high quality for a variety of industrial applications. As a consequence, the study of the structural, electronic, electrical, optical, etc. properties of organic plasma polymer thin films received special attention to solid state and material scientists.

1.2 Review of the Earlier Research Works

Nowadays, material preparation and processing have become one of the most active areas of research in the development of science and technology. In this respect, plasma polymerization is one of the unique methods of preparing pinhole free, highly resistive, chemically inert polymer thin films from almost any organic vapor and also from the metallic and inorganic elements. The advancement of scientific interest in different technological applications of plasma polymerized thin films has drawn much attention of the scientists and researchers. A brief review on various properties of plasma polymerized thin films and their applications are described below:

Yasuda [1] proposed the Competition-Ablation-Polymerization mechanism for glow discharge polymerization and identified two regimes of plasma polymerization in which the mechanisms differ dramatically i.e. the monomer-deficient plasma and the energy-deficient plasma. Indeed the composite plasma process parameter W/F_M has shown to be very efficient to control the chemical structure of the polymer. Before characterization one needs to know the chemical species of the plasma polymers and their chemical combinations. Yasuda et al. [9] and Westwood et al. [10] conducted significantly important investigations on the elemental compositions and empirical formulae of repeating units of plasma polymers produced from a variety of organic compounds using various kinds of plasma reactors. They observed two trends in the plasma polymers namely: (i) the deficiency of hydrogen and halogens which were attached to the carbon in the monomers and (ii) the incorporation of oxygen in the polymers even though the monomers did not contain oxygen. They also determined the empirical formulae of repeating units of plasma polymerized films. Having these observations, they concluded that the incorporation of oxygen was a consequence of the post plasma reaction of trapped free radicals with ambient oxygen.

The structural, optical and electrical behaviors of plasma polymerized thin films have been widely studied. It is known that Fourier transformed infrared (FTIR), spectroscopic analysis, X-ray photoelectron spectroscopy (XPS), X-ray diffraction (XRD), scanning electron microscopy (SEM), atomic force microscopy (AFM), elemental analysis (EA) etc. provide information about the chemical structure of the materials. Diferential thermal analyses (DTA) and thermogravimetric analyses (TGA) provide information about thermal

behavior of the plasma polymers. For optical characterization of plasma polymerized thin films e.g. to determine the presence, nature and extent of conjugation in materials, impurity states, optical energy gaps, direct and indirect transitions, refractive index, extinction coefficients etc. , ultraviolet visible (UV-vis) spectroscopic method is being frequently used by many investigators. For electrical characterization, the direct current (DC) and alternating current (AC) electrical properties are widely studied.

Xiong-Yan Zhao [11] discussed the development, potential applications and future directions of opto-electronic polymer thin films deposited by glow discharge plasma technique, especially the film properties required for applications in opto-electronic devices. Dung Thi Tran et al. [12] prepared composite membranes by the deposition of plasma-polymerized allylamine films onto a porous polyimide substrate. The relationship between the plasma conditions and the membrane characteristics was described in terms of monomer flow rate, plasma discharge power, plasma polymerization time, and so on. SEM images indicated that the thickness of the plasma polymer layer increased and the membrane skin pore size decreased gradually with increasing plasma polymerization time. The FTIR spectra demonstrated the appearance of amine groups in the plasma deposited polymer.

Jacob et al. [13] described the fabrication of an organic polymer thin film from a monomer based on Lavandula angustifolia. Several polymer thin films were manufactured with thicknesses ranging from 200 nm to 2400 nm. The energy gap of the polymer thin film was measured to be 2.93 eV. The results showed that the organic polymer thin film demonstrates the possibility of an environment friendly, cost effective organic semiconductor. Bhuiyan et al. [14] prepared thin films of m- xylene by plasma polymerization method using a capacitively coupled reactor. They revealed from polarized light microscopy and infrared (IR) spectroscopic studies that films were smooth, pinhole free and structurally different from m-xylene. The ac conductivity, dielectric constant and dielectric loss tangent have been measured. The observed data suggests that on heat treatment the plasma polymerized m-xylene (PPm-X) film stabilizes.

Shah Jalal et al. [15] studied the conduction mechanism in plasma polymerized m-xylene (PPm-X) thin films deposited using a capacitive coupled glow discharge reactor and concluded that the Poole-Frenkel type of conduction was most probable in PPm-X thin films. Xiao-Qin et al. [16] reported that the glow discharge polymer (GDP) films each with a

thickness of about 5μm were deposited by low-pressure plasma polymer apparatus. The influence of heat treatment on the structure of GDP film is characterized by FTIR. The optical transparency and optical band of GDP film are investigated by UV-vis spectrum. The results show that with increasing temperature, the relative content of CH_3 decreases, while the relative contents of CH_2 and CH increase. The H content in GDP film decreases.

Chowdhury et al. [17] investigated plasma-polymerized diphenyl (PPDP) thin films and reported that the surface morphology of the PPDP film was observed to be uniform and pinhole-free. The IR analysis revealed that structures of PPDP thin films were different from that of the monomer diphenyl. It was found that the surface and bulk atomic concentrations of the constituent elements were not identical. Zaman and Bhuiyan [18] investigated plasma polymerized tetraethylorthosilicate (PPTEOS) thin films by elemental analysis and IR spectrometry. The chemical structure of plasma polymerized thin films was observed to be different than that of the monomer. From the elemental analysis the chemical compositions of PPTEOS were found to be $C_{9.40}H_{12.30}$ $(SiO_4)_{0.90}$.

Akther and Bhuiyan [19] investigated plasma polymerized N, N, 3, 5-tetramethylaniline (PPTMA) and reported that PPTMA thin films were formed with certain amount of conjugation, which modified on heat treatment. From the UV-Vis absorption spectra, allowed direct transition (E_{qd}) and indirect transition (E_{qi}) energy gaps were determined to be 2.80 and 1.56 eV, respectively. While E_{qd} increased a little, E_{qi} decreased, on heat treatment of PPTMA. The calculated values of *B* for all the samples indicated an increase in structural order/conjugation in PPTMA thin films on heat treatment.

Sequential lowering of the optical band gap (4.30-2.00 eV) was observed with increasing pyrolysis temperature up to 773 K in vacuum for three hours in plasma polymerized acrylonitrile (PPAN) by Bhuiyan et al. [20]. Formation of a weak charge transfer complex between PPAN and iodine with nitrile nitrogen in the PPAN structure was observed by Bhuiyan and Bhoraskar [21] due to the doping of iodine with PPAN. Bazaka and Jacob [22] deposited transparent, smooth and uniform organic films by plasma polymerized non-synthetic Terpinen-4-ol monomer and reported the refractive index, extinction coefficient and band gap to be 1.55, 0.0007 and 2.67 eV respectively and selected as a potential candidate for electronics, optics and biomedical industries applications.

Chifen et al. [23] reported on the synthesis of nano-porous silicon oxide (SiO_2) layers by gas phase polymerization reactions of hexamethydisiloxane and oxygen. The results of XPS and FTIR showed an SiO_2-like surface chemistry and virtually complete removal of the organic components. These materials offer a very high surface area-to-volume ratio suitable for sensing applications. Bae et al. [24] investigated plasma polymerized cyclohexane and ethylcyclohexane organic thin films, deposited on Si(100), glass and copper substrates at 25–100 °C by plasma enhanced chemical vapor deposition (PECVD) method. The impedance analyzer was utilized for the measurement of *I–V* curve for leakage current density and found the best leakage current density of a cyclohexane thin film was around 5.5×10^{-12} A/cm^2 while that of ethylcyclohexane thin film was about 4.5×10^{-12} A/cm^2.

Filho et al. [25] made use of cleaner technologies and environmental friendly reagents to produce polar organic films with adsorption properties to be used as sensors in the environmental field. They obtained the films by plasma deposition of 2-propanol which were characterized by IR and Raman spectroscopies. The films with higher adsorption capacity were characterized by XPS. They analyzed some films through *I–V* and quartz crystal microbalance (QCM) measurements to investigate their application on sensing. They concluded that this film could be used as selective membrane for sensors. Takai et al. [26] investigated the properties of diamond like carbon (DLC) thin films obtained in a capacitively coupled, RF powered, PECVD system. A precursor used was pyrrole, one of the most known monomers for conductive polypyrrole polymer processing. All deposited films were transparent in the IR range. They found the resistivity decreased to $\rho \approx 3.5$ kΩ cm at 400 W and by using nitrogen as a doping element.

Rajan et al. [27] reported the structural, electrical, and optical properties of plasma-polymerized pyrrole and iodine-doped pyrrole. A comparative study of the IR spectra of the monomer and polymer pyrrole gives information that the ring structure is retained during plasma polymerization. Iodine doping considerably increases the conductivity of the polymer film and decreases the optical band-gap energy. Bazaka et al. [28] presents the effect of iodine doping on optical and surface properties of polyterpenol thin films deposited from non-synthetic precursor by means of plasma polymerization. Spectroscopic ellipsometry studies showed that iodine doping reduce the optical band gap of pristine from 2.82 to 1.50 eV and doped samples respectively. Higher levels of doping notably reduced the transparency of

films, an issue if material is considered for applications that require high transparency. Doping had no significant effect on the surface profile or roughness of the film. Hajduk et al. [29] show that doping influences on surface morphology, cristallinity and optical properties of polymer. Doping mechanism and changes of polymer electronic structure have been proposed in this paper.

Çapan et al. [30] deposited arachidic acid onto a quartz crystal using a standard Langmuir–Blodgett (LB) thin film deposition procedure. Quartz Crystal Microbalance (QCM) technique was used to monitor the reproducibility of the LB film monolayer and was employed to study the organic vapor sensing properties of chloroform, toluene, benzene, ethyl alcohol and isopropyl alcohol. They concluded that the response of the sample against chloroform was fast, large and reversible. Truica-Marasescu et al. [31] investigated low- and atmospheric-pressure plasma co-polymerizations of binary gas mixtures of C_2H_4 and NH_3 or N_2, respectively, for depositing N-rich plasma polymer coatings for biomedical applications.

Plasma polymerized tert-butylacrylate (PP-t-BA) film was prepared using tert-butylacrylate monomer under 100 Pa of vapor pressure with varying RF power of 10–250 W and continuous wave RF power of 13.56 MHz by Hidenobu Aizawa et al. [32]. Results showed that deposition rates of PP-t-BA film were proportional to the polymerization time at 100 Pa of monomer pressure under the same RF power. Olayo et al. [33] reported the influences that both electron energy and density of plasma bear on thin film formation are examined in the case of iodine-doped polyaniline polymerization. The results indicate that the electric conductivity of polyaniline by plasma is a function of the iodine content and that such content is a function of the combined conditions of both reactor and plasma.

Enlow et al. [34] described the formation of high index of refraction polymer thin films using a novel plasma polymerization deposition process. Thin films of plasma polymerized ferrocene were deposited on substrates and subsequently characterized. The chemical nature of the polymer thin films was characterized using FTIR and XPS spectroscopy. They concluded that plasma polymerization was an enabling technology for the fabrication of photonic thin films that utilize solid state precursors. The response of resistive-type sensors based on thin hexamethyldisiloxane layers to relative humidity was evaluated by Guermat et al. [35]. Humidity sensitive layers were plasma polymerized at low frequency glow discharge using a capacitively coupled parallel plate reactor. Films with a greater

thickness showed a significant decrease in the humidity sensing capability. FTIR analysis revealed the presence of SiH bonding groups, which are frequently linked to the film density. The increase in the plasma discharge power induced also a significant decrease in the diffusion process of water vapour inside the sensitive layer bulk.

Zhao et al. [36] reported on plasma-polymerized 4-biphenylcarbonitrile (PPBPCN) thin films deposited by plasma polymerization technique. Structural and morphological characterizations revealed that a conjugated PPBPCN thin film with a high retention of the aromatic ring structure of the starting monomer can be deposited at a low discharge power. They found that the plasma-synthesized film was homogeneous and quite suitable for the measurement of dielectric properties. Hence they concluded that the dielectric constant of PPBPCN thin films decreased with frequency and increased with temperature. Cho et al. [37] studied the polymer-like organic thin films, deposited at room temperature and different RF powers by plasma enhanced chemical vapor deposition (PECVD) method using ethylcyclohexane as precursor. They mainly investigated the effects of the RF plasma power to compare the optical properties as well as the electrochemical properties of the organic films. Benítez et al. [38] obtained thin polymeric films by plasma polymerization of dimethylsiloxane (DMSO) which are widely used as protective coatings on optical reflective surfaces and decorative parts.

Bazaka and Jacob [39] reported that organic thin films have myriad of applications in biological interfaces, micro-electromechanical systems and organic electronics. Polyterpenol thin films fabricated via RF plasma polymerization have been substantiated as a promising gate insulating and encapsulating layer for organic optoelectronics, sacrificial place-holders for air gap fabrication as well as antibacterial coatings for medical implants. The effect of oxygen ambience on the structure and properties of potassium lithium niobate films prepared on glass substrates by pulsed laser ablation technique are studied by Jayasree et al. [40]. They also investigated the influence of annealing on the properties of vacuum deposited films. They found resistivity in the range of kΩ m for DC resistance measurement on the films deposited at non-reactive ambience. Plasma polymerized organic thin films have been deposited on Si(100), glass and metal substrates at 25~100 °C using thiophene and toluene precursors by PECVD method by Bae et al. [41] In order to compare physical and electrochemical properties of the as-grown thin films, the effect of the RF (13.56 MHz)

plasma power in the range of 30~100 W and the deposition temperature on the corrosion protection efficiency and optical property were mainly studied. Saravanan et al. [42] reported that polyaniline thin films prepared by RF plasma polymerisation. FTIR and UV–vis–NIR measurements were carried out on the pristine and Si ion irradiated polyaniline thin films for structural evaluation and optical band gap determination. The FTIR spectrum indicates that the structure of the irradiated sample is altered. The optical studies showed that the band gap of irradiated thin film had been considerably modified due to the rearrangement in the ring structure and the formation of C≡C terminals. This results in extended conjugated structure causing reduction in optical band gap.

An atmospheric pressure glow-like dielectric barrier discharge in helium with small admixtures of methyl methacrylate (MMA) is used for the deposition of thin polymethyl methacrylate (PMMA) films by Geyter et al. [43]. The effect of discharge power and feed composition (monomer concentration) on film properties have been investigated by means of FTIR, XPS and AFM. They concluded that the deposition parameters should carefully choosen in order to obtain a high deposition rate and a high retention of ester groups in the plasma-polymerized MMA films. Xi Jin and Daqing Zhu [44] reported that the influence of curing temperature (CT) on the optical properties of 6FDA/ODA poly (amic acid)-polyimide (PAA-PI) films was characterized by measuring ATR-FTIR spectra, refractive index (RI) and birefringence of the films. Ahner et al. [45] reported the development of the optical, electrical and structural properties of two spin-on MSQ low-k dielectrics over a low-temperature range. Optical, electrical and structural parameters fluctuate very sensitive on changing the curing temperature, so usage of those materials within a low-temperature range requires a very stable curing process to achieve reproducible material properties.

Afroze and Bhuiyan [46] had prepared plasma polymerized 1, 1, 3, 3-tetramethoxy-propane (PPTMP) thin films of different thicknesses through glow discharge of 1, 1, 3, 3-tetramethoxypropane using a capacitively coupled reactor. They revealed from SEM that as-deposited PPTMP thin films were smooth, uniform and pinhole free. IR investigation had indicated the formation of conjugation along with C=O bonds and C-O-C bond owing to rearrangement of oxygen due to heat treatment of PPTMP thin films. A red shift in the maximum absorption wavelength of the UV-vis spectra for all the PPTMP thin films was observed compared to the monomer maximum absorption wavelength. Elashmawi et al [47]

reported the complex formation between polyvinyldene fluoride and different concentrations (10 wt%) of iodine were prepared by casting method using dimethyl sulfoxide as a common solvent. UV-VIS analysis suggests that the addition of iodine leads to formation of charge transfer complex with two different modes. The conductivity and dielectric measurements were carried out on these films as a function of frequency at various temperatures. The addition of iodine significantly improved the ionic conductivity. The conductivity–temperature plots were found to follow an Arrhenius nature. The decrease in dielectric permittivity was observed with increasing frequency and temperature.

Sarker and Bhuiyan [48] deposited plasma-polymerized 1-benzyl-2-methylimidazole (PPBMI) thin films onto glass substrates by glow discharge technique. SEM revealed that the surface morphology of PPBMI thin films was uniform and flawless. FTIR spectroscopy analysis showed that the chemical composition of PPBMI films was different from that of the BMI. From the UV-vis spectra direct and in- direct transition energy gaps were determined to be between 3.10 and 3.35 eV and 1.80 and 1.95 eV, respectively, for as-deposited PPBMI thin films of different thicknesses. Both direct and indirect transition energy gaps increase with increasing thickness and decrease upon heat treatment. Chowdhury and Bhuiyan [49] reported that highly adhering plasma-polymerized diphenyl (PPDP) thin films were grown by a dry and flawless process in glow discharge. Optical properties were evaluated from UV–Vis spectroscopic measurements of as-deposited, heat treated and aged (as-deposited and heat treated) PPDP thin films. The results were discussed in the light of possible structural modification in PPDP thin films on heat treatment and aging. Plasma Polymerization technique was employed to prepare thin films of polyaniline on aluminium substrate and its elctrical properties were investigated by Padwal [50] et. al. The electrical conductivity of the film was found to be of the order of 10^{-12} $ohm^{-1}cm^{-1}$. The electrical conductivity was considerably increased after doping the film by iodine vapours. The conductivity recorded after doping was of the order of 10^{-5} $ohm^{-1}cm^{-1}$. Thus by appropriate doping the conductivity of the polyaniline film formed can be controlled and set to desired level.

Hosono et al. [51] reported the effects of the discharge conditions on the structure and conductivity of the plasma polymerized polypyrrole (PPPy) films. They found that the difference in the structure of the polymer backbone of the PPPy films does not crucially affect

on the conductivity. Bae et al. [52] investigated the plasma polymerized cyclohexane and tetraethoxysilane (TEOS) hybrid thin films deposited on silicon substrates at room temperature with varying RF power by PECVD method. They concluded that the dielectric constant of thin films increases with increasing plasma power. Soo-Jin Park et al. [53] reported the effects of fluorination of polyimide thin films on surface and dielectric characteristics were studied using XPS and dielectric spectrometry, respectively. The thermal and mechanical properties of the film were characterized by TGA and tensile strengths, respectively. The fluorine content of the polyimide thin film increased with increasing treatment concentration, resulting in decreasing dielectric constant of the film. Komino et al. [54] investigated the relationship between molecular orientation and J–V characteristics, in some indium tin oxide (ITO)/X/Al structures. The results have shown that the orientation change of the poly 3-hexylthiophene (P3HT) chain causes a reproducible loop of the J–V characteristics in P3HT thin film. A series of PMMA molecules with different molecular weights and arachidic acid has been used to fabricate alternate layer LB films onto aluminum coated glass substrates and electrical properties of these LB films have been investigated by Çapan et al. [55]. I–V measurements showed that there is a polarity in the alternate layer LB films. Schottky barrier height values have been calculated using alternate layer type (AL-type) LB films.

Jiang et al. [56] fabricated polymer dielectric films by PECVD which have unique properties due to their dense crosslinked bulk structure. These spatially uniform films exhibit good adhesion to a variety of substrates, excellent chemical inertness, high thermal resistance, and are formed from an inexpensive, solvent-free, room temperature process. The dielectric constant (ε_r) and dielectric loss (tan δ) of the films were investigated over a range of frequencies up to 1 MHz and the dielectric strength (breakdown voltage) (F_b) was characterized by the I-V method. Spectroscopic ellipsometry was performed to determine the film thickness and refractive index. The PECVD processing pressure had a significant effect on final film structure and the film's physical density had a strong impact on dielectric breakdown strength. Afroze and Bhuiyan [57] reported that PPDEAEMA is stable up to 550 K. The $E_{q\mathrm{d}}$ and $E_{q\mathrm{i}}$ decrease with an increase in thickness and are found to be about 3.25–3.45 and 1.65–1.90 eV, respectively, for as deposited PPDEAEMA thin films of different

thicknesses. The effect of heat treatment on the optical properties in relation to structural changes of PPDEAEMA is also discussed. As temperature increases, both $E_{q\mathrm{d}}$ and $E_{q\mathrm{i}}$ decrease. The Urbach energy E_{u} of the PPDEAMEA thin films increases with the increase in film thickness and heat treatment temperature. The steepness parameter β decreases with thickness and heat treatment temperature.

Majumder and Bhuiyan [58] had employed electrical glow discharge technique for the preparation of plasma polymerized vinylene carbonate (PPVC) thin films at room temperature by a parallel plate capacitively coupled reactor. The structural investigation of the monomer VC and PPVC was performed by FTIR spectroscopy. They observed that Ohmic current conduction in the low voltage region and non-Ohmic conduction in the high voltage region. Matin and Bhuiyan [59] reported that plasma polymerized 2, 6, diethylaniline (PPDEA) thin films were deposited at room temperature on to glass substrates by a capacitively coupled parallel plate glow discharge reactor. They found that the surfaces of the PPDEA thin films were uniform and pinhole free from the scanning electron micrographs. The observation by energy dispersive X-ray analysis had indicated the presence of carbon, nitrogen and oxygen in the PPDEA thin films.

Akther and Bhuiyan [60] reported that plasma-polymerized *N*,*N*,3,5-tetramethylaniline (PPTMA) thin films were deposited onto glass substrates at room temperature by a capacitively coupled plasma polymerization system using TMA as a precursor. Infrared (IR) spectroscopy, elemental analysis and UV–vis spectroscopy revealed that there are conjugations in the matrix of the PPTMA thin films. From UV–vis spectroscopy they found that indirect energy gap varies from 1.49 to 1.86 eV with film thickness. Khare et al. [61] found that at higher fields and temperatures, the observed conduction behavior could be consistently described by the Richardson- Schottky emission in ferrocene mixed PMMA films grown by the isothermal immersion technique. The increase in current due to doping has been attributed to the formation of charge transfer complexes.

Wang [62] et al. showed an approach for polymerization to produce PMMA was developed, in which the reaction was initiated by the glow discharge electrolysis (GDE) rather than chemical initiators. The following parameters such as the applied voltage, discharge

time, the content of MMA, the amount of a suspension stabilizer (polyvinyl alcohol), polymerization temperature and time were examined in detail, which could affect the conversion, molecular weight and polydispersity index. PMMA was characterized by gel permeation chromatography (GPC), FTIR, cold field emission scanning electron microscopy (FESEM), nuclear magnetic resonance and TGA. Results indicate that using the GDE technique to initiate the polymerization reaction is successful, because the product obtained has the same properties with one obtained by chemical method, for example, in chemical structure, toxicity and thermal stability. Moreover, the polymer particles for the former are smaller than the latter. The kinetic observation was that the polymerization of MMA initiated by the GDE plasma obeys the first order of reaction with an obvious induction period. Park [63] et al. fabricated a poly(methyl methacrylate-co-methacrylic acid) (PMMA-co-MAA) and titanium dioxide (TiO_2) composite to use as a gate insulator in pentacene-based organic thin-film transistors (OTFTs). The dispersion stability was confirmed by observing the sedimentation time of TiO_2 nanoparticles in the PMMA-co-MAA solution, which is essential to avoid a severe gate-leakage current in OTFTs. From the measured capacitance-frequency characteristics, a dielectric constant value of 4.5 was obtained for the composite film and 3.3 for the PMMA-co-MAA film.

Sarker and Bhuiyan [64] studied *J-V* characteristics over the temperature range from 300 to 423 K for plasma-polymerized 1-benzyl-2-methylimidazole (PPBMI) thin films of thicknesses 100, 150, 200 and 250 nm in aluminum/PPBMI/aluminum (Al) sandwich configuration and found that the dominant conduction mechanism is space charge limited conduction (SCLC). Mathai et al. [65] reported the *J-V* characteristics of polyfurfural thin films lying in the thickness range of 1300–2000 Å indicate that Schottky conduction mechanism is dominant in plasma polymerized furfural thin films. Kumar et al [66] suggested that the conduction mechanism in the plasma polymerized eucalyptus oil film is a Schottky type. The non-linearity in the *J-V* behaviour at higher voltages was explained by phonon-assisted tunneling model by Pipinys et al. [67]. Sivaraman and Anantharaman [68] revealed the mechanism of electrical conduction in PA thin films for different temperatures and found that the mechanism of carrier transport in these thin films is SCLC.

Electrical conduction mechanism and dielectric properties of thermally evaporated N-(p-dimethylaminobenzylidene)-p-nitroaniline (DBN) thin films were studied by El-Nahass et al. [69]. The DBN films were prepared by thermal evaporation sandwiched between two gold electrodes of thickness 50 nm which act as ohmic contacts with the DBN films. The temperature dependence of the direct current conductivity of the DBN thin films reveal that the conduction is through a thermally activated process having two conduction mechanisms. The electrical conduction of the films follows a mechanism in which the electron or hole hops from one localized site to the next. So the dc conductivity indicates a thermally activated carrier hopping rate which increases with increasing temperature. Mathai et al. [70] focused on the electrical properties of ac plasma polymerized aniline thin films with a view to determining the dominant conduction mechanism. The *J-V* characteristics in symmetric and asymmetric electrode configuration for polyaniline thin films of different thicknesses were investigated. *J-V* plot for symmetric electrode configuration shows that the conduction in the lower region of the applied voltage is found to be ohmic while in the higher range of the applied field, it is found to be non-ohmic and the dominant conduction mechanism is Schottky-type. The optical and electrical characterizations of plasma polymerized pyrrole (PPPy) films in the presence and absence of iodine were carried out by Kumar et al. [71]. From the *I-V* characteristics of the two types of polymer films they found that the conductivity of the doped PPPy was approximately two times greater than that of the undoped one. Iodine doping increased the conductivity of the PPPy thin films. A detailed analysis of the conduction mechanism showed that the conduction mechanism in the undoped PPPy thin film was Schottky type.

Saravanan [72] et al. reported on polyaniline thin films prepared by employing an RF plasma polymerization technique. Capacitance, dielectric loss, dielectric constant and alternating current (ac) conductivity were evaluated in the frequency range 100 Hz–1 MHz. Capacitance and dielectric loss decrease with increase of frequency and increase with increase of temperature. The ac conductivity was calculated from the observed dielectric constant and is explained based on the Austin–Mott model for hopping conduction. These films exhibit low dielectric constant values, which are stable over a wide range of frequencies and are probable candidates for low ε‘ applications. Thomas et al. [73] reported that the dielectric constant of PMMA was around 4.9 for 100Hz which increased to 15.7 for 100 Hz when the ceramic

content has increased to 40 Vol %. At low frequencies, space charge polarization is dominant. This composite also exhibited remarkably low dielectric loss at high frequency, which makes this composite a suitable candidate for the capacitors in high frequency application.

Zhao et al. [74] prepared a novel plasma-polymerized 1-cyanoisoquinoline (PPCIQ) thin film of desired thickness by plasma polymerization under different glow discharge conditions. The plasma-synthesized films are homogeneous and dielectric measurements show a low dielectric constant of 2.62 for the PPCIQ thin films. Darwish [75] measured ac dark current of nickel phthalocyanine thin films using ohmic gold electrodes in the frequency range 30-10^5 Hz and within the temperature range 295-385 K. The ac conductivity indicates a dominant hopping process at low temperatures. From the temperature dependence of ac conductivity, free carrier conduction with mean activation energy of 0.31 eV is observed at higher temperatures. Capacitance and loss tangent decreased with increasing frequency and increased with increasing temperature. Such characteristics are found to be in good qualitative agreement with existing equivalent circuit model assuming ohmic contacts.

Zhao et al. [76] reported that plasma-polymerized 4-biphenylcarbonitrile thin films are homogeneous and conclude that dielectric constant decreased with frequency and increased with temperature. Cho et al. [77] deposited plasma-polymer pure ethylcyclohexane thin films on Si(100) substrates at room temperature by using PECVD. They investigated the electrical and the physical properties of the plasma-polymer thin films at various deposition RF powers and annealing temperatures. An impedance analyzer was used to measure the capacitance and from the electrical property measurements, the lowest dielectric constant obtained was 1.71. Kim et al. [78] fabricated organic memory device by entirely dry process, plasma polymerized methyl methacrylate (ppMMA) thin films and were used as both tunneling layer and gate insulator layer in a floating-gate type organic memory device. The ppMMA gate insulator thin film revealed dielectric constant of 3.75 and low leakage current of smaller than 10^{-9} A/cm. Gonon and Sylvestren [79] investigated the dielectric properties of fluorocarbon thin films deposited by RF magnetron sputtering of polytetrafluroethylene. The dielectric constant and the loss factor are studied as a function of frequency (0.1 Hz-1 MHz) and temperature (room temperature to 100 °C). The value of the dielectric constant is 1.8 at optical frequencies, and around 2.3 in the 0.1 Hz–1 MHz range. Temperature dependence of the dielectric constant is

well described by a simple Debye model and this dependence leads to an activation energy of 0.66 eV.

Chowdhury and Bhuiyan [80] employed dielectric relaxation spectroscopy to investigate the behavior of the as-deposited plasma-polymerized diphenyl thin films and found ac conductivity more dependent on temperature in the low frequency region than in the high frequency region. They concluded that the conduction may be dominated by hopping of carriers between the localized states at low temperatures and thermally excited carriers from energy levels within the band gap in the vicinity of high temperature. The dielectric data analyses showed the existence of distribution of relaxation time in these materials. Kalugasalam and. Ganesan [81] studied the dielectric and conduction properties of Lead Phthalocyanine thin films prepared by vacuum deposition method. The dependence of conductivity on frequency was explained by the predominance of the hopping mechanism, as the conductivity increases with increasing frequency. Akther and Bhuiyan [82] reported the capacitance and ac electrical conductance of plasma polymerized N,N,3,5 tetramethylaniline (PPTMA) thin films, as functions of frequency ($100 < f < 105$ Hz) and temperature ($300 < T < 450$ K). The electrical conductivity is more dependent on temperature in the low frequency region than that in the high frequency region. In PPTMA thin films the conduction may be dominated by hopping of carriers between the localized states at low temperatures and thermally excited at the high temperatures. The activation energies are estimated to be about 0.05 eV in the low temperature and 0.23 eV in the high temperature. Dielectric constant decreases with the increase of frequency and that decreases with the increase of temperature but dielectric loss increases with increasing frequency with a minimum in the low frequency region. The temperature-dependence of the Cole-Cole diagram shows the existence of distribution of dielectric relaxation times in the PPTMA thin films.

Hussien [83] investigated the ac electrical conductivity of (poly-methyl methacrylate - alumina) composite. The dielectric constant, dielectric loss, AC electrical conductivity are changed with change the concentration of the filler and frequency of applied electrical field.
Abdelrazek [84] et al reported on polyethyl methacrylate (PEMA) films filled with different mass fractions of $MnCl_2$ prepared by casting method. AC conductivity behavior of all the prepared samples was investigated over the frequency range (42–5M) Hz and under different

isothermal stablilization in the temperature range 300–423 K. It suggested that the hopping mechanism is important in the conduction process, in low temperature regime.

Banerjee and Kumar [85] reported on polyaniline (PAni) nanofibers synthesized by interfacial polymerization were reinforced in the PMMA matrix in different weight ratios. The dielectric constant measured over a frequency range of 42 Hz–1 MHz and in the temperature range of 303–373 K showed dependence upon frequency, temperature and concentration of the conducting nanofibers in the composites. The σ_{ac} was interpreted as a power law of frequency. The frequency exponent was found to lie in the range from 0.4 to 0.65 and decreased with the increase in temperature, which suggested that correlated barrier hopping (CBH) was the dominant charge transport mechanism. Reda [86] investigated the σ_{ac}, dielectric permittivity and dielectric loss for pure PMMA and mixed with phthalocyanine, Ni-phthalocyanine and hematoporphyrin IX chloride laser dyes. The conductivity values for all polymer dye samples are higher than that of the pure PMMA. Capan et al. [87] found on the basis of surface plasmon resonance (SPR) measurements, under dynamic conditions, room temperature response of PMMA films to benzene vapours is found to be fast, highly sensitive and reversible.

Sadhir et al. [88] prepared thin dielectric films containing silicon nitride-type linkages by plasma polymerization of tetramethylsilane in the presence of ammonia. The dielectric constant and dissipation factor decreased with an increase in frequency. The loss tangent and dielectric constant decreased with an increase in the film deposition temperature from 25 °C to 200 °C at all the frequencies with an exception at the highest frequency. A gradual increase in dielectric constant and loss tangent was observed for the films with an increase in measurement temperature. Afroze and Bhuiyan [89] reported that PPTMP thin films might have a certain amount of conjugation which was confirmed by FTIR spectroscopic investigation. Optical properties were investigated by ultraviolet–visible spectroscopic measurements on as-deposited and aged PPTMP thin films. From the optical absorption data, absorption coefficient and direct and indirect energy band gaps were calculated for the as-deposited unaged and aged PPTMP thin films. The aging effect on the structural and optical properties is also discussed. Matin and Bhuiyan [90] reported a comparative analysis on the changes of morphological, structural and optical properties of as-deposited, heat treated and aged PPDEA thin films. DTA, TGA analysis and DTA recommended that the PPDEA is

thermally stable up to about 580 K. They found allowed direct and indirect transition energies ranging from 3.63 to 2.73 and 2.38 to 1.26 eV respectively for as-deposited, heat treated and aged PPDEA thin films of different thicknesses. They concluded that the optical parameters of as-deposited PPDEA thin films change due to heat treatment and do not change appreciably due to aging.

From the overall literature review, it is seen that plasma polymerization process is an important physical process of depositing organic thin films with properties different from their conventionally prepared counterpart. The physical, chemical, electrical and optical properties of plasma polymerized thin films are very much dependent on the types of glow discharge reactor and deposition conditions. Thin films deposited by this process are proposed to be important dielectric, insulator, sensors, optoelectronic etc. materials. In this respect plasma polymerized thin films of organic materials warrant detail investigation of their physico-chemical, structure, optical, electrical etc. properties.

PMMA is a polymer having carbon-carbon main chains. It is basically classified as insulators due to very small number of charge carriers and their low mobility [91]. It is one of the best polymeric materials broadly used for insulation devices assemble [92]. It is seen from the literature survey that PMMA and derivatives of methylmethacrylate (MMA) have gained a lot of interest among the scientists and technologists for their interesting properties and wide range of applications including sensing material, gate dielectric for organic thin film transistor, dielectric layer for field effect transistor, memory devices, etc. [93-96]. 2-(diethylamino)ethyl methacrylate (DEAEMA) is a derivative of ethyl methacrylate (EMA) which is a methacrylate ester readily polymerizes and rapidly reacts with multifunction methacrylates to form a crosslinked polymer [97].

DEAEMA is a monofunctional acrylate monomer with dual methacrylic and amine reactivity and with a polar tertiary amine functional group which offers water solubility and good adhesion. DEAEMA forms homopolymers and copolymers. It is also a very useful feedstock for chemical syntheses, because it readily undergoes addition reactions with a wide variety of organic and inorganic compounds [98-99]. Conventional PMMA and its plasma-polymerized analog (PPMMA) or plasma-treated PMMA are finding a broad array of uses in

thin film and coating applications**.** PMMA is also used in flat screen televisions, liquid crystal displays, etc. The plasma polymerization process almost always yields cross linked, pinhole free and durable surfaces. Plasma-polymerized or plasma-treated MMA films have been used as polymer membranes for the contact lens or intraocular lenses for the natural lens of the eye during eye surgery, moisture-sensing applications such as relative-humidity sensors, and optical applications such as solid-state dye layers and wavelength transformers [100]. Thin films of PMMA are of interest for a variety of applications, including organic vapor and moisture sensors, electron-beam resists, photonic waveguides and optical fibers [101]. Thus it is decided to study the optical and electrical properties of a derivative of MMA i.e. 2 (diethylamino)ethyl methacrylate in thin film form.

1.3 Aim of the study

The purpose of this work is to prepare plasma polymerized 2 (diethylamino)ethyl methacrylate in thin film and to explore the structural, optical and electrical characteristics of PPDEAEMA thin films of different thicknesses. The structural changes/chemical bonding are confirmed by FTIR and the thermal properties are investigated by TGA/DTA. From the UV-vis absorption spectroscopic measurements the direct and indirect energy band gap, Urbach energy, extinction coefficient and steepness parameter are determined.

Since iodine is frequently used as a dopant because of the ease of the doping procedure, high electro negativity and less toxicity in comparison to other halogens. The modification of the above characteristics due to the effect of heat treatment at different temperature and iodine doping for different time interval are also discussed.

The objective of this work is also to study at thin films of PPDEAEMA from the point of view of DC and AC electrical conduction. The nature of the charge transport phenomenon and the conduction mechanism involved has been studied from DC electrical conduction. The influence of film thickness and temperature on the transport properties of PPDEAEMA thin films has been presented. The effect of iodine doping on the DC electrical properties was observed.

The influence of film thickness and temperature on the AC electrical properties of PPDEAEMA thin films has been investigated. The results obtained from the AC electrical

investigation will be analyzed with the existing theories to illuminate the relaxation behavior and dielectric loss mechanism in these materials. The detail investigation of the AC conductivity and dielectric properties of plasma-polymerized thin films provide information about the conduction process, dielectric constant, relaxation process, etc. which are dependent on frequency and temperature. The change in AC electrical properties due to iodine doping was also studied.

1.4 Thesis Layout

Organization of this thesis is divided into five chapters:

Chapter 1 is the introductory chapter beginning with a general introduction followed by reviews of earlier research works, objective of the thesis and thesis layout. Chapter 2 focuses the fundamental aspects of polymer, plasma, their classification and general properties, overview of gas discharge plasma, plasma polymerization mechanism, advantages, disadvantages and applications of plasma polymerized thin films, etc.

Chapter 3 provides the existing theories on SEM, FTIR, DTA/TGA, UV-vis, AC/DC conduction. The experimental techniques related to the thermal, structural, optical and electrical characterizations of Plasma Polymerized thin films are discussed in Chapter 4 along with the description of the plasma polymerization set up, generation of glow discharge, deposition parameters, thin film formation, film thickness measurements etc.

Chapter 5 focuses the results of SEM and EDAX, DTA/TGA and FTIR spectroscopic study. Besides, the details of UV-Vis spectroscopic measurements including optical absorption, absorption coefficient, Urbach energy, extinction coefficient and steepness parameter are reported. The J-V Characteristics, conduction mechanism, activation energy and temperature dependent conductivity are discussed in this chapter. The frequency and temperature dependence of ac conductivity, dielectric constants, dielectric relaxation, loss tangent and Cole-Cole plot are also discussed.

Finally, the thesis is folded up with conclusions and suggestions for future work in Chapter 6.

References

[1] Yasuda, H., 'Plasma Polymerization', Academic Press, New York, 1985.

[2] Morosoff, N., Agostino, R. d' (Ed), 'In Plasma deposition, Treatment and Etching of Polymers', Academic Press, San Diego, CA, 1990.

[3] Inagaki, N., 'Plasma Surface Modification and Plasma Polymerization', Technomic Publishing Co. Inc., New York 1996.

[4] Zhao, X.-Y., Wang, M.-Z. and Wang, Z., 'Deposition of plasma polymerized 1-cyanoisoquinoline thin films and their dielectric properties', Plasma Process. Polym. 4, 840-846, 2007.

[5] Wu, L., Zhu, C. and Liu, M., 'Study on plasma polymerization of 1. 1. 1-trifluoroethane: deposition and structure of plasma polymer films', Desalination 192, 234-240, 2006.

[6] Zhao X.-Y., Wang, M.-Z. and Xiao, J., 'Deposition of plasma conjugated polynitrile thin films and their optical properties', Eur. Polym. J. 42, 2161-2167, 2006.

[7] Sajeev, U. S., Mathai, C. J., Saravanan, S., Ashokan, Rajeev R., Venkatachalam, S. and Anantharaman, M. R., 'On the optical and electrical properties of r.f. and a.c. plasma polymerized aniline thin films', Bull. Mater. Sci. 29, 159-163, 2006.

[8] Saravanan, S., Joseph, Mathai C., Venkatachalam, S. and Ananharaman, M. R., 'Low k thin films based on rf plasma- polymerized aniline', New J. Phys. 6, 64, 2004.

[9] Yasuda, H., Bumgarner, M. O., Marsh, H. C., Morosoff, N., 'Plasma poltmerization of some organic compounds and properties of the polymers', J. Polym. Sci. Polym. Chem., 14, 195-224, 1976.

[10] Westwood, A. R., Eur. Polym. J., 7, 377, 1971.

[11] Zhao, X.-Y., 'Opto-electronic polymer thin films deposited by glow discharge plasma technique: A review', Iranian Polym. J. 19 (11), 823-841, 2010.

[12] Dung, T. T., Shinsuke, M. and Masaaki, S., 'Characteristics of polyimide-based composite membranes fabricated by low-temperature plasma polymerization', Thin Solid Films 516(13), 4384-4390 2008.

[13] Jacob, M. V., Easton, C. D., Woods G. S. and Berndt C. C., 'Fabrication of a novel organic polymer thin film', Thin Solid Films 516(12), 3884-3887, 2008.

[14] Bhuiyan, A. H., Islam, O. and Ahmed, .S. 'IR and dielectric studies of plasma polymerized m-xylene thin films', Thin Solid Films, 238, 191-194, 1994.

[15] Shah Jalal, A.B.M., Ahmed, S., Bhuiyan, A.H., and Ibrahim, M., 'On the conduction

mechanism in plasma polymerized m-xylene thin films', Thin Solid Films, 295, 125-130, 1997.

[16] Jia, X.-Q., He, Z.-B., Niu, Z.-C., He, X.-S., Wei, J.-J., Li, R., Du, K., 'Influnce of heat treatment on the structure and optical properties of glow discharge polymer films', Acta. Phys. Sin. 62(5), 056804, 2013.

[17] Chowdhury, F.-U.-Z., Islam, A.B.M.O., and Bhuiyan, A.H. 'Chemical analysis of the plasma-polymerized diphenyl thin films', Vacuum, 57, 43-50, 2000.

[18] Zaman, M. and Bhuiyan, A. H., 'Elemental Analysis and infrared investigation of plasma polymerized Tetraethylorthosilicate thin films', J. App. Sci. Techn., 03(02), 133-137, 2003.

[19] Akther, H., Bhuiyan, A. H, 'Infrared and ultra violet-visible spectroscopic investigation plasma polymerized N, N, 3, 5- tetramethylaniline thin films', Thin Solid Films, 474, 14-18, 2005.

[20] Bhuiyan, A. H., Rajopadhye, N. R., Bhoraskar, S. V., 'A few electronic properties of thin films of plasma polymerized acrylonitrile', Thin Solid Films, 161, 187-195, 1988.

[21] Bhuiyan, A. H., Bhoraskar, S. V., 'Evidence of the formation of a charge transfer complex between iodine and plasma polymerized acrylonitrile', Thin Solid Films, 235, 43, 1993.

[22] Bazaka, K., Jacob, M. V. M, 'Synthesis of radio frequency plasma-polymerized. Non–synthetic Terpinen-4 ol thin films', Mater. Lett. 63, 1594-1597, 2009.

[23] Anye, N. C., Wolfgang, K. and Renate, F., 'Fabrication of nano-porous silicon oxide layers by plasma polymerisation methods', Mater. Lett. 61 (8-9), 1722-1724, 2007.

[24] Bae, I. S., Cho, S. H., Park, Y. S., Hong, B., Park, Z. T., Kim J.-G. and Boo J.-H., 'Synthesis and application perspective of advanced plasma polymerized organic thin films', Thin Solid Films, 506-507, 2-7, 2006.

[25] Nascimento Filho, A. P., da Silva, M. L. P., Galeazzo, E. and Demarquette, N. R., 'Use of plasma polymerized highly polar organic compound films for sensor development', Sens. Actuat. B: Chem. 91 (1-3), 370-377, 2003.

[26] Takai, O., Anita, V. and Saito, N., 'Properties of DLC thin films produced by RF PE−CVD from pyrrole monomer', Surf. Coat. Technol. 200(1-4), 1106-1109, 2005.

[27] Rajan K. John, D. Sakthi Kumar, 'Structural, electrical, and optical studies of plasma-polymerized and iodine-doped poly pyrrole', J. Appl. Polym. Sci. 83: 1856–1859, 2002.

[28] Bazaka, K., Jacob, M. V., 'Effect of Iodine Doping on Surface and Optical Properties of Polyterpenol Thin Films' Mater. Sci. Forum 654-656, 1764-1767, 2010.

[29] Hajduk, B., Weszka, J., Jarząbek, B., Jurusik, J., Domański, M., 'Physical properties of

polyazomethine thin films doped with iodine', J. Achiev. Mater.and Manuf. Eng., 24(2) 2007.

[30] Çapan, R., Açıkbaş, Y., Evyapan, M., 'A study of Langmuir–Blodgett thin film for organic vapor detection' Mater. Lett., 61(2), 417-420, 2007.

[31] Truica-Marasescu, F., Girard-Lauriault, P.-L., Lippitz, A., Wolfgang E.S. Unger, Michael R. Wertheimer, 'Nitrogen-rich plasma polymers: Comparison of films deposited in atmospheric- and low-pressure plasmas' Thin Solid Films, 516(21), 7406-7417, 2008.

[32] Aizawa, H., Kawashima, S., Kurosawa, S., Noda, K., Fujii, T., Hirata, M.,'Synthesis and characterization of plasma-polymerized tert-butylacrylate films', Thin Solid Films, 515(9), 4141-4147, 2007.

[33] Olayo, M. G., Morales, J., Cruz, G. J., Olayo, R., Ordon˜ Ez, E., Barocio, S. R. , 'On the Influence of Electron Energy on Iodine-Doped Polyaniline Formation by Plasma Polymerization', J Polym. Sci. B: Polym. Phys. 39: 175–183, 2001.

[34] Enlow, Jesse, O., Jiang, H., Grant, J., T., Eyink, K., Su, W., Bunning, T. J., 'Plasma polymerized ferrocene films', Polym., 49(19), 4042-4045, 2008.

[35] Guermat, N., Bellel, A., Sahli, S., Segui, Y., Raynaud, P., 'Thin plasma-polymerized layers of hexamethyldisiloxane for humidity sensor development', Thin Solid Films, 517, 4455, 2009.

[36] Zhao, X.-Y., Wang, M.-Z., Wang, Z. and Zhang, B.-Z., 'Structural and dielectric properties of conjugated polynitrile thin films deposited by plasma polymerization', Thin Solid Films, 516 (23), 8272-8277, 2008.

[37] Cho, S.-H., Park, Z.-T., Kim, J. -G. and Boo, J.-H., 'Physical and optical properties of plasma polymerized thin films deposited by PECVD method', Surf. Coat. Technol. 174-175, 1111-1115, 2003.

[38] Benítez F., Martínez E., Galán M., Serrat J. and Esteve J., 'Mechanical properties of plasma deposited polymer coatings', Surf. Coat. Technol. 125(1-3), 383-387, 2000.

[39] Bazaka, K., and Jacob, M. V. 'Solubility and surface interactions of RF plasma polymerized polyterpenol thin films', Mater. Expr., 2 (4), 285-293, 2012.

[40] Jayasree, V., Ratheesh, R., Ganesan, V., Reddy, V. R., Sudarsanakumar, C., Mahadevan Pillai, V. P., Nayar, V. U., 'Influence of reactive oxygen ambience on the structural, morphological and optical properties of pulsed laser ablated potassium lithium niobate thin films', Thin Solid Films, 516(24), 603-608, 2008.

[41] Bae, I.-S., Jung, C.-K., Jeong, S.-H., Cho, S.-J., Yu, Y. J., Kim, J.G., Boo, J.-H., 'Comparison of their electrical, optical, and electrochemical properties of as-grown plasma polymerized organic thin films by PECVD', Thin Solid Films, 515(2), 407-410, 2006.

[42] Saravanan, S., Anantharaman, M. R., Venkatachalam, S., Avasthi, D. K., 'Studies on the

optical band gap and cluster size of the polyaniline thin films irradiated with swift heavy Si ions', Vacuum, 82(1), 56-60, 2007.

[43] De Geyter, N., Morent, R., Van Vlierberghe, S., Dubruel P., Leys, C., Gengembre, L., Schacht, E., Payen, E., 'Deposition of polymethyl methacrylate on polypropylene substrates using an atmospheric pressure dielectric barrier discharge', Prog. Org. Coat., 64(2-3), 230-237, 2009.

[44] Jin, X. and Zhu, D., 'Influence of curing temperature on the optical properties of fluorinated polyimide thin films' Eur. Polym. J., 44(11), 3571-3577, 2008.

[45] Ahner, N., Schulz, S. E., Blaschta, F. and Rennau, M., 'Optical, electrical and structural properties of spin-on MSQ low-k dielectrics over a wide temperature range', Microelectronic Engg., 85(10), 2111-2113, 2008.

[46] Afroze, T. and Bhuiyan, A. H., 'Infrared and ultraviolet-visible spectroscopic studies of plasma polymerized 1, 1, 3, 3 - tetramethoxypropane thin films', Thin Solid Films 519 (6), 1825-1830, 2011.

[47] Elashmawi, I.S., Abdelrazek, E.M., Ragab, H.M., Hakeem, N.A., 'Structural, optical and dielectric behavior of PVDF films filled with different concentrations of iodine', Physica, B 405, 94–98, 2010.

[48] Sarker, R. B. and Bhuiyan, A. H., 'Structural and optical properties of plasma-polymerized 1-benzyl-2-methylimidazole thin films', Inter. J. Modern Phys. B (IJMPB) 25(14), 1941-1955, 2011.

[49] Chowdhury, F.-U.-Z, Bhuiyan, A.H., 'An investigation of the optical properties of plasma-polymerized diphenyl thin films', Thin Solid Films 360 (1-2), 69-74, 2000.

[50] Padwal, P., Madhuskar, S.V. and Kulkarni, S., 'Study of electrical properties of polyaniline films prepared by rf plasma polymerization', IOSR J. Appl. Phys. (IOSR-JAP)3(3), 59-61, 2013.

[51] Hosono, K., Matsubara, I., Murayama, N., Shin W. and Izu, N., 'Effects of discharge power on the structure and electrical properties of plasma polymerized polypyrrole films', Mater. Lett. 58(7-8) 1371-1374, 2004.

[52] Bae I.-S., Cho, S.-J., Choi, W.S., Cho, H.J., Hong, B., Jeong H.-D. and Boo, J.-H., 'Characterization on polymerized thin films for low-*k* insulator using PECVD', Prog. Org. Coat., 61 (2-4), 245-248 (2008).

[53] Soo-Jin Park, Ki-Sook Cho and Sung-Hyun Kim, 'A study on dielectric characteristics of fluorinated polyimide thin film', J. Colloid. Inter. Sci., 272(2), 384-390, 2004.

[54] Takeshi Komino, Hiroyuki Tajima, Masaki Matsuda, 'An attempt to measure simultaneously

molecular orientation and current–voltage characteristics in thin films', Thin Solid Films, 517(4), 1358-1361, 2008.

[55] Çapan, I., Uzunoğlu, T., Tarımc, C., Tanrısever, T., 'Electrical characterisation of poly(methyl methacrylate)/arachidic acid Langmuir–Blodgett films', Thin Solid Films, 516(24), 8975-8978, 2008.

[56] Jiang, H., Hong, L., Venkatasubramanian, V., Grant, J., T., Eyink, K., Wiacek, K., Fries-Carr, S., Enlow, J., Bunning, T. J., 'The relationship between chemical structure and dielectric properties of plasma-enhanced chemical vapor deposited polymer thin films', Thin Solid Films, 515(7-8), 3513-3520, 2007.

[57] Afroze, T. and Bhuiyan, A. H., 'Effect of heat treatment on the structural and optical characteristics of plasma deposited 2-(diethylamino)ethyl methacrylate thin films by a capacitively coupled glow discharge plasma system' , Phys. Scr., 88(4), 045502, 2013.

[58] Majumder, S. and Bhuiyan, A. H., 'DC conduction mechanic,sm in plasma polymerized vinylene carbonate thin films prepared by glow discharge technique', Polym. Sci. Series A 53 (1), 85-91, 2011.

[59] Matin, R. and Bhuiyan, A. H., 'Electrical transport mechanism in plasma polymerized 2, 6, diethylaniline thin films', Thin Solid Films, 519 (11), 3462-3467, 2011.

[60] Akther, H., Bhuiyan. A. H., 'Electrical and optical properties of plasma-polymerized N,N,3,5-tetramethylaniline thin films', New J. Phys. 7, 173, 2005.

[61] Khare, P. K., Jain, S. K. and Paliwal S. K., 'Conduction mechanism in doped polymethylmethacrylate (PMMA) films', Bull. Mater. Sci., 20, 699-705, 1997.

[62] Wang, A., Gao, J., Yuan, L., and Yang, W., 'Synthesis and characterization of polymethylmethacrylate by using glow discharge electrolysis plasma', Plasma Chem Plasma Process, 29(5), 387-398, 2009.

[63] Jaehoon Park, Jong Won Lee, Dong Wook Kim, Bong June Park, Hyoung Jin Choi and Jong Sun Choi, 'Pentacene thin-film transistor with poly(methyl methacrylate-co-methacrylic acid)/TiO_2 nanocomposite gate insulator', Thin Solid Films, 518(2), 588-590, 2009.

[64] Sarker R. B. and Bhuiyan A.H., 'Electrical conduction mechanism in plasma polymerized 1-Benzyl-2- methylimidazole thin films under static electric field', Thin Solid Films 519, 5912-5916, 2011.

[65] Mathai C. J., Anantharaman M. R., Venkitachalam S., Jayalekshmi S., 'Mechanism of electrical conduction in plasma polymerized furfural thin films', Thin Solid Films 416, 10–15, 2002.

[66] Sakthi Kumar D., Kenji Nakamura, Satoko Nishiyama, Hiromichi Noguchi, Shigeru Ishii,

Kunihiro Kashiwagi, Yasuhiko Yoshida, 'Electrical and optical properties of plasma polymerized eucalyptus oil films', J. Appl. Polym. Sci. 90, 1102–1107, 2003.

[67] Pipinys P., Rimeika A. and Lapeika V., 'DC conduction in polymers under high electric fields', J. Phys. D: Appl. Phys. 37, 828–831, 2004.

[68] Sivaraman S. and Anantharaman M. R., 'Determination of charge carrier transport in radio frequency plasma polymerized aniline thin films', J. Phys. D: Appl. Phys. 43, 055403 (6pp), 2010.

[69] El-Nahass M. M., Zeyada H. M., El-Samanoudy M. M., El-Menyawy E. M., 'Electrical conduction mechanism and dielectric properties of thermally evaporated N-(p-dimethylaminobenzylidene)-p-nitroaniline thin films', J. Phys.: Condens. Matter. 18(22), 5163-5173, 2006.

[70] Mathai C. J., Saravanan S., Jayalekshmi S., Venkatachalam S., Anantharaman M. R., 'Conduction mechanism in plasma polymerized aniline thin films' Mater. Lett. 57, 2253, 2003.

[71] Kumar D. S., Kenji Nakamura, Satoko Nishiyama, Shigeru Ishi, Hiromichi Noguchi, Kumihiro Kashiwage and Yasuhiko Yoshida, 'Optical and electrical characterization of plasma polymerized pyrrole films', J. Appl. Phys., 93, 2705, 2003.

[72] Saravanan S., Mathai C. J., Venkatachalam S , and Anantharaman M. R., Low *k* thin films based on rf plasma-polymerized aniline, New J of Phys., 6, 64, 2004.

[73] Thomas P., Ernest Ravindran R.S., Varma K.B.R., 'Dielectric properties of Poly(methyl methacrylate) (PMMA)/CaCu3Ti4O12 Composites'.

[74] Zhao X. Y., Wang M. Z., Wang Zhi, 'Deposition of Plasma-Polymerized 1-Cyanoisoquinoline Thin Films and Their Dielectric Properties' Plasma Process. Polym., 4, 840–846, 2007.

[75] Darwish S., 'Capacitance Measurements and AC Conductivity of Nickel Phthalocyanine Films', Inter. J. Pure and Appl. Phys., 1(2) 165-172, 2005.

[76] Zhao X.Y., Wang Ming-zhu, Wang Zhi, Zhang Bing-zhu, 'Structural and dielectric properties of conjugated polynitrile thin films deposited by plasma polymerization', Thin Solid Films, 516, 8272–8277, 2008.

[77] Hong S.-J. Cho, Bae I.-S., J.-H. Boo and Park Y. S., Study on the Plasma-Polymer Thin Films Deposited by Using PECVD and Application Tests for Low-k Insulator, J. Korean Phys. Soc., 53(3), 1634-1637, (2008).

[78] Hee-sung Kim, Boong-Joo Lee, Gun-Su Kim, and Paik-Kyun Shin, 'Floating-Gate Type Organic Memory with Organic Insulator Thin Film of Plasma Polymerized Methyl Methacrylate', Jpn. J. Appl. Phys., 52, 021601, 2013.

[79] Gonon, P. and Sylvestren, A., 'Dielectric properties of fluorocarbon thin films deposited by radio frequency sputtering of polytetrafluoroethylene', J. Appl. Phy., 92(8), 4584-4589, 2002.

[80] Chowdhury, F.–U.-Z., Bhuiyan, A. H., 'Dielectric properties of plasma polymerized diphenyl thin films', Thin Solid Films, 370 (1-2), 78-84, 2000.

[81] Kalugasalam, P., Ganesan, DR. S., 'Dielectric and ac conduction studies of lead phthalocyanine thin film', Chalcogenide Lett. 6(9), 469 – 476, 2009.

[82] Akther, H., Bhuiyan, A. H., 'Dielectric properties of plasma polymerized N,N,3,5 tetramethylaniline thin films', Surface Rev. and Lett., 18(1&2), 53-60, 2011.

[83] Hussien, Bahaa, 'The D.C and A.C. Electrical Properties of (PMMA -Al2O3) Composites', Eur. J. Scientific Res., 52(2), 236-242, 2011.

[84] Abdelrazek, E. M., Elashmawi, I. S., Ragab, H. M., 'Manifestation of $MnCl_2$ fillers incorporated into the polymer matrices in their dielectric properties', Physica B, 403, 3097–3104, 2008.

[85] Banerjee, S., Kumar, A., 'Dielectric behavior and charge transport in polyaniline nanofiber reinforced PMMA composites', J. Phys. and Chem. Solids, 71, 381–388, 2010.

[86] Reda, S. M. 'Electric and dielectric properties of some luminescent solar collectors based on phthalocyanines and heamatoporrphyrin doped PMMA', Dyes and Pigments, 75, 526-532, 2007.

[87] Capan, R., Ray, A. K., Hassan, A. K. and Tanrisever, T., 'Poly(methyl methacrylate) films for organic vapour sensing', J. Phys. D: Appl. Phys., 36, 1115–1119, 2003.

[88] Sadhir, R. K., Saunders, H. E, Schoch, K. F., Bennett, A. I., 'Electrical properties of plasma polymerized thin films deposited at high substrate temperature', Electrical Electronics Insulation Conference, 25-28 Sep,1989. Chicago '89 EEIC/ICWA Exposition, Proceedings.

[89] Afroze, T., Bhuiyan A. H., Effect of Aging on the Optical Properties of Plasma Polymerized 1,1,3,3-Tetramethoxypropane Thin Films, Adv. in Polym. Tech. 32(2), 21347, 2013.

[90] Matin, R. Bhuiyan, A. H., 'Heat treatment and aging effect on the structural and optical properties of plasma polymerized 2,6-diethylaniline thin films', Thin Solid Films 520(21), 6463–6470, 2012.

[91] Soman, Vijay V., Kelkar, Deepali, S., 'DC electrical study of modified PMMA, PVC and their blend', Macromolecular Symposia; 290(1), 30-36, 2010.

[92] Namouchi, F., Smaoui, H., Fourati, N., Zerrouki, C., Guermazi H., Bonnet J. J., 'Investigation on electrical properties of thermally aged PMMA by combined use of FTIR and impedance spectroscopies', J. Alloys Comp., 469, 197–202, 2009.

[93] Park, Ji Hoon, Hwang, D. K., Lee, Jiyoul, Im Seongil, Kim Eugene, 'Studies on poly(methyl

methacrylate) dielectric layer for field effect transistor: Influence of polymer tacticity'. Thin Solid Films, 515, 4041–4044, 2007.

[94] Ao, Wei, Lim, Jae-Sung and Shin, Paik-Kyun, 'Preparation and Characterization of Plasma Polymerized Methyl Methacrylate Thin Films as Gate Dielectric for Organic Thin Film Transistor', J. Elec. Engg. Technol., 6(6), 836~841, 2011.

[95] Kim Jung-Min, Lee Dong-Hoon, Yoon Tae-Sik, Lee Hyun Ho, Lee Jong-Wook, and Kima Yong-Sang, 'Electrical Charging/Discharging Properties of Organic Memory Device Using CdSe Nanoparticles/PMMA Blend as the Tunneling Layer', Electrochem. Solid-State Lett., 14 (6) 238-240, 2011.

[96] Deshmukh, S. H., Burghate, D. K., Akhare, V. P., Deogaonkar, V. S., Deshmukh, P. T. and Deshmukh, M. S., 'Electrical conductivity of polyaniline doped PVC–PMMA polymer blends', Bull. Mater. Sci., 30(1), 51–56, 2007.

[97] 'Amended Final Report on the safety assessment of Ethyl Methacrylate', Int. J. Toxicology, 21, 63-79, 2002.

[98] Technical Data Sheet 213, © Polysciences, Inc. www.polysciences.com.

[99] TI/CP 0007 e March 2012 BASF Group www.specialty-monomers.basf.com.

[100] Jeon, H. S., Wyatt, J., Harper- Nixon, D., Weinkauf, D.H., 'Characterization of Thin Polymer-Like Films Formed by Plasma Polymerization of Methylmethacrylate: A Neutron Reflectivity Study', J Polym. Sci. Part B: Polym. Phys., 42, 2522–2530, 2004.

[101] Thomas, Casserly B. and Karen, Gleason, K., 'Effect of Substrate Temperature on thePlasma Polymerization of Poly(methyl methacrylate)', Chem. Vap. Depos. 12, 59–66, 2006.

2.1 Introduction

Polymers affect every day of our life. These materials have so many varied characteristics and applications that their usefulness can only be measured by our imagination. Polymers are the materials of past, present and future generations. Polymeric materials have a vast potential for exciting new applications in the imminent future. Polymer uses are being developed in such diverse areas such as: conduction and storage of electricity, molecular based information storage and processing, molecular composites, unique separation membranes, new forms of food processing and packaging, health, housing, and transportation. Plasma polymerization is a novel and inexpensive technique for the fabrication of quality polymer coatings and thin films [1-4]. Organic monomer vapors can be polymerized at low temperatures using plasma treatment. This is a versatile technique to produce polymer thin films of organic compounds that do not polymerize under normal chemical polymerization techniques. Starting in the 1960s, scientists have successfully explored the plasma techniques in material science, including plasma polymerization [5-6]. Inspired to the use of plasma polymer as a dielectric film during the early development of microelectronic field at that time, the systematic investigations of plasma polymerization were followed by the rapid advancement of polymer science. Nowadays, the advantages of plasma polymerization have been fully recognized not only in the field of microelectronics but also covering many potential applications in optical field, polymer science, sensors, membrane and surface modification of biomedical materials [7]. Therefore, it is of interest to develop polymer thin films of high quality for a variety of industrial applications. As a consequence, the study of the structural, electronic, electrical, optical, etc. properties of organic polymer thin films received special attention of solid state and material scientists.

2.2 Fundamental Aspects of Polymers

2.2.1 Polymer

The term ‘polymer’ is derived from the Greek words: *polys* meaning *many*, and *meros* meaning *parts*. A polymer is a substance composed of molecules with large molecular mass composed of repeating structural units, or monomers, connected by covalent chemical bonds. Many polymers are made by repeating the same small molecule over and over again (Fig.2.1).

In some cases the repetition is linear to form linear chain in others the chains are branched or inter connected to form three-dimensional networks. The repeat unit is usually equivalent to the monomer, or starting material from which it is formed. A single mer is called a monomer, and the term polymer means many mer units.

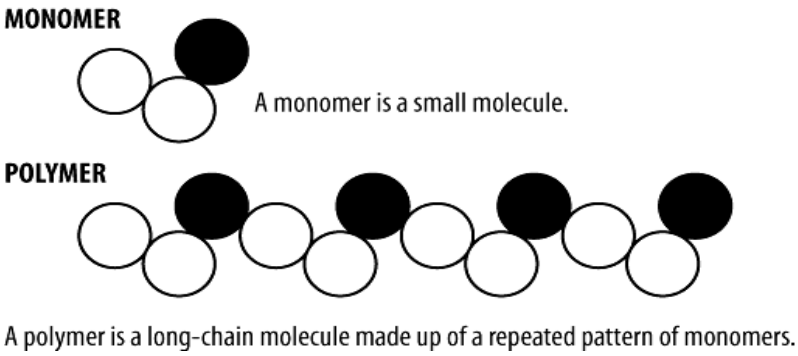

Fig. 2.1 Structure of monomer and polymer.

Polymers are categorized as organic compounds since it contain carbon. The most common element found in polymers, besides carbon, is hydrogen. All polymers must then be manufactured through polymerization reactions.

2.2.2 Characteristics of Polymers:

The important characteristics of polymer are given below:

(i) Low density and coefficient of friction,

(iii) Good corrosion resistance and mouldability,

(v) Excellent surface finish can be obtained and produced with close dimensional tolerances,

(vi) Poor tensile strength and temperature resistance, low mechanical properties,

(vii) Can be produced transparent or in different colors,

(viii) Very resistant to chemicals,

(ix) Can be both thermal and electrical insulators,

(x) Very light in weight with significant degrees of strength,

(xi) Can be processed in various ways and is economical.

2.2.3 Classification of polymers

Depending on the different functional groups and structures in the field of macromolecules, polymers are classified in various ways as shown in Fig.2.2.

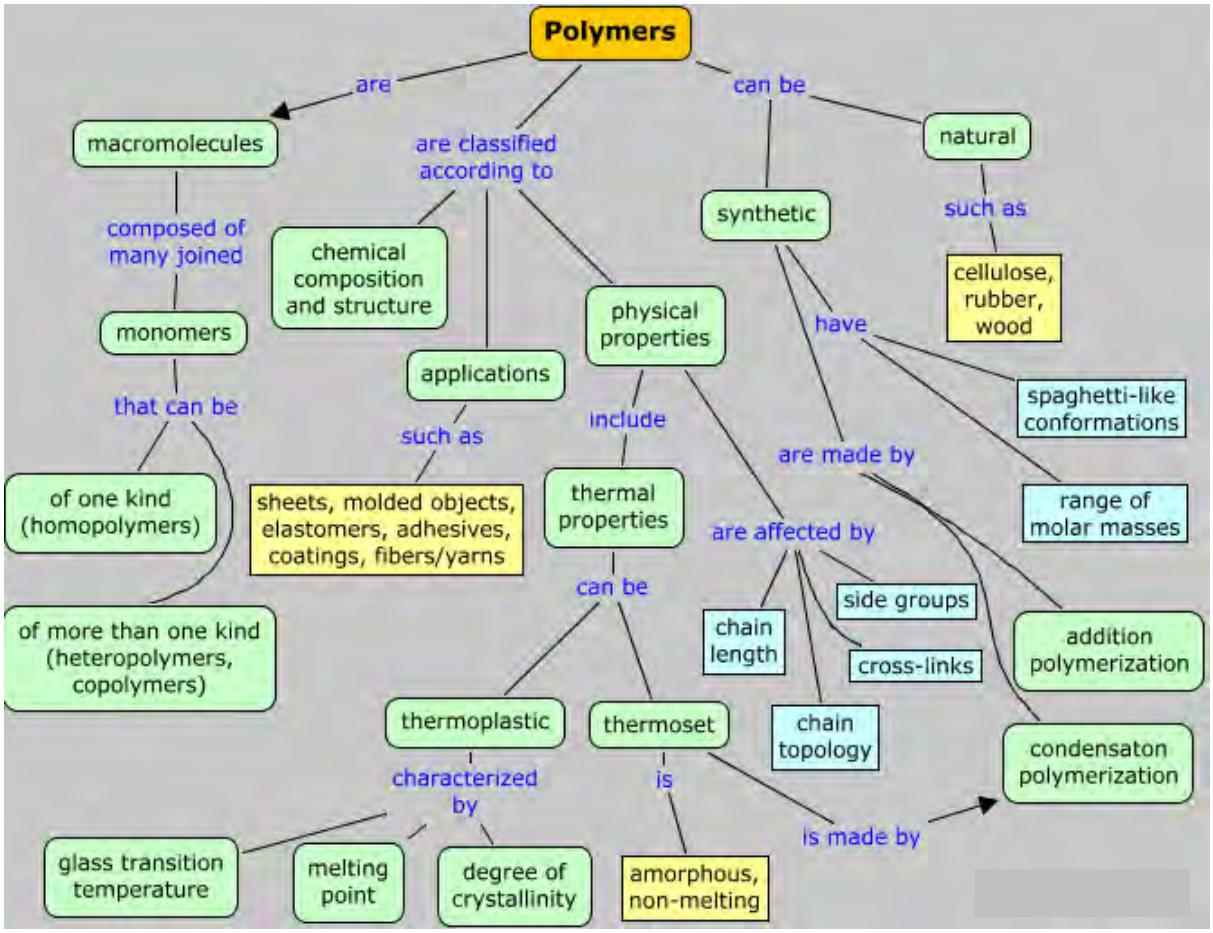

Fig. 2.2 Classification of polymers

Polymers can be classified according to different molecular structures such as:

(i) Linear and Branched polymers

By using different starting materials and processing techniques, polymers can be of different molecular structures. As illustrated in Fig. 2.3 these structures can be classified into four different categories: (a) linear, (b) branched, (c) crosslinked, and (d) network. In linear polymers, the mers are joined together end to end in single chains (Fig. 2.3a). Polymers may also have a molecular structure in which side-branch chains are connected to the main ones, as

shown schematically in Fig. 2.3(b). These polymers are called branched polymers. The branches result from side reactions that occur during the synthesis of the polymer.

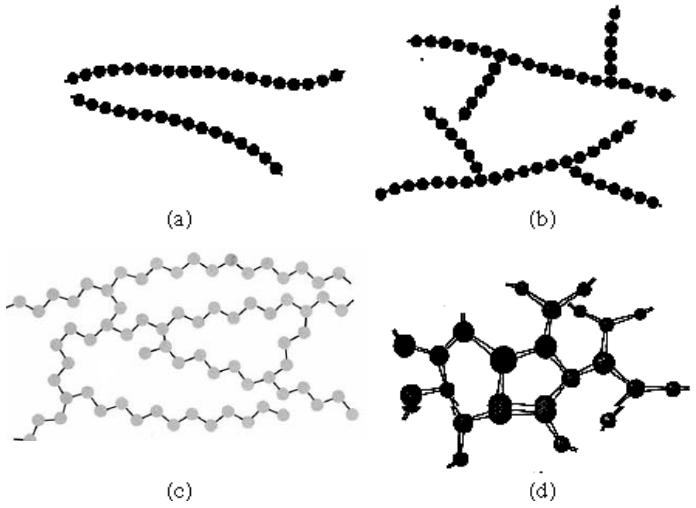

Fig. 2.3. Schematic illustrations of (a) linear, (b) branched, (c) crosslinked, and (d) network (three-dimensional) molecular structures. The circle designate individual mer units.

(ii) Crosslinked polymers

In crosslinked polymers, adjacent linear chains are joined to one and another at various positions along their lengths as depicted in Fig. 2.3(c). Generally, crosslinking is accomplished by additive atoms or molecules that are covalently bonded to the chains. The formation of covalent bonds which holds portions of several polymer chains together is called cross-linking. Extensive cross-linking results in a random three-dimensional network of interconnected chains. As one might expect, extensive cross-linking produces a substance which has more rigidity, hardness, and a higher melting point than the equivalent polymer without cross-linking. Almost all the hard and rigid plastics we use are cross-linked. These include Bakelite, which is used in many electric plugs and sockets, melamine, which is used in plastic crockery, and epoxy resin glues.

Depending upon the type of the constituent, polymers can also be classified as:

Homopolymer and copolymer

A homopolymer (Fig. 2.4a) is a polymer which is formed from only one type of monomer. This is in contrast to a heteropolymer or copolymer where the polymer contains at

least two monomers. Since a copolymer consists of at least two types of constituent units (also structural units), copolymers can be classified based on how these units are arranged along the chain as shown in Fig. 2.4.

Fig. 2.4 Types of copolymers (a) Homopolymers, (b) Alternating copolymer, (c) Statistical copolymers, (d) Block copolymers and (e) Graft copolymers.

2.2.4 Polarity of Molecules

A molecule is polar if the centre of negative charge does not coincide with the centre of positive charge. Such a molecule constitutes a dipole, two equal and opposite charges separated in space. If the molecule possesses a dipole moment μ, which is equal in magnitude to the product of charge with the charge separation d (the distance d is between the centre of the charges), then $\mu = ed$. The charge separation mentioned above occurs due to the polarity of bonds. We know, two atoms joined by a covalent bond share electrons; their nuclei are held by the same electron cloud. But in most cases the two nuclei do not share electrons equally; the electron cloud denser about one atom than other. One end of the bond is thus relatively negative and other end is relatively positive; i.e. there are a -ve pole and +ve pole. Such a bond is said to be a polar bond or to possess polarity. On the presence of permanent dipole moments, polymer material can be divided into:

(i) Polar Polymers: A polar polymer is rigidly fixed in a single conformation together with its polar groups; Permanent dipoles are preset in polar polymer. The examples of polar polymers are polymides, polytetrafluoro-ethylene, polyvinylchloride etc.

(ii) Non- polar Polymers: A non-polar polymer is flexible and has pendant side groups which can rotate freely. Permanent dipole moments arc not present in non -polar polymers and for this reason the dielectric constant of these polymers is low.

2.2.5 Polymerization

Two or more monomers either organic or inorganic when subjected to certain condition that gives rise to a polymer i.e. the process by which the polymer is formed is known as polymerization process or reaction. Classically, polymerization reaction which yield linear, high molecular weight products have been divided into two main groups on the basis of a comparison of the structure of the repeating unit of the polymer formed with the structure of the monomer from which the polymer is derived. Polymerization is a process of reacting monomer molecules together in a chemical reaction to form three-dimensional networks or polymer chains.

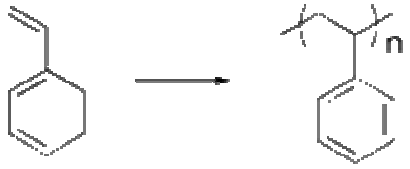

Fig.2.5 Polymerization

There are many forms of polymerization and different systems exist to categorize them. An example of alkene polymerization (Fig. 2.5), in which each Styrene monomer unit's double bond reforms as a single bond with another styrene monomer and forms polystyrene. In chemical compounds, polymerization occurs via a variety of reaction mechanisms which vary in complexity due to functional groups present in reacting compounds. Functional groups or atoms are: reactive hydrogen (-H), hydroxyl group (-OH), carboxyl group (-COOH), amino group ($-NH_2$), halogen atoms (-Cl, -Br) and C=C double bond, etc.

The process of polymerization may be divided into two ways (i) Chemical process and (ii) Physical process.

2.2.5.1 Chemical Processes or Conventional Polymerization Processes

A variety of methods are employed for producing polymer films and the three most important groups are step growth, addition, and free radical polymerization [8].

(i) Step-growth Polymerization

Step-growth polymerization is a polymerization process that involves a chemical reaction between multifunctional monomer molecules. In a step-growth reaction, the growing chains may react with each other to form even longer chains. This applies to chains of all lengths. Thus, a monomer or dimer may react in just the same way as a chain hundreds of monomer units long. This is in contrast to a chain-growth polymerization, where only monomers may react with growing chains (In chain-growth polymerization, two growing chains can't join together the way they can in a step-growth polymerization).

(ii) Addition Polymerisation

Chain-growth polymerization or addition polymerization involves the linking together of molecules incorporating double or triple chemical bonds. These unsaturated monomers (the identical molecules which make up the polymers) have extra internal bonds which are able to break and link up with other monomers to form the repeating chain.

*n*M (monomer) --> -(-M-)$_n$- (polymer)

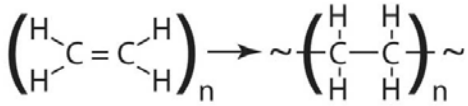

Fig. 2.6 Addition polymerization

Addition polymerization (Fig.2.6) is involved in the manufacture of polymers such as polyethylene, polypropylene and polyvinyl chloride (PVC).

(iii) Free Radical Polymerization

A free radical is an atomic or molecular species whose normal bonding system has been modified such that an unpaired electron remains associated with the new structure. The radical is capable of reacting with an olefinic monomer to generate a chain carrier which can retain its activity long enough to propagate a macro molecular chain under the appropriate conditions. Radical polymerization (Fig. 2.7) is a type of polymerization in which the reactive center of a polymer chain consists of a radical. The polymerization reaction is initiated by three classes of free-radical initiators:

(i) Certain compounds that can be broken down in two radicals at temperatures just above room temperature. Such compounds include organic peroxides such as Benzoyl peroxide and certain azo compounds such as Azobisisobutyronitrile.

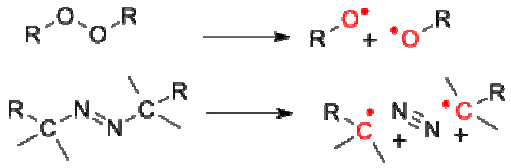

Fig. 2.7 Decomposition of a peroxide (top) and of a azo compound (bottom).

(ii) Photosensitive molecules, which under the influence of light, get into an excited state or react with other molecules, forming radicals.

(iii) A redox--system with transfer of one electron during the reaction. This often involves a metal-ion such as in the reaction of a ferrous ion with hydrogen peroxide to a ferric ion in which a hydroxyl radical is formed.

Except these methods, thin polymer films can be prepared in the two ways: one includes wet process like Langmuir-Blodgett (LB), spreading, dipping or solvent casting methods and the other is dry processing, such as physical vapor deposition (PVD) and chemical vapor deposition (CVD).

2.2.5.2 Physical Processes

The important processes of film formation are that (i) Evaporation and (ii) Plasma polymerization.

(i) Theory of Evaporation

The thermal evaporation method is simple and can produce good quality film and hence this method becomes a good technique for thin film fabrication. The Vacuum evaporation [9] is a kind of technique for the preparation of thin films, which includes sublimation and a condensation process. As the name implies vacuum evaporation technique consists of vaporization of the solid material by heating it to sufficiently high temperature and condensing it onto a cooler substrate to form a film. The deposition of thin films by vacuum evaporation consists of several distinguishable steps:

i) Transition of a condensed phase, which may be solid or liquid into the gaseous state.

ii) Vapor traversing the space between the evaporation source and the substrate at reduced gas pressure.

iii) Condensation of the vapor upon arrival on the substrates.

The liquid vapor transformation is called evaporation and solid to vapor transformation is called sublimation. Thus by evaporation method films of high quality are produced with a

minimum of interfering conditions. In practice they are applicable to all substances and to a. great range of thicknesses.

(ii) Plasma Polymerization

As this technique is used in the preparation of the organic thin films to be investigated in the present study, a little detail about plasma and plasma polymerization is documented in the following sections.

2.3 Plasma and Plasma Polymerization

2.3.1 Plasma

Sir William Crookes, an English physicist, identified a fourth state of matter, now called plasma, in 1879. Plasma temperatures and densities range from relatively cool and tenuous (like aurora) to very hot and dense (like the central core of a star). Ordinary solids, liquids, and gases are both electrically neutral and too cool or dense to be in a plasma state. The word ‘plasma’ was first applied to ionized gas by Dr. Irving Langmuir, an American chemist and physicist, in 1929. Fig. 2.8 illustrates schematic ranges of plasma systems occur in terms of densities and temperatures. Plasma research is yielding a greater understanding of the universe. Besides the astroplasmas there are two main groups of laboratory plasmas, i.e. the high-temperature or fusion plasma and the so-called low temperature plasma or gas discharge. Generally subdivision can be made between plasmas, which are in thermal equilibrium, and those, which are not in thermal equilibrium [10-11].

Thermal equilibrium implies that the temperature of all species (electrons, ions, neutral species) is the same. Often the term 'Local thermal equilibrium (LTE) is used, which implies that the temperatures of all plasma species are the same in localized areas in the plasma. On the other hand, interstellar plasma matter is typically not in thermal equilibrium also called ‘non-LTE’. The gas discharge plasmas can also be classified into LTE and non-LTE plasmas. This subdivision is typically related to the pressure in the plasma. Indeed a high gas pressure implies many collisions in the plasma, leading to an efficient energy exchange between the plasma species and hence equal temperatures. A low gas pressure, on the other hand, results in only a few collisions in the plasma species due to inefficient energy transfer. In recent years, the field of gas discharge plasma applications has rapidly expanded [12-14].

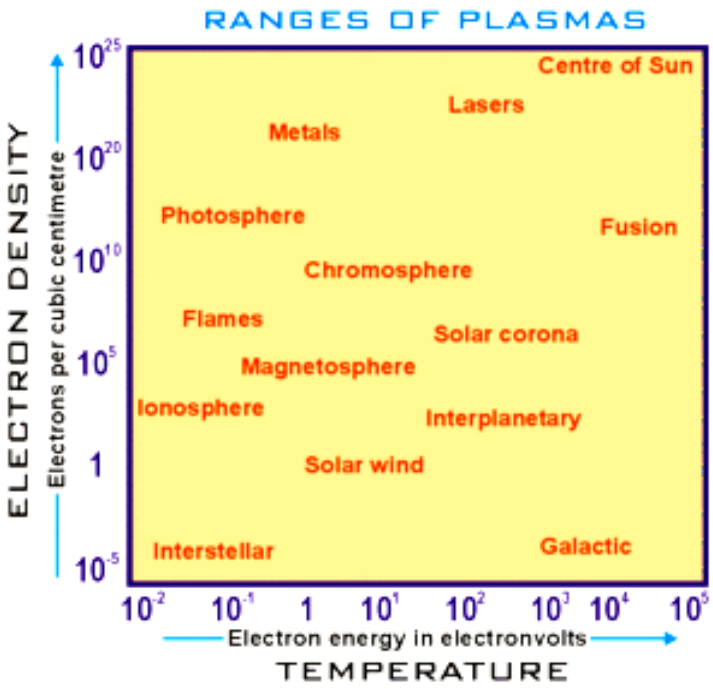

Fig. 2.8 Schematic ranges of plasma.

Plasma is a state of matter similar to gas in which a certain portion of the particles are ionized. Heating a gas may ionize (reduce the number of electrons in) its molecules or atoms, thus turning it into plasma, which contains charged particles: positive ions and negative electrons and shown in Fig. 2.9. Ionization can be induced by other means, such as strong electromagnetic field applied with a laser or microwave generator, and is accompanied by the dissociation of molecular bonds, if present. The presence of a non-negligible number of charge carriers makes the plasma electrically conductive so that it responds strongly to electromagnetic fields. Plasma, therefore, has properties quite unlike those of solids, liquids, or gases and is considered a distinct state of matter. Like gas, plasma does not have a definite shape or a definite volume unless enclosed in a container; unlike gas, under the influence of a magnetic field, it may form structures such as filaments, beams and double layers.

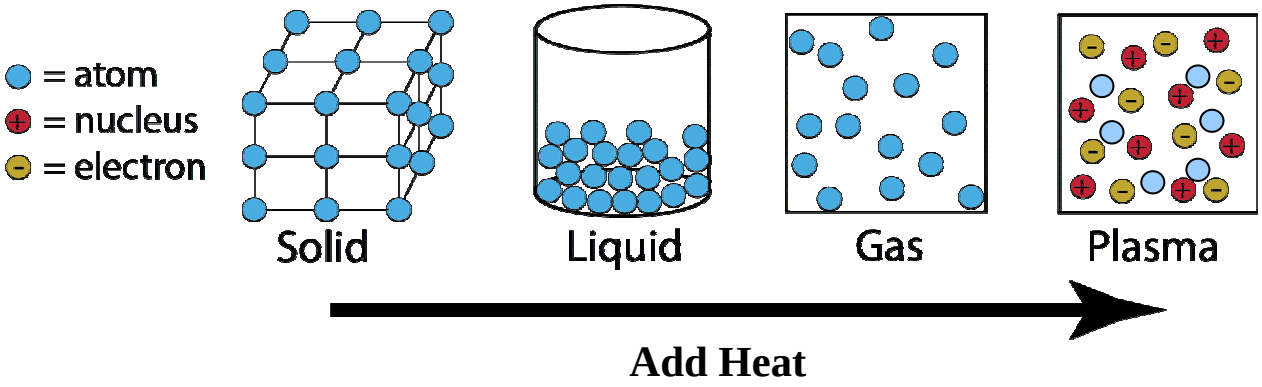

Fig. 2.9 Different states of matter

An ionized gas consists mainly of positively charged molecules or atoms and negatively charged electrons. Energy is needed to strip electrons from atoms to make plasma. The energy can be of various origins: thermal, electrical, or light (ultraviolet light or intense visible light from a laser). A gaseous complex that may be composed of electrons, ions of polarity, gas atoms and molecules in the ground or any higher state of any form of excitation as well as of light quanta is referred to as plasma. The ionization degree can vary from 100% (fully ionized gases) to very low values (partially ionized gases). With insufficient sustaining power, plasmas recombine into neutral gas. Although plasma is loosely described as an electrically neutral medium of positive and negative particles, a definition can have three criteria:

(i) The plasma approximation: Charged particles must be close enough together that each particle influences many nearby charged particles, rather than just interacting with the closest particle (these collective effects are a distinguishing feature of plasma). The plasma approximation is valid when the number of charge carriers within the sphere of influence (called the Debye sphere whose radius is the Debye screening length) of a particular particle are higher than unity to provide collective behavior of the charged particles.

(ii) Bulk interactions: The Debye screening length (defined above) is short compared to the physical size of the plasma. This criterion means that interactions in the bulk of the plasma are more important than those at its edges, where boundary effects may take place.

(iii) **Plasma frequency**: The electron plasma frequency (measuring plasma oscillations of the electrons) is large compared to the electron-neutral collision frequency (measuring frequency

of collisions between electrons and neutral particles). When this condition is valid, electrostatic interactions dominate over the processes of ordinary gas kinetics.

2.3.2 Plasma Polymerization

Plasma polymerization is defined as the formation of polymeric materials under the influence of plasma conditions. The solid materials deposited under plasma conditions are generally referred to as plasma polymers, but they are unique and distinct from traditional polymers in that they lack the repeat structure that typically defines a polymer chain. Additionally the materials tend to be highly cross linked (Fig.2.10), and not soluble in any chemical solvents. One of the advantages of plasma polymers is the fact that they tend to deposit as thin, pin hole free films in a relatively simple one step process.

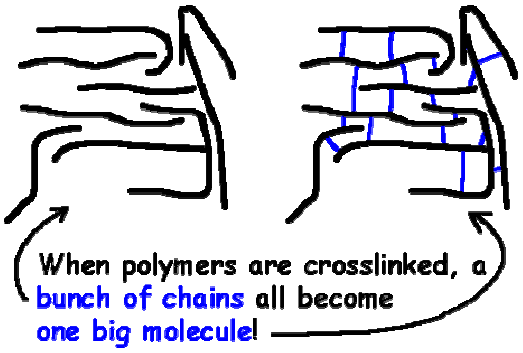

Fig. 2.10 Cross linked plasma polymer

Plasma polymerization is an attractive technique for producing polymer-like organic materials (usually in the form of thin films) with the aid of a plasma discharge. The deposition of plasma polymer films is based on the fragmentation of an organic monomer in electrical discharges and the transport of radicals to the substrate where the films grow. In the plasma polymerization process, a monomer gas is pumped into a vacuum chamber where it is polymerized by plasma to from a thin, clear coating. The monomer starts out as a liquid. It is converted to a gas in an evaporator and is pumped into the vacuum chamber. A glow discharge initiates polymerization. Glow discharge is a technique in polymerization which forms free electrons which gain energy from an electric field, and then lose energy through collisions with neutral molecules in the gas phase. This leads to many chemically reactive species, which then lead to a plasma polymerization reaction [15]. The electric discharge process for plasma polymerization is the “low-temperature plasma” method, because higher temperatures cause

degradation. The excited electrons created in the glow discharge ionize the monomer molecules.

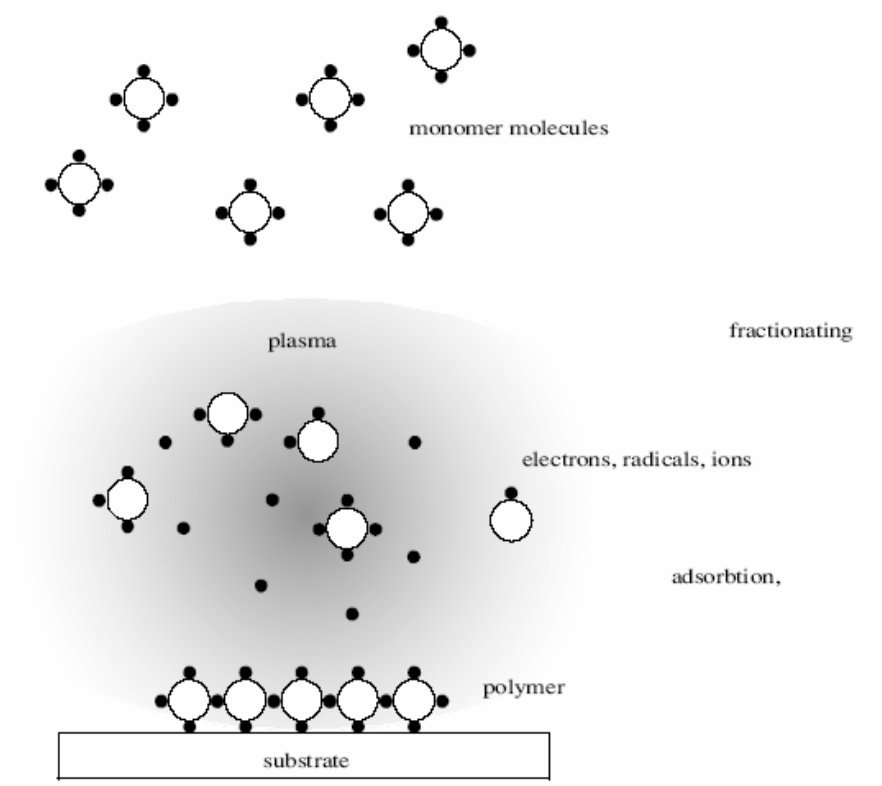

Fig. 2.11 A schematic plasma polymerization process.

The monomer molecules break apart (fractionate) create free electrons, ions, exited molecules and radicals. The radicals absorb, condense and polymerize on the substrate. The electrons and ions crosslink, or create a chemical bond, with the already deposited molecules, creating a harder, denser coating. A schematic plasma polymerization configuration is presented in the Fig. 2.11. The materials obtained by plasma polymerization are significantly different from conventional polymers and also different from most inorganic materials. Hence plasma polymerization should be considered as a method of forming new types of materials rather than a method of preparing conventional polymers. This polymerization process covers a wide interdisciplinary area of physics, chemistry, science of interfaces and materials science and so on [16-19]. Thus plasma polymerization is a versatile technique for the deposition of films with functional properties suitable for a wide range of modern applications.

To explain the reaction mechanism, many investigators discussed the effects of discharge conditions such as polymerization time monomer pressure, discharge current, and discharge power and substrate temperature on the polymerization rate. In many cases, polymers formed by plasma polymerization show distinguished chemical composition and chemical and physical properties from those formed by conventional polymerization, if the same monomer is used for both the polymerization. Comparison of the structures of plasma polymers and conventional polymers is shown in the Fig. 2.12.

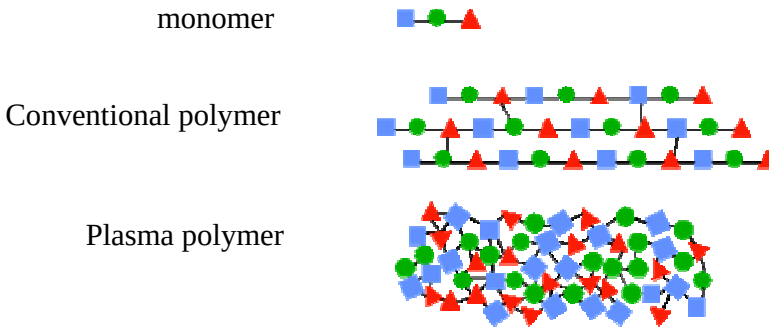

Fig. 2.12 Comparison of the structures of plasma polymers and conventional polymers.

Polymers are formed, from solid or liquid monomers, by plasma-induced polymerization through essential chemical reaction that is believed to be conventional molecular polymerization that occurs with the influence of plasma. Thus, the capability of plasma polymerization to form an ultra thin film containing a minimal amount of flaws is unique and is a valuable asset. Among the many types of electric discharge, glow discharge is by far the most frequently used in plasma polymerization. Some other models were proposed based on ion or electron bombardment.

2.4 General characteristics of plasma polymers

The properties of plasma polymers differ greatly from those of conventional polymers. While both types are dependent on the chemical properties of the monomer, the properties of plasma polymers depend more greatly on the design of the reactor and the chemical and physical characteristics of the substrate on which the plasma polymer is deposited [1]. The location within the reactor where the deposition occurs also has an effect on the resultant polymer's properties [20]. In fact by using plasma polymerization with a single monomer and

varying the reactor, substrate, etc. a variety of polymers, each having different physical and chemical properties, can be prepared. A common characteristic of plasma polymers is the adhesion ability [1]. The most significant difference between conventional polymers and plasma polymers is that plasma polymers do not contain regular repeating units. Due to the number of different propagating species present at any one time as discussed above, the resultant polymer chains are highly-branched and are randomly terminated with a high degree of cross-linking [21]. All plasma polymers contain free radicals as well. The amount of free radicals present varies between polymers and is dependent on the chemical structure of the monomer. Because the formation of the trapped free radicals is tied to the growth mechanism of the plasma polymers, the overall properties of the polymers directly correlate to the number of free radicals [20].

Plasma polymers also contain an internal stress. If a thick layer (e.g. 1 μm) of a plasma polymer is deposited on a glass slide, the plasma polymer will buckle and frequently crack. The curling is attributed to an internal stress formed in the plasma polymer during the polymer deposition. The degree of curling is dependent on the monomer as well as the conditions of the plasma polymerization. Most plasma polymers are insoluble and infusible. These properties are due to the large amount of cross-linking in the polymers, previously discussed. Consequently the kinetic path length for these polymers must be sufficiently long, so these properties can be controlled to a point. The permeabilities of plasma polymers also differ greatly from those of conventional polymers. Because of the absence of large-scale segmental mobility and the high degree of cross-linking within the polymers, the permeation of small molecules does not strictly follow the typical mechanisms of “solution-diffusion”. Really the permeability characteristics of plasma polymers fall between these two ideal cases.

2.5 Thin Film Deposition Techniques

Thin films are thin material layers ranging from fractions of a nanometre to several micrometres in thickness. The act of applying a thin film to a surface is known as thin-film deposition. Thin-film deposition is any technique for depositing a thin film of material onto a substrate or onto previously deposited layers. Different deposition techniques are described below:

i) Plasma-enhanced chemical vapor deposition (PECVD) is a process used to deposit thin films from a gas state (vapor) to a solid state on some substrate. There are some chemical reactions involved in the process which occur after creation of plasma of the reacting gases. The plasma is generally created by RF (AC) frequency or DC discharge between two electrodes. Plasma is any gas in which a significant percentage of the atoms or molecules are ionized. Processing plasmas are typically operated at pressures of a few mTorr to a few Torr. Plasmas with low fractional ionization are of great interest for materials processing because electrons are so light, compared to atoms and molecules, that energy exchange between the electrons and neutral gas is very inefficient. Therefore, the electrons can be maintained at very high equivalent temperatures – tens of thousands of K, equivalent to several eV average energy – while the neutral atoms remain at the ambient temperature. These energetic electrons can induce many processes that would otherwise be very improbable at low temperatures, such as dissociation of precursor molecules and the creation of large quantities of free radicals. A second benefit of deposition within a discharge arises from the fact that electrons are more mobile than ions. As a consequence, the plasma is normally more positive than any object it is in contact with, as otherwise a large flux of electrons would flow from the plasma to the object. The voltage between the plasma and the objects it contacts is normally dropped across a thin sheath region. Ionized atoms or molecules that diffuse to the edge of the sheath region feel an electrostatic force and are accelerated towards the neighboring surface. Thus, all surfaces exposed to the plasma receive energetic ion bombardment. The potential across the sheath surrounding an electrically-isolated object (the floating potential) is typically only 10–20 V, but much higher sheath potentials are achievable by adjustments in reactor geometry and configuration. Thus, films can be exposed to energetic ion bombardment during deposition. This bombardment can lead to increases in density of the film, and help remove contaminants, improving the film's electrical and mechanical properties.

ii) Chemical vapor deposition (CVD) is a chemical process used to produce high-purity, high-performance solid materials. The process is often used in the semiconductor industry to produce thin films. In a typical CVD process, the wafer (substrate) is exposed to one or more volatile precursors, which react and/or decompose on the substrate surface to produce the desired deposit. Frequently, volatile by-products are also produced, which are removed by gas flow through the reaction chamber. These processes differ in the means by which chemical

reactions are initiated (e.g., activation process) and process conditions. Microfabrication processes widely use CVD to deposit materials in various forms, including: monocrystalline, polycrystalline, amorphous and epitaxial. These materials include: silicon, carbon fiber, carbon nanofibers, filaments, carbon nanotubes, SiO_2, silicon-germanium, tungsten, silicon carbide, silicon nitride, silicon oxynitride, titanium nitride, and various high-k dielectrics. The CVD process is also used to produce synthetic diamonds.

iii) Physical vapor deposition (PVD) is a variety of vacuum deposition and is a general term used to describe any of a variety of methods to deposit thin films by the condensation of a vaporized form of the material onto various surfaces (e.g., onto semiconductor wafers). The coating method involves purely physical processes such as high temperature vacuum evaporation or plasma sputter bombardment rather than involving a chemical reaction at the surface to be coated.

iv) Ion plating is a physical vapor deposition (PVD) process that is sometimes called ion assisted deposition (IAD) or ion vapor deposition (IVD) and is a version of vacuum deposition. Ion plating utilizes concurrent or periodic bombardment of the substrate and depositing film by atomic-sized energetic particles. Bombardment prior to deposition is used to sputter clean the substrate surface. During deposition the bombardment is used to modify and control the properties of the depositing film. Ion plating can be done in a plasma environment where ions for bombardment are extracted from the plasma or it may be done in a vacuum environment where ions for bombardment are formed in a separate ion gun. Ion plating is used to deposit hard coatings of compound materials on tools, adherent metal coatings, optical coatings with high densities, and conformal coatings on complex surfaces.

v) Atomic layer deposition (ALD) is a thin film deposition technique that is based on the sequential use of a gas phase chemical process. The majority of ALD reactions use two chemicals, typically called precursors. These precursors react with a surface one-at-a-time in a sequential manner. By exposing the precursors to the growth surface repeatedly, a thin film is deposited.

2.6 Different Types of Glow Discharge Reactors

Glow discharge reactor is the important part of plasma polymerization system. Because reactor geometry influences the extent of charge particle bombardment on the growing films which affects the potential distribution in the system, Different kinds of reactors (Fig. 2.13) including capacitatively coupled and inductively coupled rf reactors, microwave, dual-mode (MW/RF), etc, can be used for plasma polymerization processes [11-22]. The presence of insulating layers on the electrodes deflects plasma current into any surrounding conducting areas and thus leads to gross plasma non-uniformity or plasma extinction. Therefore, when insulating materials are involved, AC power is usually employed so that power may pass through the insulator by capacitative coupling. The most widely used reactor configurations for plasma polymerization can be broadly divided in to three classes.

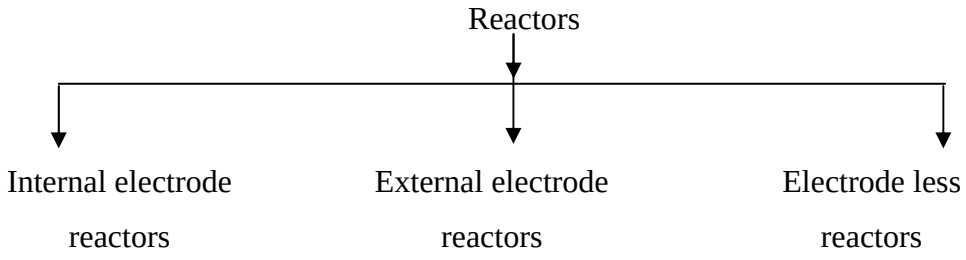

Reactors with internal electrodes have different names, e.g. flat bed parallel plates, planar, diode etc. Their main features are power supply, coupling system, vacuum chamber, rf driver electrode, grounded electrode, and eventually one or most substrate holders. .

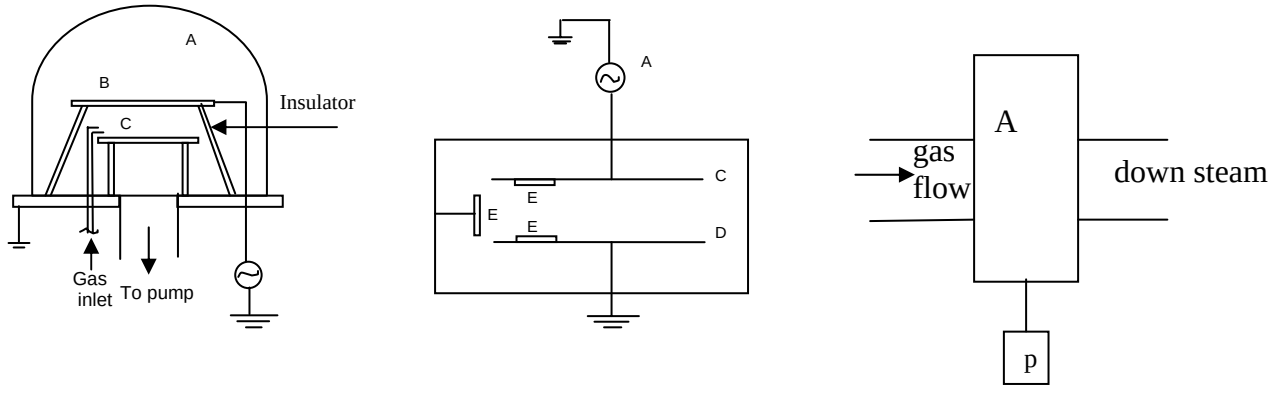

Fig. 2.13 Different types of reactor configuration used for plasma polymerization. Schematic of a (a) bell jar reactor, (b) parallel plate internal electrode reactor, (c) electrode less microwave reactor.

Among the internal electrode arrangements a bell-jar-type reactor with parallel plate metal electrodes is most frequently used by using AC (1-50 kHz) and rf fields for plasma excitation. The vacuum chambers can be made either of glass or of conductive materials, such as metal. In the case of bell-jar reactors, no particular care is taken for the grounded electrode apart from its area. On the contrary, the design and arrangement of the cathode require special attention: a metallic shield surrounding the electrode highly improves the glow confinement inside interelectrodic space; electrode material and area greatly affect the extend of sputtering on the target. In the current research, capacitively coupled reactor (glow discharge plasma) system was used for the formation of thin films.

2.6.1 An Overview of Gas Discharge Plasma

Plasma polymerization take place in a low pressure (or low temperature) plasma that is provided by a glow discharge operated in an organic gas or vapor (monomer) at low pressure between two electrodes. When a sufficient high potential difference is applied between two electrodes placed in a gas, the later will break down into positive ions and electrons, giving rise to a gas discharge. The mechanism [1] of the gas breakdown is shown in Fig. 2.14 and can be explained as follows: a few electrons are emitted from the electrodes due to the omnipresent cosmic radiation.

However, when a potential difference is applied the electrons are accelerated by the electric field in front of the cathode and collide with the gas atoms. The most important collisions are the inelastic collisions leading to excitation and ionization. The excitation collisions create new electrons and ions. The ions are accelerated by the electric field toward the cathode, where they release new electrons by ion-induced secondary electron emission. The electrons give rise to new ionization collisions, creating new ions and electrons. These processes of electron emission at the cathode and ionization in the plasma make the glow discharge self-sustaining plasma.

Another important process in the glow discharge is the phenomenon of sputtering, which occurs at sufficiently high voltage. When the ions and fast atoms from the plasma bombard the cathode, they not only release secondary electrons, but also atoms of the cathode materials, which is called sputtering. This is the basis of the use of glow discharges for analytical spectrochemistry. The ions can be detected with a mass spectrometer and the excited

atoms or ions emit characteristic photons, which can be measured with optical emission spectrometry. Alternatively, the sputtered atoms can also diffuse through the plasma and they can be deposited on a substrate, this technique used in materials technology e.g. for the deposition of thin films.

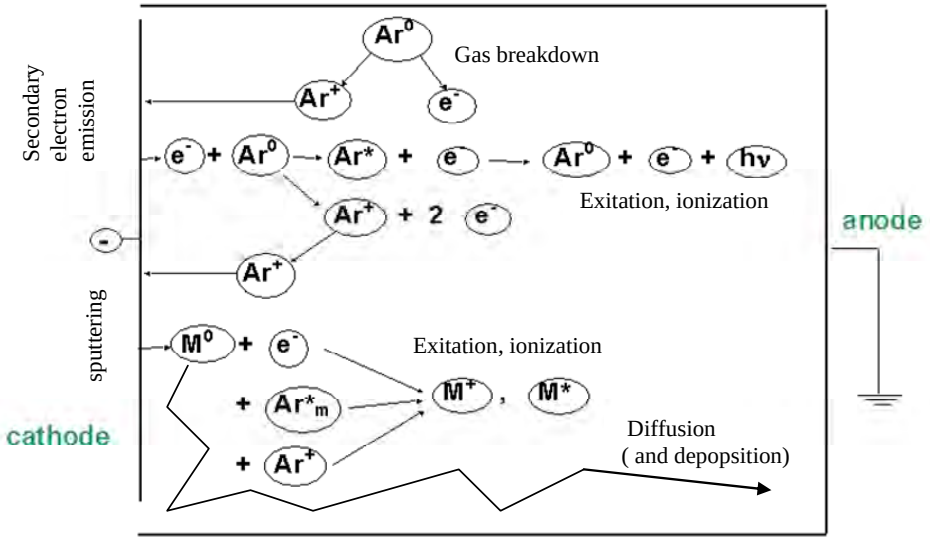

Fig. 2.14 Schematic overview of the basic processes in a glow discharge.

Two types of polymerization processes may occur during plasma processes: plasma induced polymerization and plasma-state polymerization. Plasma induced polymerizations occur only with unsaturated monomers and are essentially step-growth polymerizations initiated by the reactive species contained in the plasma. Plasma-state polymerizations are atomic processes that can only occur in plasma and produced non-polymer-forming byproducts. When a monomer gas enters the plasma region, it instantly becomes a complex mixture of the original monomer, forming ionized and excited species and fragments, as well as gaseous products that do not participate in the polymerization. When a polymerizable and chemically reactive material is introduced to plasma, particles can be deposited, ablated and redeposited if they collide with a solid surface before they are evacuated. The plasma is constantly in contact with the reactor walls, the solid substrate and the substrate mount and polymer-forming intermediates and gas by-products originate from these solids, as well. Within a given monomer-reactor system, the total reactor pressure at constant temperature is a function of only the feed rate and the pumping rate. However, once plasma is initiated, the situation changes dramatically; the pressure becomes a function of the reactions occurring within the plasma.

Extending the definition of ablation to include ablation of the solid phase and fragmentation of the gas-phase species, ablation processes contribute to pressure decrease.

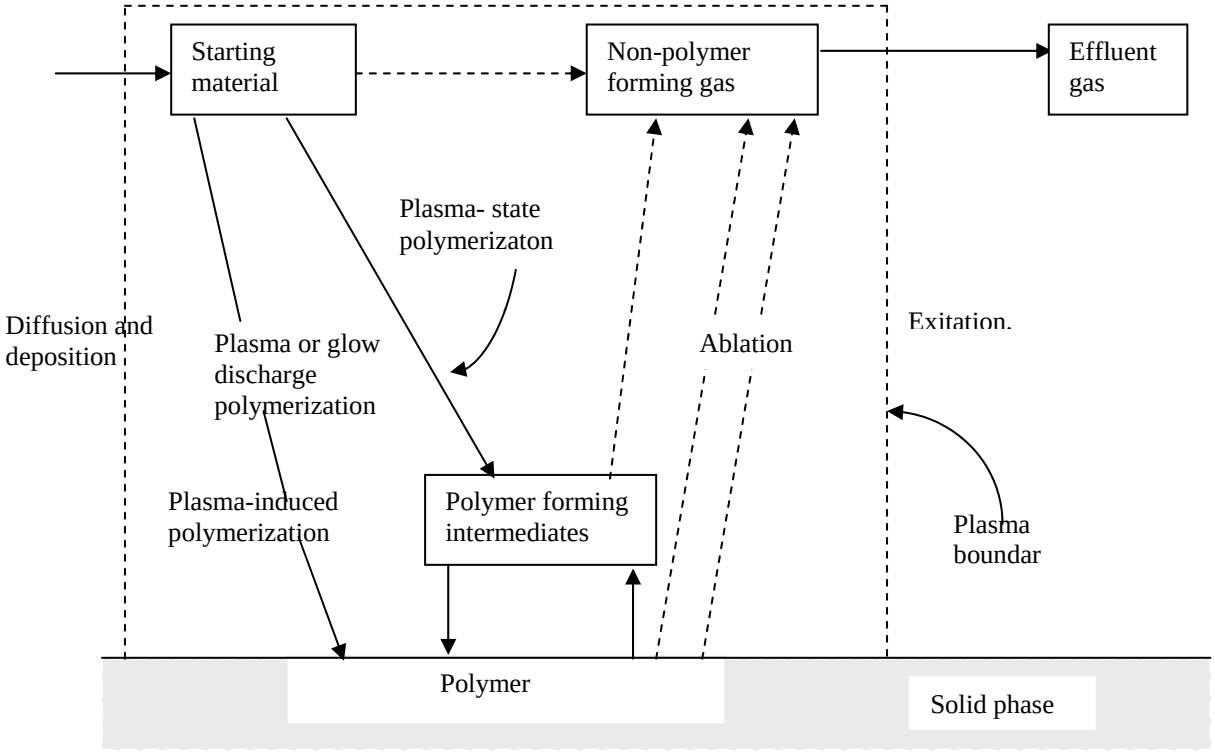

Fig. 2.15 Competetive ablation and polymerization, scheme of glow discharge polymerization.

In other words, if polymerization processes dominate, a pressure drop is expected when the plasma is ignited; if ablation processes dominate, a pressure increase is expected. This type of behavior is an example of the Competitive Ablation and Polymerization (CAP) model of plasma polymerization developed by Yasuda and Hsu [23] and depicted in Fig. 2.15.

2.6.2 Direct Current Glow Discharge

Plasma polymerization process takes place usually in a low temperature generated by glow discharge. The space between the electrodes becomes visible when a glow discharge is established; the actual distribution of light in the glow discharge is significant and is dependent on the current-voltage characteristics of the discharge [1]. When a constant potential difference is applied between the cathode and anode, a continuous current will flow through the discharge; giving rise to a direct current (DC) glow discharge. In a dc glow discharge the electrodes play an essential role for sustaining the plasma by secondary electron emission. The potential

difference applied between the two electrodes is generally not equally distributed between cathode and anode, but it drops almost completely in the first millimeters in front of the cathode. However, for most of the other applications of dc glow discharges (sputtering, deposition, chemical etching, analytical chemistry etc.), the distance between cathode and anode is generally short. So normally a short anode zone is present beside cathode dark space and negative glow, where the slightly positive plasma potential returns back to zero at the anode.

A DC glow voltage can operate over a wide range of discharge conditions. The pressure can vary from below 1 Pa to atmospheric pressure. The product of pressure and distance between the electrodes is a better parameter to characterize the discharge. For instance, at lower pressure, the distance between cathode and anode should be longer to create a discharge with properties comparable to these of high pressure with small distance. The discharge can operate in a rare gas (most often argon or helium) or in a reactive gas (N_2, O_2, H_2, CH_4, SiH_4, SiF_4, etc.), as well as in a mixture of these gases.

2.6.3 Alternating Current Glow Discharge

The mechanism of glow discharge generation will basically depend on the frequency of the alternation. At low frequencies (60 Hz), the effect is simply to form dc glow discharges of alternating polarity. However the frequency is higher than 6 GHz the motion of ions can no longer follow the periodic changes in field polarity. But above 500 kHz the electrode never maintains its polarity long enough to sweep all electrons or ions, originating at the opposite electrode, out of the inter-electrode volume. In this ease the regeneration of electrons and ions that are lost to the walls and the electrodes takes place within the body of the plasma. The mechanism by which electrons pick up sufficient energy to cause bond dissociation or ionization involves random collisions of electrons with gas molecules, the electron picking up an increment of energy with each collision. A free electron in a vacuum under the action of an alternating electric field oscillates with its velocity 90° out of phase with the field, which obtains no energy, on the average, from the applied field. The electron can gain energy from the field only as a consequence of elastic collisions with the gas atoms, as the electric field converts the electron's resulting random motion back to ordered oscillatory motion. Because of its interaction with the oscillating electric field, the electron gains energy on each collision until

it acquires enough energy to be able to make an inelastic collision with a gas atom, In that case the process of these inelastic collisions is termed volume ionization.

Thus the transfer of energy from the electric field to electrons at high frequencies is generally accepted as that operative in microwave discharges. It has also been put forward as that applicable to the widely used rf of 13.56 MHz.

2.6.4 Capacitively Coupled (cc) Radio-Frequency (rf) Discharge

If an AC voltage (up to kHz) is used, the discharge is still basically of a DC type and each electrode really acts as a cathode and anode alternatively. The frequencies generally used for the alternating voltages are typically in the radio frequency (rf) range.

Capacitively coupled (cc) discharge can also be generated by alternating voltages in another frequency range. Therefore, the term 'alternating current' (AC) discharges as opposed to dc discharges might be more appropriate. The term 'capacitively coupled' refers to the way of coupling the input power into the discharges i.e. by means of two electrodes and their sheaths forming a kind of capacitor. The cc rf discharges which also results from the differences in mass between electrons and ions, is the phenomenon of self bias. The self-bias or dc-bias is formed i) when both electrodes differ in size and ii) when a coupling capacitor is present between the rf power supply and the electrode or when the electrode is non conductive (because it then acts as a capacitor). When a certain voltage is applied over the capacitor formed by the electrodes, the voltage over the plasma will initially have the same value as the applied voltage. When the applied voltage is initially positive the electrons will be accelerated toward the electrode. Hence the capacitor will be rapidly charged up by the electron current and the voltage over the plasma will drop. When the applied potential changes polarity after one half-cycle, the voltage over the plasma changes with the same amount. The capacitor will now be charged up by the ion current and the voltage over the plasma will, therefore drop as well, but this second drop is less pronounced, because of the much lower mobility of the ions and hence the lower ion flux. At the next half-cycle, the applied potential and hence also the voltage over the plasma, again changes polarity. The voltage over the plasma drops again more rapidly because the capacitor is again charged up by the electron. flux. This process repeats itself, until the capacitor is finally sufficiently negatively charged so that the ion and electron fluxes

integrated over one rf-cycle are equal to each other. This results in a time-averaged negative dc bias at the rf-powered electrode.

Because of the negative DC bias, the ions continue to be accelerated toward the rf-powered electrode, and they can, therefore cause sputtering of the rf-electrode material. In fact, the cc rf discharge often resembles a DC glow discharge with a similar subdivision in different regions, similar operating conditions, and with similar processes occurring in the plasma.

2.7 Possible Growth Mechanism of Plasma Polymerization

The mechanism of reaction by which plasma polymerization occurs is quite complex and cannot be specifically described for the general case. Operational parameters such as monomer flow rate, pressure, frequency, and power affect the deposition rate and structure of the plasma film. The electrons or atoms generated by partial ionization of the molecules are the principle sources for transferring energy from the electric field to the gas in all glow discharges [24, 25]. In plasma polymerization, free electrons gain energy from an imposed electrical field and then transfer the energy to neutral gas molecules, which lead to the formation of many chemically reactive species. By applying greater power to the rf source, the energy per unit mass of the monomer is increased and may bring about changes in the fragmentation process. As a result, free radicals may become entrapped in the plasma-polymerized film and increase in concentration with increasing rf power. The deposition of polymer films in low-pressure plasma is a complex phenomenon involving reactions, which occur both in the plasma phase and at the surfaces bounding the plasma.

The study of plasma polymerization kinetics is commonly employed to elucidate polymerization mechanisms. With this background a comparison of the polymer formation rates of various monomers by plasma polymerization would provide an overview of the kind of reaction mechanism responsible for plasma polymerization.

The probable chain growth polymerization is represented by

$$M_n^* + M \longrightarrow M^*_{n+1}$$

Where M_n^* is the reactive chain carrying species and M is the monomer molecules. But Yasuda and Lamaze [26] on the basis of their observation on plasma polymerization ruled out the chain growth polymerization. The rapid step-growth mechanism is very likely to be the

reaction in plasma polymerization and this reaction is expressed as:

$$[M_m{*}+M_n{*} \longrightarrow M_{m+n}{*}] \times N$$

Where N represents the number of repetitions of similar reactions. In this case, the reaction occurs between molecules.

In case of parylene polymerization, **M** is a difunctional reactive species and the overall polymerization can be represented by

$$n{*}M{*} \longrightarrow {*}(M_n){*}$$

If the reactive species are monofunctional *(M*)*, such as free radical R*, the reaction is given by

$$M_m{*}+M_n{*} \longrightarrow M_{m+n}$$

Which is essentially a termination process that occurs in free radical polymerization and does not contribute without additional elementary steps. Yasuda and Lamaze [27] pointed out that the reactivation of the product of an elementary reaction was bound to occur in plasma.

The overall polymerization mechanism based on the rapid step-growth principle shown in Fig. 2.16. The figure shows the overall reaction, which contains two major routes of rapid step-growth. Cycle (C-1) is via the repeated activation of the reaction products from monofunctional activated species, C-2 is via difunctional or multifunctional activated species.

Cycle - 1

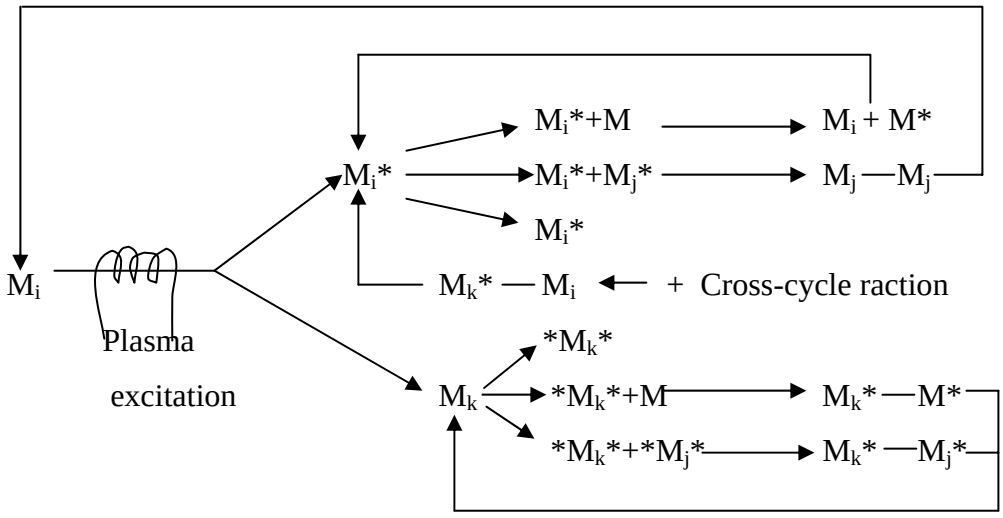

Cycle - 2

Fig.2.16 Schematic representation of bicycle step growth mechanism of plasma polymerization.

Here, M_x refers to neutral species that can be original monomer molecule or any of the dissociation products including some atoms, such as hydrogen, chlorine, fluorine and others;

M* activated species; ***M*** difunctional activated species and the subscripts i, j, k indicate the difference in the size of the species involved (i=j is possible, thus i=j=1 for initial monomer.)

One of the most important features of plasma polymers is that a large quantity of free radicals is often trapped in the polymer. Although, the amount varies with the type of monomer and the conditions of the plasma polymerization, it is safe to consider that plasma polymers contain a certain amount of trapped free radicals. Therefore, the free radicals play important role in plasma polymers. In plasma polymerization, deposition rates and polymer film densities have been shown to vary with substrate temperature and discharge power. Some authors have observed that deposition rate decreases with increasing substrate temperature. Polymeric films produced by plasma polymerization have branched and cross-linked structures and are difficult to dissolve in organic solvents. Their structure is irregular and amorphous and there may be no distinction between the main chain and branches.

2.8 Advantages and Disadvantages of Plasma Polymers

Plasma polymerization offers a number of advantages [28-29] over other polymerization methods and in general. The most significant advantage of plasma polymerization is its ability to produce polymer films of organic compounds that do not polymerize under normal chemical polymerization conditions [20]. Organic compounds that could be polymerized under normal chemical polymerization conditions are also be polymerized by this process. Nearly all monomers, even saturated hydrocarbons and organic compounds without a polymerizable structure such as a double bond, can be polymerized with this technique [27]. The main advantage of plasma polymerization is that it can occur at moderate temperatures compared to conventional chemical reactions because of cracking of monomers and the formation of radicals occurs by electron impact reactions in the plasma. Another important advantage to this process is that polymers can be directly attached to a desired surface while the chains are growing, which reduces steps necessary for other coating processes such as grafting. Plasma polymerization is used to deposit films with thickness from several tens to several thousands of angstroms (500°A to 1 μm). Multilayer films or films with grading of chemical and physical characteristics can be easily prepared. Next advantage is the ease of application of the polymers as coatings versus conventional coating processes. While coating a substrate with conventional polymers requires a number of steps, plasma

polymerization accomplishes all these in essentially a single step [30]. This leads to a cleaner and 'greener' synthesis and coating process, since no solvent is needed during the polymer preparation and no cleaning of the resultant polymer is needed either. Another 'green' aspect of the synthesis is that no initiator is needed for the polymer preparation since reusable electrodes cause the reaction to precede. The resultant polymer coatings also have a number of advantages over typical coatings. These advantages include being nearly pinhole free, highly dense and that the thickness of the coating can easily be varied [31]. Plasma-polymerized films are generally chemically inert, insoluble , mechanically tough, and thermally stable have been used in a wide variety of applications such as protective coating, electrical, optical and biomedical films. This technique is useful in applications such as biomedical where controlling and modifying surface is important. Several advantages of plasma polymerized films:

- Consistently even, thin, clear films can be deposited.
- Because the films are highly cross linked, they have a low solubility and good corrosion resistance. They also have excellent resistance to most chemicals.
- Good surface uniformity and relatively easy procedure.

The specific advantages of plasma-deposited films are summarized in here:

i) Conformal: Because of the penetrating nature of low-pressure gaseous environment in which mass transport is governed in part by both molecular (line of sight) diffusion and convective diffusion, complex geometry shapes can be treated.

ii) Pinhole-free: Under common reaction conditions, the plasma film appears to coalesce during formation into a uniform over layer free of voids. Transport studies and electrical property studies suggest this continuous barrier structure.

iii) Barrier film: The pinhole-free and dense, cross-linked nature of these films suggests they have potential as barrier and protective films.

iv) Unique substrates: Plasma-deposited polymeric films can be placed upon almost any solid substrate including metals, ceramics, and semiconductors. Other surface grafting or surface modification technologies are highly dependent upon the chemical nature of the substrate.

v) Good adhesion to the substrate: The energetic nature of the gas phase species in the plasma reaction environment can induce some mixing and implantation between the

film and the substrate. The plasma polymer coatings have good adhesion to both metallic and plastic surfaces.

vi) Unique film chemistry: The chemical structure of the polymeric over layer films produced by rf plasma deposition cannot be synthesized by conventional organic chemical methods. Complex gas phase molecular rearrangements account for these unique surface chemical compositions.

vii) Easy preparation: Once the apparatus is set up and optimized for a specific deposition, treatment of additional substrates is rapid and simple. Through careful control of the polymerization parameters, it is possible to tailor the films with respect to specific chemical functionality, thickness, and other chemical and physical properties.

Disadvantages

The main disadvantages are:

- Polymerized coatings have low abrasion resistance.
- Low deposition rates. Only very thin films can be deposited economically on high production items.
- The process doesn't discriminate against what is coated. Everything in the coating range of the polymerization process is coated, or can become part of the coating.
- The process, used in mass production, is still in its infancy. More capabilities will likely be available as improvements to the process occur, the chemistry produced on a surface is often not well defined, and sometimes a complex branched hydrocarbon polymer will be produced.
- Contamination can be a problem and care must be exercised to prevent extraneous gases, grease films, and pump oils from entering the reaction zone.

In spite of the drawbacks, plasma polymerization is far well developed process for many types of modification that simply cannot be done by any other technique.

2.9 Applications of Plasma-polymerized Organic Thin Films

Plasmas are used in a large number of application fields. The most important application is probably in the microelectronics industry and in materials technology, for surface treatment, etching of surfaces (e.g., for the fabrication of integrated circuits), deposition of thin protective coatings, plasma polymerisation, plasma modification of polymers and other surfaces.

Because a lot of chemical reactions take place in the plasma, several types of discharges (mainly atmospheric pressure glow discharges and dielectric barrier discharges) find also increasing interest for environmental applications (e.g., the destruction of volatile organic compounds) and biomedical applications (e.g., the sterilisation of materials).

Surface modification is probably another most important application field, plasma processes appear to have some distinct advantages compared to conventional processes. Plasma polymers are used as dielectric and optical coating to inhibit corrosion. A number of different plasma technologies are essential to different steps in the fabrication of ICs. The use of plasmas as lamps, more specifically fluorescent lamps is probably the oldest application. Nowadays, new types of so-called electrode less lamps are being developed, and the use of low temperature plasmas for displays as large and flat television screens. Applications of plasma-polymerized films are associated with biomedical uses, the textile industry, electronics, optical applications, chemical processing and surface modification [30-34]. The main advantage of plasma polymerization is that it can occur at moderate temperatures compared to conventional chemical reactions because of cracking of monomers and the formation of radicals occurs by electron impact reactions in the plasma. Segui described two applications and the problems that prevent their industrial application, i.e. the reactor geometry and neutralization of free radicals in the case of micro capacitors and contact openings and mobile charge quantity reduction in the case of component passivation.

References

[1] Yasuda, H., 'Plasma Polymerization', Academic Press, New York, 1985.

[2] Biederman H. and Osada Y., 'Plasma Polymerization Process', Elsevier Science, Publishers, Amsterdam, 1992.

[3] Sunny, V., Narayanan T. N., Sajeev U. S., Sakthi Kumar D., Yoshida Y. and Anantharaman M. R., 'Evidence for intergranular tunnelling in polyaniline passivated α-Fe nanoparticles', Nanotechnology 17, 4765, 2006.

[4] Saravanan, S., Anantharaman, M. R., Venkatachalam S. and Avasthi D. K., 'Studies on the Optical Band Gap and Cluster Size of the Polyaniline Thin Films Irradiated with Swift Heavy Si Ions', Vacuum 82(1) , 56-60, 2007.

[5] Goodmann, J., The formation of thin polymer films in the gas discharge J. Polym. Sci., 44,

551, 1960.

[6] Bradley A.P., Hammes J. P., 'Electrical Properties of Thin Organic Films', J. Electrochem. Soc., 110(1), 15 -22, 1963.

[7] Hynek, Biederman, 'Plasma Polymer Films', Imperial College Press, UK, 2004.

[8] Cowie, J. M. G., 'Polymers: Chemistry and Physics of Modern Materials', Blackie Academic and Professionals, UK, 2nd Ed., 1991.

[9] Andrew Gulhrie, 'Vacuum Technology', John Wiley and Sons, Inc, New York, 1963.

[10] Biederman, H., Osada, Y., 'Plasma Chemistry of Polymers', Adv. in Polym. Sci.,Berlin, Germany, 1990.

[11] Bogaerts, A., Neyts, E., 'Gas discharge plasma and their applications', Spectrochimica Acta Part B, 57, 609-658, 2002.

[12] Lieberman, M. A, Lichtenberg, A. J., 'Principles of Plasma Discharges and Materials Processing', John Wiley and Sons, New York, 1994.

[13] Grill, A., "Cold Plasma in Materials Fabrication: From Fundamentals to Applications", IEEE press, New York, 1994.

[14] Bogaerts, L., Wilken, V., Hoffmann, R., Gijbels, K., Wetzig 'Comparison of modeling calculations with experimental result for rf glow discharge optical emission spectroscopy', Spectrochimi. Acta Part B, 57 , 109-119, 2002.

[15] Shen, M., Alexis, T. Bell, 'Plasma Polymerization' Washington D.C. American Chemical Society, 1979.

[16] Biederman, H. and Stavinska, D., 'Plasma polymer films and their future prospects', Surf. Coat. Technol. 125 (1-3), 371-376, 2000.

[17] Nakamura, K., Watanabe, M., Zhou, M., Fujishima, M., Tsuchiya, M., Handa, T., Ishii, S., Noguchi, H., Kashiwagi, K. and Yoshida, Y., 'Plasma polymerization of cobalt tetraphenylporphyrin and the functionalities of the thin films produced', Thin Solid Films 345, 99-103, 1999.

[18] Chowdhury, F.-U.-Z. , Bhuiyan A. H., 'An investigation of the optical properties of plasma-polymerized diphenyl thin films', Thin Solid Films 360, 69-74, 2000.

[19] Han, M. G. and Im, S. S., 'Dieleetric spectroscopy of conductive polyaniline salt films', J. Appl. Polym. Sci. 82, 2760-2769, 2001.

[20] Gaur, S. and Vergason, G., 'Plasma Polymerization:Theory and Practice'. Vergason Technology, Inc. http://www.vergason.com/pdf/Plasma_Polymerization_Theory.pdf. 2011.

[21] Zang, Z., 'Surface Modification by Plasma Polymerization and Application of Plasma Polymers as Biomaterials', Johanneses Gutenberg University of Mainz, 2003.

[22] Yasuda, H., Vossen, J. L., and Kern, W., 'Thin Film Processes', Academic Press, New York, 1978.

[23] Yasuda, H. and Hsu T., Surf. Sci. 76, 232, 1978.

[24] Hopwood, J, 'Review of Inductively Coupled Plasmas for Plasma Processing'. Plasma. Source. Sci. Technol., 1, 109-116, 1992.

[25] Yasuda, H. and Hirotsu, T, J., Polym. Sci.,Polymer Chemistry Edition, 16, 313-17, 1978.

[26] Yasuda, H. and Lamaze, C. E, J. Appl. Polym. Sci., 17, 1533, 1973.

[27] Zang, Z., 'Surface Modification by Plasma Polymerization and Application of Plasma Polymers as Biomaterials' Johanneses Gutenberg University of Mainz, 2003.

[28] Vurzel, F. B., Acad. Sci., Moscow, USSR, 'Plasma Chemistry Technology, Application', Inst. Plasma Chem. and Technol., Carlsbad, CA,1983.

[29] Mathai, C. J., Saravanan, S., Jayalekshmi S., Venkitachalam S., Anantharaman M. R., 'Conduction mechanism in plasma polymerized aniline thin films', Mater Lett. 57, 2253-2257, 2003.

[30] Yasuda, H., 'Glow Discharge Polymerization', J. Polym. Sci.: Macromolecular Reviews 16 (1), 1981.

[31] Van Os M., 'Surface Modification by Plasma Polymerization: Film Deposition, Tailoring of Surface Properties, and Biocompatibility', The Netherlands: University of Twente, Enschede, 2000.

[32] Hammer, T., 'Applications of plasma technology in environmental techniques' Contrib Plasma Phys. 3, 441-462, 1999.

[33] Lindford, R. G., 'In Applications of Electroactive Polymers'; Scrosati, B (Ed); Chapman and Hall, London 1-28, 1993.

[34] Segui, Y. and Bui Ai, 'Microelectronic applications of plasma- polymerized films', Thin Solid Films 50, 321-324, 1978.

4.1 Introduction

Plasma polymerization and deposition are finding increasing use in a variety of applications. Plasma polymers are formed as a result of recombination of reactant species due to monomer fragmentation by plasma discharges. Plasma polymers have very different macroscopic properties from those of conventional linear polymers with the same starting monomer(s). Indeed, unexpected properties of plasma polymers are being uncovered constantly. A complete understanding of the plasma polymerization processes and the properties of plasma polymers requires fundamental knowledge of plasma sources, plasma physics/chemistry in the gas phase, and surface chemistry/kinetics at the plasma-substrate interface. This chapter describes the experimental details related to thermal, structural, optical and electrical characterization of PPDEAEMA, substrate materials, capacitively coupled plasma polymerization set up, film thickness measurement, the techniques applied for characterization of thin films, such as SEM, DTA/TGA, FTIR for structural; UV-vis Spectroscopy for optical, DC and AC measurements for electrical characterizations are discussed in details.

4.2 The monomer

2-(Diethylamino)ethyl methacrylate (DEAEMA) from Aldrich is the starting material for preparing plasma polymerized thin films. It is a clear light yellow color liquid. Its physical and chemical properties are given below:

Molecular formula	:	$C_{10}H_{19}NO_2$
Linear Formula	:	$H_2C=C(CH_3)CO_2CH_2CH_2N(C_2H_5)_2$
Molecular Weight	:	185.26
Boiling point	:	80 ºC (10 mmHg)
Flash point	:	170 ºF
Density	:	0.922 g/cm^3
Decomposition	:	176-178 ºC
Refractive index	:	1.444

The chemical structure of the monomer is given in Fig.4.1.

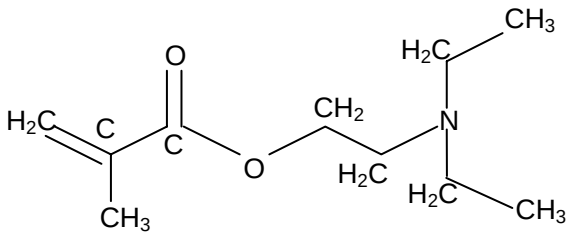

Fig. 4.1 The chemical structure of 2-(Diethylamino)ethyl methacrylate.

4.3 Substrate and their cleaning Process

A thoroughly cleaned substrate is a prerequisite for the preparation of films with reproducible properties. The substrates used were pre-cleaned glass slides (Sail brand, China) purchased from local market. Before thin film deposition the substrates were cleaned with acetone and distilled water. The cleaned glass plates were then dried by a drier.

4.4 Capacitively Coupled Plasma Polymerization Set-up

In this work, plasma polymerized thin film would be formed by using a locally fabricated capacitively coupled plasma polymerization system situated in the Material Science Laboratory, Deptartment of Physics, Bangladesh University of Engineering and Technology (BUET). The glow discharge plasma deposition process consists of the following steps shown in Fig. 4.2

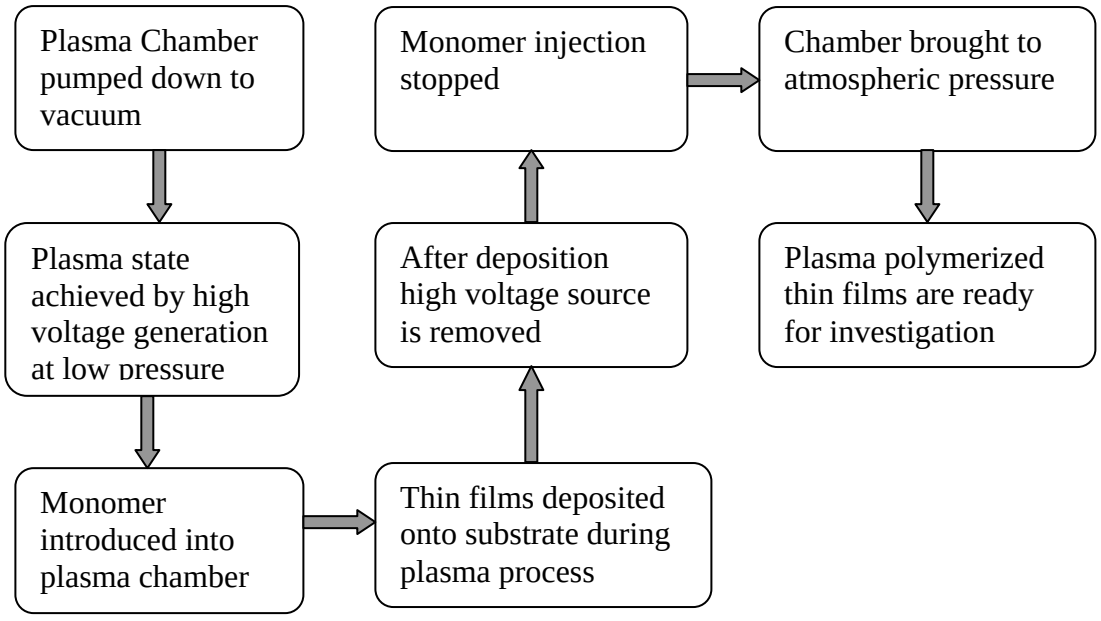

Fig. 4.2 A Block diagram for preparation of plasma polymerized thin

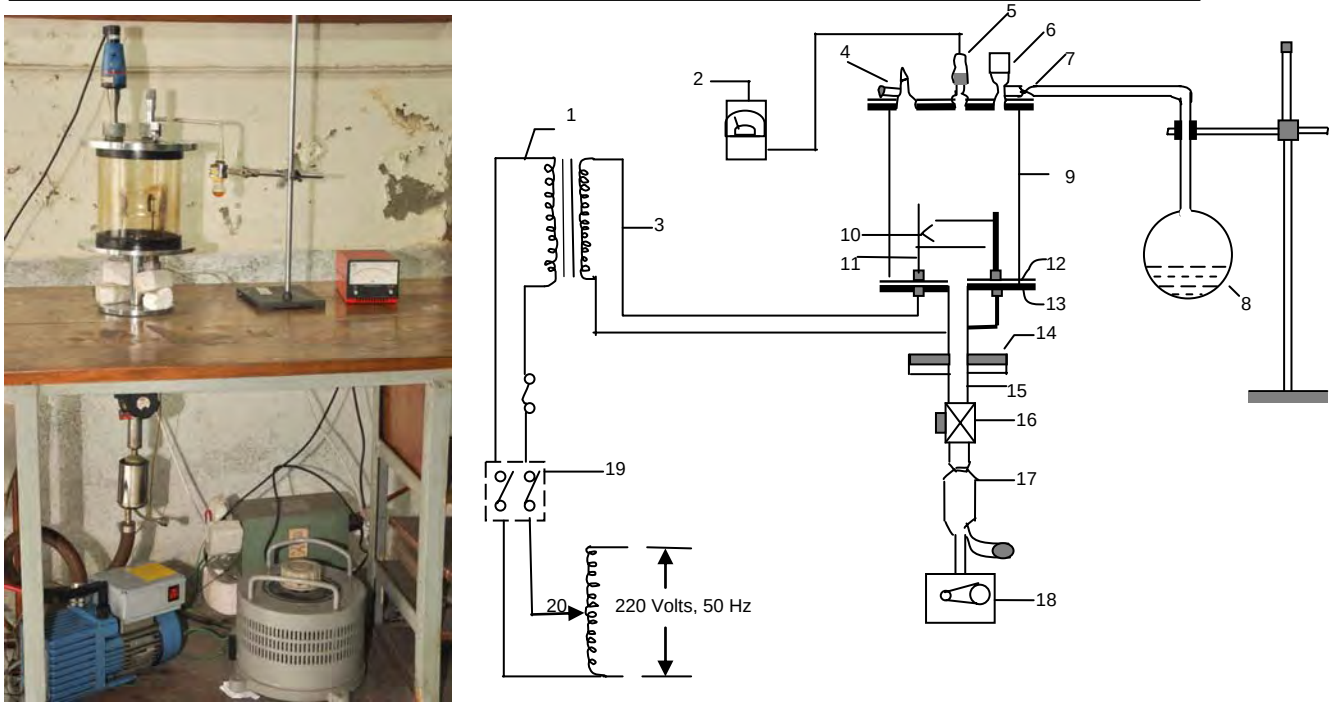

(a) (b)

Fig. 4.3. (a) Plasma polymerization set-up in laboratory and (b) schematic diagram of the plasma polymerization system (1, high voltage power supply; 2, pirani gage; 3, high tension leads; 4, gas inlet valve; 5. gauge head; 6, monomer injection valve; 7, flow meter; 8, monomer container; 9, Pyrex glass dome; 10, metal electrodes; 11, electrode stands; 12, gasket; 13, lower flange; 14, bottom flange; 15, brass tube; 16, valve; 17, liquid nitrogen trap; 18, rotary pump; 19, switch and 20, variac).

In the present set-up capacitatively coupled electrode system was used. Two circular stainless steel plates of diameter 0.09 m and thickness of 0.001 m are connected to the high voltage copper connectors. The inter-electrode separation can be changed by moving the electrodes through the electrode stands. After adjusting the distance between the electrodes they are fixed with the stands by means of screws. The substrates are usually kept on lower electrodes for plasma deposition. Pumping unit is used for evacuating the plasma reaction camber. In order to create laboratory plasma, first step is pumping out the air/gas from the plasma chamber. In this system a rotary pump of vacuubrand (Vacuubrand GMBH & Co: Germany) is used. The input power supply for plasma excitation comprises of a step-up high-tension transformer and a variac. The voltage ratio at the output of the high-tension transformer is about 16 times that of the output of the variac. The maximum output of the variac is 220V and that of the transformer is about 3.5 kV with a maximum current of 100 mA. The deposition rate increases with power at first and then becomes independent of power

at high power values at constant pressure and flow rate. The glow discharge plasma deposition set-up is shown in Fig.4.3. The monomer injecting system consists of a conical flask of 25 ml capacity and a glass tube with capillarity at the end portion. The capillary portion is well fitted with metallic tube of the nozzle of the high vacuum needle valve. The conical flask with its components is fixed by stand-clamp arrangement.

The plasma chamber (Fig. 4.4) consists of a cylindrical Pyrex glass jar having 0.l5 m in inner diameter and 0.18 m in length. The top and bottom edges of the glass bell-jar are covered with two rubber L-shaped (height and base 0.015m, thickness, 0.001 m) gaskets.

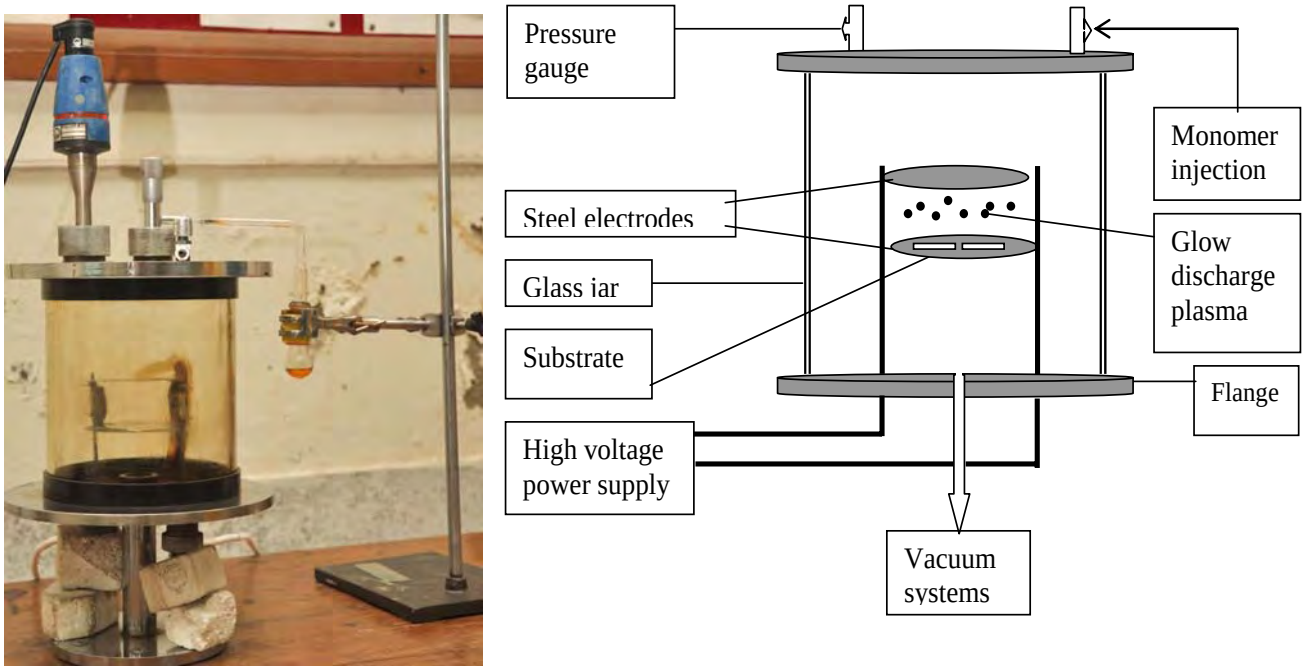

Fig.4.4 Plasma reaction chamber: (a) photograph and (b) schematic diagram: 1, Pressure gauge; 2, Monomer inlet; 3, Monomer container; 4, Steel electrodes; 5, To vacuum pump; 6, AC power supply; 7, Glass cylinder, 8, electrode stands, 9, Monomer, 10, Upper flange and 11, lower flange.

The cylindrical glass jar is placed on the lower flange. The lower flange is well fitted with the diffusion pump by an I joint. The upper flange is placed on the top edge of the glass-jar. The flange is made up of brass having 0.01 m in thickness and 0.25 m in diameter. A vacuum pressure gauge head (Laybold AG) and a meter (Thermotron^{TM} 120) of Laybold, Germany, are used lo measure inside pressure of the plasma deposition chamber. On the upper flange a laybold pressure gauge head, Edwards high vacuum gas inlet valve and a monomer injection valve are fitted. In the lower flange two highly insulated high voltages

feed-through are attached housing screwed copper connectors of 0.01m high and 0.004 m in diameter via Teflon insulation. A metal frame of dimension l.5m x 0.76m x 0.09m is fabricated with iron angle rods, which can hold the components described above. The upper and lower bases of the frame are made with polished wooden sheets. The wooden parts of the frame are varnished and the metallic parts are painted to keep it rust free. The pumping unit is placed on the lower base of the frame. On the upper base a suitable hole is made in the wooden sheet so that the bottom flange can be fitted with nut and bolts.

The system pressure of the gas flow is determined by the feed in rate of gas and the pumping out rate of a vacuum system. The monomer flow rate is determined by a flow meter. So flowmeters are used in plasma polymerization system to control the monomer deposition rate, In the plasma polymerization set up a flowmeter (Glass Precision Engineering LTD, Meterate, England) is attached between the needle valve and the monomer bottle.

4.5 Generation of Glow Discharge Plasma in the Laboratory

The chamber of the plasma polymerization unit and monomer container is evacuated to about 0.01 mbar.

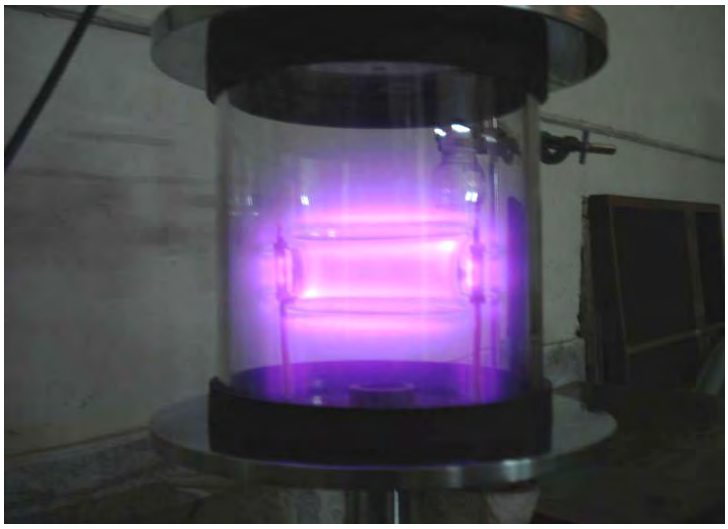

Fig. 4.5. Glow discharge plasma during deposition.

The monomer vapor is then injected to the chamber slowly for some time. A high-tension transformer along with a variac is connected to the feed-through attached to the lower flange. While increasing the applied voltage, light purple colors monomer plasma is produced across the electrodes. Fig. 4.5 shows the photograph of glow discharge plasma across the

electrodes in the capacitatively coupled parallel plate discharge chamber. In laboratory PPDEAEMA thin films were prepared using a capacitively coupled glow discharge system. The deposition times for these films were varied from 50 minute to 75 minutes in order to get films of different thicknesses.

4.6 Optimized deposition conditions

PPDEAEMA thin films were prepared at different experimental conditions such as: different time limit, different power etc. The deposition rate can be significantly altered by changing such deposition parameters as input power, monomer flow, or pressure within the deposition chamber. For instance, similar deposition set-up has demonstrated a significant reduction in the film growth rate for increased levels of input power. The decrease in the deposition rate was attributed to a higher degree of fragmentation of the monomer molecule and subsequent increase in the degree of cross-linking of the resultant polymer film. In addition, the process of ablation is likely to be more prominent in the case of high power conditions, etching back the newly formed film. Hence, it is possible to produce films of desired thickness to suit given application by controlling such deposition conditions as time and applied power [16],

In order to find out the most suitable experimental conditions which would be the desired deposition parameter of PPDEAEMA thin films, the thickness at different deposition time and FTIR analyses of the thin films deposited at different powers were considered. The FTIR spectra in Fig. 4.6 show that the same vibrational groups are present in all films deposited at different plasma powers. From Fig. 4.7 it is observed that the relative intensity of some absorption bands change with increasing plasma power. It is well known that the C=O absorption is almost always one of the most characteristic in the entire spectrum and also most likely to be the most intense spectral feature in carbonyl compounds.

Also conjugation plays an important role in the observed carbonyl frequency which includes connection to conjugation, to a C=C or another C=O [17]. From Fig 4.6 it is clear that absorption band at around 1720 cm^{-1} due to C=O stretching and a broad absorption band at 1650-1550 cm^{-1} due to C=C stretching are most prominent in the FTIR spectra found for 40 W rather than 50 and 30 W.

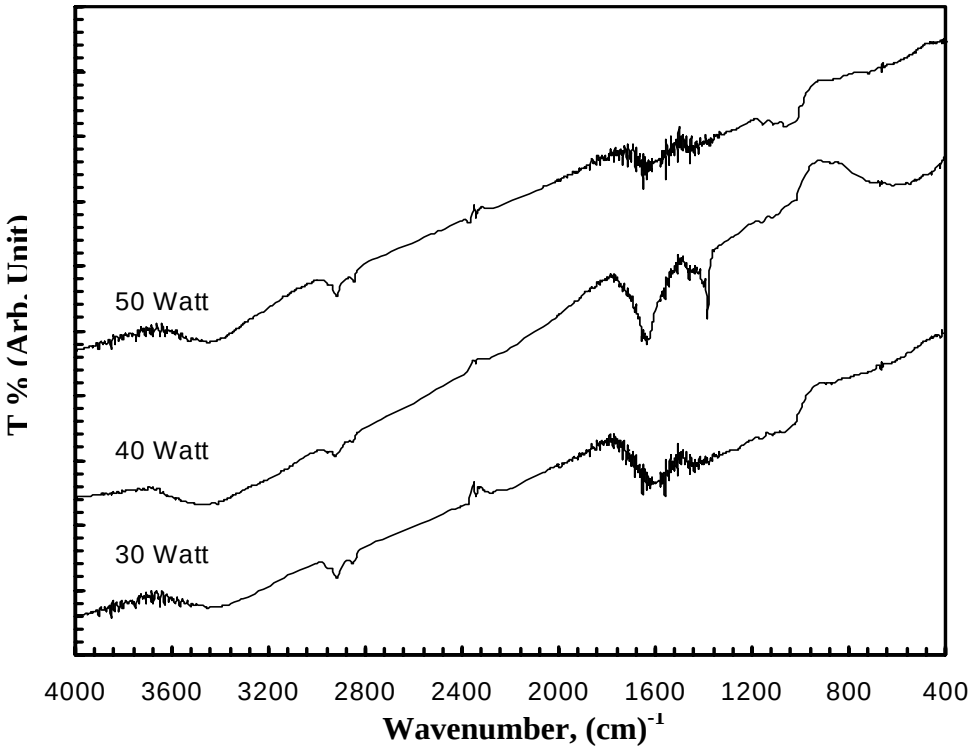

Fig. 4.6. The FTIR spectra of as deposited PPDEAEMA at 30, 40 and 50 Watt.

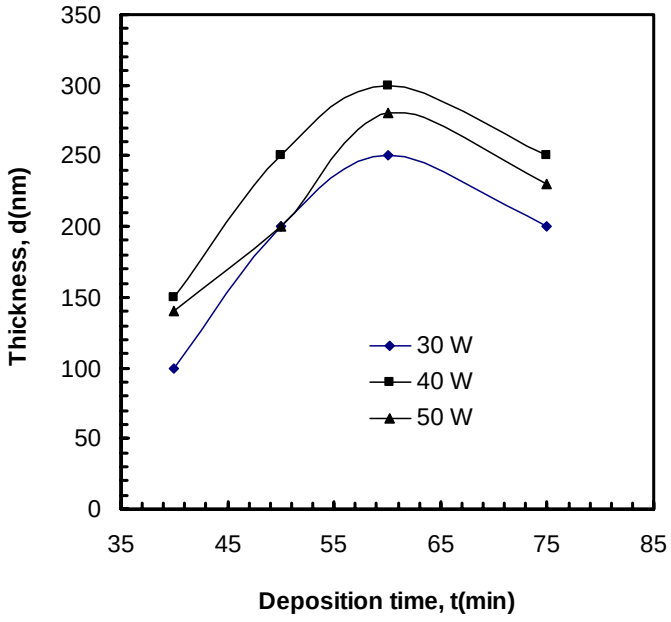

Fig. 4.7 Variation of thickness with different deposition time for the PPDEAEMA thin films.

It is perceived from Fig. 4.7 that at 30 W the plasma is low to gain the film thickness properly and at 50 W the plasma is high which results in slower deposition of the thin films, with the increase in time. Thus the PPDEAEMA thin films were prepared at 40 W plasma

powers for different measurements. The deposition time was varied from about 40 to 75 min to get the film thicknesses ranging from 100 to 300 nm. The optimized conditions for thin film formation for the present study:

- placing the substrate on the top of the lower electrode.
- deposition time 1 hour.
- electrode separation is 4 cm.
- deposition power 40 W.
- pressure during deposition is about 13.3 Pa.

4.7 Heat Treatment of PPDEAEMA

For the UV-Vis spectroscopic investigation and SEM study, PPDEAEMA thin films were heat treated at 373, 473 and 573 K in air for one hour (temperature rising rate was 5 K/min and followed by furnace cooling system) using a programmable Muffle furnace and Thermconcept (Eurotherm) temperature controller, Germany. For FTIR analysis PPDEAEMA powder was heat treated at a constant temperature of 473 and 573 K in air for one hour by keeping on glass slide using the same furnace and conditions.

4.8 Modification of PPDEAEMA thin films with iodine

Besides good chemical and thermal stability, plasma polymers are highly crosslinked and are characterized by high electrical resistance[1-5]. Many researcher has been devoted to enhance the conductivity of polymers by doping using suitable dopants [6-9]. Iodine is frequently used as a dopant because of the ease of the doping procedure. It was shown by several techniques (e.g. UV-vis spectroscopy, X-ray induced photoelectron spectroscopy and Raman spectroscopy) that, next to absorbed I_2, charge transfer complexes in the form of I_3- and/or I_5- are formed upon iodine doping of polyacetylene [10-12]. The same charge transfer complexes of iodine were found after iodine doping of other conjugated polymers, trimers and monomers. It is now generally accepted that the conductivity in conjugated polymers after doping is governed by the charge carriers generated by charge transfer complexes [13-14].

The PPDEAEMA thin films were doped by iodine in order to introduce charge carriers into the plasma polymer structure. The samples were doped by placing in a desiccator containing iodine crystals for a certain period of time at room temperature. After doping, the colour of

the PPDEAEMA thin films becomes dark brown which indicates the successful introduction of the iodine in PPDEAEMA thin films. The iodine doped PPDEAEMA thin films were subjected to atmospheric conditions at room temperature before and after iodine doping. All the measurements on doped thin films were taken place after storage in air for the same time period.

4.9 Measurement of Thickness of the Thin Films

Thickness is the single most vital film parameter. It may be measured either by in-situ examining of the rate of deposition, or after the film is taken out of deposition chamber. Techniques of the first type often called as monitor method generally allow both monitoring and controlling of the deposition rate and film thickness. Any physical quantity related to film thickness can in principle be used to measure the film thickness. It may be measured either by several methods with varying degrees of accuracy. The methods chosen on the basis of their convenience, simplicity and reliability. Several of the common methods are i) Multiple-Beam Interferometry, ii) using a Hysteresis graph and other methods used in film-thickness determination with particular reference to their relative merits and accuracies. Since the film thicknesses are generally of the order of a wavelength of light, various types of optical interference phenomena have been found to be most useful for measurement of film thicknesses. Multiple-Beam Interferometry technique was employed for the measurement of thickness of the thin films. This technique described below:

4.9.1 Multiple-Beam Interferometer

This method utilizes the resulting interference effects when two silvered surfaces are brought close together and are subjected to optical radiation. This interference technique, which is of great value in studying surface topology in general, may be applied simply and directly to film thickness determination. When a wedge of small angle is formed between unsilvered glass plates, which arc illuminated by monochromatic light, broad fringes are seen arising from interference between the light beams reflected from the glass on the two sides of the air wedge. Where the path difference is an integral and odd number of wavelengths, bright and dark fringes occur. If the glass surfaces of the plates are coated with highly reflecting layers, one of which is partially transparent, then the reflected fringe system consists of very

fine dark lines against a bright background. A schematic diagram of the multiple-beam interferometer along with a typical pattern of Fizeau fringes from a film step is shown in Fig 4.8.

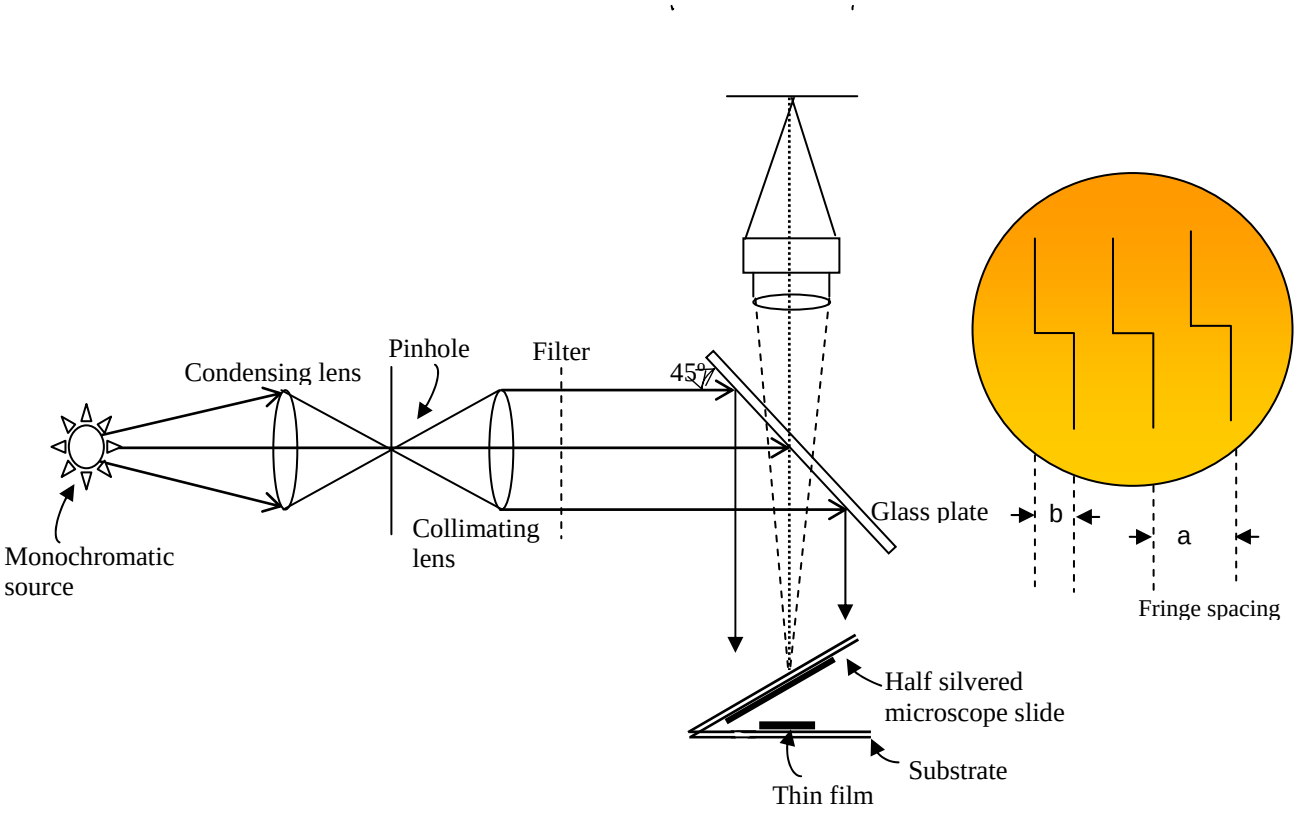

Fig.4.8 Schematic diagram of multiple-beam interferometer and schematic diagram of Fizeau fringes observed due to interference in Multile beam Interferrometric Technique. The step height 'b' and width (Fringe spacing) 'a' of the interference fringes.

As shown in this figure, the film whose thickness is to be measured is over coated with a silver layer to give a good reflecting surface and a half-silvered microscope slide is laid on top of the film whose thickness is to be determined, The thickness of the film d can then be determined by the relation $d = \frac{\lambda b}{2a}$, where λ is the wavelength and *b/a* is the fractional discontinuity identified in the figure. In general, the sodium light is used, for which λ = 5893 A°. In practice, several half-silvered slides of varying thickness and therefore of varying transmission are prepared, and one of these is selected for maximum resolution.

Fig. 4.9 Traveling microscope arrangement for film thickness measurement.

Accurate determinations of fringe spacing are difficult and time consuming; but a method of image comparison, which considerably improves the ease, and rapidity of measurement has recently been developed. Alternatively, a simple film- thickness gauge utilizing Newton's rings may be developed, which involves no critical adjustment of wedges, etc., and which reduces error in film-thickness determination. The traveling microscope arrangement for film thickness measurement set up is shown in Fig. 4.9. It might be mentioned that the Tolansky method of film-thickness measurement is the most widely used and in many respects also the most accurate and satisfactory one. The thickness of the plasma polymerized films deposited on glass substrates was measured by using a multiple-beam interferometric method [15]. For film thickness measurement separate glass slide has been used in addition to the sample substrates. Teflon tape was used to cover 50% area of the cleaned glass, which was not exposed to plasma environment during plasma polymerization. After deposition, the Teflon tape was carefully removed from the glass slide. The step generated on the surface of the glass slide was used to measure the film thickness.

4.10 Experimental Techniques employed for characterization of PPDEAEMA thin films

In this research work, thin films of PPDEAEMA were investigated using different experimental techniques. Following are the different techniques or procedure used to study the different properties of the PPDEAEMA thin films:

1. Scanning electron microscopy (SEM) for surface morphological studies.

2. Differential thermal analysis (DTA) and Thermogravimetric analysis (TGA) to study the thermal properties of the films.
3. Fourier transformed infrared (FTIR) spectroscopy for identifying different functional groups in the PPDEAEMA films.
4. Ultraviolet visible (UV-vis) spectroscopic analyses to study the optical properties.

The experimental procedures to study the above mentioned properties are described below:

4.11 Scanning Electron Microscopy

Fig. 4.10 A photograph of a Scanning Electron Microscope

The PPDEAEMA thin films were deposited onto glass substrates for SEM. Glass substrate of surface area 1.0 cm × 1.0 cm was used for SEM measurements. Scanning electron micrographs of PPDEAEMA thin film surfaces were taken using a SEM (S-50, FEI Quanta Impact, The Netherlands) (Fig. 4.10). As deposited, heat treated (at 573 K for an hour) and iodine doped PPDEAEMA thin films were used in this investigation. Energy Dispersive X-ray of the samples was recorded at the same time by an EDS attached to the SEM.

4.12 Differential Thermal Analysis and Thermogravimetric Analysis

DTA/TGA is the simplest and most widely used thermal analysis technique. A little amount of PPDEAEMA powder was scrapped off from the substrates to study DTA/TGA. The DTA/TGA scans of PPDEAEMA were taken in air environment using a computer controlled TG/DTA 6300 (Fig. 4.11) system connected to an EXSTAR 6000 station, Seiko Instruments Inc., Japan. The TG/DTA module uses a horizontal system balance mechanism. The heating rate was 10 K/min in air. The specifications of the instrument are : sample weight≤ 200 mg, Temperature range: 300 K to 1573 K, TGA measuring range ±200 mg (0.2 μg), DTA Measuring Range≤ 1000 μV(0.06μV), Gas flow 1000 m/min.

Fig. 4.11 TG / DTA 6300 system

4.13 Fourier Transform Infrared Spectrometry

A schematic diagram of an FTIR instrument is as shown in Fig. 4.12. An IR spectrum shows the frequencies of IR radiation absorbed and the % of the incident light that passes through the molecule without being absorbed. For organic molecules, the IR spectrum can be divided into three regions. Absorptions between 4000 and 1300 cm^{-1} are primarily due to specific functional groups and bond types. Those between 1300 and 909 cm^{-1}, the fingerprint

region, are primarily due to more complex interactions in the molecules; and those between 909 and 650 cm^{-1} are usually associated with the presence of benzene rings in the molecule.

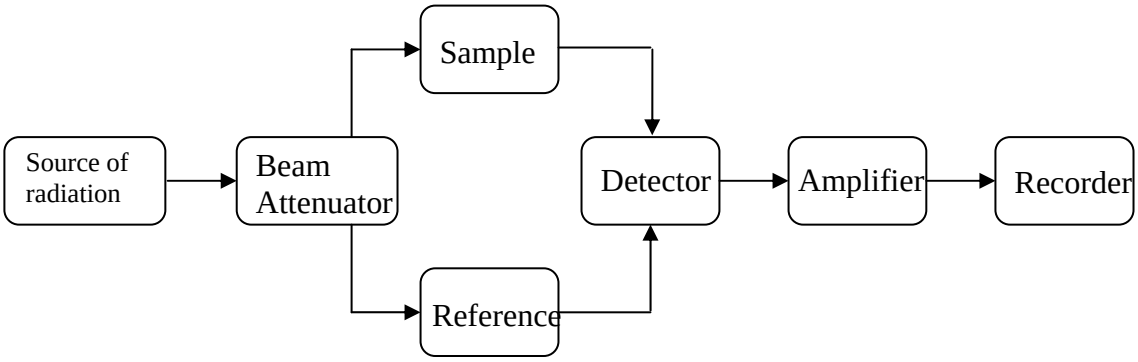

Fig. 4.12 A schematic diagram of an FTIR Spectrophotometer.

Fig. 4.13 The FTIR spectrometer 8900.

The FTIR spectra of DEAEMA and as deposited, heat treated (at 473K and 573 K for an hour) and iodine doped PPDEAEMA were recorded at room temperature using a double-beam IR spectrophotometer (Shimadzu–FTIR 8900 spectrophotometer, Japan) (Fig. 4.13). All the spectra were recorded in transmittance (T %) mode in the wavenumber range 4000-400 cm^{-1} at room temperature. A drop of monomer was put between two thin potassium bromide (KBr) pellets to record the FTIR spectrum. A little amount of PPDEAEMA powder collected from substrates was taken to make pellets after mixing with KBr and FTIR for different as deposited and heat treated samples were taken.

4.14 Ultraviolet Visible Spectroscopy

The instrument used in UV-VIS spectroscopy is called a UV-VIS spectrophotometer. In this work dual-beam UV-VIS spectrophotometer is used and a schematic diagram of the dual-beam UV-VIS spectrophotometer is given in Fig.4.14.

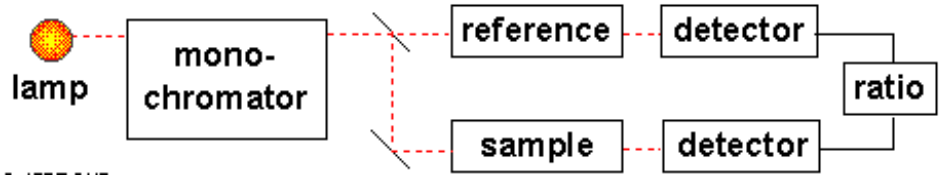

Fig. 4.14 A Schematic of a dual-beam UV-vis spectrophotometer.

The optical properties of the PPDEAEMA thin films deposited onto glass substrates having a dimension of 18 mm×18 mm×2 mm were studied by UV-Vis spectroscopic measurements. UV-Vis absorption spectra were recorded using a dual beam UV-Vis spectrophotometer (SHIMADZU UV-1601, Japan) in the wavelength range of 190-1100 nm at room temperature. The absorption spectra were recorded for as-deposited, heat treated at 473 and 573 K for 1 hour and iodine doped (for different period of time) PPDEAEMA thin films.

Fig. 4.15 A UV-vis Spectrophotometer

Samples of thicknesses 100,150, 200, 250 and 300 nm were used for UV-Vis spectroscopic studies. A blank glass slide was used as the reference during the optical

absorption measurement of PPDEAEMA thin films. Fig. 4.15 shows the dual beam UV-Vis spectrophotometer used in our research work (BCSIR Lab, Dhaka).

4.15 Sample Preparation for DC/AC Electrical Studies

For the studies of the electrical conductivity, we have prepared sample in the metal-insulator-metal (M-I-M) sandwich form. Here, for the M-I-M structure we have used 'Al' as the metal electrode. To obtain Al-PPDEAEMA-Al sandwich structure we have to proceed through three steps:

i) Deposition of 'Al' electrode on the well cleaned glass substrate

ii) Deposition of PPDEAEMA thin film on the 1^{st} electrode.

iii) Deposition of counter (2^{nd}) electrode on the PPDEAEMA thin film with proper masking.

4.16 Electrode preparation for electrical measurements

Electrode material: Aluminium (Al) (purity of 4N British chemical standard) was used as electrode material prior to deposition Al has been reported to have good adhesion to glass slide. Al film has advantages of easy self-healing burn-out of flaws in sandwich structure.

Electrode deposition: Metal electrodes of aluminium were deposited using an Edward coating unit E-306 A (Edward, U K) (Fig. 4.16). All of the components of the coating unit were properly cleaned with acetone. For thin film deposition, especially the physical deposition technique known as evaporation requires a good degree of vacuum. The process of deposition starts, by creating vacuum in the deposition chamber, usually of the order of 1.33×10^{-4} Pa or less. The actual deposition is followed by this vacuum. The process of deposition chamber evacuation begins usually at atmospheric pressure and then proceeds to high vacuum. The most common pumping arrangement for production of high vacuum consists of a positive displacement mechanical pump for initial evacuation followed by a vapor-stream pump, usually called diffusion pump. Diffusion pumps essentially are vapor ejectors and cannot discharge directly into the atmosphere. A mechanical pump is therefore required for the removal of the output discharge as well as for the initial evacuation. The second operation is commonly termed rough pumping or roughing. This is to reduce the pressure in the diffusion system and to bring it to the correct operating range. When suitable operating pressure

conditions are reached, the diffusion pump can take over. The mechanical pump is now used to maintain proper discharge pressure conditions for the diffusion pump at the fore line connection.

Fig. 4.16 The Edward vacuum coating unit E 306A

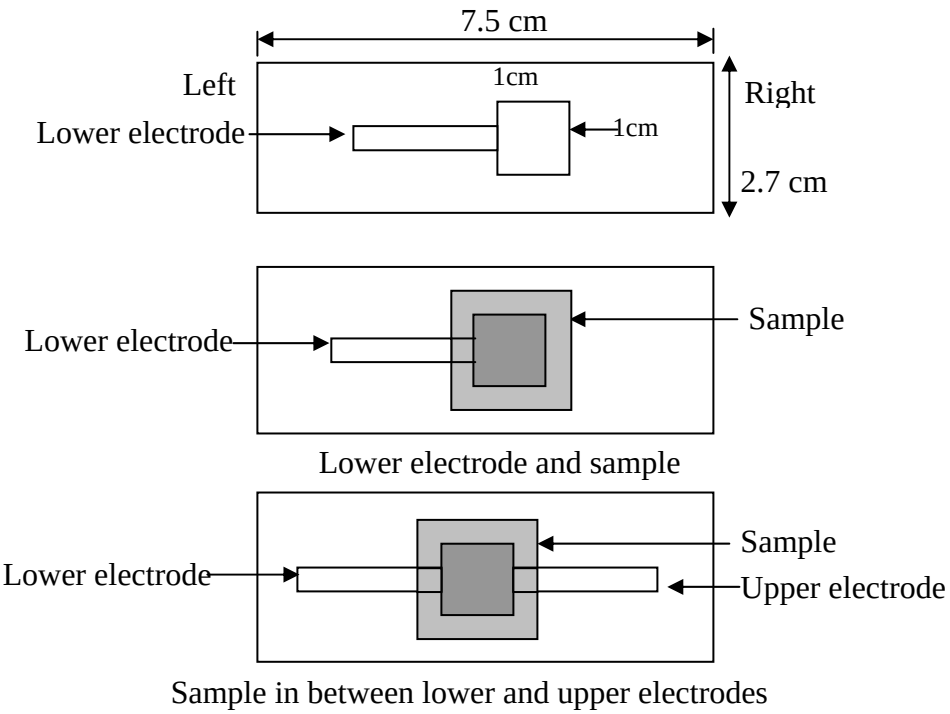

Fig. 4.17 Electrode – sample configuration.

This operation is called fore pumping or backing. The system was evacuated by an oil diffusion pump backed by an oil rotary pump. The glass substrates were masked with a 0.08m x 0.08m x0.001m engraved brass sheet for the electrode deposition. The electrode assembly used in this study is shown in Fig. 4.17. The glass substrates with mask were supported by a metal rod 0.1 m above the tungsten filament. For the electrode deposition Al was kept on the tungsten filament. The filament was heated by low-tension power supply of the coating unit. The low-tension power supply was able to produce 100 A current at a potential drop of 10 V. During evacuation of the chamber by diffusion pump, the diffusion unit was cooled by the flow of chilled water and its outlet temperature was not allowed to rise above 305 K. When the penning gauge reads about 1.33×10^{-3} Pa, the Al on the tungsten filament was heated by low-tension power supply until it was evaporated. After deposition of the 1st Al electrode on the cleaned glass substrate by conventional thermal evaporation technique under a pressure of about $2.66\text{x}10^{-3}$ Pa, the glass substrates were taken out of the vacuum coating unit and placed on the lower electrode of the plasma polymerization chamber. Then the PPDEAEMA thin films were deposited on the top of the Al electrode surface. After the deposition of the PPDEAEMA thin films on the first electrode the samples were taken out of the polymerization chamber and brought to the vacuum coating unit. The counter electrode (2) of aluminum was deposited in the same condition as described above, by using a suitable mask such that the effective area of the M-I-M structure is about 10^{-4} m^2.

4.17 DC electrical measurements

Suitable electrical contacts were made with the Al electrode by fine conducting wire of Cu using silver paste. Now the samples are ready for DC and AC electrical measurements. The electrical measurements were carried out in the PPDEAEMA films by loading the samples in a cylindrical metal holder. The measurements were carried out under dynamic vacuum of about 1.33 Pa. The current flowing through the films was measured by using a high impedance Keithley 614 electrometer. The DC bias voltage was applied by an Agilent 6545A stabilized DC power supply. The DC measurements were carried out at different constant temperatures (298, 323, 348, 373, 398 and 423 K).

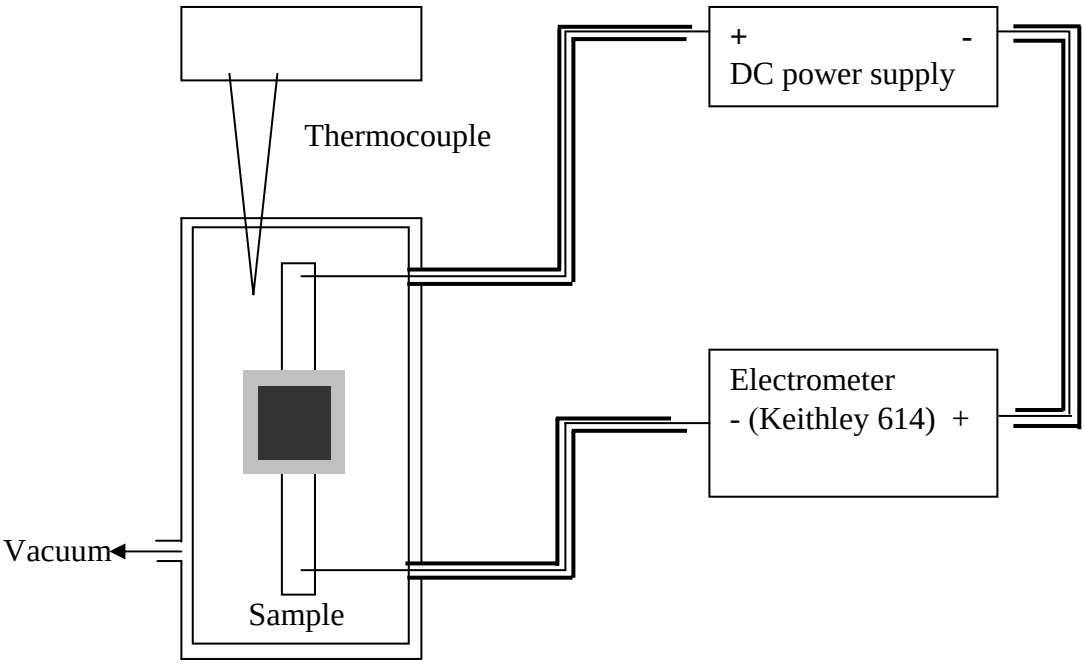

Fig. 4.18 A schematic circuit diagram of DC measurements.

Fig. 4.19 Arrangement for dc measurements

The sample chamber as well as the samples were heated by a heating coil wrapped around the specimen chamber. A Chromel-Alumel thermocouple mounted on the sample holder, with the fused end in contact with the PPDEAEMA thin film, permitted temperature measurements using a 197A digital microvoltmeter (DMV). The block diagram for DC measurements and dc measurement set up are shown in Fig. 4.18 and 4.19 respectively.

4.18 Measurement of dielectric properties by an Impedance Analyzer

The AC measurement was performed in the frequency range from 10^1 to 10^6 Hz and temperature range 298-423 K, by a low frequency (LF) Impedance analyzer, Agilent 4192A, 5Hz-13MHz, Agilent Technologies Japan, Ltd. made in Japan.

Electrical Specification and Characteristics of dielectric measuring system:

(i) Measuring Frequency (f) : 50-500 kHz

(ii) Capacitance (C_x): (a) Measurement range 270-2.2 nm, (b) Minimum 2.2nm.

(iii) Conductance (G_x):(a) Maximum range 10.2ms, (b) Minimum ranges 1.2 μs.

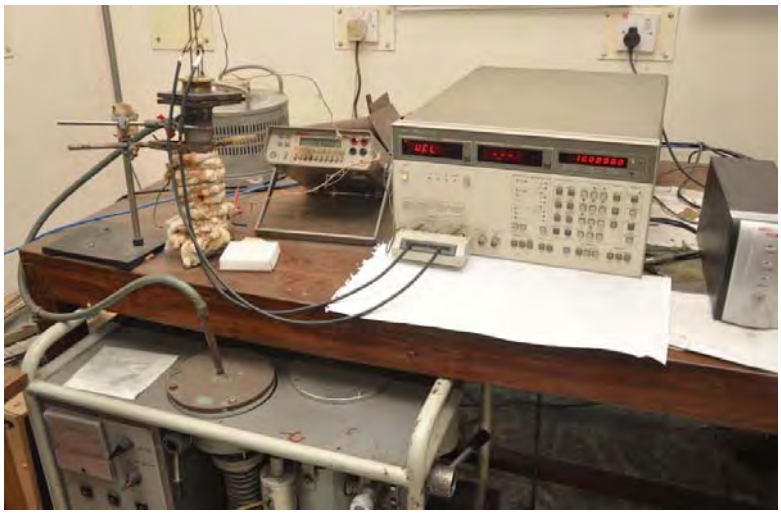

Fig. 4.20 Photographs of the Impedance Analyzer and the ac electrical measurement set-up.

The temperature was recorded by a Chromel- Alumel thermocouple placed very close to the sample which was connected to a Keithley 197A DMV. To avoid oxidation, all measurements were performed in a vacuum of about 13.3 Pa. Photographs of the Impedance analyzer and AC measurement set-up are shown in Figs. 4.20 (a, b).

References

[1] Hozumi, N., Takao, T., Ohki, Y., 'Dielectric Loss Measurement of Plasma Polymerized Ethylene Films in Vacuo and Effect of Hydrogen Treatment,' Jpn. J. Appl. Phys., 21, 195, 1982.

[2] Hozumi, N., Takao, T., Kasama, Y, Ohki Y., 'Effect of Atmosphere on Dielectric Properties of Plasma Polymerized Ethylene', Jpn. J. Appl. Phys., 22, 636, 1983.

[3] Sawa, G., Yamanaka, S., Nakamura, S., Yamaguchi, S., 'Improvement of Dielectric Properties of

Plasma Polymerized Styrene with Hydrogen Plasma Treatment', Jpn. J. Appl. Phys., 20, L201, 1981.

[4] Nakano, T., Kasama, Y., Ohki, Y., Yahagi, K., 'Effect of Carrier Gas on Structure of Plasma Polymerized Tetrafluoroethylene Films', Jpn. J. Appl. Phys., 24, 83, 1985.

[5] Boeing, H. V., 'Fundamentals of Plasma Chemistryand Technology' Technomic: Lancaster, PA, 1988.

[6] Chiang, C.K., Druy, M.A., Gau, S.C., Heeger, A.J., Louis, E.J., MacDiarmid, A.G., Park, Y.W., Shirakawa, H., 'Synthesis of Highly Conducting Films of Derivatives of Polyacetylene, (CH)x', J. Am. Chem. Soc., 100, 1013, 1978.

[7] Chiang, C. K., Gau, S. C., Fincher, C. R., Park, Y. W., Mac Diarmid, A. G. and Heeger, A. J., 'Polyacetylene, $(CH)_x$: *n*-type and *p*-type doping and compensation', Appl. Phys. Lett., 33, 18, 1978.

[8] Kaneto, K., Yoshino, K., Inuishi, Y., 'Electrical and optical properties of polythiophene prepared by electrochemical polymerization', Solid State Commun., 46, 389, 1983.

[9] Bhat, N. V., Joshi, N. V., 'Structure and properties of plasma-polymerized thin films of polyaniline', Plasma Chem. Plasma Proc., 14, 151, 1994.

[10] Hsu, S. L., Signorelli, A. J., Pez, G. P., Baughman, R. H., 'Highly conducting iodine derivatives of polyacetylene: Raman, XPS and x-ray diffraction studies', J. Chem. Phys., 69, 106, 1978.

[11] Salaneck, E. W., Thomas H. R., Bigelow R.W., Duke C. B., Plummer E. W., Heeger A. J., Mac Diarmid A. G., 'Photoelectron spectroscopy of iodine doped polyacetylene', J. Chem. Phys., 72, 3674-3678, 1980.

[12] Bhuiyan, A.H., Bhoraskar, S. V, 'Evidence of the formation of a charge-transfer complex between iodine and plasma-polymerized acrylonitrile', Thin Solid Films, 235, 43-46, 1993.

[13] Tassaing, T., Besnard, M., Yarwood, J., 'A mid infrared study of dynamic processes in iodine–pyridine charge transfer complexes', Chem. Phys., 226, 71-82, 1998.

[14] Groenewoud, L.M.H., Engbers, G.H.M., White, R., Feijen, J., 'On the iodine process of plasma polymerized thiophene layers' Synthetic Metals, 125, 429-440, 2002.

[15] Tolansky, S., 'Multiple Beam Interferometry of Surfaces and Films', Clarendon Press, Oxford, 1948.

[16] Bazaka, K., Mohan, V. Jacob and Robert, A. Shanks, 'Fabrication and Characterization of RF Plasma Polymerized Thin Films from 3, 7-Dimethyl-1,6-octadien-3-ol for Electronic and Biomaterial Applications', Adv. Mater. Res., 123-125, 323-326, 2010.

[17] Meyers, R.A. (Ed.), 'Interpretation of Infrared Spectra, A Practical Approach John Coates in Encyclopedia of Analytical Chemistry', 10815–10837, John Wiley & Sons Ltd, Chichester, 2000.

6.1 Conclusions

2-(diethylamino)ethyl methacrylate (DEAEMA) is one of the derivatives of ethyl methacrylate (EMA) which is a methacrylate ester readily polymerizes and rapidly reacts with multifunction methacrylates to form a crosslinked polymer. A parallel plate capacitively coupled glow discharge reactor was successfully used to prepare PPDEAEMA thin films of desired thickness onto glass substrate, at room temperature, by plasma polymerization technique. The core findings of the morphological, thermal, structural, optical, direct current electrical and alternating current dielectric properties of as deposited and modified (heat treated and iodine doped) PPDEAEMA thin films are summarized.

The SEM observations confirm that the as-deposited, heat treated (at 573 K) and iodine doped PPDEAEMA thin films are uniform and pinhole free. The EDAX observations indicate the presence of C, N, O in both the as deposited and heat treated PPDEAEMA thin films. Iodine doped sample indicates the presence of iodine along with C, N and O.

The TGA analysis demonstrates that PPDEAEMA is stable up to 550 K whereas the heat treated PPDEAEMA is stable upto 660 K which show that heat treated PPDEAEMA is more stable. The mass loss may be caused by the thermal breakdown of the PPDEAEMA and expulsion of higher molecular mass hydrocarbons, oxygen containing compounds etc. The DTA curves exhibit exothermic broad band.

The FTIR spectra of PPDEAEMA indicate the details of functional groups present in the PPDEAEMA thin films. The chemical structure of DEAEMA retains to some extent in the PPDEAEMA. During plasma polymerization decomposition of $-CH_3$ occurs, so $-CH_2-$ is observed for as deposited and heat treated spectra. The band C-O-C characterizes the presence of esters, C-N characterize the presence of amides. The presence of C=O and C=C are most prominent in all the spectra. The FTIR spectra of iodine doped PPDEAEMA show shifts in band which may be due to the formation of charge transfer complex to either amine nitrogen site or oxygen site during iodine doping. The absorption coefficient, allowed direct transition, E_{qd}, and allowed indirect transition, E_{qi}, energy gaps of as deposited , heat treated (at 573 K for 1 hour) and iodine doped

PPDEAEMA thin films were determined from the Ultraviolet-visible absorbance spectra and thus Urbach energy, steepness parameter, extinction coefficient were calculated. The E_{qd} and E_{qi} decrease with the increase in thickness and found to be about 3.30 to 3.40 eV and 1.80 to 2.05 eV respectively, for as deposited PPDEAEMA thin films of different thicknesses. Effect of heat treatment on the optical properties in relation to structural changes of PPDEAEMA is also discussed. As temperature increases, both the E_{qd} and E_{qi} decrease. The Urbach energy E_u of the PPDEAMEA thin films increase with the increase in film thickness and heat treatment temperature. The steepness parameter β decrease with thickness and heat treatment temperature. The E_{qd} of iodine doped PPDEAEMA thin films is about 2.93 eV which remains almost stable for different period of iodine doping. The change in energy gap in comparison to as deposited PPDEAEMA thin films indicate that there is a charge transfer complex formation between PPDEAEMA and iodine.

J-V characteristics are determined as a function of voltage and temperature. It is observed that the current increases linearly with the applied voltage in the low voltage region i.e. it shows ohmic behavior and SCLC in the higher voltage region in Al/PPDEAEMA/Al structure sample in the experimental thickness and temperature. The values of current densities are smaller for thin films of higher thicknesses at the same voltage. This may be due to the probable change in physical properties during the formation of the plasma polymerized thin films. Since film morphology is highly thickness dependent and better morphology (lower roughness) is usually observed for smaller thickness, which causes increased charge mobility thus increased conductivity could be observed. The slope of the J-d plot also confirms that the most probable type of charge conduction in PPDEAEMA thin films is SCLC. The carrier mobility was found about 9.48×10^{-19} to 2.78×10^{-18} m^{-2} $V^{-1}s^{-1}$. The free carrier density and the trap density are calculated to be about 1.78×10^{23} to 2.10×10^{22} m^{-3} and 6.88×10^{23} to 1.58×10^{24} m^{-3} respectively for different thicknesses. Activation energies were found to be about 0.12 to 0.20 eV and 0.16 to 0.28 eV for 2 V and 30 V for PPDEAEMA thin films of different thicknesses. These small values of the activation energies suggest the existence of the shallow traps levels in PPDEAEMA thin films and consequently reveal the thermally activated hopping conduction in this material.

The ac electrical conductivity increases sharply as the frequency increases but at very high frequency (near about 10^5 Hz) it starts to become almost stable and it increases a little with the increase of temperature. Ac conductivity reveal that Debye type mechanism is operative in the low frequency region and in the high frequency the values of n are high enough that required for Debye type relaxation process. It is found that the activation energy of PPDEAEMA thin films is very low about 0.02 eV which reveal that conduction may be dominated by hopping of carriers between the localized states at low temperature and thermally excited carriers in the high temperature region. Dielectric constant of PPDEAEMA thin films increases with increasing film thickness and decreases with increasing frequency which may be due to the complex nature of the deposition process of thin films in glow discharge. The characteristic dependence of dielectric constant on frequency could be explained by space charge accumulation at the structural interface of the PPDEAEMA thin films. Dielectric constant decrease slightly as the temperature increases from 298 to 348 K and above this temperature the decrease is quite greater. The strong temperature dependence of dielectric constant at higher temperature is attributed to the thermally activated electron hopping mechanism. Dielectric loss increases with increasing frequency with loss peaks found at higher frequency which was shifted towards lower frequency as the thicknesses of the films increase. Dielectric loss increases as the temperature increase from 298 to 398 K. The temperature dependence of Cole-Cole plot depicts the existence of relaxation distribution with respect to temperature and frequency.

Finally, it is perceived from the summarized findings of the structural, optical and electrical properties of the as deposited, heat treated and iodine doped PPDEAEMA thin films that modifications affect these properties to some extent. The annotations are new additions to the present knowledge of the scientists and researchers in this area of research. These outcomes may help in searching for various applications of this material.

6.2 Suggestions for future work

In this work an attempt is made to investigate the structural, optical and electrical properties of as deposited, heat treated and iodine doped PPDEAEMA thin films. It is

observed that both the optical and electrical properties are thickness and temperature dependent. These properties are also affected by iodine doping.

To study the thickness dependence more precisely the FTIR spectra could be taken and analyzed for the films of different thickness separately to know the probable structural change due to the thickness. The AFM images could also be taken to observe the smoothness of the PPDEAEMA thin films. The XPS investigation which provides quantitative information of the element present could be carried on to study the bonding of different functionalities and chemical states in the thin films of different thickness.

In this work iodine doping was carried out by chamber method but it could also be done by in situ iodine doping process. More PPDEAEMA thin films could be iodine doped for electrical measurement to observe the thickness dependence and dependence upon iodine doping period and also to ensure the dc/ac conduction mechanism.

The aging effect on the structural, optical and electrical properties could also be experimented.

The conductivity of the PPDEAEMA thin films increases after reaction with iodine can be used for the sensing of iodine. More research would be needed to develop a sensor suitable for practical application.

3 Introduction

There are several methods for structural characterization of plasma polymerized thin films such as SEM, EDX analysis, TGA, DTA, FTIR spectroscopy. For optical characterization Ultraviolet and visible absorption spectroscopy is widely used. The direct current (DC) field behavior of a material provides information about the nature of charge carriers, their mobility, conduction mechanism etc., whereas a study in alternating current (AC) electrical field behavior provides information about the electrical nature of the molecular or atomic species which constitutes the dielectric materials, ac conductivity, dielectric relaxation etc. This chapter describes all these techniques from theoretical aspects.

3.1 Scanning Electron Microscopy

The SEM is one of the techniques widely used to obtain surface morphological information of plasma polymerized thin films. This technique has also been used to evidence to see the uniformity and defects of the films produced by plasma. In a SEM, a tiny electron beam is focused onto the sample. Simultaneous to scanning the beam across a selected sample area, generated signals are being recorded and thereby an image is formed pixel by pixel. Valuable information about morphology, surface topology and composition can be obtained. The SEM uses a focused beam of high-energy electrons to generate a variety of signals at the surface of solid specimens. The surface of the object is scanned with the electron beam point by point whereby secondary electrons are set free. The intensity of this secondary radiation is dependent on the angle of inclination of the object's surface. The secondary electrons are collected by a detector that sits at an angle at the side above the object. The signal is then enhanced electronically. The magnification can be chosen smoothly (depending on the model) and the image appears a little later on a viewing screen. The signals that derive from electron-sample interactions reveal information about the sample including external morphology (texture), chemical composition, and crystalline structure and orientation of materials making up the sample [1-2]. Fig. 3.1 represents a schematic diagram of an SEM. In most applications, data are collected over a selected area of the surface of the sample, and a 2-dimensional image is generated that displays spatial variations in these properties. Areas ranging from approximately 1 cm to 5 microns in width can be imaged in a scanning mode using

conventional SEM techniques (magnification ranging from 20X to approximately 30,000X, spatial resolution of 50 to 100 nm).

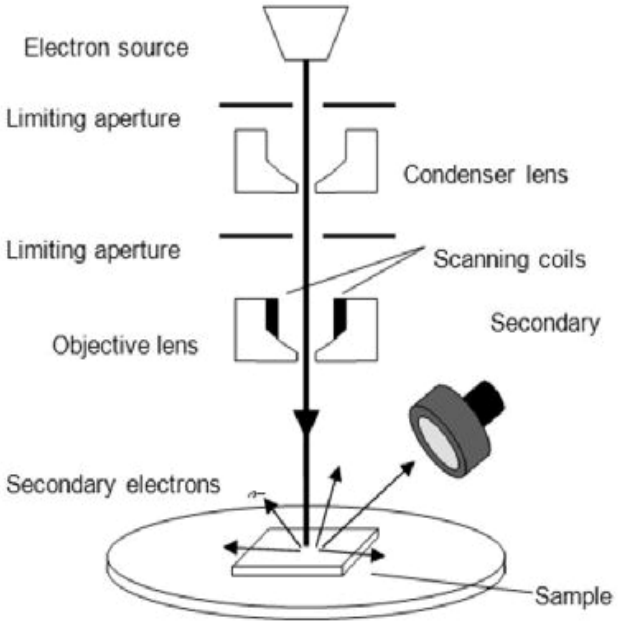

Fig.3.1 A schematic diagram of an SEM.

For compositional investigation an Energy-Dispersive Spectrometer (EDS) attached to the SEM system is used. In case of EDS, the energy of the X-rays is detected using an energy dispersive detector. The X-ray 'count', which is an arbitrary measure of the X-ray intensity, is then plotted against the detected energy. Characteristic X-rays form different elements present in the specimen is the basic phenomenon behind elemental analysis in the region reached by electrons. The PPDEAEMA thin films were deposited onto glass substrates for scanning electron microscopy (SEM). Scanning electron micrographs of PPDEAEMA thin film surfaces were taken using a Scanning Electron Microscope (S-50, FEI Quanta Impact, The Netherlands). Energy Dispersive X-ray of the samples was recorded at the same time by an Energy-Dispersive X-ray Spectrometer (EDS) attached to the SEM.

3.2 Thermogravimetric analysis and Differential thermal analysis

Thermogravimetry is the branch of thermal analysis which examines the mass change of a sample as a function of time in the isothermal mode. TGA is used to characterize the decomposition and thermal stability of materials under a variety of conditions, and to examine the kinetics of the physico-chemical process occurring in the sample. Thermo gravimetric

analysis is a technique in which the mass of a substance is measured as a function of temperature while the substance is subjected to a controlled temperature program. This can be very useful to investigate the thermal stability of a material, or to investigate its behavior in different atmospheres (e.g. inert or oxidizing). It is suitable for use with all types of solid materials, including organic or inorganic materials. Such analysis relies on a high degree of precision in three measurements: weight, temperature, and temperature change. As many weight loss curves look similar, the weight loss curve may require transformation before results may be interpreted. A derivative weight loss curve can be used to tell the point at which weight loss is most apparent. TGA is commonly employed in research and testing to determine characteristics of materials such as polymers, to determine degradation temperatures, absorbed moisture content of materials, the level of inorganic and organic components in materials, decomposition points of explosives, and solvent residues. The technique can analyze materials that exhibit either mass loss or gain due to decomposition, oxidation or loss of volatiles (such as moisture). It is especially useful for the study of polymeric materials, including thermoplastics, thermosets, elastomers, composites, films, fibers, coatings and paints.

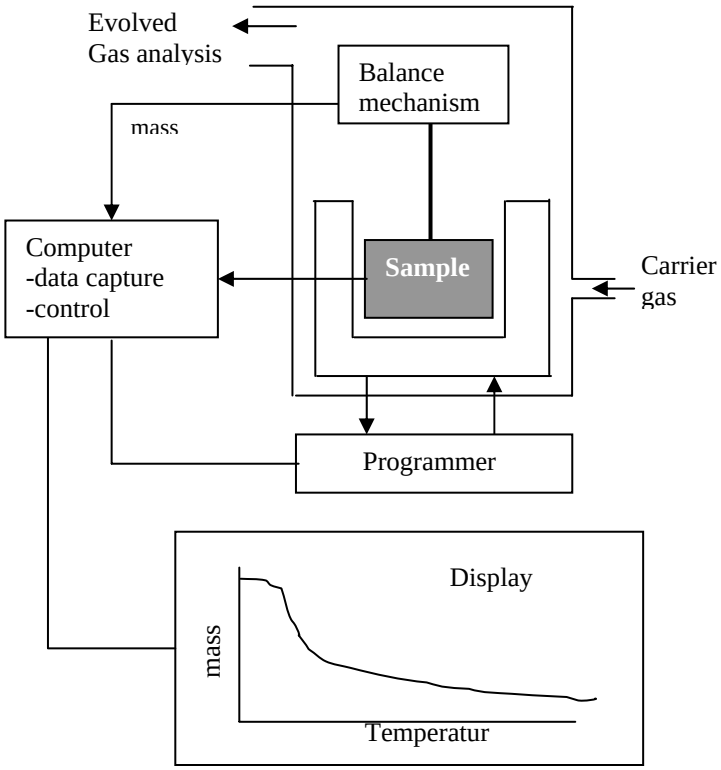

Fig.3.2 A pictorial set-up for TGA measurements.

Fig.3.2 shows the sample balance beam and reference balance beam are independently supported by a driving coil/pivot. When a weight change occurs at the beam end, the movement is conveyed to the opposite end of the beam via the driving coil/pivot, when optical position sensors detect changes in the position of a slit. The signal from the optical position sensor is sent to the balance circuit. The balance circuit supplies sufficient feedback current to the driving coil so that the slit returns to the balance position. The current running to the driving coils to the sample side and the current running to the driving coil on the reference side is detected and converted into weight signals.

Simultaneous TGA/DTA measures both heat flow and weight changes (TGA) in a material as a function of temperature or time in a controlled atmosphere.

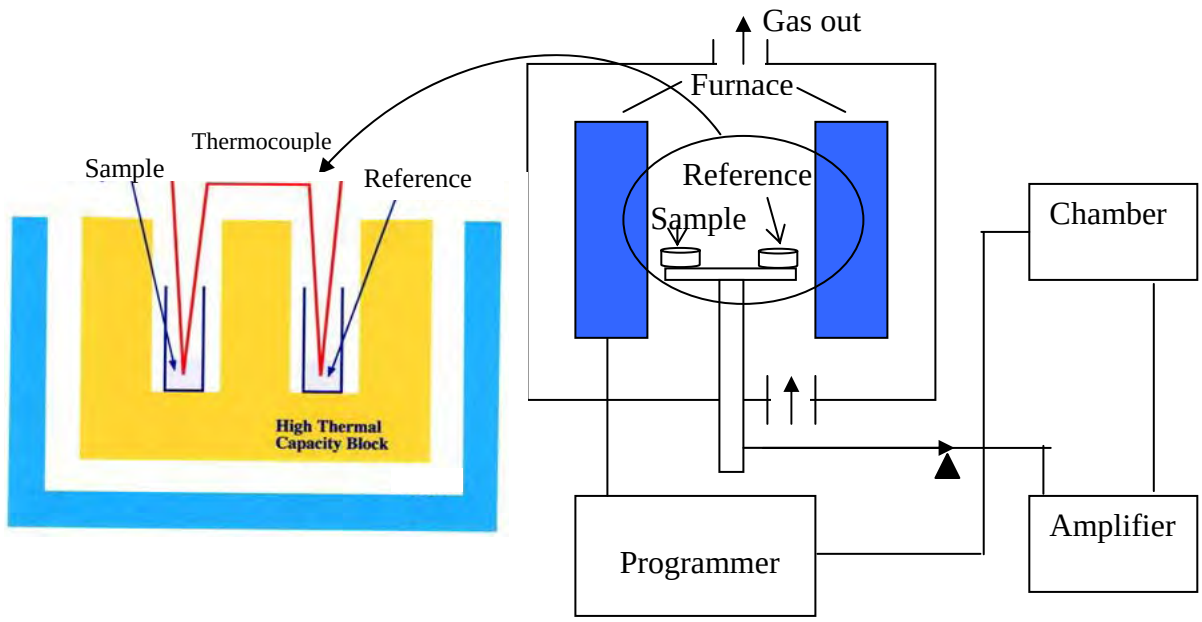

Fig. 3.3 The Basic Differential Thermal Analysis Apparatus

DTA is a thermoanalytic technique. Differential thermal analysis is the most widely used and is probably a very suitable method for the identification and estimation purposes of materials. The chemical or physical changes which are not accompanied by the change in mass on heating are not indicated in thermogravimetric but there is a possibility that such changes may be indicated in DTA. In DTA, the material under study and an inert reference are made to undergo identical thermal cycles, while recording any temperature difference between sample and reference. This differential temperature is then plotted against time, or

against temperature (DTA curve or thermogram). Changes in the sample, either exothermic or endothermic, can be detected relative to the inert reference. Thus, a DTA curve provides data on the transformations that have occurred, such as glass transitions, crystallization, melting and sublimation. The area under a DTA peak is the enthalpy change and is not affected by the heat capacity of the sample. A DTA consists of a sample holder comprising thermocouples, sample containers and a ceramic or metallic block; a furnace; a temperature programmer; and a recording system. Fig. 3.3 shows the basic Differential Thermal Analysis apparatus.

The key feature is the existence of two thermocouples connected to a voltmeter. One thermocouple is placed in an inert material such as Al_2O_3, while the other is placed in a sample of the material under study. As the temperature is increased, there will be a brief deflection of the voltmeter if the sample is undergoing a phase transition. This occurs because the input of heat will raise the temperature of the inert substance, but be incorporated as latent heat in the material changing phase.

3.3 Fourier transform infrared spectroscopic analyses

FT-IR stands for Fourier Transform Infra Red, the preferred method used to obtain an infrared spectrum of absorption, emission, photoconductivity or Raman scattering of a solid, liquid or gas. In infrared spectroscopy, IR radiation is passed through a sample. Some of the infrared radiation is absorbed by the sample and some of it is passed through (transmitted). The resulting spectrum represents the molecular absorption and transmission, creating a molecular fingerprint of the sample. Like a fingerprint no two unique molecular structures produce the same infrared spectrum. This makes infrared spectroscopy useful for several types of analysis. An FTIR spectrometer simultaneously collects spectral data in a wide spectral range. This confers a significant advantage over a dispersive spectrometer which measures intensity over a narrow range of wavelengths at a time. The type of absorption spectroscopy depends upon the type of transition involved and accordingly the frequency range of the EM radiation absorbed. If the transition is from one vibrational energy level to another, then the radiation is from the infrared portion of the EM spectrum and the technique is known as IR spectroscopy. The EM spectrum is shown in the Fig.3.4. The portion of the infrared region is most useful for analysis of organic compounds is not immediately adjacent

to the visible spectrum, but is that having a wavelength range from 2,500 to 16,000 nm, with a corresponding frequency range from 1.9 X 10^{13} to 1.2 X $l0^{l4}$Hz.

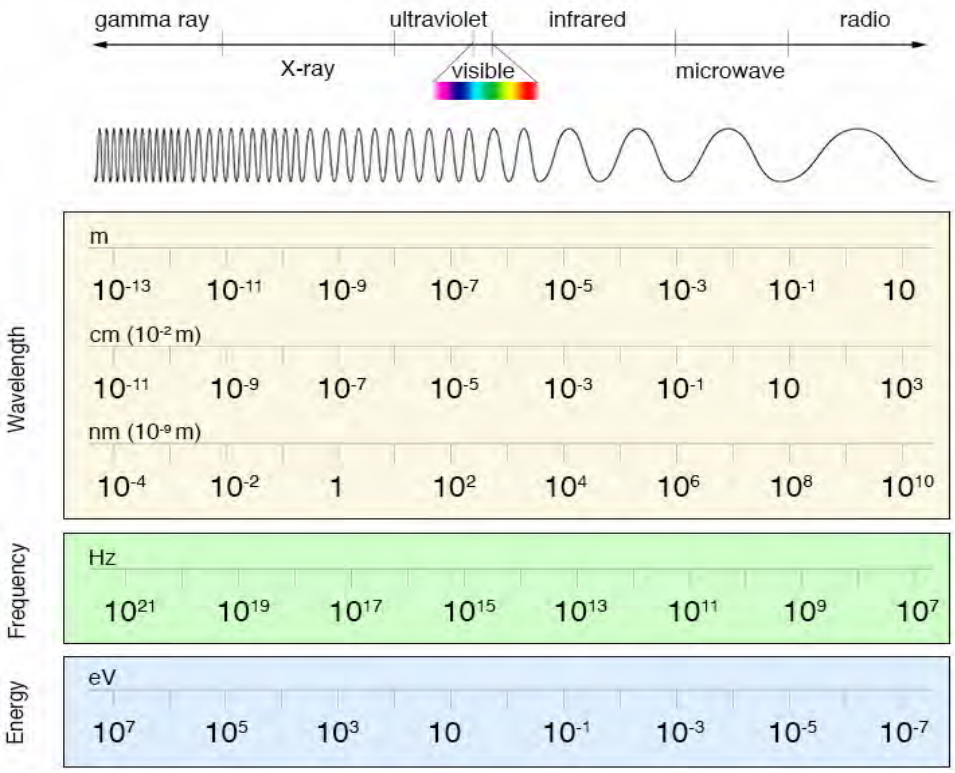

Fig.3.4 The Electromagnetic spectrum.

Photon energies associated with this part of the infrared radiation are not large enough to excite electrons, but may induce vibrational excitation of covalently bonded atoms and groups. Any structural change like addition, substitution, of groups or atoms in a molecule affects the relative mode of vibration of the group. Organic functional groups differ from one another both in the strength of the bonds, and in the masses of the atoms involved. Molecules are flexible, moving collections of atoms. The atoms in a molecule are constantly oscillating around average positions, Bond lengths and bond angles are continuously changing due to this vibration. A molecule absorbs IR radiation when the vibration of the atoms in the molecule produces an oscillating electric field with the same frequency as the frequency of incident IR "light". All of the motions can be described in terms of two types of molecular vibrations. One type of the vibration, a stretch, produces a change of bond length.

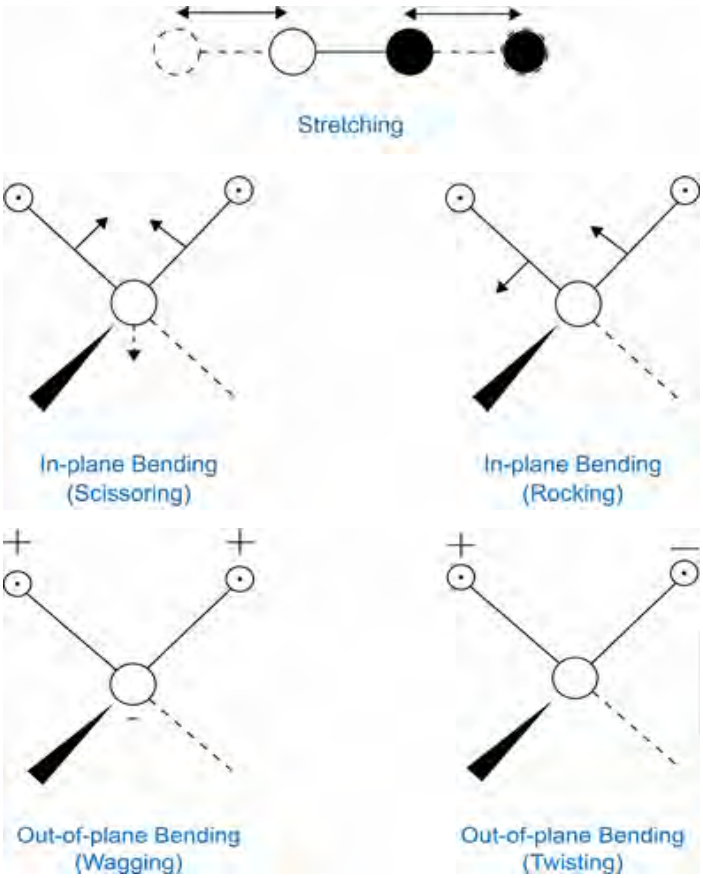

Fig. 3.5 Different kinds of molecular vibrations.

A stretch is a rhythmic movement along the line between the atoms so that inter atomic distance is either increasing or decreasing. The second type of vibration, a bend, results in a change in bond angle. These are also sometimes called scissoring, rocking, etc. motions. Each of these two main types of vibration can have variations. A stretch can be symmetric or asymmetric. Bending can occur in the plane of the molecule or out of the plane; it can be scissoring, like blades of a pair of scissors, or rocking, where two atoms move in the same direction. Molecular asymmetry is a requirement for excitation by infrared radiation and fully symmetric molecules do not display absorbance in this region unless asymmetric stretching or bending transitions are possible. A molecule absorbs only those frequencies of IR light that match vibrations that cause a change in the dipole moment of the molecule.

Assignments for stretching vibrations can be approximated by the application of Hook's law. In the application of the law, 2 atoms and their connecting bond are treated as a simple harmonic oscillator composed of 2 masses joined by a spring. The following equation, derived from Hook's law, states that, the vibrational frequency

$$\bar{\nu} = \frac{1}{2\pi c}\left[\frac{f}{\frac{M_x M_y}{M_x + M_y}}\right]^{1/2}$$

Where c is the velocity of light (cm/sec), F is the force constant of bond (dynes/cm), M_x and M_y is the mass of atom x and atom y, respectively.

In a complicated molecule many fundamental vibrations are possible, but not all are observed. Fig. 3.5 shows different kinds of molecular vibrations. Some motions do not change the dipole moment for the molecule; some are so much alike that they coalesce into one band. even though an IR spectrum is characteristic for an entire molecule, there are certain groups of atoms in a molecule that gives rise to absorption bands at or near the same wave number, ν,(frequency) regardless of the rest of the structure of the molecule. These persistent characteristic bands enable to identify major structural features of the molecule [3-4].

3.4 Ultraviolet and visible absorption spectroscopy

UV-VIS light can cause electronic transitions. When a molecule absorbs UV-VIS radiation, the absorbed energy excites an electron into an empty, higher energy orbital. The absorbance of energy can be plotted against the wavelength to yield a UV-VIS spectrum (Fig. 3.4). Molecular absorption in the UV-VIS region of the electromagnetic spectrum is dependent on the electronic structure of the molecule. Absorption of energy is quantized, resulting in the elevation of electrons from orbital in the ground state to higher energy orbital in an excited state. The relationship between the energy absorbed in an electronic transition and the frequency (ν) of radiation producing the transition is $\Delta E = h\nu$, where h is the Planck's constant. ΔE is the energy absorbed in an electronic transition in a molecule from a low energy state (ground state) to a high energy state (excited state). The energy absorbed is dependent on the energy difference between the ground state and the excited state; the smaller the difference in energy, the longer the wavelength. Each wavelength of light has a particular energy associated with it. If that particular amount of energy is just right for making an energy jump, then that wavelength will be absorbed and its energy will have been used in promoting an electron. Since the relationship between wavelength and frequency is given by the following equation $\lambda = \frac{\nu}{c}$, therefore, it is obvious that higher the frequency, the lower the

wavelength is, i.e., the shorter the wavelength, the greater the energy of the light absorbed and vice versa. The electronic energy levels of simple molecules are widely separated and usually only the absorption of a high energy photon, that is one of very short wavelength, can excite a molecule from one level to another. In complex molecules the energy levels are more closely spaced and photons of near ultraviolet and visible light can effect the transition. These substances, therefore, will absorb light in some areas of the near ultraviolet and visible regions.

A close relationship exists between the color of a substance and its electronic structure. A molecule or ion will exhibit absorption in the visible or ultraviolet region when radiation causes an electronic transition within its structure. Thus, the absorption of light by a sample in the ultraviolet or visible region is accompanied by a change in the electronic state of the molecules in the sample. The energy supplied by the light will promote electrons from their ground state orbitals to higher energy, excited state orbitals or antibonding orbitals. Potentially, three types of ground state orbitals may be involved:

i) σ (bonding), ii) π (bonding) and iii) n (non-bonding) atomic orbital

In addition, two types of antibonding orbitals may be involved in the transition:

i) σ* (anti-bonding) and ii) π* (anti-bonding) orbital

A bond is actually an interaction between two or more atoms or groups of atoms which holds the atoms together. This interaction results from the sharing of electrons in (normally) incomplete shells of adjacent atoms. The predicted paths (orbital) of the bonding electrons about the nucleus give each atom a particular shape which affects the way it bonds with the adjacent atoms. A molecule can have a combination of different types of bond orientations. Bonding occurs where there is a single electron in an orbital intended for two electrons. Antibonding occurs where both electrons are present in an orbital and this inhibits bonding. A transition in which a bonding s electron is excited to an antibonding σ orbital is referred to as σ to σ* transition. In the same way π to π* represents the transition of one electron of a lone pair (non-bonding electron pair) to an antibonding π orbital. The possible electronic transitions which can occur by the absorption of ultraviolet and visible light are shown in Fig. 3.6. In each possible case, an electron is excited from a full orbital into an empty anti-bonding orbital. Each jump takes energy from the light, and a big jump obviously needs more energy than a small one.

$\sigma \rightarrow \sigma^*$ transitions: An electron in a bonding σ orbital is excited to the corresponding antibonding orbital. The energy required is large. For example, methane (which has only C-H bonds, and can only undergo $\sigma \rightarrow \sigma^*$ transitions) shows an absorbance maximum at 125 nm. Absorption maxima due to $\sigma \rightarrow \sigma^*$ transitions are not seen in typical UV-Vis. spectra (200 - 700 nm).

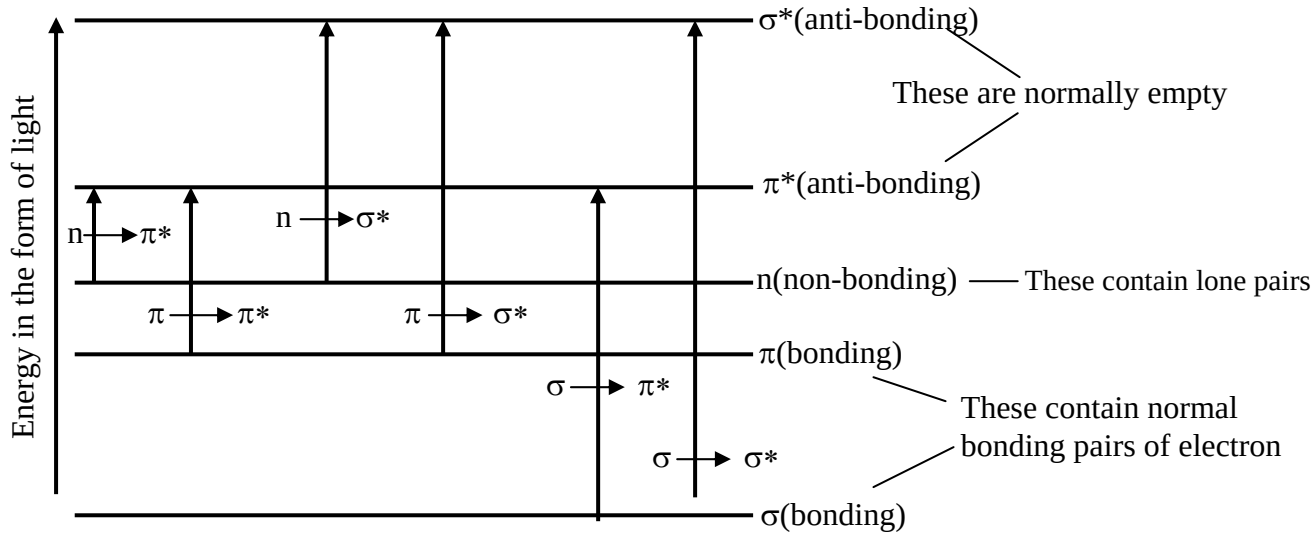

Fig. 3.6 The possible electronic transitions occur by the absorption of ultraviolet and visible light.

***n* $\rightarrow \sigma^*$ transitions:** Saturated compounds containing atoms with lone pairs (non-bonding electrons) are capable of $n \rightarrow \sigma^*$ transitions. These transitions usually need less energy than $\sigma \rightarrow \sigma^*$ transitions. They can be initiated by light whose wavelength is in the range 150 - 250 nm. The number of organic functional groups with $n \rightarrow \sigma^*$ peaks in the UV region is small.

***n* $\rightarrow \pi^*$ and $\pi \rightarrow \pi^*$ transitions:**

Most absorption spectroscopy of organic compounds is based on transitions of *n* or π electrons to the π^* excited state (Fig.3.7). This is because the absorption peaks for these transitions fall in an experimentally convenient region of the spectrum (200 - 700 nm). These transitions need an unsaturated group in the molecule to provide the π electrons.

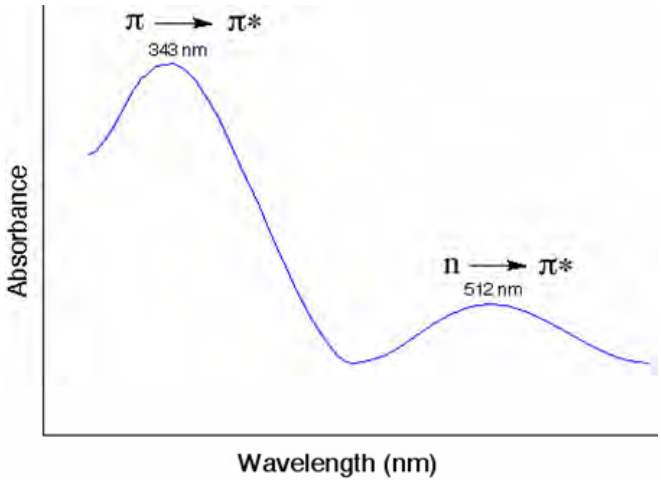

Fig. 3.7 $n \rightarrow \pi^*$ and $\pi \rightarrow \pi^*$ transitions.

Thus, the characteristic energy of a transition and hence the wavelength of absorption is a property of a group of atoms rather than the electrons themselves. When such absorption occurs, two types of groups can influence the resulting absorption spectrum of the molecule [5-6].

3.4.1 Beer –Lambert Law: The law of Absorption

Lambert's law states that the fraction of the incident light absorbed is independent of the intensity of the source. Beer's law states that the absorption is proportional to the number of absorbing molecules. Combining these two laws gives the Beer-Lambert law. The absorption spectrum can be analyzed by Beer-Lambert law, which governs the absorption of light by the molecules. It states that, 'When a beam of monochromatic radiation passes through a homogeneous absorbing medium the rate of decrease in intensity of electromagnetic radiation in UV-VIS region with thickness of the absorbing medium is proportional to the intensity coincident radiation.

$$I = I_0 e^{-\alpha d} \quad \text{.....(3.1)}$$

$$\log_e \left(\frac{I_0}{I} \right) = \alpha d \quad \text{.....(3.2)}$$

Where I_o is the intensity of the incident radiation, I is the intensity of the transmitted radiation, d is the path length of the absorbing species and α is the absorption coefficient. Thus the absorption coefficient is equal to the cross section area that a quantum needs for clear passage. This cross section area is the effective cross section area of an absorbing molecule.

The proportion not absorbed is the same as the probability of a quantum not being absorbed. The absorption spectrum can be analyzed by Beer-Lambert law. It states that, "When a beam of monochromatic radiation passes through a homogeneous absorbing medium the rate of decrease in intensity of electromagnetic radiation in UV-VIS region with thickness of the absorbing medium is proportional to the intensity of coincident radiation". The intensity of transmittance I, is expressed as the inverse of intensity of absorbance. The absorption co-efficient α , can be calculated from the absorption data using the relation (5,2)

$$\alpha = \frac{2.303A}{d} \tag{3.3}$$

where $A = \log_{10}\left(\frac{I_0}{I}\right)$ is the Absorbance.

3.4.2 Direct and Indirect Optical Transitions

In solid state physics and related applied fields, the band gap , also called an energy gap or stop band, is a region where a particle or quasiparticle is forbidden from propagating. For insulators and semiconductors, the band gap represents the minimum energy difference between the top of the valence band and the bottom of the conduction band. Fundamental absorption refers to the annihilation or absorption of photons by the excitation of photons by the excitation of an electron from the valence band up into the conduction band, leaving a hole in the valence band. Both energy and momentum must be conserved in such a transition. However, the top of the valence band and the bottom of the conduction band are not generally at the same value of the electron momentum. In a direct band gap, the top of the valence band and the bottom of the conduction band occur at the same value of momentum, as in the schematic below. In an indirect band gap semiconductor, the maximum energy of the valence band occurs at a different value of momentum to the minimum in the conduction band energy, which is shown in Fig. 3.8. The difference between the two is most important in optical devices. Since a photon can provide the energy to produce an electron-hole pair and each photon of energy E has momentum $p = \frac{E}{c}$, where c is the velocity of light. An optical photon has energy of the order of 10^{-19} J, and, since $c = 3 \times 10^8$ ms^{-1}, a typical photon has a very small amount of momentum. A photon of energy E_g, where E_g is the band gap energy, can produce an electron-hole pair in a direct band gap semiconductor quite easily, because the

electron does not need to be given very much momentum. However, an electron must also undergo a significant change in its momentum for a photon of energy E_g to produce an electron-hole pair in an indirect band gap semiconductor. This is possible, but it requires such an electron to interact not only with the photon to gain energy, but also with a lattice vibration called a phonon in order to either gain or lose momentum.

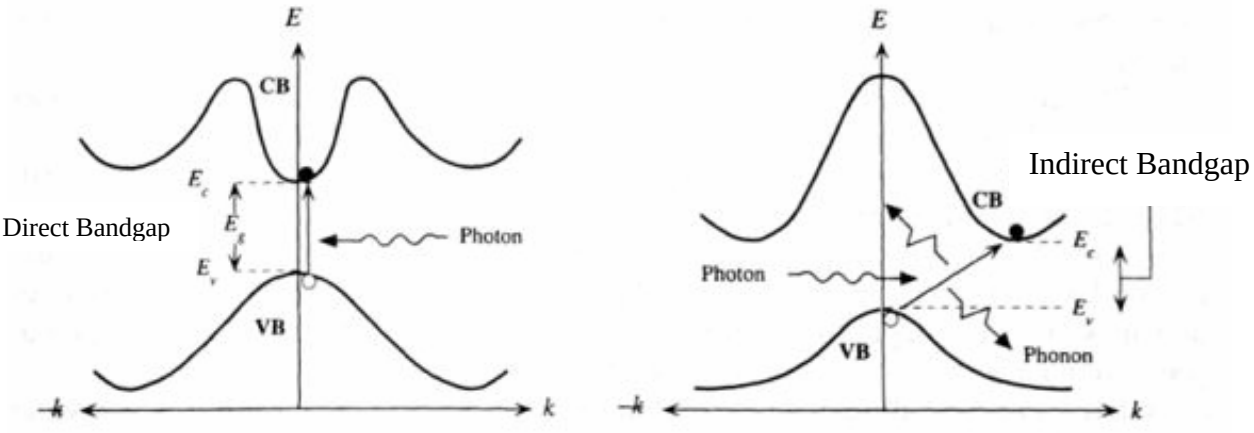

Fig. 3.8 Photon absorption in a direct band gap and an indirect band gap material.

The indirect process proceeds at a much slower rate, as it requires three entities to intersect in order to proceed: an electron, a photon and a phonon. This is analogous to chemical reactions, where, in a particular reaction step, a reaction between two molecules will proceed at a much greater rate than a process which involves three molecules. The same principle applies to recombination of electrons and holes to produce photons. The recombination process is much more efficient for a direct band gap semiconductor than for an indirect band gap semiconductor, where the process must be mediated by a phonon. To estimate the nature of absorption a random phase model is used where the k momentum selection rate is completely related. The integrated density of states N(E) has been used and defined by

$$N(E) = \int_{-\alpha}^{+\alpha} g(E)dE \quad \text{.....(3.4)}$$

The density of states per unit energy interval may be represented by $g(E) = \frac{1}{V}\sum \delta(E - E_n)$ Where V is the volume, E is the energy at which g(E) is to be evaluated and E_n is the energy of the n th state. If $g_v \propto E^p$ and $g_c \propto (E\text{-}E_{opt})$, where energies are

measured from the valence band moility edge in the conduction band (mobility gap), and substituting these values into an expression for the random phase approximation, the relationship obtained $\nu^2 I_2(\nu) \infty (h\nu - E_0)^{p+q+1}$, where $I_2(\nu)$ is the imaginary part of the complex permittivity. If the density of states of both band edges is parabolic, then the photon energy dependence of the absorption becomes $\alpha h\nu \infty \nu^2 I_2(\nu) \infty (h\nu\text{-}E_{opt})^2$

So for higher photon energies the simplified general equation which is known as Tauc relation is $$\alpha h\nu = B(h\nu - E_{opt})^n \qquad \text{.....(3.5)}$$ where $h\nu$ is the energy of absorbed light, n is the parameter connected with distribution of the density of states and *B* is the proportionality factor. The index n equals 1/2 and 2 for allowed direct transition and indirect transition energy gaps respectively [7]. Thus, from the straight-line plots of $(\alpha h\nu)^2$ versus hν and $(\alpha h\nu)^{1/2}$ versus hν the direct and indirect energy gaps of insulators and/or dielectrics can be determined. The fundamental absorption refers to band to band optically induced transitions and it manifests itself by a rapid rising in the absorption used to determine the optical band gap as well as the internal structure [8-9].

3.5 Direct Current Electrical Conduction

The direct current electrical properties of a material provide information about the nature of charge carriers, their mobility, conduction mechanism etc. Electrical conduction in amorphous organic insulating solids has received considerable interest because of their importance in electronic devices. Charge transport measurements in disordered insulators can provide information about the electronic structure of these materials. The disorder in the atomic configuration is thought to cause localized electronic states or groups of states within the material. In the case of organic solids, the conductivity due to electrons excited from valence band to conduction band is negligible and a complex behavior of the dc electronic conduction is observed for these types of materials.

3.5.1 Conductivity of thin films

Electrical properties of polymer thin films are very important. Polymers are insulators and they are not supposed to conduct electrical current, but the electrical properties are changed when subjected to high electric fields and temperatures for long time, and consequently polymers starts to conduct. An insulator is a material which contains very few

volume-generated carriers, in many instances considerably less than one per cm^3, and thus has virtually no conductivity. But the conductivity of the thin film materials which have energy gaps greater than about 2 eV or so, the electrical properties may bear no resemblance to what is intrinsically expected of such a material. This is because it is becoming increasingly clear that the electrical properties of thin film insulators are determined not by the intrinsic properties of the insulator but by other properties, such as the nature of the electrode-insulator contact. A suitable (ohmic) contact is capable of injecting additional carriers into the insulator, far in excess of the bulk-generated carriers. Also the application of a few volts bias is capable of causing inordinately high fields to be generated in a thin film insulator at the cathode-insulator interface. For fields in excess of 10^6 Vcm^{-1}, field-emission injection of relatively large currents from the cathode into the conduction band of the insulator is possible. There are also several reasons for believing that the observed conductivity in thin film insulators is due often to extrinsically rather than intrinsically bulk-generated carriers. For example, at room temperature, the intrinsic current density carried by an insulator is only of the order of 10^{-12} Acm^{-2}. This is many orders of magnitude smaller than the current densities for materials which have energy gaps greater than 3 eV. A second point is that the observed thermal-activation energy associated with the conductivity of the films is much smaller than would be expected ($\approx E_g/2$) if the conductivity were intrinsic in nature. The source of the extrinsic conductivity is thought to be the inherent defect nature of evaporated/deposited chemical compound films. Another important fact to be considered in thin film insulators is traps. Insulating films deposited onto amorphous (e. g., glass) substrates are usually, at best, polycrystalline, and in many cases are amorphous. For crystalline sizes of 100 A, trapping levels as high as 10^{18} cm^{-3} are possible because of grain-boundary defects alone; in vacuum-deposited CdS, trapping densities as high as 10^{21} cm^{-3} have been reported. Furthermore, vacuum-deposited films contain large stresses which induce further trapping centers.

It follows then that thin film vacuum-deposited insulators can contain a large density of both impurity and trapping centers. A judicious study of electrical conduction in vacuum-deposited thin films cannot be accomplished without consideration of these possibilities. Since study of the conductivity of thin films deals primarily with insulators having large energy gaps ($\geq$3 eV), it is concerned mainly with the electron rather than the hole carrier, although the results in general can be applied equally well to either type of carrier. The reason

for this is twofold. First, the hole mobility is usually is much lower than the electron mobility, and thus the hole contribution to the conductivity can usually, but not always, be neglected. Second, in practical insulating films, where, the trapping density is high, the tendency is for a free hole to be trapped quickly and thus become immobilized.

3.5.2 Metal-Insulator Contacts

In order to measure the conductivity of an insulator, it is necessary to connect electrodes to its surfaces in order to facilitate injection of electrons into, and their withdrawal from, the bulk of the insulator. Clearly, the conductivity of the insulator per se will determine the conductivity of the system, since it is much lower than that of the electrodes. In terms of the energy-band picture, the action of the insulator is to erect between the electrodes a potential barrier, extending from the electrode Fermi level to the bottom of the insulator conduction band. This barrier impedes the flow of electrons from one electrode to the other, which would normally flow virtually unimpeded if the insulator were not there (i.e., metal-metal contact). Clearly, then, the height of the potential barrier is an important parameter in conductivity studies in metal-insulator systems. Furthermore, the height of this barrier is determined by the relative alignment of the electrode and insulator energy bands. In thermal equilibrium the vacuum and Fermi levels is continuous through the system. The vacuum level represents the energy of an electron at rest just outside the surface of the material, and the energy difference between the vacuum and Fermi levels is called the work function of the material. It would appear that the equilibrium conditions can be satisfied only when the work function of the metal ψ_m and that of the insulator ψ_i are equal. However, the equilibrium condition is satisfied when $\psi_m \neq \psi_i$**,** [Fig. 3.9] because of charge transfer from the electrode to the insulator or vice versa.

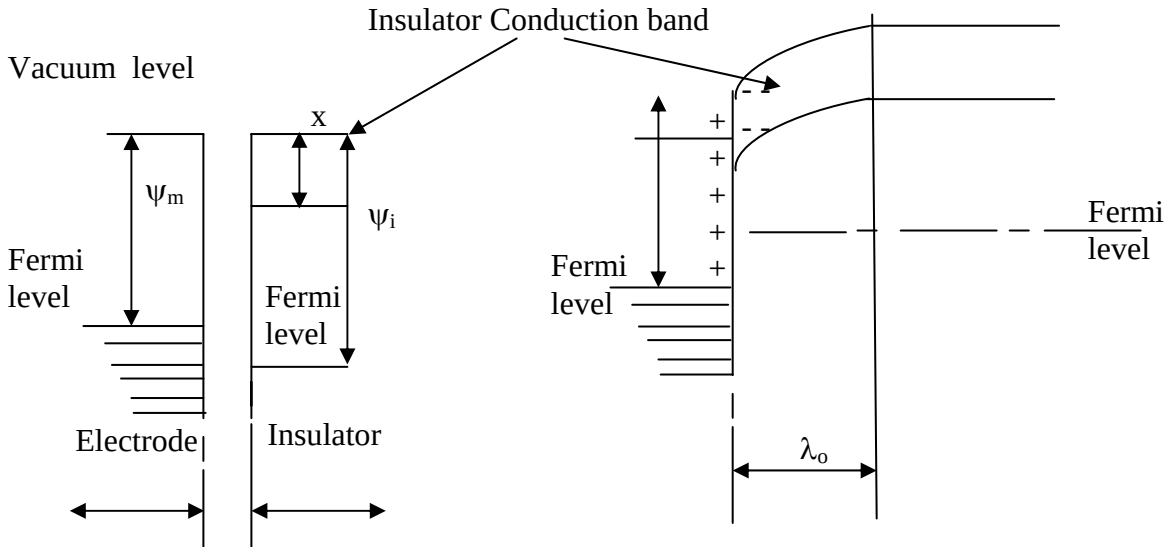

Fig. 3.9 Energy diagram representing of the ohmic contact when $\psi_m < \psi_i$.

The shape of the potential barrier just within the surface of the insulators depends on whether or not the insulator is intrinsic or extrinsic, and on the relative magnitudes of the work functions of the metal and insulator, among other things. At reasonable applied fields there will normally be a sufficient supply of carriers available to enter the insulator from the cathode (negatively biased electrode) to replenish the carriers drawn out of the bulk of the insulator. Under these conditions the *I-V* characteristics of the sample will be determined by the bulk properties of the insulator; we thus refer to this conduction process as being bulk-limited. At high fields, or if the contact is blocking, the current capable of being supplied by the cathode to the insulator will be less than that capable of being carried in the bulk of the insulator. Under these conditions the *I-V* characteristics of the sample will be controlled primarily by conditions existing at the cathode-insulator interface; this conduction process is referred to as being emission-limited or contact-limited. The types of contact that can exist at a metal-insulator interface fall into three categories: (i) ohmic contact, (ii) neutral contact, (iii) blocking contact.

3.5.3 Factors Influencing the Electrical Properties

The following factors influence the electrical properties: [8]

i) Size effect i.e. surface scattering and tunneling of charge carriers,

ii) Method of film preparation i.e. deposition method and deposition parameters.

iii) Electrode effect

iv) Degree of film continuity

v) Existence of high electric field phenomenon i.e. small voltage applied across very small dimension produces high field effects in thin films.

3.5.4 Types of Conduction mechanism

The various types of conduction mechanism in insulating film have been extensively studied. In general an insulator possesses very few charge carriers at normal temperatures and large energy gap. In most cases, insulating films are amorphous in nature and the usual model of sharply defined energy bands can not be readily applied, but fuzzy tails arise both at the top of the valence band and the bottom of the conduction band [10]. A relatively high density of

charge carriers may be present due to structural imperfection and they tend to be localized or trapped at these centers which causes the insulating property having low mobilities. In general, amorphous solid has very complicated conduction mechanism, in which electrons, ions and holes influence on the current transport. Different electrical phenomena may arise by insulating films when sandwiched between combinations of metal and semiconductor electrodes. The various conduction processes may take place in case of wide gap semiconductors and insulators depending on the trap density, the depth of the trap energy levels below the conduction band and the size of the Schottky barrier at the contacts. The different mechanisms are described below:

3.5.4.1 Schottky mechanism

The Schottky mechanism is the emission of electrons into the conduction bandof an insulator from the metal contact electrode by thermal activation over the electric field which lowers the metal-insulator interfacial barrier. The phenomena, that the lowering of the potential barrier height by the interaction of the applied electric field and the image force is called Schottky effect. The abrupt changes in potential at the metal-insulator interface as seen in the energy diagram are physically unrealistic, since abrupt changes in potential imply infinite electric fields. Actually the potential step changes smoothly, as a result of the image force. This image force arises as a result of the metal surface's becoming polarized (positively charged) by an escaping electron. This escaping electron in turn exerts an attractive force $F_{im} = -\frac{e^2}{16\pi\varepsilon_0\varepsilon' x^2}$ on the electron. So, the potential energy of the electron due to this image force is given by

$$\phi_{im} = -\frac{e^2}{16\pi\varepsilon_0\varepsilon' x} \tag{3.6}$$

where, x is the distance of the electron from the electrode surface, e is the electronic charge, ε_0 is the permittivity of free space and ε' is the dielectric constant of the insulator. The image force effects play an important role in the conduction process when the current is electrode limited. The potential step with respect to the Fermi level at a neutral barrier with attendant image potential as a function of the distance x from the interface is given by,

$$\varphi(x) = \varphi_0 + \varphi_{im} = \varphi_0 - \frac{e^2}{16\pi\varepsilon_0\varepsilon' x} \tag{3.7}$$

where φ_0 is the Coulombic barrier height of the electrode-polymer interface. The barrier potential $\phi(x)$ in the presence of image forces is illustrated by the line AB in Fig. 3.10.

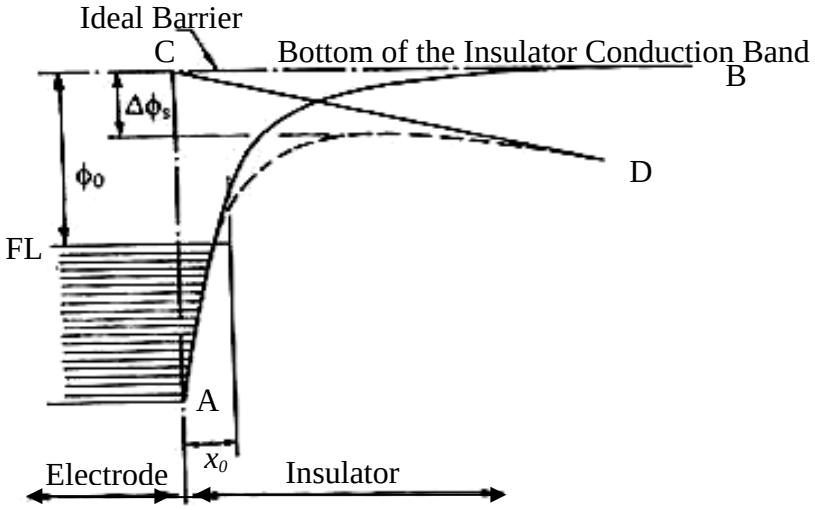

Fig. 3.10 Schottky effect at a neutral contact.

Clearly eq. (3.6) is not valid at the electrode surface, since φ= -∞ there. Schottkey assumed that the image force holds only for x greater than some critical value x_0. For $x < x_0$, he assumed a constant image force; that is, the potential energy is a linear function of x, and such that it matches the bottom of the electrode conduction band at the surface.

When an electric field exists at a metal-insulator interface, it interacts with the image force and lowers the potential barrier (Fig. 3.10). The line CD represents the potential due to a uniform field, which when added to the barrier potential φ(x) produces the potential step shown by the dotted line which is seen to be $\Delta\varphi_s$, lower than without the electric field. The potential energy of the barrier under the influence of the field with respect to the Fermi level of the electrode is given by

$$\phi(x) = \phi_0 - \frac{e^2}{16\pi\varepsilon'\varepsilon_0 x} - eFx \tag{3.8}$$

This equ^n has a maximum at $x_m = \left(\frac{e}{16\pi\varepsilon'\varepsilon_0 F}\right)^{1/2}$. The change $\Delta\varphi_s = \varphi_0 - \varphi(x_m)$ in the barrier height due to the interaction of the applied field with the image potential is thus given by

$$\Delta\phi_s = \left(\frac{e^3}{4\pi\varepsilon'\varepsilon_0}\right)^{1/2} F^{1/2} \equiv \beta_s F^{1/2} \tag{3.9}$$

where, $\beta_s = \left(\frac{e^3}{4\pi\varepsilon'\varepsilon_0}\right)^{1/2}$ is the Schottky coefficient, ε' is the high frequency dielectric constant. Because of image-force lowering of the barrier, the electrode-limited current does not saturate according to the Richardson law

$$J = AT^2 \exp\left(-\frac{\phi_0}{kT}\right) \tag{3.10}$$

but rather obeys the Richardson-Schottky law

$$J = AT^2 \exp\left(-\frac{\phi_0 - \Delta\phi_s}{kT}\right) \tag{3.11}$$

$$J = AT^2 \exp\left(\frac{\beta_s F^{1/2} - \phi_0}{kT}\right) \tag{3.12}$$

$$J = AT^2 \exp\left(-\frac{\phi_0}{kT}\right) \exp\frac{\beta_s F^{1/2}}{kT} \tag{3.13}$$

where $A = 4\pi ek^2/h^3$ is the Richardson constant,

F = static electric field =V/d

V = applied voltage,

d = film thickness

T = Temperature in K

k = Boltzmann constant

The Richardson-Schottky effect in insulators appears to have been first observed by Emptage and Tantraporn [11], who reported a log I vs. $F^{1/2}$ relationship in their samples; since then there have been many other reported similar observations.

3.5.4.2 Poole-Frenkel effect

The original theory of PF effect was put forward by Frenkel [12]. PF effect is also known as field-assisted thermal ionization process. This process is the bulk analog of the Schottky effect at an interfacial barrier. This effect is lowering of a Coulombic potential barrier when it interacts with an electric field as shown in Fig. 3.11.

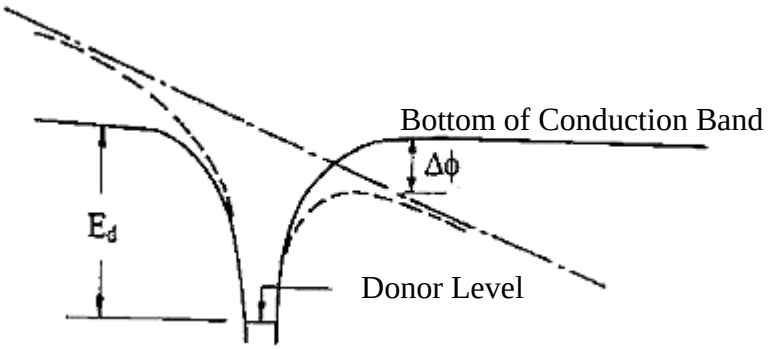

Fig. 3.11 Poole-Frenkel effect at a donor center.

Since the potential energy of an electron in a Coulombic field $-\frac{e^2}{4\pi\varepsilon_0\varepsilon' x}$ is four times that due to the image-force effects, the PF reduction of a Coulombic barrier $\Delta\varphi_{PF}$ in a uniform electric field is twice that due to the Schottky effect in a neutral barrier:

$$\Delta\phi_{PF} = 2\Delta\phi_s = 2\left(\frac{e^3}{4\pi\varepsilon'\varepsilon_0}\right)^{1/2} F^{1/2} \equiv \beta_{PF} F^{1/2}$$

Here, β_{PF} is the PF coefficient defined by

$$\beta_{PF} = 2\left(\frac{e^3}{4\pi\varepsilon'\varepsilon_0}\right)^{1/2} = 2\beta_s \tag{3.14}$$

This result was first applied by Frenkel to the host atoms in bulk semiconductors and insulators. He argued that the ionization potential E_g of the atoms in a solid is lowered by an amount given by (3.14) in the presence of a uniform field. Thus the conductivity is obtained by substituting E_g-$\Delta\varphi_{PF}$ for E_g in $I=e\mu N_c F$ exp(-$E_g/2kT$) yielding a field-dependent conductivity of the form

$$\sigma = \sigma_0 \exp\left(\frac{\beta_{PF} F^{1/2}}{2kT}\right) \tag{3.15}$$

where $\sigma_0 = e\mu N_c F$ exp (-$E_g/2kT$) is the low-field conductivity, e is the electronic charge, μ is the mobility, F is the field in the insulator, N_c is the effective density of states in the insulator, E_g is the insulator gap, k is Boltzmann's constant, and T is the absolute temperature. Equation (3.15) may be written in the form

$$J=J_0 \exp\left(\frac{\beta_{PF} F^{1/2}}{2kT}\right) \tag{3.16}$$

where $J_0 = \sigma_0 F$ is the low-field current density.

It is to be noted that although $\Delta\phi_{PF} = 2\Delta\phi_s$, the coefficient of $F^{1/2}$ in the exponential is the same for both Richardson-Schottky and PF characteristics. Since traps abound in an insulator and that a trap having a Coulombic-type barrier would experience the PF effects at high fields, thereby increasing the probability of escape of an electron immobilized therein, the current density in thin film containing shallow traps is given by

$$J = J_0 \exp\left(\frac{\beta_{PF} F^{1/2} - \phi_c}{kT}\right) \tag{3.17}$$

where, ϕ_c is the ionization potential of the PF centers.

Therefore, the general expression for the current density, *J*, that holds equally well for both the PF and the Schottky mechanisms is of the form

$$J = J_0 \exp\left(\frac{\beta F^{1/2} - \phi}{kT}\right) \tag{3.18}$$

For a constant applied voltage at a particular temperature the current density expression (Eq. 3.18) can be written as $\log J \approx d^{1/2}$. Thus, for the PF or the Schottky mechanism the plot of log*J* against the square root of the film thickness, $d^{1/2}$, should be a straight line.

3.5.4.3 Space charge limited conduction process

Space charge means charges in space, i.e. in a region where there is a concentration of charges in the form of electrons, holes or ions. These charges may be mobile or localized, but constitute non-uniform localized field. Transport of the charges under the influence of non-uniform electric field is called SCLC, which is observed in many polymer insulating materials [13].

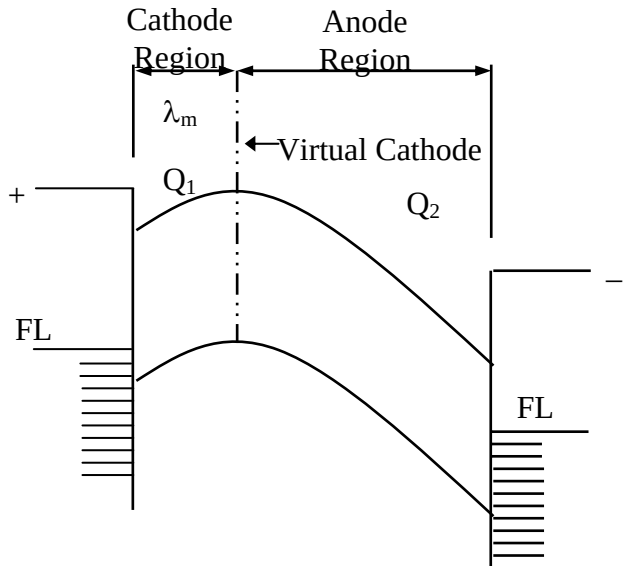

Fig. 3.12 Energy diagram illustrating virtual cathode, cathode region, and anode region under space-charge-limited condition.

An insulator which does not contain donors and which is sufficiently thick to inhibit tunneling will not normally conduct significant current. If an ohmic contact is made to the insulator, the space charge injected into the conduction band of the insulator is capable of carrying current; this process is termed SCLC. In order to gain physical insight into this process, let us consider what happens when a bias is applied to system shown in Fig.3.12, that is, an insulator having two ohmic contacts on its surfaces. The result of the applied bias is to add positive charge to the anode and negative charge to the cathode. When the voltage bias increases, the net positive charge on the anode increases and that on the cathode decreases. Calling the charge on the cathode Q_1, that on the anode Q_2 and the negative space-charge density $\rho(x)$, the condition of electrical neutrality demands that

$$\int_0^d \rho(x)dx = Q_1 + Q_2 \tag{3.19}$$

$$\int_0^{\lambda_m} \rho(x)dx + \int_{\lambda_m}^{d} \rho(x)dx = Q_1 + Q_2$$

where λ_m is chosen such that

$$\int_0^{\lambda_m} \rho(x)dx = Q_1 \tag{3.20}$$

$$\int_{\lambda_m}^{d} \rho(x)dx = Q_2 \tag{3.21}$$

The insulator has thus been divided into portions with λ_m as the boundary separating the two. The significance of equations (3.20) and (3.21) is that the positive charge on either contact is neutralized by an equal amount of negative charge contained between the contact and the plane at $x = \lambda_m$. From a consideration of equations (3.20) and (3.21) and the fact that Q_1 decreases and Q_2 increases with increasing voltage, it will be clear that the virtual cathode moves closer to the cathode as the applied voltage increases, that is, the cathode region decreases and the anode region increases. Eventually, when $Q_1 = 0$, the virtual coincides with the physical cathode-insulator interface. Under this condition, the anode region extends throughout the whole of the insulator, and an ohmic contact no longer exists at the cathode-

insulator interface. Thus, for further increasing voltage bias, the conduction process is no longer space-charge-limited, but rather it is emission-limited.

Trap-free insulator: By assuming that the anode region extends throughout the insulator, so we may neglect the diffusion current. Thus, the current density may be written as

$$J = \rho(x)\,\mu F$$

From Poisson's equation, $$\frac{dF}{dx} = -\frac{\rho(x)}{\varepsilon'\varepsilon_0}$$

Using the boundary conditions, the Mott and Gurney [14] equation for current density

$$J = \frac{9\mu\varepsilon'\varepsilon_0 V^2}{8d^3} \tag{3.22}$$

where μ is the mobility of the charge carrier, ε' is the dielectric constant, ε_0 is the permittivity of free space, V is the applied voltage and d is the thickness of the insulator. The interesting features of eq. (3.22) are that it predicts that SCL current is proportional to V^2 and inversely proportional to d^3, both these predictions have since been confirmed by experiment. However, equ^n. (3.22) predicts much higher currents than are observed in practice, and also that SCL currents are temperature-insensitive, which is also contrary to observation.

Defect Insulator: The theory of SCL currents in defects insulators is due initially to Rose [15]. If the insulator contains traps, a large fraction of the injection space charge will condense therein, which means that the free carrier density will be much lower than in a perfect insulator. Furthermore, since the occupancy of traps is a function of temperature, the SCL current is temperature-dependent. By separating the space charge into a trapped ρ_t and a free ρ_f component thus, $J = \rho_f \mu F$ and $\frac{dF}{dx} = -\frac{\rho_f + \rho_t}{\varepsilon'\varepsilon_0}$.

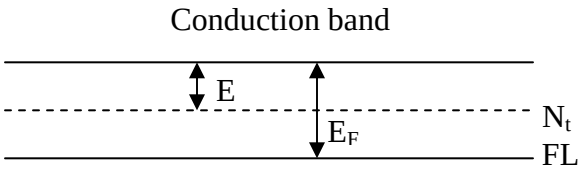

Fig. 3.13 Energy diagram showing shallow traps.

If the insulator contains N_t shallow traps (Fig.3.13) positioned an energy E_t below the conduction band then

$$\rho_f = eN_C \exp\left(-\frac{E_F}{kT}\right) \tag{3.23}$$

and

$$\rho_t = eN_t \exp\left(\frac{-(E_F - E_t}{kT}\right) \tag{3.24}$$

Thus trapping factor, θ is defined as

$$\theta \equiv \frac{\rho_f}{\rho_t} = \frac{N_c}{N_t}\exp\left(-\frac{E_t}{kT}\right) \tag{3.25}$$

where N_c is the effective density of states in the conduction band, and N_t is the density of trapping levels situated at an energy E_t below the conduction band edge.

Therefore, SCLC current density with traps can be expressed as

$$J = \frac{9\mu\varepsilon'\varepsilon_0 V^2}{8d^3}\theta \tag{3.26}$$

It is clear that the effect of shallow trapping centers into the theory by way of the factor θ, and since it is independent of V, $J \alpha V^2$ as in the trap-free case.

For trap-free SCLC, θ = 1. According to equation (3.26), J varies as d^{-1} in the Ohmic region and as d^{-3} in the SCLC region for the trap-filled SCLC part. For a fixed V, the dependence of *logarithm of J* on *logarithm of d* should be linear with slope $l \geq -3$.

Lampert [16] calculated the voltage at which the transition from the ohmic to shallow trap SCLC region (V_{tr}) occurs is given by

$$V_{tr} = \frac{8}{9} n_0 \frac{ed^2}{\varepsilon'\varepsilon_0} \tag{3.27}$$

where volume generated free carrier density, n_0 is independent of both μ and J. Lampert [16] has pointed out that if sufficient charge is injected into the insulator, the traps will become filled (trap-filled limit, V_{TFL}). Further injected charge then exists as free charge in the conduction band and contributes in to the current. Beyond the TFL, the *J-V* characteristic can be given by eq. (3.22) rather than eq. (3.26). Fig. 3.14 shows schematically a typical *I-V* characteristic for an insulator having a shallow discrete trapping level. At the lower voltages ($V<V_{tr}$), the characteristic is ohmic, because the bulk generated current exceeds the SCL current. In the voltage range $V_{tr}<V<V_{TFL}$ the SCLC predominates and $I \alpha V^2$, (Eq. 3.26). When $V= V_{TFL}$ sufficient charge has been injected into the insulator to fill the gaps. Hence, as V just exceeds V_{TFL} the current rises rapidly such that for $V> V_{TFL}$, the *I-V* characteristic obeys

the trap-free law, (Eq. 3.22). Clearly, from the structure exhibited in the characteristic, much information about the traps in insulators can be deduced from the experimental data.

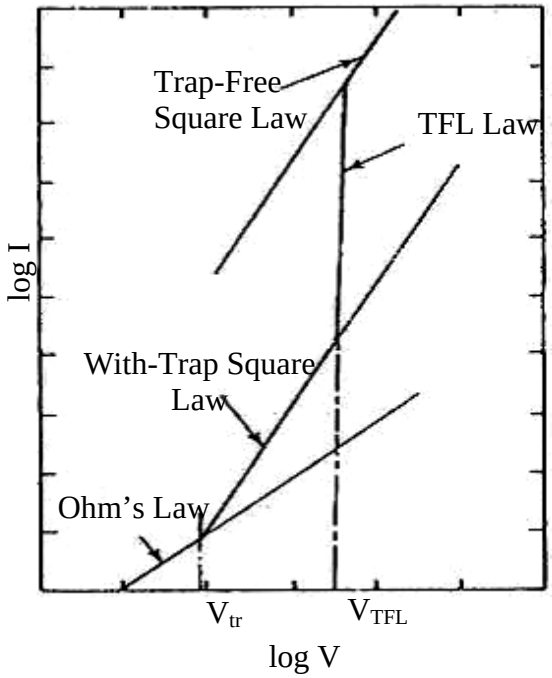

Fig. 3.14 SCLC *I-V* characteristic for an insulator containing shallow traps.

3.5.4.4 Tunneling effect-for very thin insulators

If the energy of an electron is less than the interfacial potential barrier in a metal-insulator-metal junction upon which it is incident, classical physics predicts certain reflection of the electron at the interface; that is the electron can not penetrate the barrier and hence its passage from one electrode to the other is precluded. Quantum theory however contradicts this idea. The quantum mechanical wave function $\psi(x)$ of the electron has finite values within the barrier and since $\psi(x)\ \psi^*(x)dx$ is the probability of finding the electron within the incremental range x and x+dx, this means that the electron can penetrate the forbidden region of the barrier. The wavefunction decays rapidly with depth of penetration of the barrier from the electrode-insulator interface and for barriers of macroscopic thickness is essentially zero at the opposite interface indicating zero probability of finding the electron there. However if the barrier is very thin (<50 Å), the wavefunction has a nonzero value at the opposite interface. For this case, there is a finite probability that the electron can pass from one electrode to other by penetrating the barrier. The penetration probability of an electron from one electrode to the other through the insulator is much dependent on the applied electric

field. The effects of temperature, effective mass of electron in the conduction band, image forces, dielectric constant and shape of the potential barrier must all be taken into account in calculating the tunnel currents.

Experimental results show the possibilities for direct tunneling from one metal to the other in films having thickness less than 100 Å. When tunneling takes place from the metal to the conduction band of the insulator the effect of space charges, image forces and traps present in the insulator on the potential barrier should be considered.

3.6 Electronic Conduction in Polymers

Electrical conductivity of materials is a property which spans a very wide range. Organic compounds typically have conductivities eighteen orders of magnitude smaller than those of metals, and the polymeric subgroup falls at the low-conductivity end, with polyethylene and polystyrene being amongst the best insulator known. In contrast, metallic superconductors have immeasurably high conductivities in their low temperature, superconducting regimes.

Electrical conduction may occur through the movement of either electrons or holes. The basic equation for the conductivity is $\sigma = q\, n\, \mu$ (3.28) where the conductivity σ is resolved into three factors: the charge q, concentration n and drift mobility μ of the carriers. The later parameter (i. e. mobility) parameter characterizes the ease with which the charged species will move under the influence of the applied electric field. There may be contributions to the conductivity from different types of carriers, notably electrons and holes in electronic conductors, and cation and anion pairs in ionic conductors. In most polymeric materials it is very difficult to observe any electronic conductivity at all and conductivity usually depends on the movements of adventitious ions. Electronic conduction in organic, molecular compounds differs in several ways from the more familiar kind in metals and inorganic semiconductors like silicon and germanium. The well-known band theory of atomic lattices has provided the essential basis of concepts and language for the discussion of conduction in molecular solids. An important feature of the band system is that electrons are delocalized or spread over the lattice. Some delocalization is naturally expected when an atomic orbital of any atom overlaps appreciably with those of more than one of its neighbors, but delocalization reaches an extreme form in the case of a regular, 3-dimensional lattice. In a full band there can be no net flow of electronic charge under an external electric field.

Intrinsic conduction can therefore only occur when electrons are promoted across the band gap into the conduction band by some means. Then both this electron and hole in the valence band can contribute to net charge flow. Promotional energy can be obtained by direct photon absorption or by raising the temperature when an occasional electron may receive sufficient thermal energy from the lattice. As the temperature is increased the charge carrier concentration increases strongly with temperature. This dominates the temperature dependence of the conductivity, giving it an Arrhenius - like character. It is difficult to generalize about the temperature dependence of dc conduction whether it is ionic or electronic since so many processes are possible. Ohmic (low field) conduction whether ionic or electronic, gives exponential temperature dependence, given by

$$J = J_0 \exp \frac{-\Delta E}{kT} \tag{3.29}$$

where J_0 is a constant and ΔE is the activation energy for carrier generation.

3.6.1 Hopping Conduction

In amorphous semiconductors hopping between localized states is well known. A group of states or levels due to impurities, physical disorder, or band tails in the band gap may exist close to the Fermi level resulting in an adequate concentration of electrons in these states and adequate concentration of empty states. Thermal excitation and de-excitation of an electron from a full state to an empty one now can occur.

That is, for a random distribution of atoms the density of electronic energy states tails into what is normally the forbidden zone, and electrons in these tails are localized. There is then not so much an energy gap as a mobility gap. In other words there is an intermediate range of electronic energy states in which the mobilities are very low. Conduction via localized electrons implies discrete jumps across an energy barrier from one site to the next as shown in Fig. 3.15. An electron may either hop over, or tunnel through, the top of the barrier, the relative importance of these two mechanisms depending on the shape of the barrier and the availability of thermal energy. For variable range hopping the electrical conductivity is given by $\sigma = \sigma_o \exp[-\left(\frac{T_o}{T}\right)^{\frac{1}{d+1}}]$ (3.30) where "d" is

the dimensionality of transport, σ is the conductivity, σ_o is the initial value of conductivity, T is the absolute temperature and T_o is the activation energy in terms of temperature.

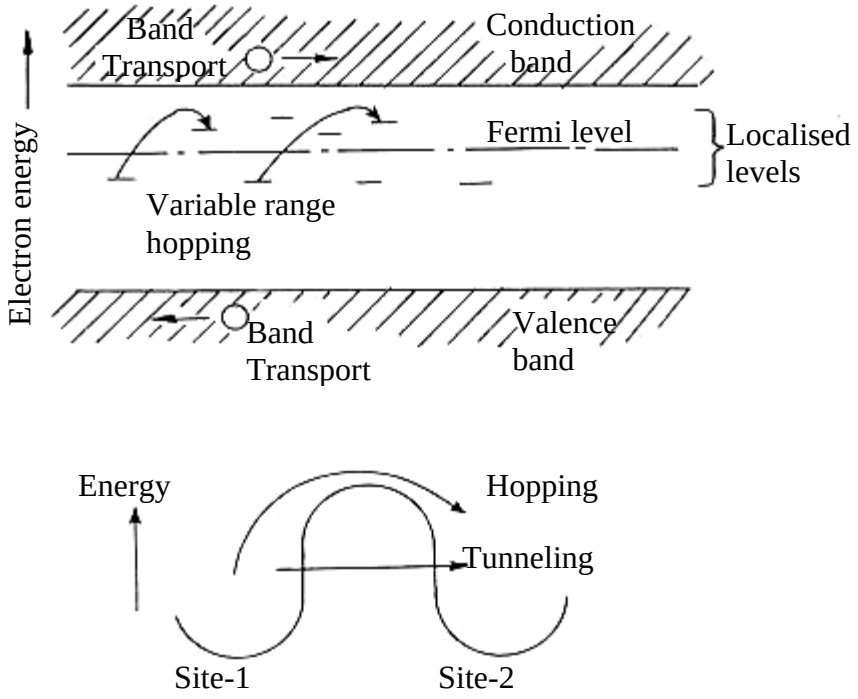

Fig. 3.15 Diagram of electron-transfer mechanisms between adjacent sites separated by a potential energy barrier.

3.6.2 Ionic Conduction

Ionic conduction consists of the transit of ions (atoms of positive or negative charge) from one site to another via point defects called vacancies in the crystal lattice. At ambient temperatures very little ion hopping takes place, since the atoms are at relatively low energy. For ionic conductivity, transport of one or more types of ions across the material is necessary. In an ideal crystal all constituent ions are arranged in regular periodic fashion and are often stacked in a close-packed form. Thus there is little space for an ion to diffuse. Often, the available space is just enough for vibration around its equilibrium position. However, at any non-zero temperature there exist defects. These could, for example, be positional disorder due to deviation from ideal stacking. The degree of such disorder can vary from one material to another or even from one temperature or pressure to another in the same material. The current

density J flowing through a specimen across which an electric field E is applied can be expressed as

$$J = \sinh(\frac{eaE}{2kT}) \tag{3.31}$$

where E is the electric field, a is the distance between neighboring potential wells, e is the electronic charge. Although it is not possible to identify the ions experimentally, it may be assumed that they are mainly derived from fragments of polymerization catalyst, degradation and dissociation products of the polymer itself, and absorbed water.

3.7 Plasma Polymers as Dielectrics

Polymer dielectric films, ranging in thickness from less than 100 Å to several microns, have become increasingly useful for basic investigations of surface phenomena and thin film electrical conductivity and for thin film electronic device and circuit development. Plasma polymers contain a certain number of polar groups independent of whether the monomer was polar or non-polar. And this presence of polar groups has significant role for the relatively high dielectric losses in plasma polymers. Most conventional polymers are non-polar and their dielectric losses are extremely low. Polar polymer has dielectric losses significantly higher. The dielectric constants of plasma polymerized films are slightly higher than those of the conventional polymers.

3.7.1 Brief Description of dielectrics

Dielectrics are materials which have no free charges; all electrons are bound and associated with the nearest atoms. An external electric field causes a small separation of the centers of the electron cloud and the positive ion core so that each infinitesimal element of volume behaves as an electric dipole. Dielectrics may be subdivided into two groups (Fig. 3.16):

Polar Dielectric: A polar dielectric is one in which the individual molecules possess a permanent dipole moment even in the absence of any applied field; that is, the center of positive charge is displaced from the center of negative charge. In this case the dipole moment is ordinarily randomly oriented, but which become more or less oriented by the application of an external electric field.

Non polar Dielectric: A non polar dielectric is one where the molecules possess no dipole moment unless they are subjected to an electric field.

A capacitor essentially consists of two conducting surface separated by a layer of an insulating medium called dielectric. The conducting surfaces may be in the form of either circular or rectangular plates or be of spherical or cylindrical shape. The purpose of a capacitor is to store electrical energy by electrostatic stress in the dielectric.

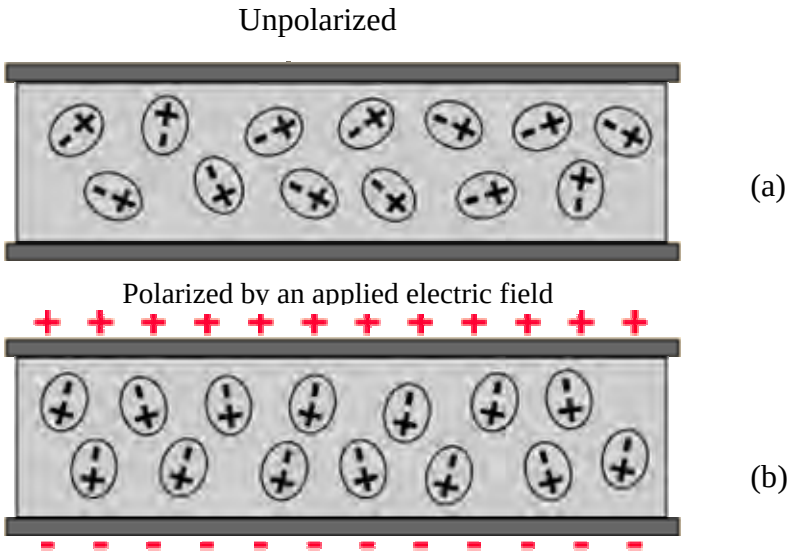

Fig. 3.16 Polar dielectric (a) unpolarized and (b) polarized by an applied electric field.

3.7.2 Polarization and its classification

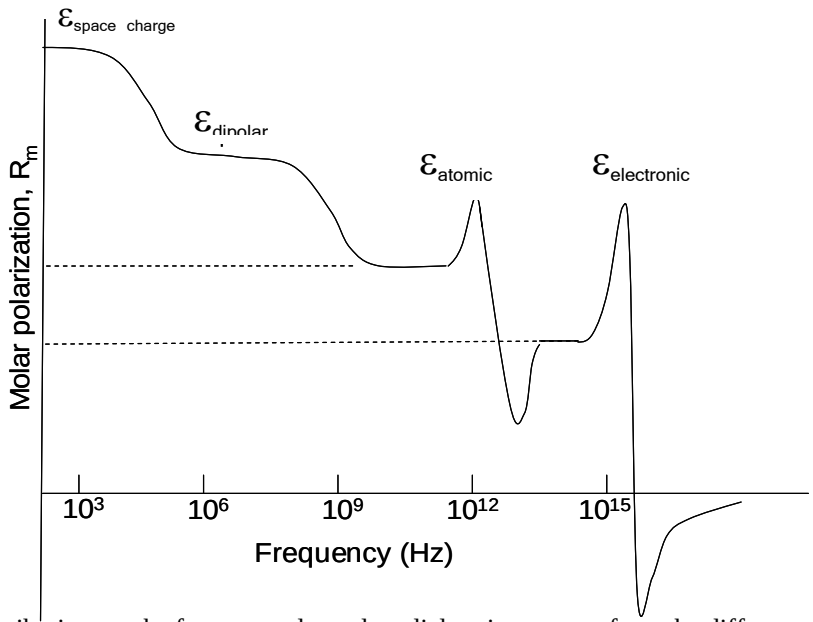

Fig. 3.17 Contributions to the frequency-dependent dielectric constant from the different charge configurations.

A dielectric subjected to a homogeneous field carries a dipole moment per unit volume. Dipole moment per unit volume is called the polarization of the dielectric. When a polymer is subjected to the influence of an applied electric field, different processes of polarization take place due to the distortion and alignment of the molecules. With changing the field, both the distortion of the molecules and their average orientations change. Different types of polarization occur at different range of frequencies. The molar polarization of a material is found to depend on the frequency of the applied alternating electric field as depicted in Fig. 3.17. The response of the atoms and molecules to an electric field leading to the formation and/or orientation of dipoles is known as polarization mechanisms. The total polarization consists by the following types of polarization mechanisms (Fig. 3.18):

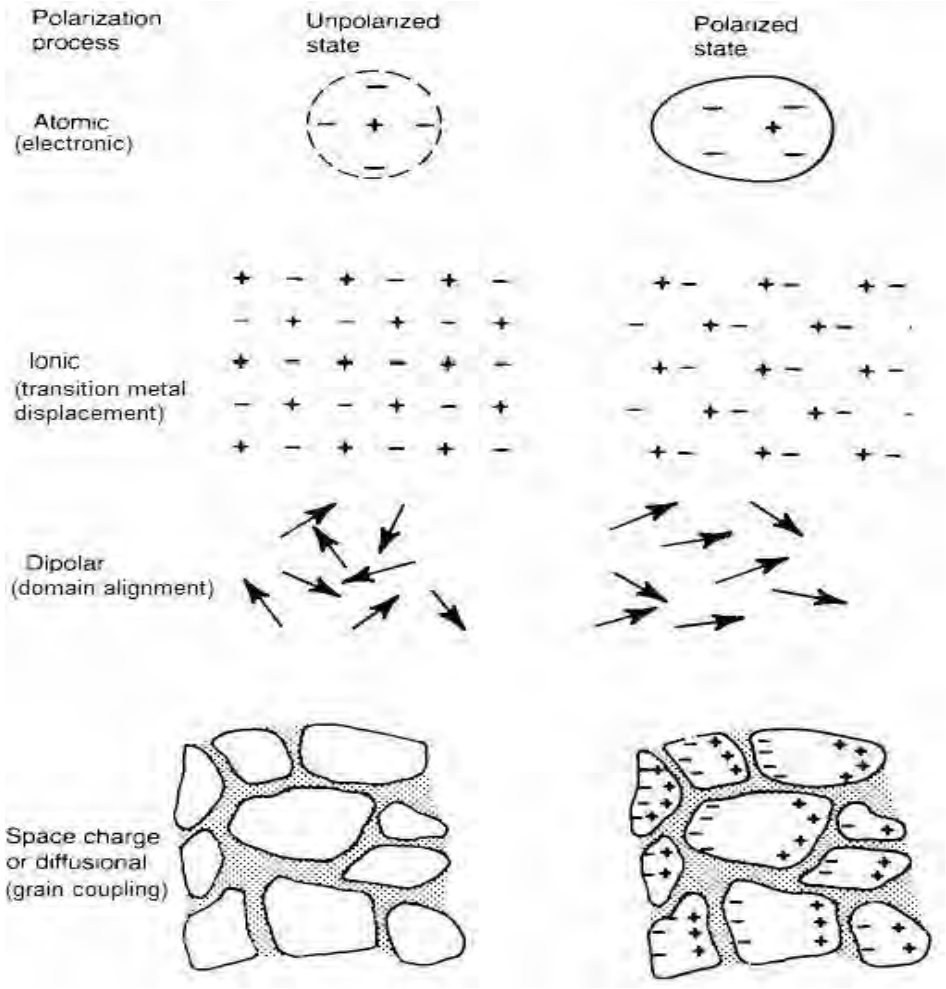

Fig. 3.18 Schematic representation of different mechanisms of polarization.

3.7.2.1 Deformation polarization

Both electronic and atomic polarizations are displacements of positive and negative charge centers within the molecule, or alternatively, molecular deformation or molecular distortion. Therefore these processes may be called displacement or deformation or distortion polarization, and dipole moment produced in this way is called an induced dipole moment. The processes are described below:

Electronic polarization is a result of dipole moments induced by the electric field. Atoms are composed of heavy nuclei surrounded by negative electron clouds. In the absence of an external field the movements of the electrons are such that the resultant orbital paths are symmetrical about the nucleus as shown schematically in Fig. 3.19(a). These orbital paths become distorted by an external electric field because the paths of the electrons tend to shift against the direction of the applied field as shown in Fig. 3.19(b). A dipole is thus induced since the atom carries a dipole moment and this dipole moment is proportional to the field strength and the proportionality factor is called the electronic poarizability of the atom. This dipole is in effect positive on the left-hand side for the assumed direction of the field.

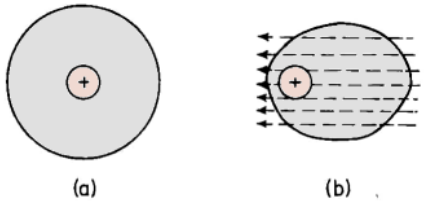

Fig. 3.19 Electronic polarization; (a) no field; (b) electric field.

Atomic polarization results from an unsymmetrical sharing of electrons when two different atoms combine to form a molecule. An external field applied to a polymer molecule can distort the arrangement of the atomic nuclei termed as atomic polarization. As nuclei is heavier than electron atomic polarization can not occur at high frequencies as electronic polarization. Atomic polarization is observed when the electronic cloud is deformed under the force of the applied field, so that the negative and positive charges are formed. This type of polarization is illustrated in Fig. 3.20 for an HCl molecule in which the hydrogen atom and the chlorine atom are both polarized. In this case the electron of the hydrogen atom is attracted into the unfilled outer shell of the chlorine atom.

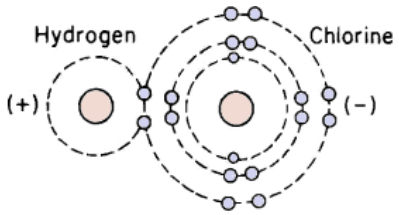

Fig. 3.20 Molecular structure of HCl illustrating atomic dipoles.

3.7.2.2 Orientational or dipolar polarization

In this mechanism the material (usually liquid or gaseous) must have natural dipoles which can rotate freely. In thermal equilibrium, the dipoles will be randomly oriented and thus carry no net polarization. If two different atoms A and B form a chemical bond, one of the two is more apart with one or more of its valence electrons than the other. As a result, the bond between A and B is at least partly ionic. If the bond between A and B has ionic character, it is obvious that the molecule AB carries an electric dipole moment even in the absence of an applied field, such a dipole moment is called permanent. The magnitude of the dipole moment is given by the product of the average charge transferred from A to B and the internuclear distance. For a molecule consisting of more than two atoms, several bonds may carry a permanent dipole moment of the molecule as a whole is obtained by vector addition of the moments associated with the various bonds. When an external field is applied to a molecule carrying a permanent dipole moment, the permanent dipole moment aligns along the direction of the field. The contribution of this process of orientation of the permanent dipoles to the polarization is called orientational polarization. Fig 3.21. shows orientation of dipoles by polarization, (a) random orientation of polar domains, (b) application of high DC electric field (polarization), (c) remnant polarization after the electric field is extinguished.

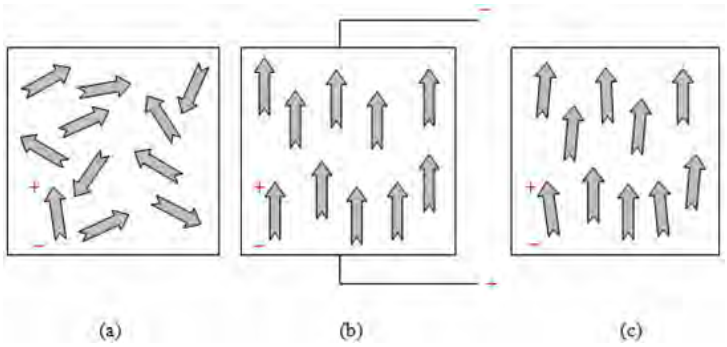

Fig 3.21 Orientation of dipoles by polarization, (a) random orientation of polar domains, (b) application of high DC electric field (polarization), (c) remnant polarization after the electric field is extinguished.

3.7.2.3 Ionic polarization

In ionic polarization a solid material must have some ionic character. Automatically it has internal dipoles, but these built-in dipoles exactly cancel each other and unable to rotate. The external field then induces net dipoles by slightly displacing the ions from their rest position. When in a molecule some of the atoms have an excess positive or negative charge (resulting from the ionic character of the bonds)-, an electric field will tend to shift positive ions relative to negative ones. This leads to an induced moment of different origin from the moment induced by electron clouds shifting relative to nuclei. The ionic polarization (Fig. 3.22) occurs due to shift of the ions relative to each other.

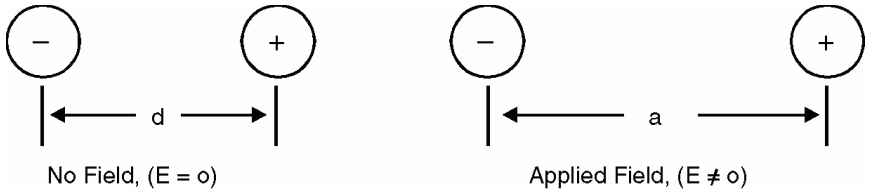

Fig.3.22 Schematic diagram of ionic polarization

3.7.2.4 Interfacial polarization

Surfaces, grain boundaries, interphase boundaries may be charged, i.e. they contain dipoles which may become oriented to some degree in an external field and thus contribute to the polarization of the material. In a real crystal there inevitably exist a large number of defects such as lattice vacancies, impurity centers, dislocations etc. Free charge carriers, migrating through the crystal, under the influence of an applied field, may be trapped by, or pile up against a defect. The effect of this will be the creation of a localized accumulation of charge which will induce its image charge on an electrode and give rise to a dipole moment. This constitutes a separate mechanism of polarization in the crystal, and is given the name interfacial polarization.

3.7.2.5 Space-charge polarization

Space-charge polarization is produced by charge carriers, such as free ions that can migrate for some distance through the dielectric. When the movement of such carriers is impeded by interfaces such as occur where two different dielectrics meet, or if the carriers are arrested in the material, space charges result. When there is no applied electric field the arrangement of these space charges is random and there is no net effect. However, in the presence of an electric field, the positive charge carriers will tend to take positions, relative to

the negative charge carriers, in the direction of the field as shown in Fig. 3.23. Fig. 3.23(a) shows the positions of the charge carriers when there is no field. On the one hand, a vertical line through the center of the charges in Fig. 3.23(a) will have zero net charge to the right and left of it. On the other hand, a vertical line through the center of Fig. 3.23(b) will have net positive charge to the left and net negative charge to the right.

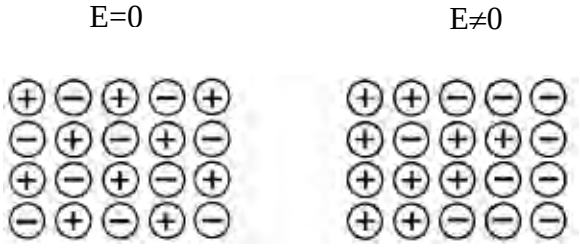

Fig. 3.23 Schematic diagram of space charge polarization.

3.8 Theory of Dielectrics

Thin films produced through glow discharge are known to have free radicals or polar groups independent of the nature of monomers. Owing to this reason, these polymers are good candidates for the investigation of dielectric properties. The ac conductivity and dielectric properties of plasma polymerized thin films provide information about the conduction process, dielectric constant, relaxation process, etc. which are dependent on the frequency and temperature. If a material contains polar molecules, they will generally be in random orientations when no electric field is applied. An applied electric field will polarize the material by orienting the dipole moments of polar molecules. This decreases the effective electric field between the plates and will increase the capacitance of the parallel plate structure. The dielectric must be a good electric insulator so as to minimize any DC leakage current through a capacitor. A capacitor is a system of two conductors separated by an insulator or vacuum. The two conductors have charges with equal magnitude and opposite sign. The potential difference V between the conductors is proportional to charge, Q and the capacitance is $C = \frac{Q}{V}$. In a parallel plate capacitor separated by a distance d, with same area A, the uniform electric field between the plates is $E = \sigma / \varepsilon_0$, where σ = surface charge density and $\varepsilon_0 = 8.85 \times 10^{-12}$ F/m, permittivity of the free space. Then the potential difference between

the two plates is $V=Ed=\frac{1}{\varepsilon_0}=\frac{Qd}{A}$ .So the capacitance of a parallel plate capacitor in free space is $C_0=\frac{Q}{V}=\frac{\varepsilon_0 A}{d}$.

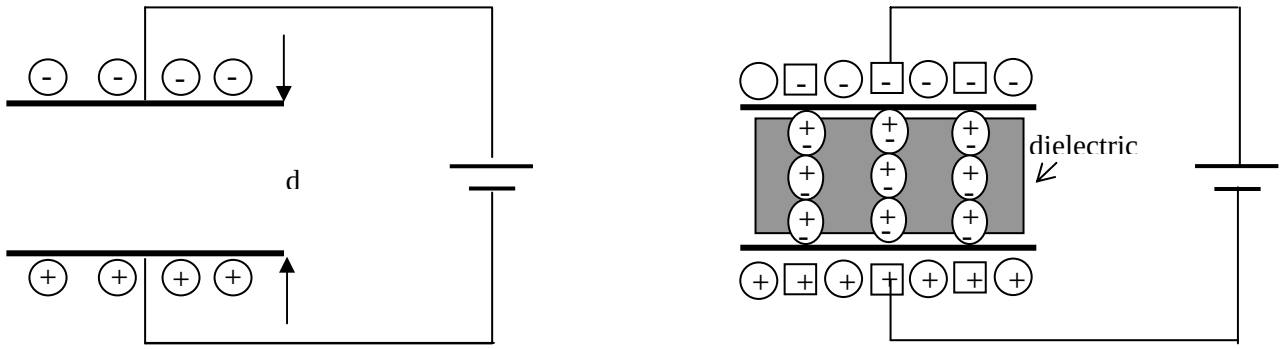

Fig. 3.24 Parallel plate capacitor (a) without dielectric and (b) with dielectric.

The capacitance of a set of charged parallel plates is increased by the insertion of a dielectric material (Fig. 3.24). Since dielectrics are non-conducting substances, there are no free charges/electrons. Hence there is no possibility of movement of free charges. However, when dielectric material is subjected to an external electric field dipole moment is induced arising out of stretching and reorientation of molecules of dielectrics. Collective effect of all molecular dipole moments is accumulation of net charges of dielectric, which produce a field that opposes external applied field. The capacitance is inversely proportional to the electric field between the plates, and the presence of the dielectric reduces the effective electric field. The dielectric is characterized by a dielectric constant ε', and the capacitance is multiplied by that factor. The capacitance of a parallel plate capacitor having a dielectric medium is expressed as

$$C_p=\frac{\varepsilon_0\varepsilon' A}{d} \quad \text{.....(3.32)}$$

where ε_0 is the permittivity of free space, ε' is the dielectric constant of the medium, A is the surface area of each of the plates/electrodes and d is the thickness of the dielectric. Hence it can be said that the ratio of C_p to C_0 is the dielectric constant of the material i.e. $\varepsilon'=C_p/C_0$. Thus it can be written as $\varepsilon'=\varepsilon'/\varepsilon_0$. The dielectric constant is therefore also known as the relative permittivity of the material. As the dielectric constant presents the ratio of the similar

type of quantities, it is dimensionless. When a dielectric is placed between charged plates, the polarization of the medium produces an electric field opposing the field of the charges on the plate. The dielectric constant ε' is defined to reflect the amount of reduction of effective electric field as shown below. The permittivity is a characteristic of space, and the relative permittivity or 'dielectric constant' is a way to characterize the reduction in effective field because of the polarization of the dielectric. The capacitance of the parallel plate arrangement is increased by factor ε'.

In other words dielectric constant represents the ratio of the electrical energy of the field set up in a dielectric material to that set up in vacuum. Dielectric materials are electrical insulators i.e have direct current resistivities greater than about 10^8 ohm-cm. Insulators have the very useful ability to store electrical charge. A common device used for this purpose is a capacitor. The capacitance of such a device measures the extent to which it is able to store charge. A real capacitor can be represented with a capacitor and a resistor. The parameters such as angular frequency (ω) of the applied field, the parallel resistance R_P, parallel capacitance C_p and the series resistance R_S and series capacitance C_s are related to the dielectric constant ε', dielectric dissipation factor ε'' and loss tangent as:

$$\varepsilon' = \frac{C_p}{C_0} \quad \text{……..……(3.33)}$$

$$\varepsilon'' = \frac{1}{R_p C_0 \omega} \quad \text{……..……..(3.34)}$$

and

$$\tan\delta = \frac{\varepsilon''}{\varepsilon'} = \frac{1}{R_p C_p \omega} = G_p / 2\pi f C_p \quad \text{…….……(3.35)}$$

The ac conductivity, σ_{ac}, was calculated using eqn.

$$\sigma_{ac} = G_p d/A \quad \text{…….(3.36)}$$

The dependence of ac conductivity, σ_{ac}, on frequency may be described by the power law [17]:

$$\sigma_{ac}(\omega) = A\omega^n \quad \text{……(3.37)}$$

where A is a proportionality constant and ω (=2πf, f is the linear frequency) is the angular frequency and n is the exponent, which generally takes the value less than unity for Debye type mechanism and is used to understand the conduction/relaxation mechanism in

amorphous materials. The dielectric behavior of a material is usually described by Debye dispersion equation [18, 19]:

$$\varepsilon^*(\omega,T) = \varepsilon' - i\varepsilon'' \quad \text{……..……(3.38)}$$

where ε^* is the complex dielectric permittivity, ε' (energy dissipated per cycle) is the real part of complex dielectric permittivity and ε'' (energy stored per cycle) is the imaginary part of the complex dielectric permittivity.

$$\varepsilon' = \varepsilon_\infty + \frac{\varepsilon_s - \varepsilon_\infty}{1+\omega^2\tau^2} \quad \text{……..……(3.39)}$$

$$\varepsilon'' = \frac{(\varepsilon_s - \varepsilon_\infty)\omega\tau}{1+\omega^2\tau^2} \quad \text{…….……..…....(3.40)}$$

where ε_s is the static dielectric constant, ε_∞ is the high frequency dielectric constant and the quantity τ is a characteristic time constant, usually called the dielectric relaxation time, it refers to a gradual change in the polarization following an abrupt change in applied field. The dielectric loss tangent is expressed by

$$\tan\delta = \frac{\varepsilon''}{\varepsilon'} \quad \text{…….(3.41)}$$

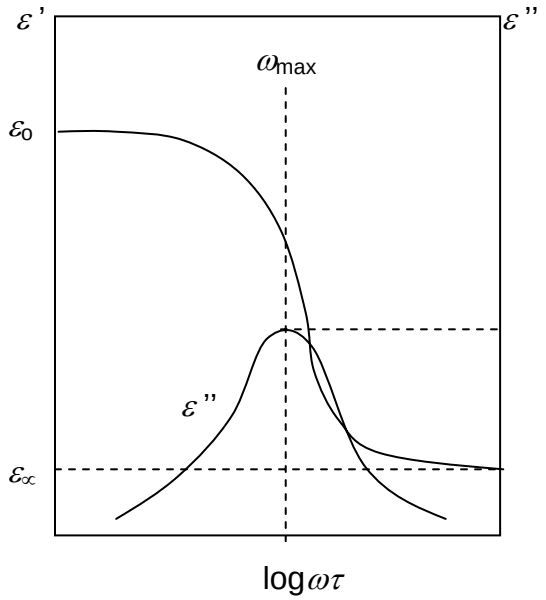

Fig.3.25 Debye dielectric dispersion curves.

The graphs of ε' and ε'' against frequency of the applied field (logarithmic scale) through the dispersion regions show (Fig. 3.25) that the maximum loss value occurs when $\omega\tau$

= 1, corresponding to a critical frequency $\omega_{max} = 1/\tau$, and location of this peak provides the easiest way of obtaining the relaxation time from the experimental results.

The activation energy (ΔE) of the relaxation process is related to the relaxation time by the Arrhenius equation: $\tau = \frac{1}{2\pi f_{max}} = \tau_0 \exp\left(\frac{\Delta E}{k_B T}\right)$ ……..(3.42)

where f_{max}, is the frequency of maximum loss for a given temperature, τ_0 is a constant and T is the absolute temperature and k_B is the Boltzman constant. ΔE was evaluated in the present work from the slope of the plot $\ln f_{max}$, versus *1/T*.

When an electric field acts on any matter the latter dissipates a certain quantity of electric energy that transforms into heat energy (Fig. 3.26). This phenomenon is commonly known as 'the expense' or 'loss' of power, meaning an average electric power dissipated in matter during a certain interval of time. As a rule the loss of power in a specimen of material, all other conditions being equal, is directly proportional to the square of the electric voltage applied to the specimen. Most of the dielectrics display a characteristic feature: under a given voltage the dissipation of power in these dielectrics depends on the voltage frequency; the expense of power frequency, voltage and capacitance and also depends on the material of dielectric. The amount of power losses in a dielectric under the action of the voltage applied to it is commonly known as 'dielectric loses'.

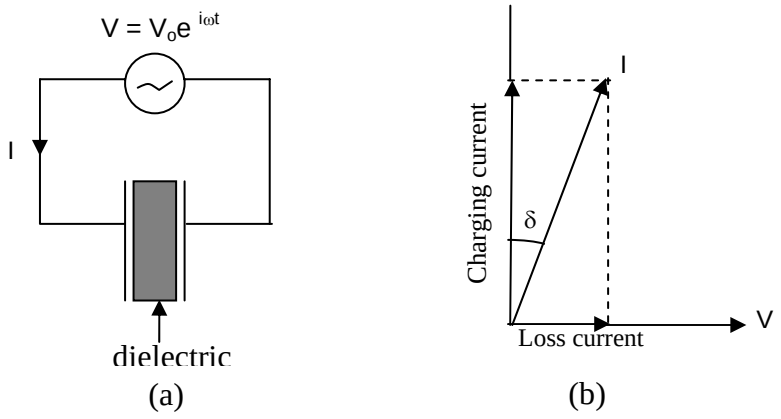

Fig. 3.26 AC losses in a dielectric : (a) circuit diagram, (b) simplified diagram of current-voltage relationship.

This is the general term determining the loss of power in an electrical insulation both at a direct and an alternating voltage.

If an alternating electric field E with amplitude E_0 and angular frequency ω is applied across a dielectric material , then it can be written in the form $E=E_0\cos \omega t$. This will produce polarization which alternates in direction, and if the frequency is high enough, the orientation of any dipoles which are present will inevitably lag (Fig. 3.27) behind the applied field. Mathematically this can be expressed as a phase lag in the electric displacement:

$D=D_0 \cos(\omega t-\delta)=D_1 \cos \omega t + D_2 \sin \omega t$, where $D_1 = D_0 \cos \delta$ and $D_2 = D_0 \sin\delta$.

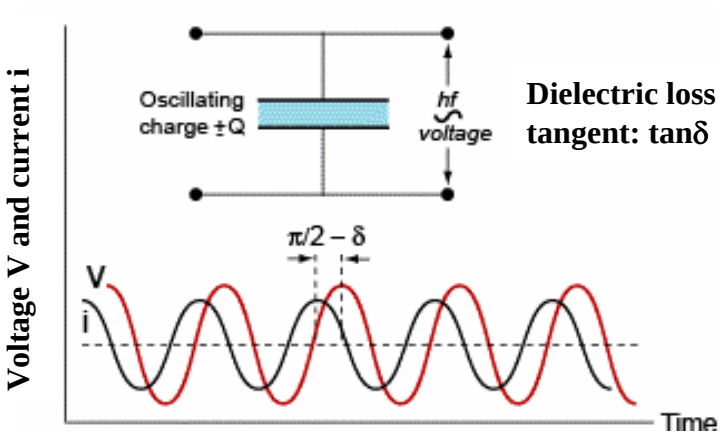

Fig. 3.27 Phase lag δ.

These leads to $\varepsilon' = \frac{D_1}{\varepsilon_0 E_0}$ and $\varepsilon'' = \frac{D_2}{\varepsilon_0 E_0}$ Linked by the relation $\tan\delta = \frac{\varepsilon''}{\varepsilon'} = \frac{Energy\ dessipated\ \ per\ cycle}{Energy\ stored\ \ per\ cycle}$, where ε'' is called the dielectric loss factor and $\tan\delta$ is usually called the dielectric loss tangent or dissipation factor. ε' and ε'' are experimentally observable quantities which may be used to characterize the dielectric dispersion over a range of frequencies.

3.9 The Cole-Cole function

The difference in dielectric constant measured at low and high frequencies is called the strength of the relaxation. By eliminating the parameter $\omega\tau$ between equations. (3.39) and (3.40), it can be obtained

$$\left(\varepsilon' - \frac{\varepsilon_s - \varepsilon_\infty}{2}\right)^2 + \varepsilon''^2 = \left(\frac{\varepsilon_s - \varepsilon_\infty}{2}\right)^2 \quad \text{.....(3.43)}$$

This is the equation of a circle, centre $[(\varepsilon_s + \varepsilon_\infty)/2, 0]$, radius $(\varepsilon_s - \varepsilon_\infty)/2$, so that a plot of ε' against ε'' should give a semicircle.

Relaxation in polymers show broader dispersion curves and lower loss maxima than those predicted by the Debye model and $\varepsilon' - \varepsilon''$ curve fails under the semicircle. This led Cole and Cole [20] to suggest the following semi-empirical equation for the dielectric relaxation of polymers

$$\varepsilon^* = \varepsilon_\infty + \frac{\varepsilon_s - \varepsilon_\infty}{1 + (i\omega\tau)^\alpha} \quad \text{.....(3.44)}$$

where $0 < \alpha \leq 1$. Davison and Cole has improved the above equation as

$$\varepsilon^* = \varepsilon_\infty + \frac{\varepsilon_s - \varepsilon_\infty}{(1 + i\omega\tau)^\beta} \quad \text{.....(3.45)}$$

where $0 < \beta \leq 1$. The parameter β is representative of relaxation time distribution. If ε'' is plotted against ε', this equation represents a circle with the centre at $(\varepsilon_s + \varepsilon_\theta)/2, 1/[2(\varepsilon_s + \varepsilon_\infty)\cot \beta\pi/2]$ and radius $1/[2(\varepsilon_s + \varepsilon_\infty)\csc \beta\pi/2]$

From the Fig.3.28, $Sin\theta = [\frac{1}{2}(\varepsilon_s - \varepsilon_\infty)]/[\frac{1}{2}(\varepsilon_s - \varepsilon_\infty)\csc \beta\pi/2]$

or $\theta = \beta\pi/2$ ....(3.46)

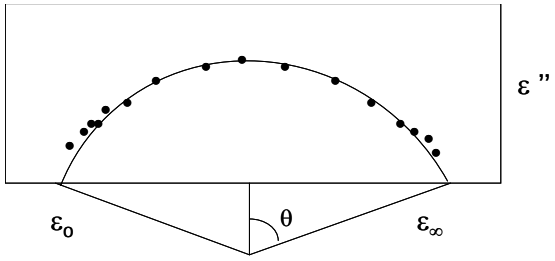

Fig. 3.28 A Cole-Cole circular arc plot constructed from the ε' *and* ε'' data.

References

[1] Danilatos, G. D., ‘Foundation of environmental scanning electron microscopy’. Advances in Electronics and Electron Phys., 71, 109, 1988.

[2] Goldstein, G. I. , Newbury, D. E., Echlin, P., Joy, D. C., Fiori, C., Lifshin, E., ‘Scanning electron microscopy and X-ray microanalysis’, Plenum Press, NY, 1981.

[3] Silverstein, R. M., Bassler G. C., Morrill T. C., 'Spectrometric identification of organic compounds', John Willey and Sons, New York, 1981.

[4] Hatakeyma, T. and Quinn, F. X., 'Fundamentals and applications to Polymer science', John Willey and Sons, 1997.

[5] Lambert, J. H., David. A. Lightner, Shurvel, H. F. and Graham, Cooks R., 'Introduction to organic spectroscopy', Macmillan Publishing Co., New York, 1987.

[6] Tauc, J., 'Optical properties of Solids', Abeles, F., Ed., North-Holland, Amsterdam, 1972.

[7] Tauc, J., "Optical Properties of Solids", F. Abeles Ed. North-Holland, Amsterdam, 1972.

[8] Ilican, S., Caglar, M., Caglar, Y., J. Optelectron. Adv. Mater. 9 (5), 1414, 2007.

[9] Yakuphanoglu, F., Sekerci, M., Optica. Appl., XXXV, 209, 2005.

[10] Ohring, M., 'The Material Science of Thin Films', Academic Press, USA, 1992.

[11] Emtage, P. R., Tantraporn, W., 'Schottky emission through thin insulating films', Phys. Rev. Lett., 8, 267, 1962.

[12] Frenkel, J., 'On pre-breakdown phenomena in insulators and electronic semi-conductors', Phys. Rev., 54, 647, 1938.

[13] Seanor, D. A., 'Electrical Properties of Polymers', Cambridge University Press, Cambridge, London, 1979.

[14] Mott, N. F., Gurney, R. W., 'Electronic Processes in Ionic Crystals', Clarendon Press, Oxford, 168, 1940.

[15] Rose, A., 'Space-charge-limited currents in solids', Phys. Rev., 97, 1538, 1955.

[16] Lampert, M. A., 'Simplified theory of space-charge-limited currents in an insulator with traps', Phys. Rev., 103, 1648, 1956.

[17] Mott, N. F. and Davis, E. A., 'Electronic Processes in Non Crystalline Materials', Clarendon Press, Oxford, 1979.

[18] Blythe, A. R., 'Electrical Properties of Polymers' Cambridge University Press, Cambridge, 69-71, 1979.

[19] Amar, N., Gould, R. D. and Saleh, A. M., 'Space-charge-limited conductivity in evaporated α-form metal-free ohthalocyanine thin films', Vacuum, 50, 53, 1998.

[20] Horng-Jer, T., 'Interfacial polarization phenomenon in the recrystallization of poly(butylenes succinate)', Polymer, 49, 2328, 2008.

5. Results and discussion

5.1 Introduction

This chapter presents the results obtained from different characterization techniques employed to determine the different properties of PPDEAEMA thin films and their analyses by using existing theories.

The surface morphology, thermal and structural /chemical characteristics of plasma polymerized thin films is analyzed by SEM, EDX, DTA/TGA and FTIR respectively. The study of UV- vis spectroscopic analyses provides the insight about the optical properties of the PPDEAEMA thin films. The optical energy gaps, the allowed direct and indirect transitions are determined and Urbach energy, steepness parameter and extinction coefficient are calculated to specify PPDEAEMA thin films.

The dc electrical conduction mechanism is discussed from the measurement of current density-voltage characteristics and its temperature dependence. The ac electrical conductivity, dielectric constant and loss tangent were investigated as function of frequency and temperature and attempts were made to explain the relaxation behavior and ac conductivity in PPDEAEMA thin films.

The PPDEAEMA thin films were heat treated at different temperature and the comparative analyses of structural, optical and dc/ac electrical properties are given in this chapter.

This chapter also presents comparative study of different characteristics of PPDEAEMA thin films with iodine doped ones and discuss the possible interactions of iodine with PPDEAEMA.

5.2 Surface Morphology

The SEM micrographs of as deposited and heat treated (at 573 K) PPDEAEMA thin films prepared at optimized condition and of 200 nm thickness, with magnifications 1000x and 50000x respectively are presented in Fig.5.1.

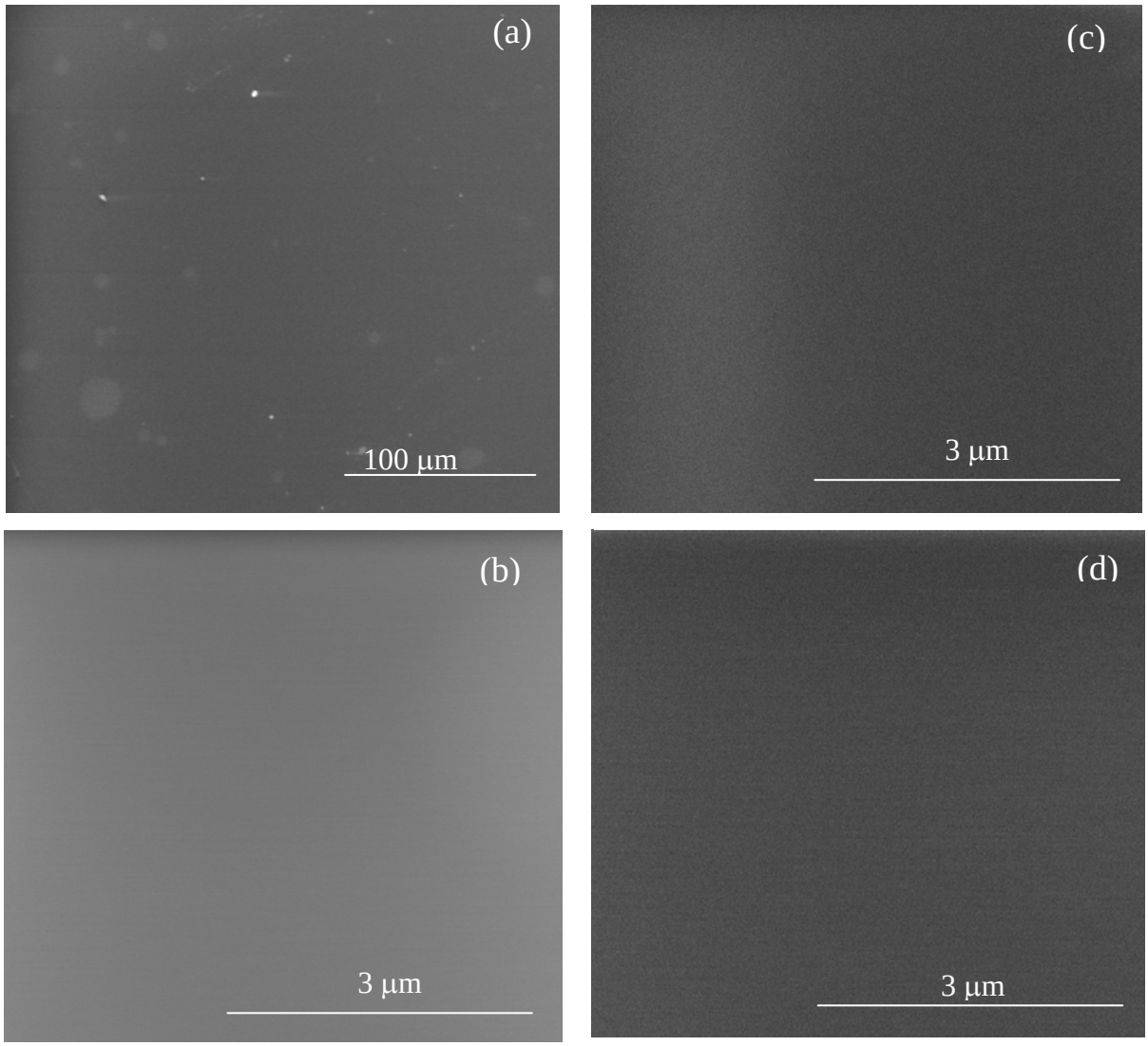

Fig. 5.1 The SEM micrographs of (a) as-deposited with magnification 1000x, (b) as deposited with magnification 50,000x, , (c) heat treated at 573 K for 1 hour and (d) iodine doped PPDEAMEA thin films onto glass substrate, at 25.00 kV, magnification 50, 000x.

Micrographs 5.1(a) and (b) show uniform and pinhole free surface of the as-deposited PPDEAMEA film with magnification 1000x and 50000x respectively. It is observed from the Fig. 5.1(a) that the film surface contains some faint spots that arise due to the exposure to atmosphere during the time gap or transfer time between thin film preparation and SEM measurements but the films itself are pinhole free. It is well known that plasma polymerized thin films have pinhole free surface [1, 2]. Fig. 5.1(b) also illustrates pinhole free nature of the film surface, as it is very much magnified in comparison to Fig 5.1(a) the faint spots are no

more observed. Micrograph 5.1(c) shows the thin films heat treated at 573 K for 1 hour PPDEAEMA film with magnification 50000 x. Fig. 5.1(c) and (d) look similar to Fig. 5.1(b). No significant variation of the surface morphology is detected due to heat treatment and iodine doping in the micrographs in comparison with the as deposited film.

EDX of the as deposited, heat treated and iodine doped PPDEAEMA thin films were recorded at the same time by EDS attached to the SEM. EDX spectra recorded for the different PPDEAEMA are provided in Fig. 5.2 (a, b, c). The observations indicate the presence of C, N and O in PPDEAEMA thin films. Fig. 5.2(c) reveals the presence of iodine in iodine doped PPDEAEMA thin films.

Table 5.1 Wt% of the elements of as deposited, heat treated at 573 K and iodine doped PPDEAEMA.

Element	Monomer DEAEMA(Wt%) calculated)	As deposited PPDEAEMA (Wt%)	Heat treated (at 573 K) PPDEAEMA (Wt%)	Iodine doped PPDEAEMA (Wt%)
C	64.86	43.83	21.40	46.18
N	7.56	14.69	15.35	10.20
O	17.29	41.48	63.25	28.52
H	10.27	-	-	-
I	-	-	-	15.10

Table 5.1 shows wt% of the carbon, nitrogen and oxygen in monomer, as deposited, heat treated and iodine doped PPDEAEMA. Though monomer contains hydrogen but the energy of it is very low to be observed by EDX. Molecular formula of the monomer is $C_{10}H_{19}NO_2$ and molecular weight 185.26 from which the wt% of the elements of the monomer is calculated. It is seen that the wt% of carbon reduces due to the breakdown of bonds owing to the complex reaction during plasma polymerization where as the wt% of oxygen increases. The heat treated sample contains less amount of carbon as a consequence of heat treatment since carbon may form gas with hydrogen or oxygen and evaporate.

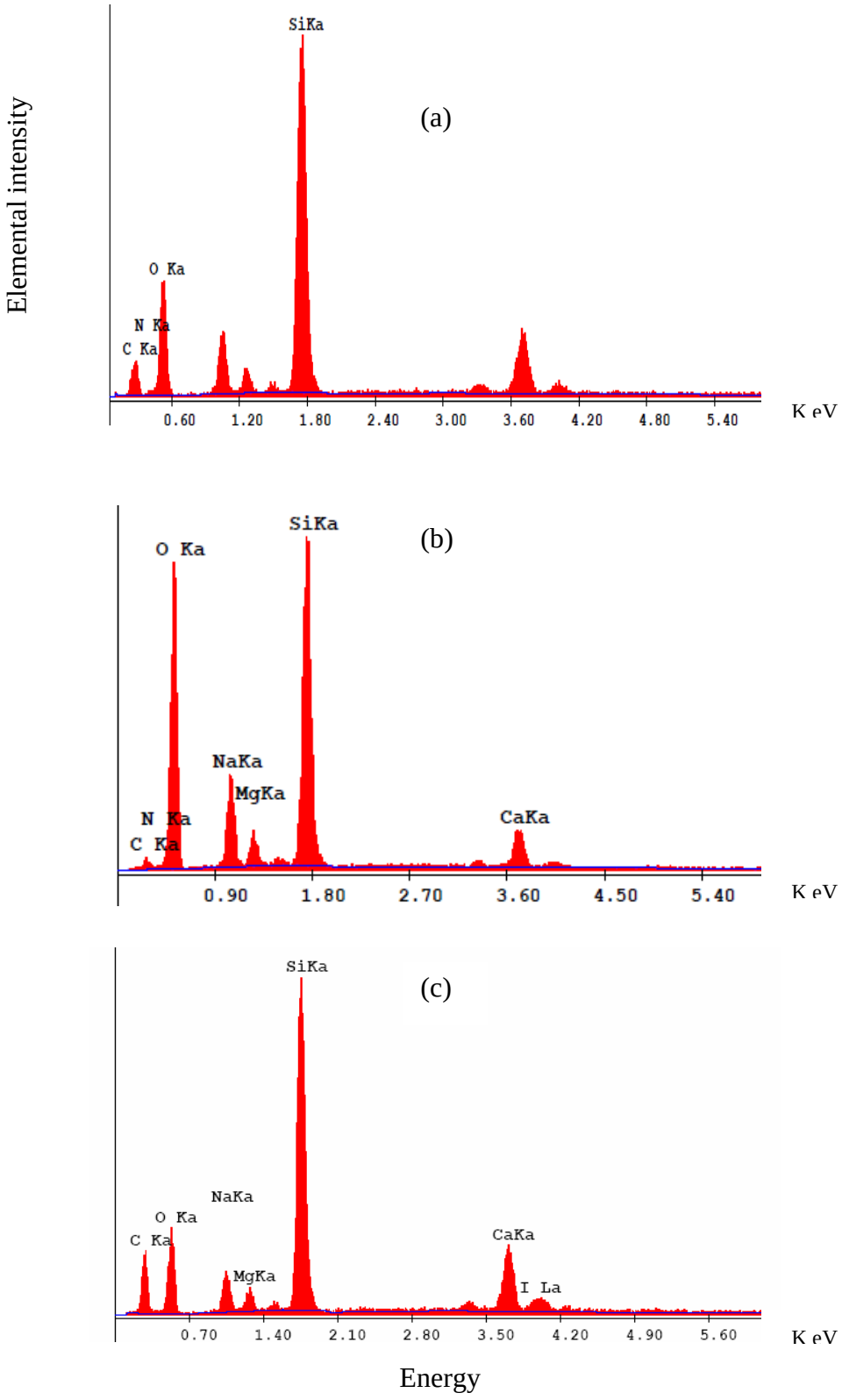

Fig. 5.2. EDX spectra of (a) as deposited, (b) heat treated at 573 K for 1 hour and (c) iodine doped PPDEMA.

The increase of oxygen in PPDEAEMA may be due to the complex reactions during plasma polymerization and post deposition reaction of the PPDEAEMA after exposure to air. A considerable amount of wt% of iodine is observed in iodine doped PPDEAEMA. The incorporation of iodine in PPDEAEMA due to the exposure to iodine vapor during iodine doping in desiccators, followed by complex interactions with radical species and dangling bonds in the structure.

5.3 Thermal studies

Thermogravimetric analysis (TGA) is widely used to estimate the percentage weight loss (wt%) of materials against temperature. The graphical representation of TGA and differential thermogravimetric analysis (DTG) curves (Fig. 5.3a) were taken for as deposited, heat treated at 573 K and iodine doped PPDEAEMA in the temperature range of 273 to 1000 K at a scan rate of 10 K/min in air and these traces reveal different stages of thermal degradation are represented by three regions A, B and C. Every region is associated with a different rate of mass loss.

In case of as deposited PPDEAEMA, the maximum weight losses in A, B and C regions are about 4%, 5% and 82% respectively. In region A, the TGA demonstrates that mass loss initiates at about 390 K which possibly arise from removal of water content (at water/moisture evolution temperature, T_w K), which is not necessarily associated with any change in the structure. The mass loss in plateau region B upto 550 K, may be attributed to the loss of non-constitutional or adsorbed water or residual moisture or unsaturated/unreacted monomer which might settle on the surface of PPDEAEMA or due to evolution of hydrogen and low molecular mass hydrocarbon gases. This corresponds to stability temperature T_s at 550 K. Above 550 K there is a rapid mass loss which results from polymer degradation. Kaniappan and Latha [3] reported that major weight loss of PMMA starts at around 570 K, which is almost same for PPDEAEMA. In region C, 50% mass loss obtained at degradation temperature T_d which is about 750 K. This mass loss may be caused by the thermal breakdown of the PPDEAEMA and expulsion of higher molecular mass hydrocarbons, oxygen containing compounds etc. Thus, it can be attributed that as-deposited PPDEAEMA is thermally stable up to about 550 K. The DTA thermogram of as deposited PPDEAEMA (Fig. 5.3b) shows an exothermic broad band which has a maximum centred around 598 K. The

DTA gives the idea that the first degradation starts at about 600 K may be due to removal of hydrogen and second decomposition starts at 780 K may be due to abstraction of carboxylic compounds. The T_w, T_s and T_d for as deposited, heat treated at 573 K and iodine doped PPDEAEMA are depicted in Table 5.2.

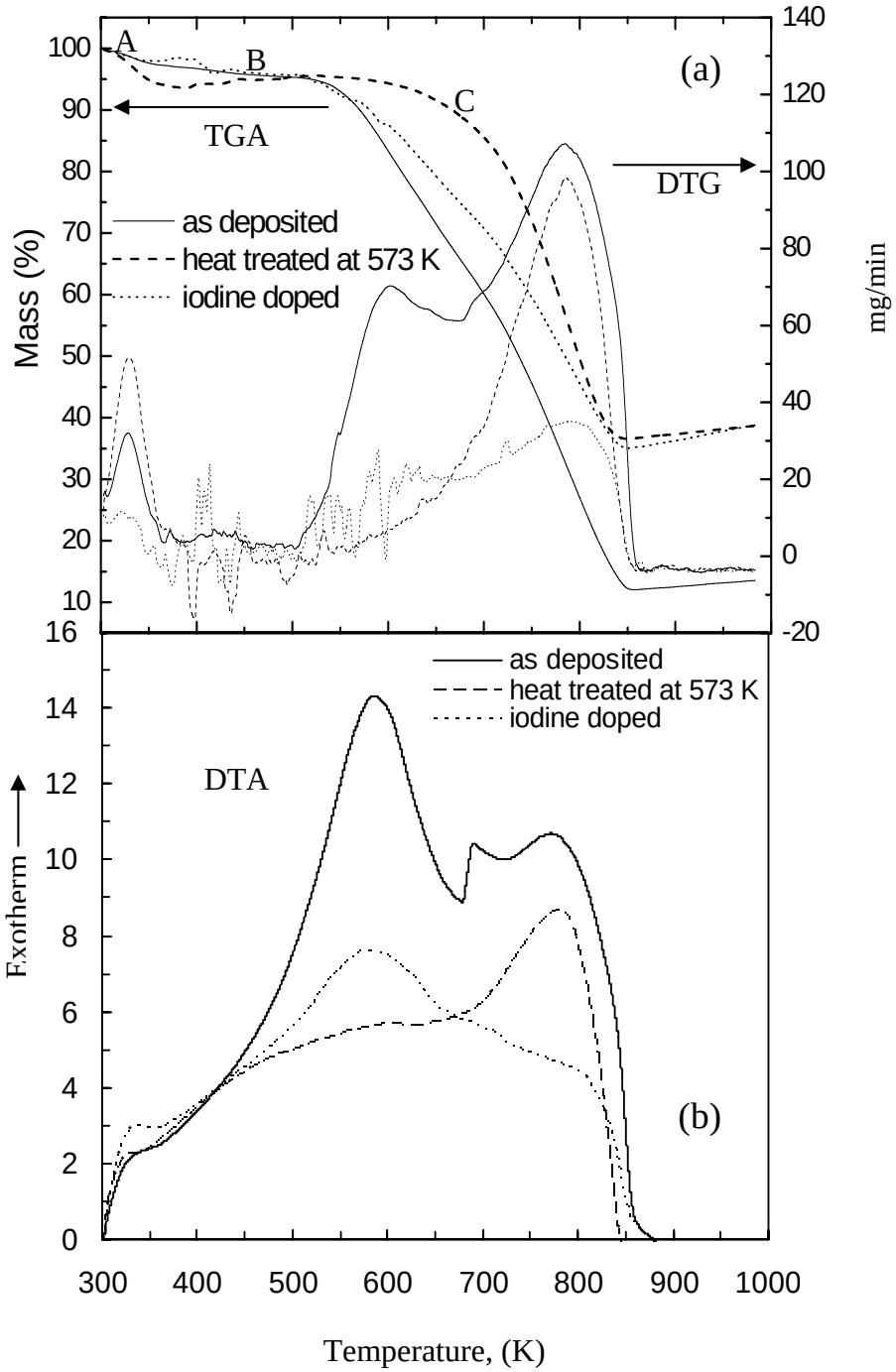

Fig. 5.3. The (a) TGA and DTG (b) DTA traces of as deposited, heat treated (at 573 K), and iodine doped PPDEAEMA taken at 10 K/min in air.

Table 5.2 Temperature corresponding to T_w, T_s and T_d for as deposited, heat treated (at 573 K) and iodine doped PPDEAEMA.

Sample	Temperature (K) corresponding to		
	T_w	T_s	T_d (50% wt loss at)
PPDEAEMA	390	550	750
PPDEAEMA, heat treated at 573 K	375	660	800
Iodine doped PPDEAEMA	350	560	770

For the heat treated PPDEAEMA, the T_w, T_s and T_d are 375, 660 and 800 K respectively. The maximum three stage weight loss in A, B and C regions is about 7%, 5% and 61% respectively. The DTG curve of as deposited PPDEAEMA shows two peaks, one is at around 600 K and another at around 800 K. The two peaks correspond two-stage degradation event which might have taken place due to the breakdown of C-H, C-N and C=C bonds, and evolution of low molecular weight hydrocarbon and/or N containing compounds. But the DTG curve of heat treated sample shows one peak around 800 K since the sample has already lost its residual moisture or hydrogen during heating at 573 K. The same trend was also observed in DTA curve of heat treated PPDEAEMA.

The iodine doped sample shows that major mass loss starts from 550 K (like as deposited PPDEAEMA) due to degradation of PPDEAEMA which is associated with exothermic peak of the DTA curve at the same temperature. The maximum weight losses in A, B and C regions are found about 5%, 5% and 60% respectively. For iodine doped PPDEAEMA, the T_w, T_s and T_d are 350, 560 and 770 K respectively. The stability of iodine doped PPDEAEMA is almost the same as that of as deposited PPDEAEMA. The intensity of DTG peak is less than that of as deposited PPDEAEMA. The DTA thermogram of iodine doped PPDEAEMA (Fig. 5.3b) shows an exothermic broad band which has a maximum centered around 580 K correspond to removal of hydrogen containing compounds or the degradation might have occurred due to the breakdown of C-H, C-N and C=C bonds, and removal of low molecular weight hydrocarbon and/or N containing compounds from the bonds and also due to the removal of iodine. As it is seen from FTIR that iodine is weakly bound to PPDEAEMA which possibly evaporate due to heating during TGA/DTA process

and shows T_s and T_d very near to as deposited. Therefore from the above discussion it can be attributed that heat treated PPDEAEMA are more stable as compared to as deposited PPDEAEMA.

5.4 Fourier transform infrared spectroscopic Analyses

5.4.1 FTIR analyses for as deposited and heat treated PPDEAEMA

The FTIR spectra of DEAEMA monomer (liquid); as deposited PPDEAEMA and heat treated (at 473 and 573 K for 1 hour) PPDEAEMA are presented in Fig.5.4 and the corresponding assignment is given in Table 5.3. In the spectrum for DEAEMA, a wide band appeared at around 3450-3200 cm^{-1} (A), indicates the presence of -OH stretching. Hydroxyl group mainly dominate this region giving rise to very characteristics band profiles. Since –OH is not present in the original monomer structure, the presence of –OH in spectrum P, may be due to exposure of the monomer to the atmosphere. This band is also observed in spectra Q, R, S. In spectrum P, the absorption band observed at 2968.2 and 2873.7 may be due to $–CH_3$- and at 2931.6 and 2804.3 cm^{-1} (B) may be due to $–CH_2$ stretching [4-5].

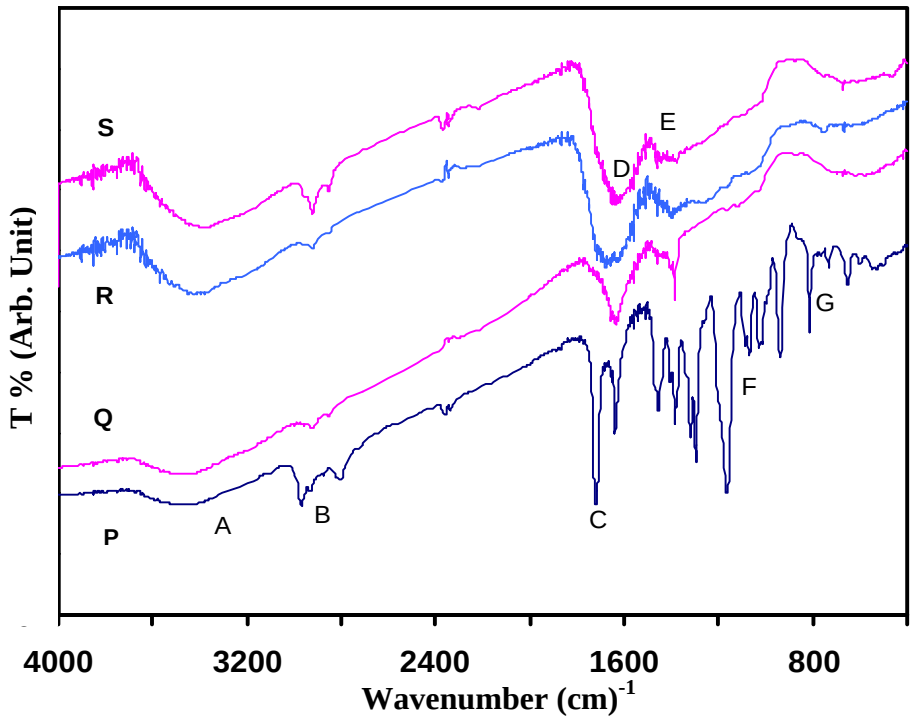

Fig. 5.4. The FTIR spectra of DEAEMA (spectrum P); as deposited PPDEAEMA (spectrum Q); and PPDEAEMA heat treated at 473 K (spectrum R); at 573 K (spectrum S).

Only -CH_2- is appeared at 2923.9, 2852.5 cm^{-1} for spectrum Q; at 2923.9 and 2854.5 cm^{-1} for spectrum R and at 2922.0 and 2852.5 cm^{-1} for spectrum S. During plasma polymerization, hydrogen may be removed from -CH_3, so -CH_2- is observed more compared to -CH_3 for Q, R and S spectra. The absorption band observed at 1720.4 cm^{-1} (C) in the spectrum of P and a weak band at 1718 cm^{-1} for Q indicate C=O stretching which confirms the material as a carbonyl compound similar to PMMA [3-4]. Some of the carbonyl groups break and crosslink occur that is why C=O band becomes weak in case of PPDEAEMA and merged with the band for C=C thus creates a broad band around 1700-1500 cm^{-1}. The C=C and C=O have close regions of absorption, so both the absorptions of C=C and C=O overlap. Because of the presence of conjugation in the structure, the intensity of absorption of C=O lowers or shifted towards lower wavelengths [6]. For heat treated PPDEAEMA weak band is observed at 1800-1650 cm^{-1} for R and S spectra.

Table 5.3 Assignments of FTIR absorption bands for DEAEMA (spectrum P); as deposited PPDEAEMA (spectrum Q) ; and PPDEAEMA heat treated at 473 K (spectrum R) ; at 573 K (spectrum S).

Assignments		***monomer***	***As deposited***	***Heat treated PPDEAEMA***	
		DEAEMA	PPDEAEMA	at 473 K	at 573 K
		P	**Q**	**R**	**S**
		Wavenumber (cm^{-1})			
-OH stretching;	**A**	3450-3200	3450-3200	3450-3200	3450-3200
-CH_3 stretching, C-H stretching doublet	**B**	2968.2, 2873.7,	weak	Weak	weak
-CH_2 -stretching asymmetric vibration of H atom		2932,	2924,	2924,	2922,
symmetric vibration of H atom		2804	2853	2855	2853
C=O stretching	**C**	1720.4	1718.4	1800-1650	
C=C stretching	**D**	1650-1550	1650-1550	1650-1550	1650-1550
CH_3, CH_2 bending	**E**	1454, 1402.2,1382.9,1319.2	1550-1300	1550-1300	1550-1300
C-N, C-O-C, C-N-C	**F**	1296,1163, 1088,1069,1028	1300-1000	1300-1000	1300-1000
=C-H	**G**	999, 814, 733	1000-700	1000-700	1000-700

The presence of C=C stretching is observed around 1650-1550 cm^{-1} (D) in all the spectra P, Q, R, S; though it is most prominent in spectrum P. The absorption peaks appeared

at 1541,1533.3,1508.2,1454, 1402.2,1382.9 and 1319.2 cm^{-1}(E) in spectrum P indicate the presence of $–CH_3$ and $–CH_2$- groups which arises due to C-H bending. The weak band in the region 1550-1300 cm^{-1} (E) arises due to C-H bending for Q, R and S spectra. In spectrum P, absorption band appeared at 1296.1 and 1163 cm^{-1} may be due to C-N (a doublet due to double bond character of the C-N bond when conjugated) stretching. The absorption band appeared at 1087.8, 1068.5 and 1028 cm^{-1}may be due to presence of functional group C-N-C for C-N stretching.

The broad absorption band observed at 1300-1000 cm^{-1} (F) may be due to C-N stretching. A sharp absorption appears at around 1150-1100 cm^{-1} indicating C-N-C due to C-N stretching. The functional group C-O-C for absorption band 1300-1000 cm^{-1} due to C-O (ester bond) stretching characterizes the presence of esters; C-N characterizes the presence of amides [4-5]. The C-H stretch vibrations for methyl and methylene are the most characteristic in terms of recognizing the compound as an organic compound containing at least one aliphatic fragment or center. The bending vibrations help to tell more about the basic structure. For example, a strong methylene /methyl band (1470 cm^{-1}) and a weak methyl band (1380 cm^{-1}), plus a band at 725–720 cm^{-1} (methylene rocking vibration) are indicative of a long-chain linear aliphatic structure (note that splitting may be observed for the 1470 and 720 cm^{-1} bands, which is indicative of a long-chain compound, and is attributed to degree of regularity for the linear backbone structure) [7].

5.4.2 FTIR analyses for iodine doped PPDEAEMA

The FTIR spectra of as deposited and iodine doped PPDEAEMA are presented in Fig.5.5 to present a comparative study of functional groups present in the PPDEAEMA and iodine doped PPDEAEMA and the assignment is given in Table 5.4. Some of the absorption bands shift due to iodine doping. The absorption peak at 2968 cm^{-1} become more intense. 2852.5 cm^{-1} band due to CH_2 stretching shifts to 2854.5 cm^{-1}. An important issue to consider with halogen substituents is the high electronegativity of the halogen atom. This can have a noticeable impact on the spectrum of neighboring group frequencies, including adjacent hydrogen atoms. In such cases, significant shifting of the C-H frequencies can occur – the direction of the shift being dependent on the location of the C-H, and whether the halogen

adds or extracts electron density from the C-H bond – adding strengthens (higher frequency) and extracting weakens (lower frequency).

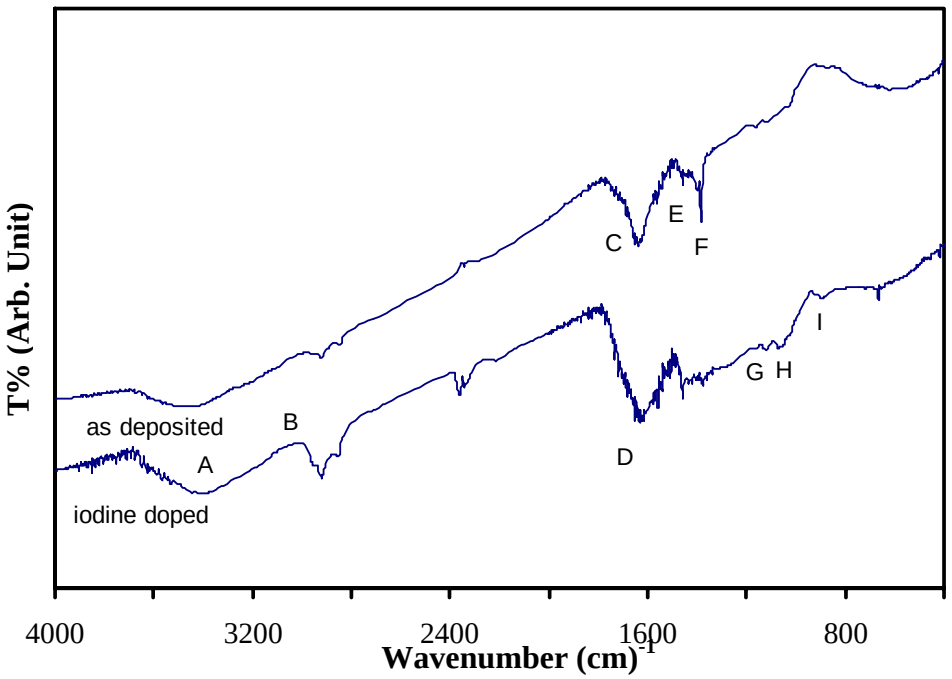

Fig. 5.5. The FTIR spectra of as deposited and iodine doped PPDEAEMA.

Table 5.4 Assignments of FTIR absorption bands for as deposited and iodine doped PPDEAEMA.

As deposited PPDEAEMA	Assignments		Iodine doped PPDEAEMA
Wavenumber (cm^{-1})			Wavenumber (cm^{-1})
3450-3200	-OH stretching;	A	3450-3200
Weak	$-CH_3$ stretching, C-H stretching doublet	B	2968.2, weak
2923.9, 2852.5	$-CH_2$ –stretching asymmetric vibration of H atom symmetric vibration of H atom		2923.9, 2854.5
1718.4	C=O stretching	C	1718.5, 1683-1650
1650-1550	C=C stretching	D	1650-1550
1550-1300	CH_3, CH_2 bending	E	1550-1300
Weak	C-N stretching	F	1272.9
-	C-O stretching	G	1122.5
-	C-N stretching	H	1072.3
-	NH_2 bending	I	894

The same influences can be observed with halogen substituted carbonyl compounds, such as acyl halides, where the bond strength of the carbonyl group is increased. In most cases, both a shift to higher frequency and an increase in absorption strength for the band are observed [7].

Absorption band at 1683-1650 cm^{-1} due to C=O stretching become more visible. An absorption peak is observed at 1272.9 cm^{-1} due to C-N stretching. Sharp absorption at 1272.9, 1122.5 and 1072.3 cm^{-1} represents C-N stretching, C-O stretching and NH_2 bending respectively. The affect of iodine on bond length is an indication of iodine doping in PPDEAEMA.

5.5 Ultraviolet and visible absorption spectra

5.5.1 UV-vis spectroscopic analyses for as deposited and heat treated PPDEAEMA thin films

The graphical representation of variation of absorbance with λ is presented in Fig. 5.6 (a) for as deposited PPDEAEMA thin films of 100, 150, 200 and 300 nm thickness which indicates that absorbance decreases rapidly up to about 500 nm and above this wavelength, it decreases slowly for all the thin films. The degree of disorder and defects present in the amorphous structure of the thin films changes due to the heat treatment. PPDEMEMA thin films were heat treated at 373 K, 473 K and 573 K for one hour to provide a deep insight about the change in energy gap in the PPDEMEMA thin films due to heat treatment. The absorbance versus λ curves for PPDEAEMA thin films of (b) 150 nm, (c)200 nm, (d) 300 nm thicknesses, heat treated at 373, 473 and 573 K for 1 hour are presented in Fig. 5.6 (b, c, d). Though the absorption peaks for 373 and 473 K PPDEAEMA thin films are higher than as deposited ones but its different for the PPDEAEMA thin films heat treated at 573 K. Since at 573 K PPDEAEMA thin films may loss some mass which is also confirmed by DTA curves which leads to the decrease in intensity of absorbance. The absorption peaks of these curves are shifted to the longer wavelength slightly. The α versus $h\nu$ curves for both as deposited and heat treated thin films of PPDEAEMA are shown in Fig. 5.7 (a, b, c, d), which displays an exponential nature at the low energy region which may arise due to the short range order or due to the presence of defects in the thin films [8]. Hence these curves can be characterized by

different slopes indicating the presence of allowed direct and indirect transitions in PPDEAEMA thin films.

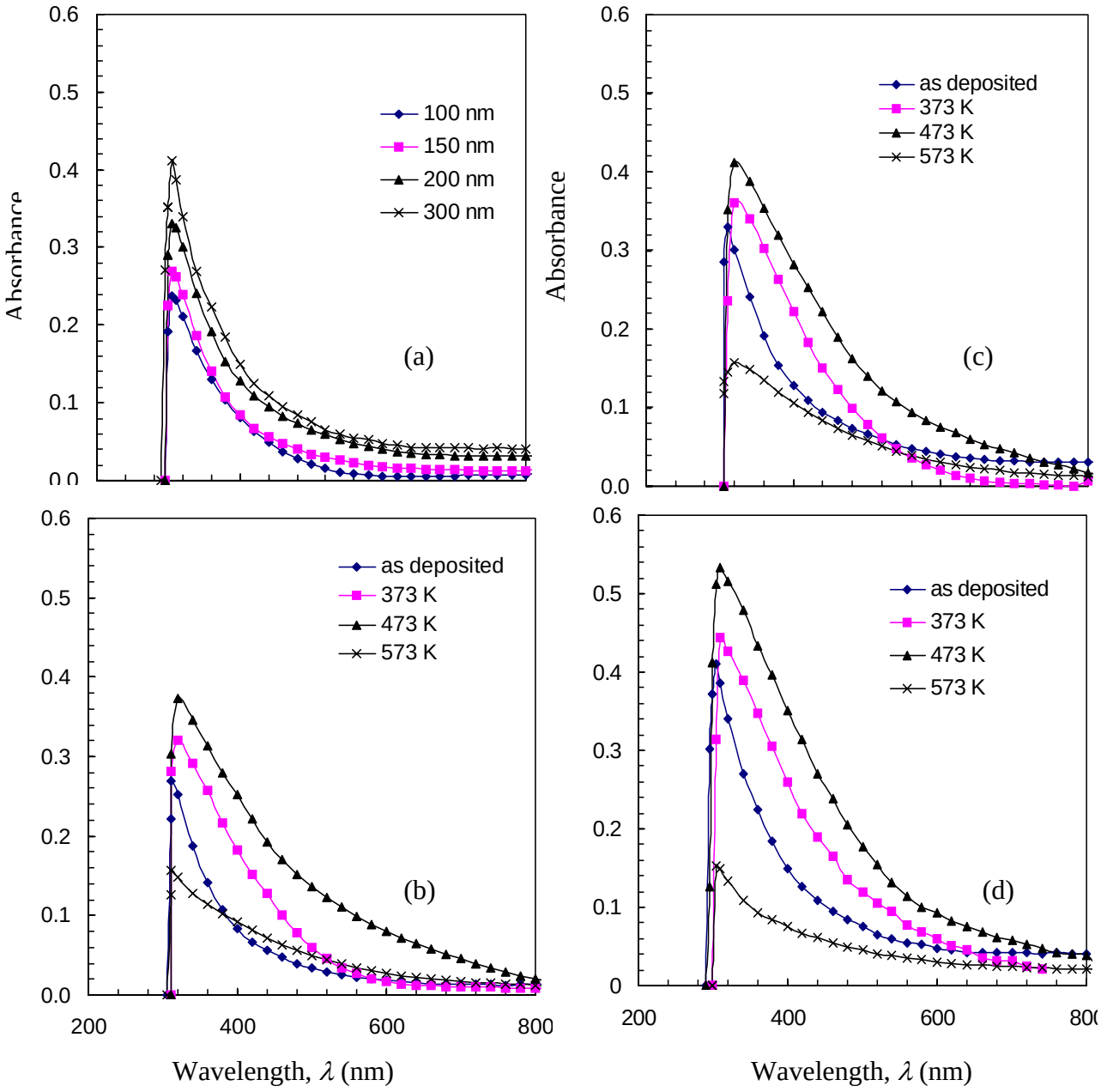

Fig. 5.6. Variation of absorbance with λ of as-deposited PPDEAEMA thin films of (a) as deposited and PPDEAEMA thin films of (b) 150 nm, (c) 200 nm, (d) 300 nm thickness heat treated at 373, 473 and 573 K for 1 hour.

The optical direct band gap E_{qd} of the PPDEAMEA thin films of as deposited and heat treated thin films were determined from $(\alpha h\nu)^2$ versus hν curves given in Fig. 5.8 (a,b,c,d) and allowed indirect band gap, $E_{qi,}$ from $(\alpha h\nu)^{1/2}$ versus hν curves given in Fig. 5.9 (a,b,c,d). The Table 5.5 contains the values of E_{qd} and E_{qi} obtained from Fig. 5.8 (a,b,c,d) and 5.9 (a,b,c,d). From the Table 5.5 we find that energy band gap decrease due to heat treatment since the interatomic spacing increases when the amplitude of the atomic vibrations increases due to the increased thermal energy.

The values of the indirect band gap shift to lower energies since higher gap states narrow the band gap. The structural rearrangement owing to heat treatment causes the band gaps to reduce, since the more conjugated the system, the smaller the energy gap. When the PPDEAEMA thin films are heat-treated, conjugation increases owing to structural rearrangement and accordingly the band gap of PPDEAEMA films reduce on heat treatment at higher temperatures.

The plots of $(\alpha h\nu)^{1/2}$ versus $h\nu$, indicate a linear behavior for the absorption edge is exponentially dependent on the incident $h\nu$ (at photon energies less than the E_g of the films, i.e. in the region of the so called Urbach spectral tail, which characterizes the slope of the exponential edge) and obeys the empirical Urbach relation, $\alpha = \alpha_0 \exp(h\nu/Eu)$,[9] where α_0 is a constant and E_u is the Urbach energy, where $\ln\alpha$ varies as a function of $h\nu$. The variation of $\ln\alpha$ with $h\nu$ for the as deposited and heat treated (at 373, 473, and 573 K) PPDEAMEA thin films is plotted in Fig. 5.10 (a, b, c, d). The exponential dependence of absorption coefficient on energy may arise from the random fluctuations of the internal fields associated with the structural disorder in many amorphous materials [10]. The dependence of the optical absorption coefficient with $h\nu$ may arise from electronic transitions between localized states. The density of these states falls off exponentially with energy which is consistent with the theory of Tauc [11].

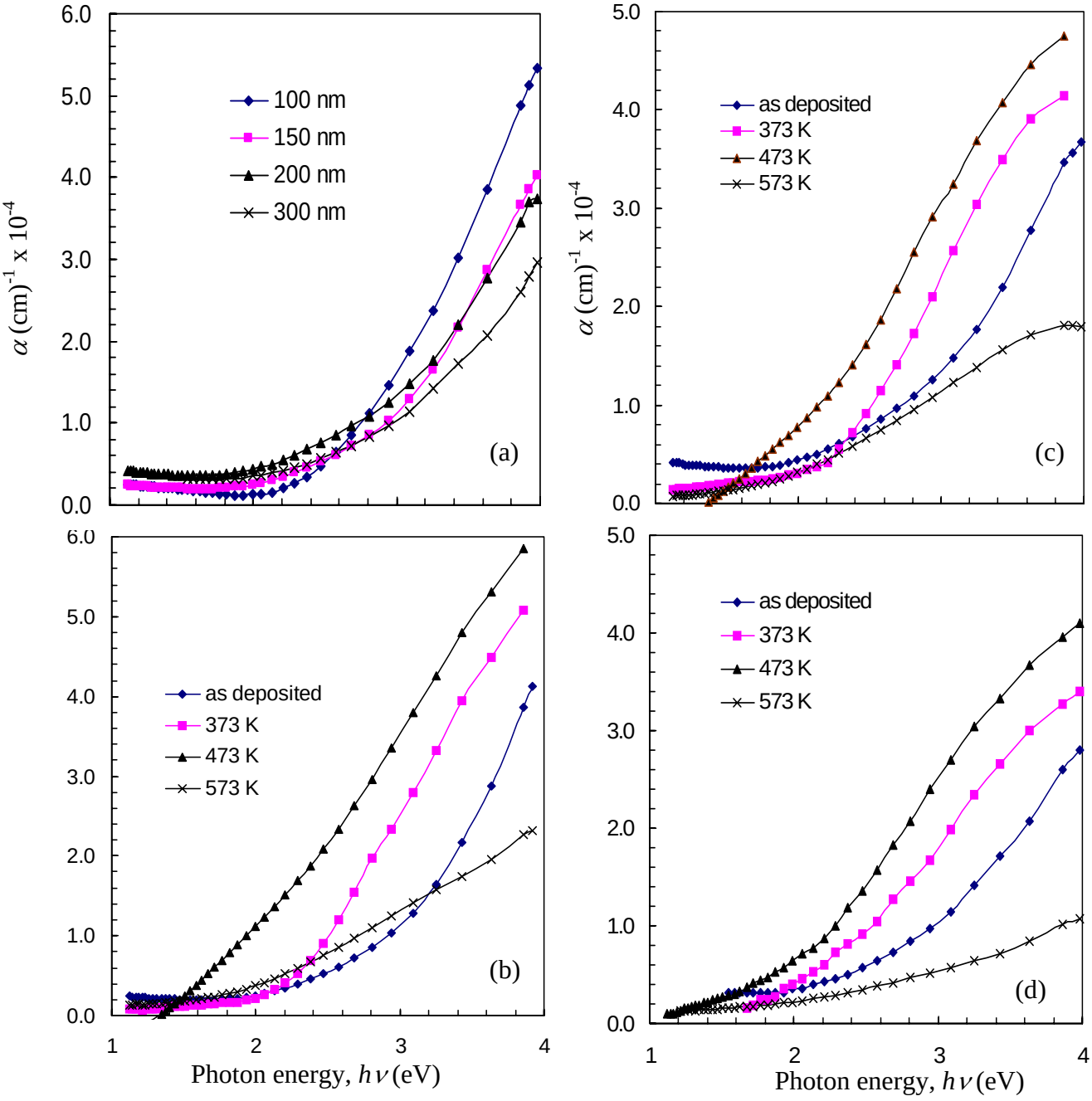

Fig. 5.7. Absorption co-efficient α, as a function of photon energy $h\nu$ for (a) as-deposited PPDEAEMA thin films of different thicknesses and PPDEAEMA thin films of (b) 150 nm, (c) 200 nm, (d) 300 nm thickness heat treated at 373, 473 and 573 K for 1 hour.

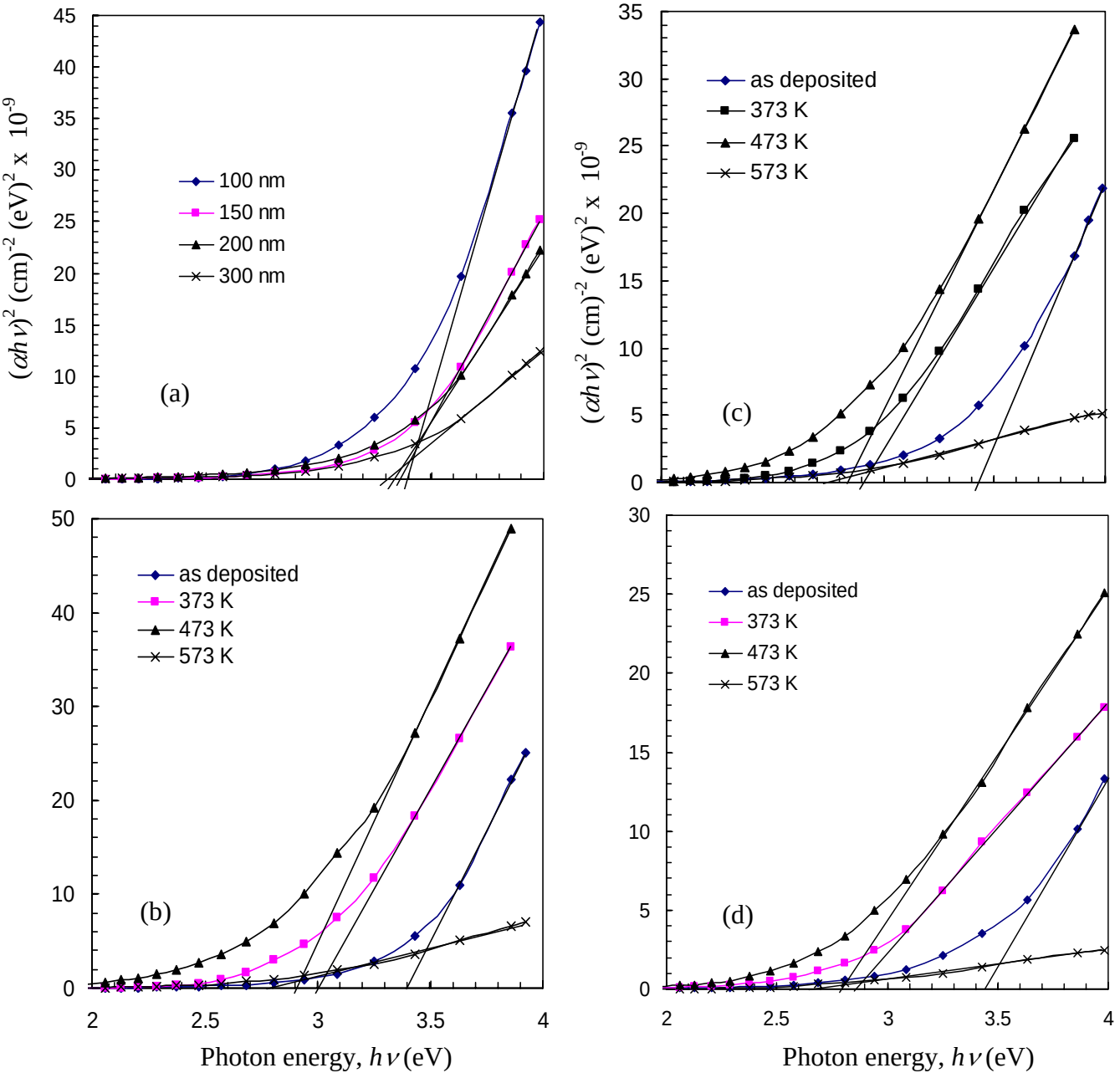

Fig. 5.8 $(\alpha h\nu)^2$ versus $h\nu$ curves for PPDEAEMA thin films of (a) as deposited and PPDEAEMA thin films of (b) 150 nm, (c) 200 nm, (d) 300 nm thickness heat treated at 373, 473 and 573 K for 1 hour.

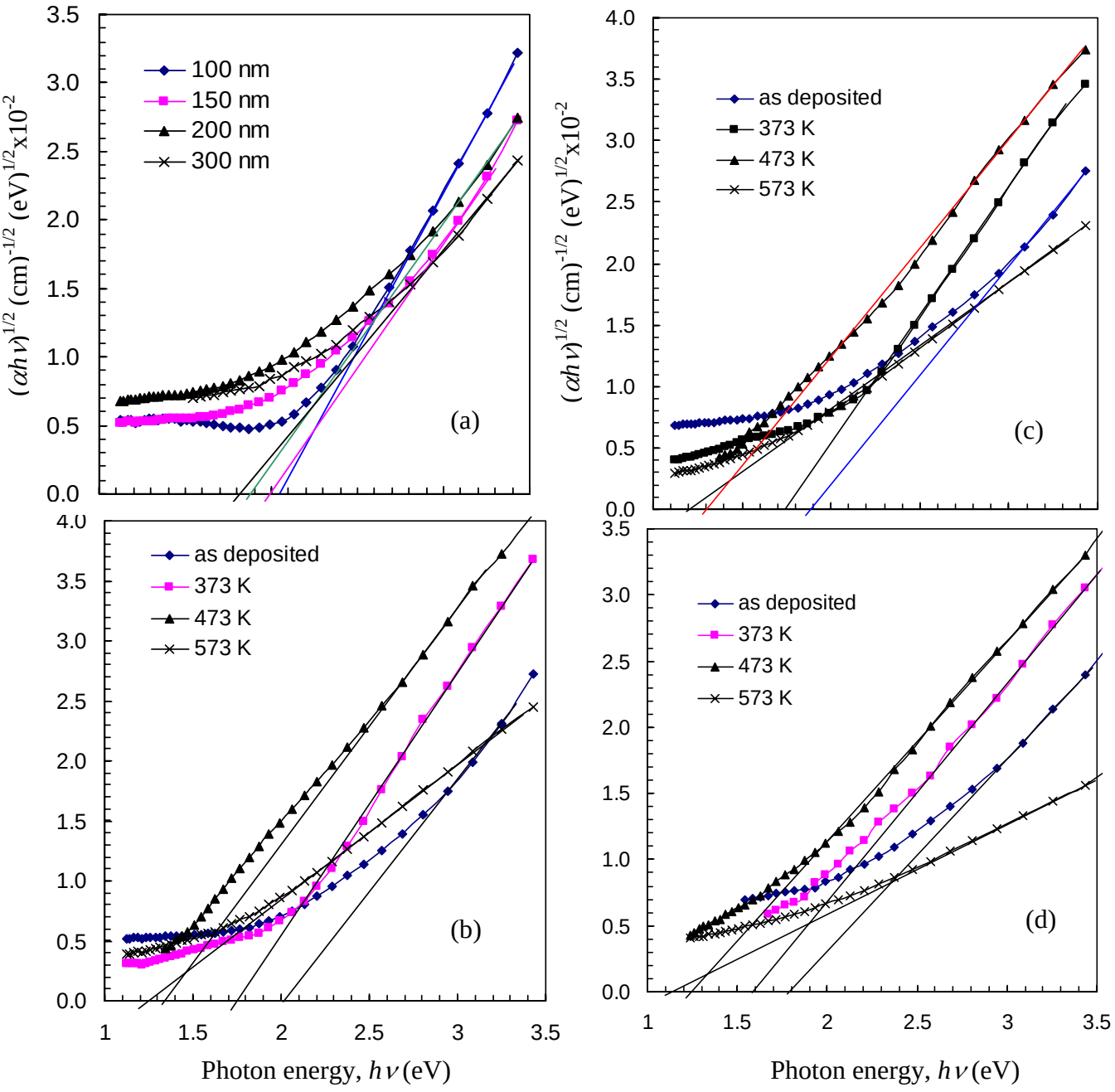

Fig. 5.9 $(\alpha h\nu)^{1/2}$ versus $h\nu$ curves for PPDEAEMA thin films of (a) as deposited and PPDEAEMA thin films of (b) 150 nm, (c) 200 nm, (d) 300 nm thickness heat treated at 373, 473 and 573 K for 1 hour.

Table 5.5. Values of allowed direct, indirect transition energy gaps for as- deposited and heat treated (at 373 K, 473 K and 573 K for 1 hour) PPDEAEMA thin films of different thicknesses.

Film thickness d(nm)	Direct transition energy gap, E_{qd} (eV)				Indirect transition energy gap, E_{qi} (eV)			
	As-deposited	Heat treated for 1 hour at			As-deposited	Heat treated for 1 hour at		
	273 K	373 K	473 K	573 K	273 K	373 K	473 K	573 K
100	3.40	-	-	-	2.05	-	-	-
150	3.36	3.00	2.91	2.80	2.00	1.80	1.35	1.25
200	3.33	2.90	2.84	2.75	1.90	1.75	1.30	1.20
300	3.30	2.85	2.80	2.70	1.80	1.60	1.25	1.15

The E_u can be evaluated as the width of the exponential absorption edge or as the width of the tails of localized states, associated with the amorphous state, in the forbidden gap. The values of E_u were calculated from the slopes of these figures using the relationship, $E_u = [d(\ln\alpha)/d(h\nu)]^{-1}$ and calculated values are given in Table 5.6.

The steepness parameter σ, which illustrates the broadening of the optical absorption edge due to electron-phonon or exciton-phonon interactions [12] can be determined from the equation $\sigma = kT/E_u$, where k is the Boltzmann constant and T is the absolute temperature. The σ values are calculated taking T=300 K and are depicted in Table 5.6.

Table 5.6. Values of allowed Urbach energy E_u and steepness parameter σ for as- deposited and heat treated (at 373 K, 473 K and 573 K for 1 hour) PPDEAEMA thin films of different thicknesses.

Film thickness d(nm)	E_u (eV)				σ			
	As-deposied	Heat treated for 1 hour at			As-deposied	Heat treated for 1 hour at		
	273 K	373 K	473 K	573 K	273 K	373 K	473 K	573 K
100	0.63	-	-	-	0.041			
150	0.69	0.63	0.77	1.08	0.037	0.041	0.034	0.024
200	0.88	0.65	0.79	1.17	0.030	0.039	0.032	0.021
300	0.94	0.74	0.85	1.26	0.028	0.035	0.030	0.019

The σ values indicate that the absorption edge changes with increasing thickness. From the absorption coefficient, the extinction coefficient can be calculated as $k(\lambda) = \alpha\lambda / 4\pi$

and $k(\nu)$ versus $h\nu$ curves are presented in Fig. 5.11 (a,b,c,d). It is clear from Fig 5.11 (a,b,c,d) that the extinction coefficient increases with increasing photon energy. Yakuphanoglu and Arslan [13] reported the increase of extinction coefficient with the increase in photon energy for some charge transfer compounds.

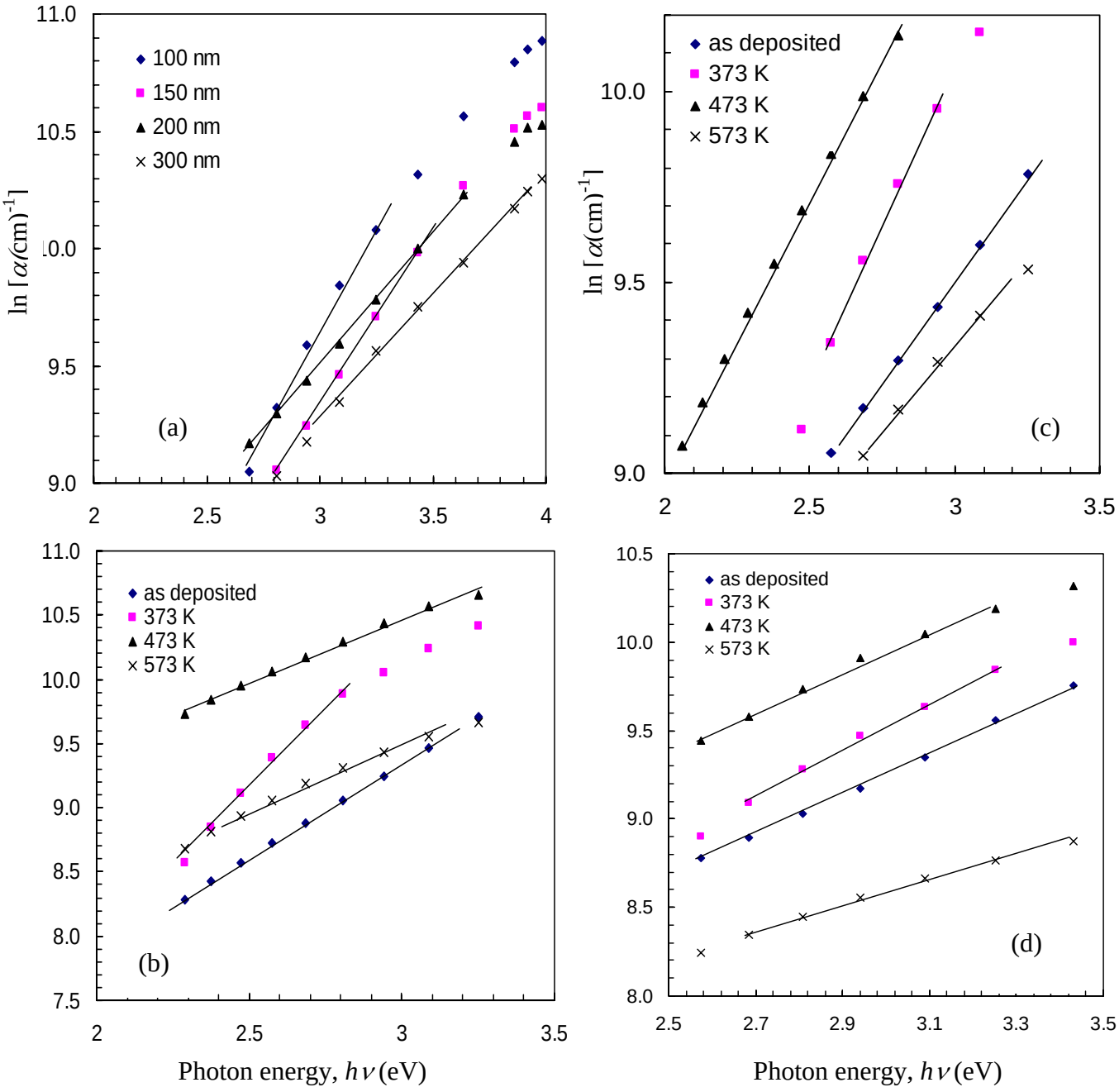

Fig. 5.10 ln α versus $h\nu$ curves for PPDEAEMA thin films of (a) as deposited and PPDEAEMA thin films of (b) 150 nm, (c) 200 nm, (d) 300 nm thickness heat treated at 373, 473 and 573 K for 1 hour.

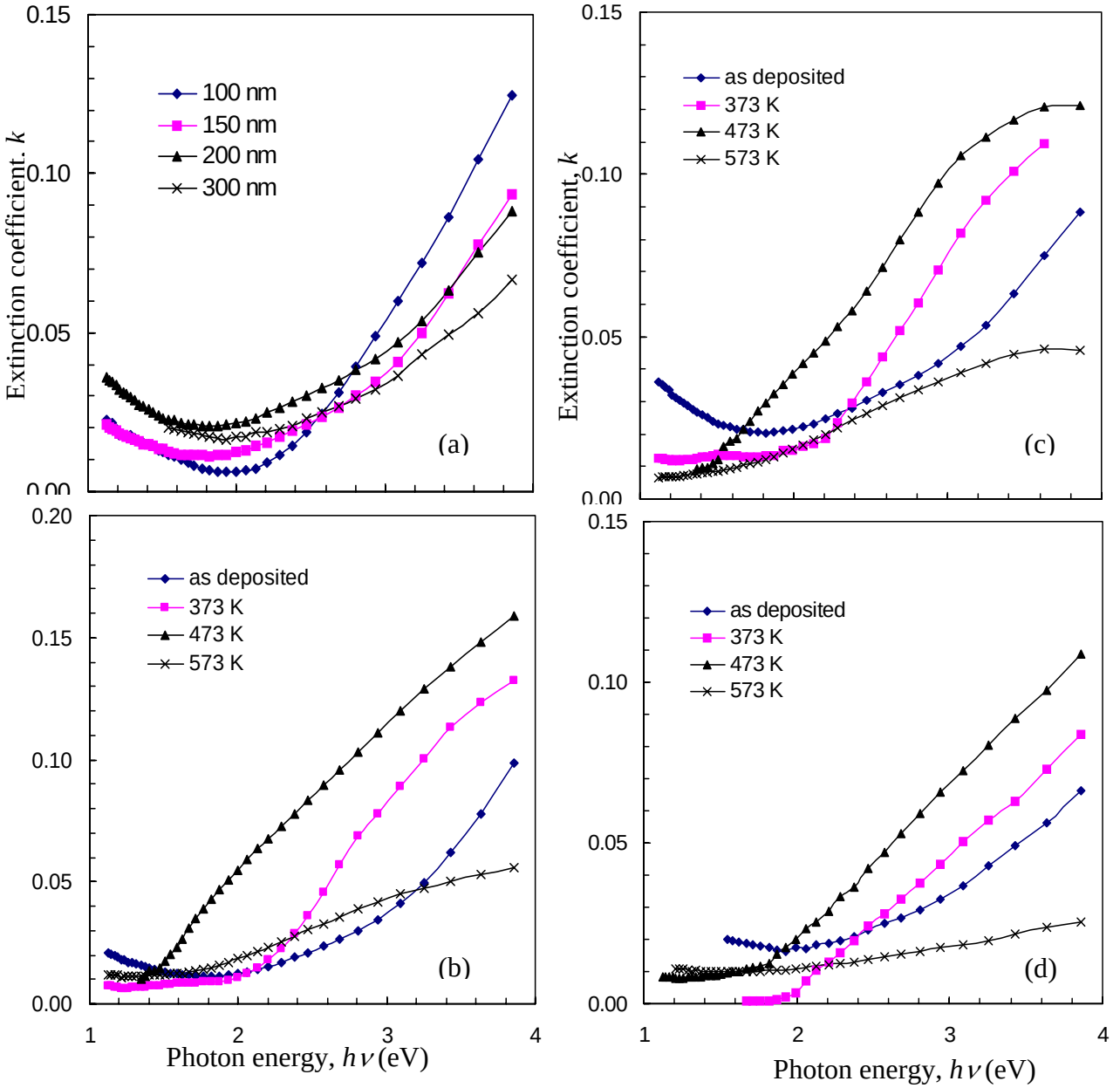

Fig. 5.11 $k(\nu)$ versus $h\nu$ curves for PPDEAEMA thin films of (a) as deposited and PPDEAEMA thin films of (b) 150 nm, (c) 200 nm, (d) 300 nm thickness heat treated at 373, 473 and 573 K for 1 hour.

5.5.2 UV-vis spectroscopic analyses of Iodine doped PPDEAEMA thin films

The PPDEAEMA thin films were subjected to iodine doping for different time span at room temperature to investigate the effect of iodine doping on the optical energy band gap. The variation of absorbance with wave length curves for PPDEAEMA thin films of different thicknesses, doped by iodine for (a) 45 min (b) 360 min and (c) 720 min are presented in Fig. 5.12 (a, b, c). There are two clear absorption peaks one (near about 300 nm) for as deposited

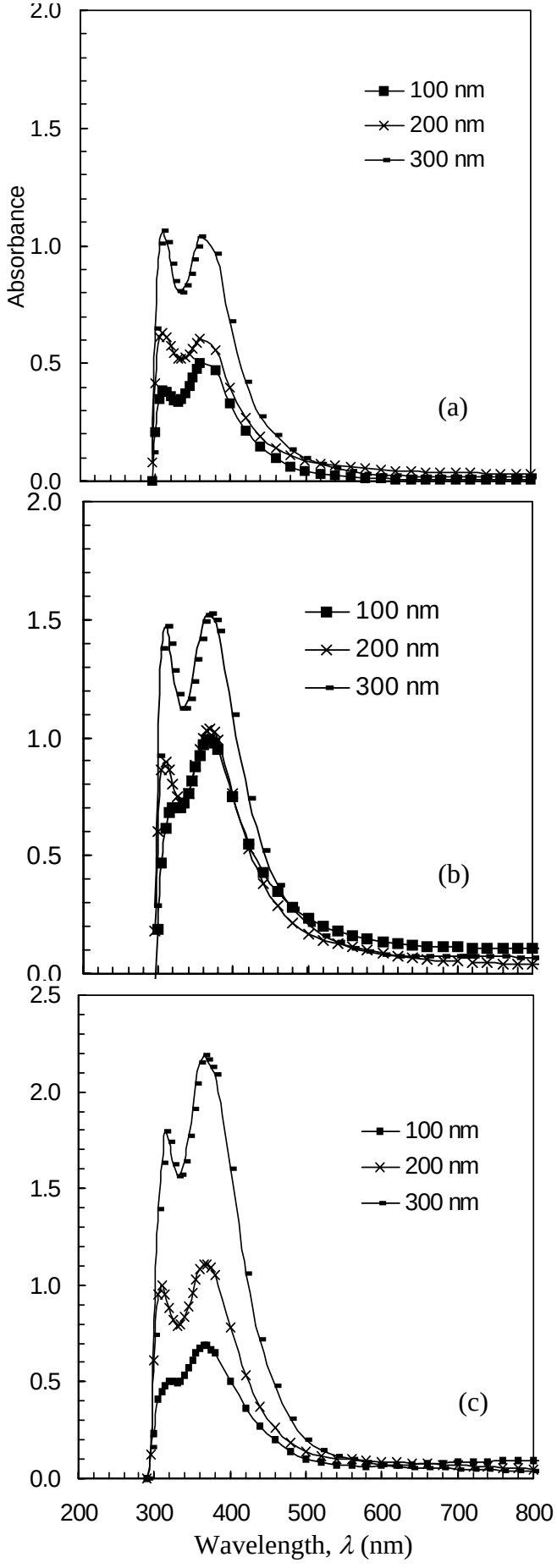

Fig. 5.12. Variation of absorbance with λ of iodine doped PPDEAEMA thin films of different thickness with different doping time : (a) 45 min, (b) 360 min and (c) 720 min.

PPDEAEMA and another (near about 370 nm) arise due to iodine doping. The absorption spectra exhibit a relatively similar change upon iodine doping which enhanced the maximum absorption wave length towards higher wavelength due to charge carriers added to the structure and a new absorption band observed at 370 nm. This band is attributed to the PPDEAEMA structure which is a weak band due to iodine doping [14-15] The peaks increases with increasing the duration of iodine exposure providing an evidence for the incorporation of iodine into PPDEAEMA [16]. The α versus $h\nu$ curves for all iodine doped PPDEAEMA thin films are shown in Fig. 5.13 (a, b, c) which displays an exponential nature at the low energy region which possibly arise due to the short range order or due to the presence of defects in the thin films [8]. So these curves can be characterized by different slopes indicating the presence of allowed direct and indirect transitions in PPDEAEMA thin films. The $(\alpha h\nu)^2$ versus $h\nu$ plot has a linear portion that, when extrapolated, cuts the energy axis. The energy at the intersection corresponds to the threshold of optical absorption and hence the optical band gap values. The direct and indirect transition energy gap E_{qd} and E_{qi} of the iodine doped PPDEAMEA thin films were determined from $(\alpha h\nu)^2$ versus $h\nu$ curves and $(\alpha h\nu)^{1/2}$ versus $h\nu$ curves respectively and shown in Fig.5.14 and 5.15. The values of the E_{qd} and E_{qi} obtained from Fig. 5.14 (a, b, c) and 5.15 (a, b, c) are depicted in Table 5.7. From the Table 5.7 we find that E_{qd} values decreases with respect to E_{qd} of as deposited PPDEAEMA thin films whereas E_{qi} values increases with respect to E_{qi} of that one. The changes of E_{qd} and E_{qi} indicate that there is a charge transfer complex arising between the host polymer and the iodine [16]. The reduction in the band gap due to iodine doping may be due to the incorporation of iodine into the polymer chain and thereby, extending the density of states more into the visible region of the electromagnetic spectrum as compared to that of the undoped case (iodine has a broad absorption band extending from the UV well into the visible region of the electromagnetic spectrum) [17]. A similar change in the band gap values upon iodine doping has already been reported for some other materials [18-20]. The decrease in the optical band gap can be correlated with the increase in electrical conductivity of the films. A probable reason for this enhancement is that the hole density of the polymer is increased by the doping of iodine. The iodine doping attracts the electrons from the molecular orbital and produces a sublevel gap or additional level in the band structure and due to the incorporation

of iodine, the band gap between the π–π* state decreases as a result of increase in the length of the π conjugated system [21-22].

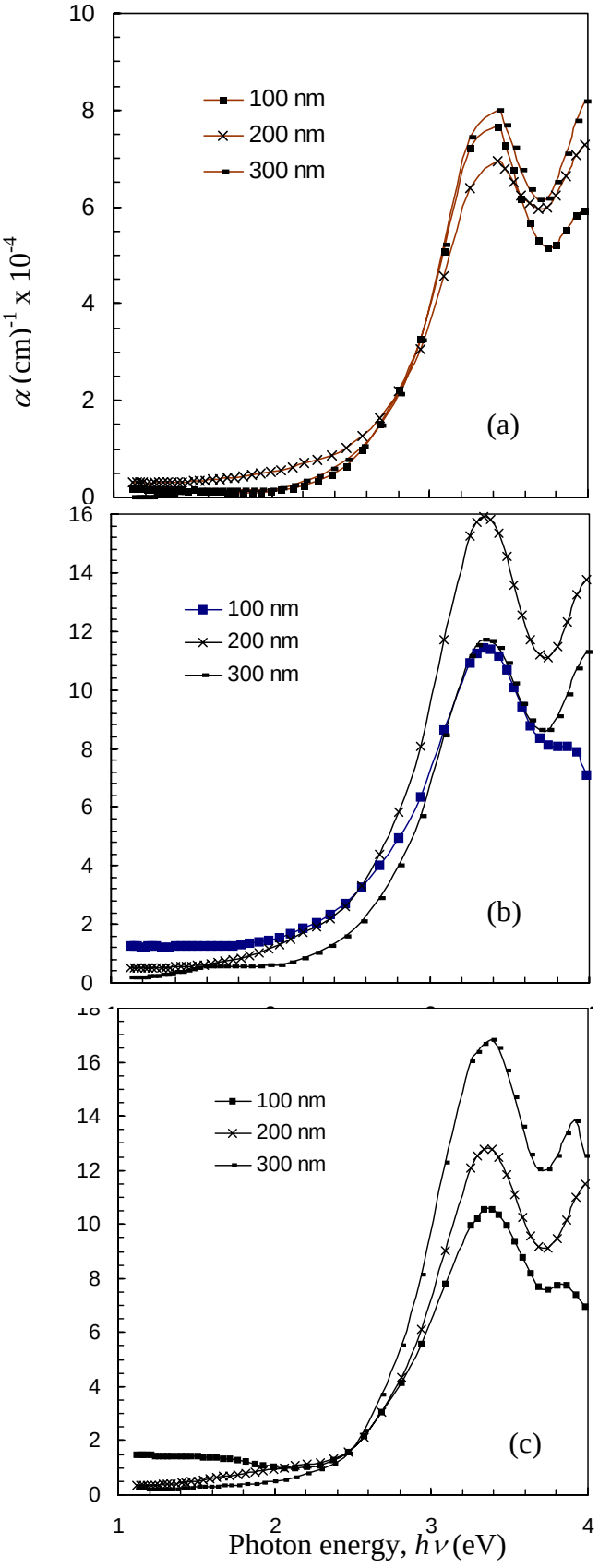

Fig. 5.13. Absorption co-efficient α, as a function of photon energy, hν of iodine doped PPDEAEMA thin films of different thicknesses with different doping time : (a) 45 min, (b) 360 min and (c) 720 min.

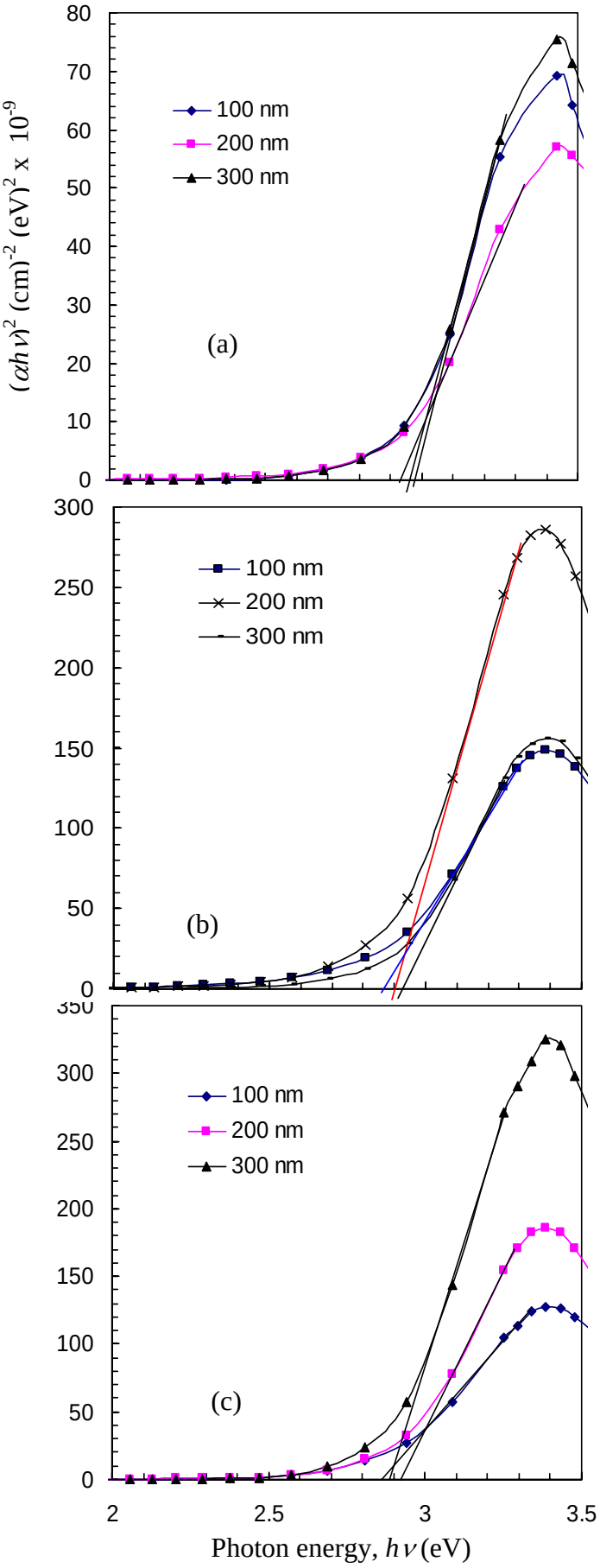

Fig. 5.14 $(\alpha h\nu)^2$ versus $h\nu$ curves for PPDEAEMA thin films of different thicknesses with different doping time : (a) 45 min, (b) 360 min and (c) 720 min.

Table 5.7. Values of allowed direct, indirect transition energy gaps for as deposited and iodine doped PPDEAEMA thin films of different thicknesses at different period of doping.

Film thickness d(nm)	Direct transition energy gap, E_{qd} (eV)				Indirect transition energy gap, E_{qi} (eV)			
	As-deposited	Iodine doped for			As-deposited	Iodine doped for		
		45 min	360 min	720 min		45 min	360 min	720 min
100	3.40	2.93	2.87	2.87	2.05	2.32	2.14	2.20
200	3.33	2.97	2. 90	2.89	1.90	2.41	2.22	2.29
300	3.30	2.98	2.92	2.92	1.80	2.50	2.32	2.32

The dependence of ln α on $h\nu$ for the iodine doped PPDEAMEA thin films of different thickness and period of doping are depicted in Fig. 5.16 (a, b, c, d). The absorption edge in the spectral range of direct optical transitions has exponential shape following the relationship [9] $\alpha\ (h\nu) = \alpha_o \exp [h\nu / E_u]$ where α_o is a constant, which is independent of temperature and E_u is the Urbach energy. The values of E_u were calculated from the slopes of these figures using the relationship, $E_u = [d(\ln\alpha)/d\ (h\nu)]^{-1}$ and calculated values are given in Table 5.6. The value of E_u slightly decreases as the thickness increases. This behavior may be due to decrease in the degree of disorder and decrease in density of defect states (which results in the reduction of tailing of bands). The σ values are calculated taking T=300 K and are depicted in Table 5.8.

The σ values suggest that the absorption edge changes with increasing thickness. From the absorption coefficient, the extinction coefficient can be calculated as $k(\lambda) = \alpha\lambda / 4\pi$ and $k(\nu)$ versus $h\nu$ curves are presented in Fig. 17 (a,b,c). It is evident from Fig 5.17 (a,b,c) that the extinction coefficient increases with increasing photon energy.

Table 5.8 Values of allowed Urbach energy E_u and steepness parameter β for as deposited and iodine doped PPDEAEMA thin films of different thicknesses.

Film thickness d(nm)	E_u (eV)				σ			
	As-deposied	Iodine doped for			As-deposied	Iodine doped for		
		45 min	360 min	720 min		45 min	360 min	720 min
100	0.63	0.40	0.73	0.43	0.041	0.056	0.035	0.060
200	0.88	0.34	0.60	0.37	0.030	0.065	0.043	0.070
300	0.94	0.33	0.44	0.34	0.028	0.078	0.058	0.077

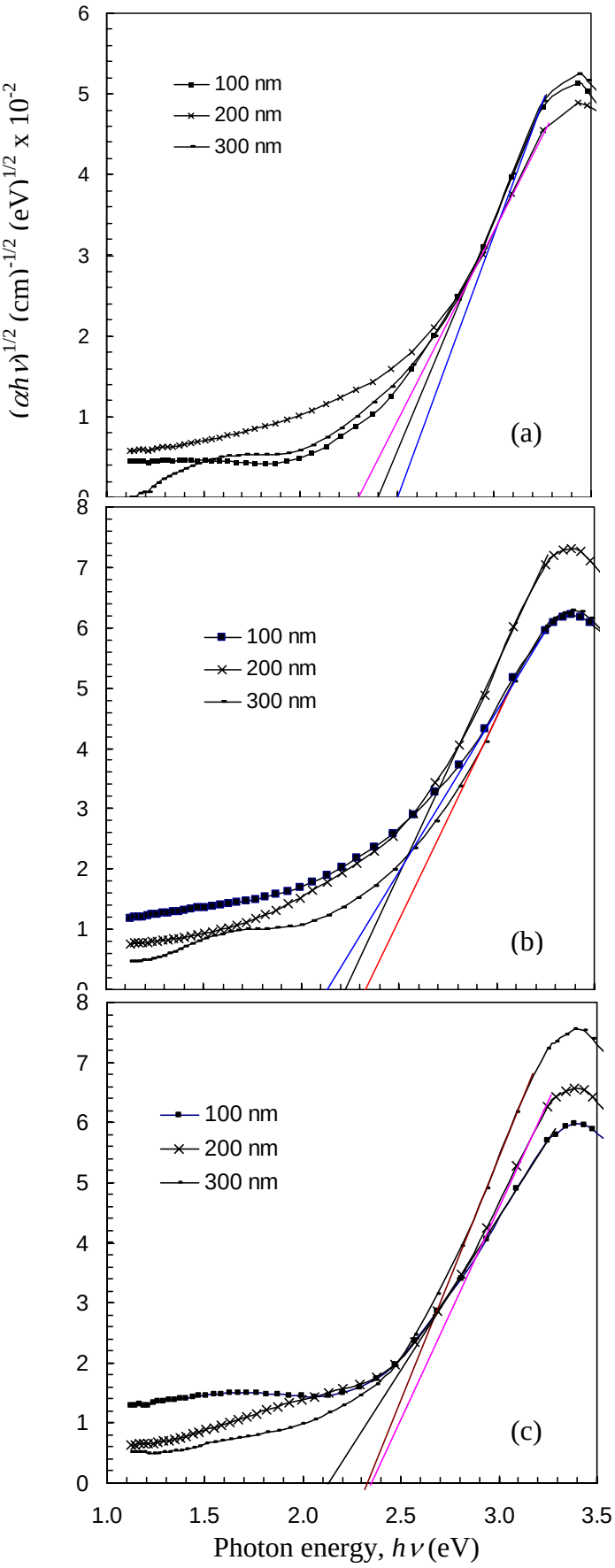

Fig. 5.15 $(\alpha h\nu)^{1/2}$ versus $h\nu$ curves for PPDEAEMA thin films of different thicknesses with different doping time : (a) 45 min, (b) 360 min and (c) 720 min.

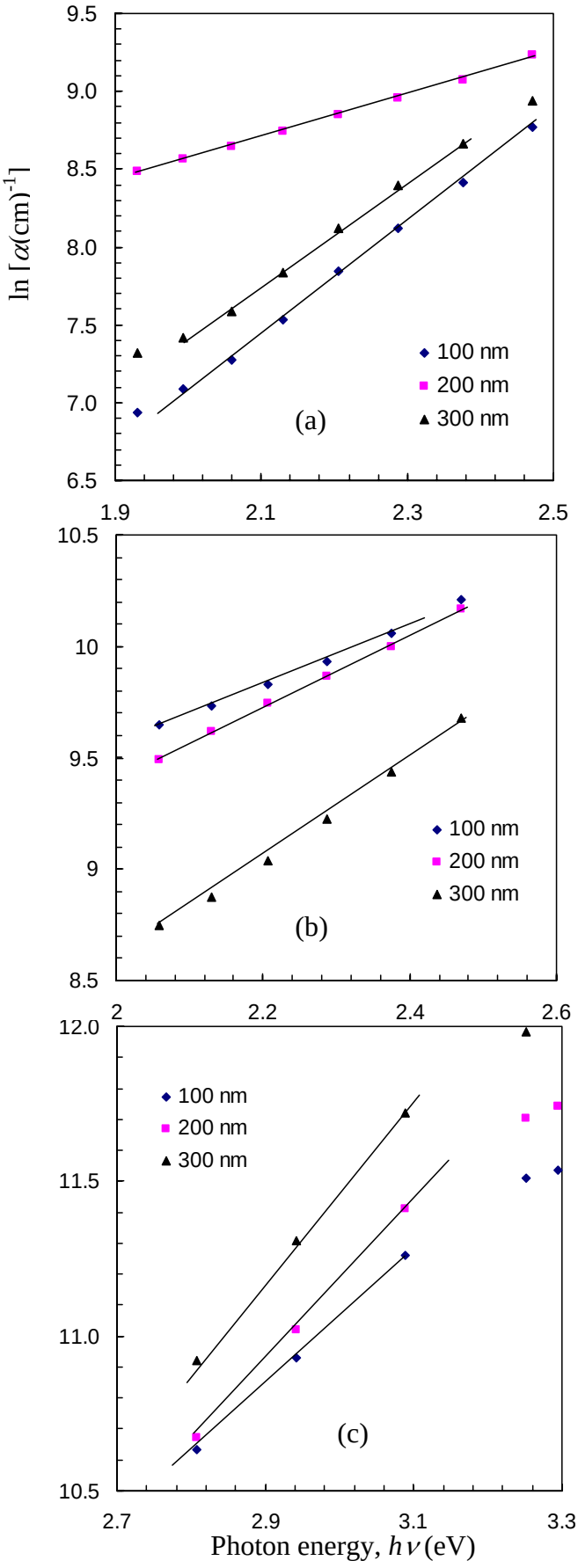

Fig. 5.16 ln α versus $h\nu$ curves for PPDEAEMA thin films of different thicknesses with different doping time : (a) 45 min, (b) 360 min and (c) 720 min.

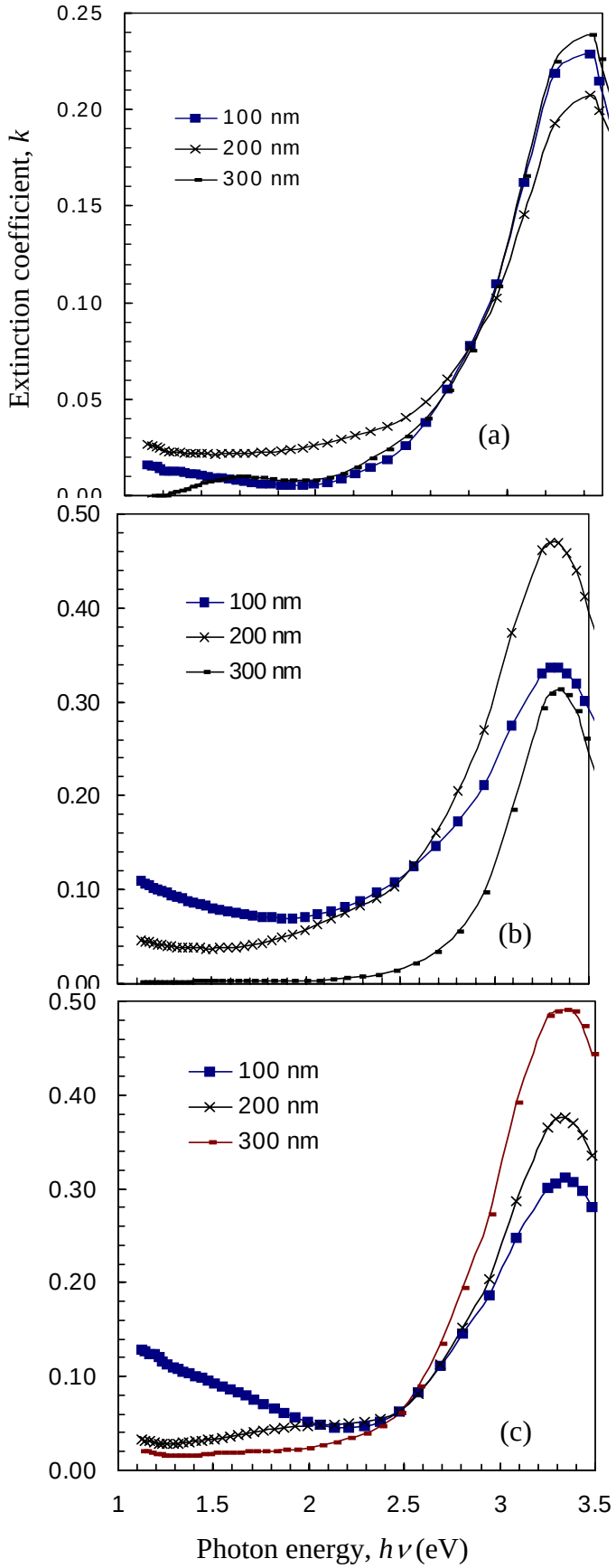

Fig. 5.17 $k\,(\nu)$ versus $h\nu$ curves for PPDEAEMA thin films of different thicknesses with different doping time : (a) 45 min, (b) 360 min and (c) 720 min.

5.6 Interaction of PPDEAEMA with iodine

PPDEAEMA thin films were exposed to iodine in desiccators containing iodine crystals for a certain period of time at room temperature. After doping, the color of the PPDEAEMA thin films changes from pale brown to dark brown which indicates the successful introduction of the iodine in PPDEAEMA thin films. So it can be attributed that iodine may incorporated in the structure of the plasma polymerized PPDEAEMA as shown below:

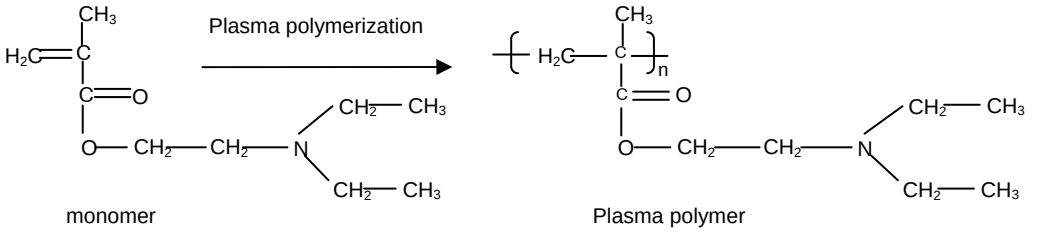

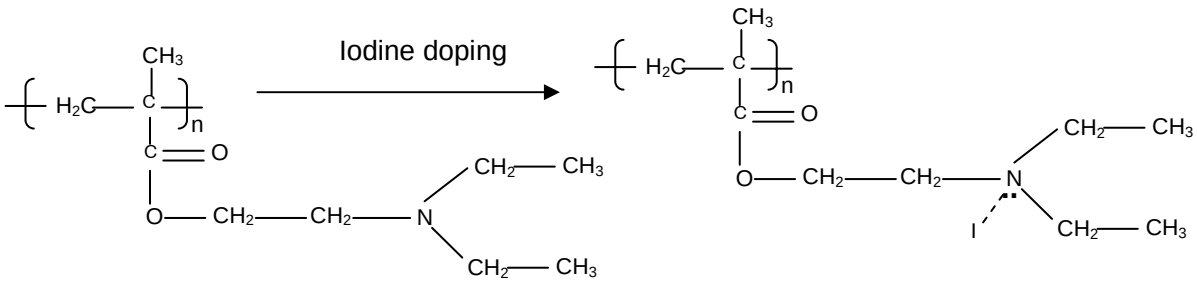

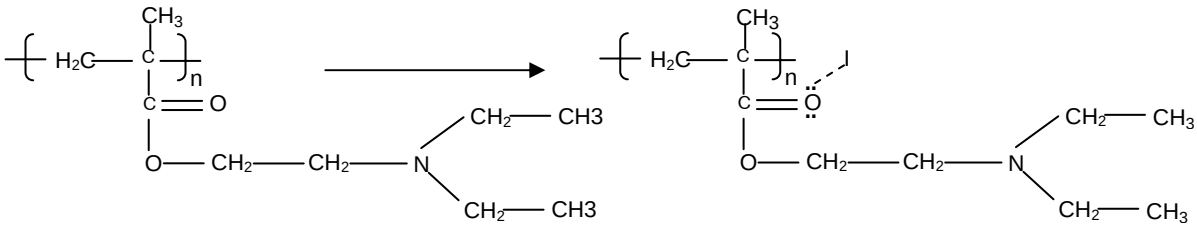

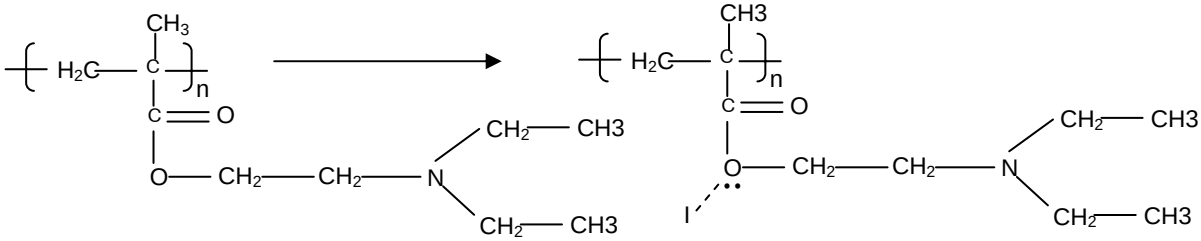

So it can be said that iodine may create bond with N or O thus affects the optical band gap, electrical conductivity etc. Iodine has 7 electrons in its last shell, so it can accept electron

from other element and usually act as acceptor. But since it has large number of electrons (53) it can donate 7 electrons also. Iodine create charge transfer complex with loosely bound lone pair of electrons of O or N of PPDEAEMA.

5.7 Current density-Voltage characteristics for as deposited PPDEAEMA thin films

There are various DC electronic conduction mechanisms by which carriers are transported under the influence of an applied electric field. Generally, one mechanism dominates the observed current but more than one conduction mechanisms may possibly operate at one particular voltage. In the process of conduction by field assisted thermal excitation the carriers are transported from the cathode into the conduction band of the contact barrier (Schottky emission). The mechanism of conduction in an organic device depends on the traps present in the polymer and the metal-polymer interface. Many experimental techniques are in existence for the determination of trap states in an organic device. The *J–V* characteristic in the SCLC regime is one among them. This technique provides information on the energy density and density of traps as well as the charge carrier motilities. Electrons/ holes may also be transported by field-assisted thermal excitation over the lower Coulombic potential barrier (PF emission) [23]. The complete *J–V* characteristics of a polymer device are determined by the carrier mobility μ, the free carrier density n_o, and the trap density N_t.

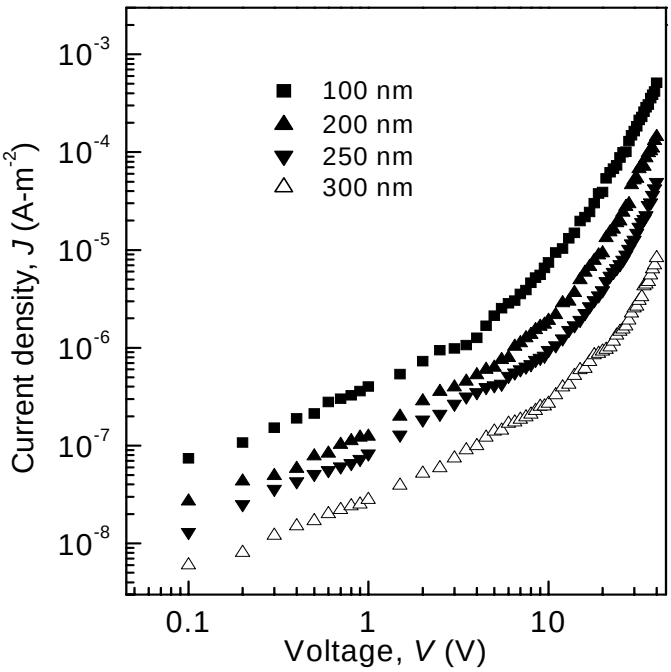

Fig.5.18 Current density versus applied voltage curve for PPDEAEMA thin films of different thicknesses at room temperature.

In order to understand the conduction behavior direct current electrical measurements were performed at varying temperatures on Al/PPDEAEMA/Al thin films of different thicknesses. The *J-V* characteristics of PPDEAEMA thin films of thicknesses of 100, 200 , 250 and 300 nm were recorded at temperatures of 298, 323, 348, 373, 398 and 423 K within the voltage range from 0.1 to 40 V. The *J-V* responses of PPDEAEMA thin films of thicknesses 100, 200, 250 and 300 nm were recorded at room temperature and are presented in Fig. 5.18 which exhibits that current density decreases with the increase in thickness. The J-V characteristics follow a power law of the form $J \alpha V^n$ with different slopes in the lower and higher voltage regions, where *n* is a power index. The values of slopes are $0.90 < n < 1.11$ and $2.24 < n < 5.28$ in the low and high voltage region respectively as depicted in Table 5.9. In all these curves there are two distinct voltage regions having slope of about 1 corresponding to ohmic conduction and of 2.24 to 5.28 in the non-ohmic region. To determine the type of probable conduction mechanism, the dependence of the current density on voltage for samples of different thicknesses is to be investigated. The variation of current density with applied voltages, of PPDEAEMA thin films of thicknesses 100, 200, 250 and 300 nm at different temperatures are presented in Fig. 5.19. It is observed that the current density increases gradually with applied voltage at low voltage region, but, the rate of increase is faster at higher voltage. The general trend of these curves reveal that each curve has two different slopes in the lower and higher voltage regions, corresponding to different conduction processes. The values of the slopes for samples of different thicknesses are tabulated in Table 5.9.

Consequently, the current conduction in the lower range of the applied voltage is found to be ohmic, while in the higher range of the applied field, the charge conduction is found to be non-ohmic. The dependence of current density both on thickness and voltage for higher voltages recommends that the current conduction may be due to either SCLC or Schottky or PF type of conduction. In a particular sample one of the conduction mechanisms will be dominant. If the applied field strength is increased to a certain value that the injected charge carrier density largely exceeds the free charge carrier density under thermal equilibrium, the system transits to SCLC conditions [25] which is influenced by traps. The defects and impurities can govern the conduction mechanism and also work as trapping centers which get occupied by the injected charge carriers from the electrode, hence they

become charged and thereby expected to build up a space charge. This build up of space charge plays the key role in the determination of the SCLC process [24].

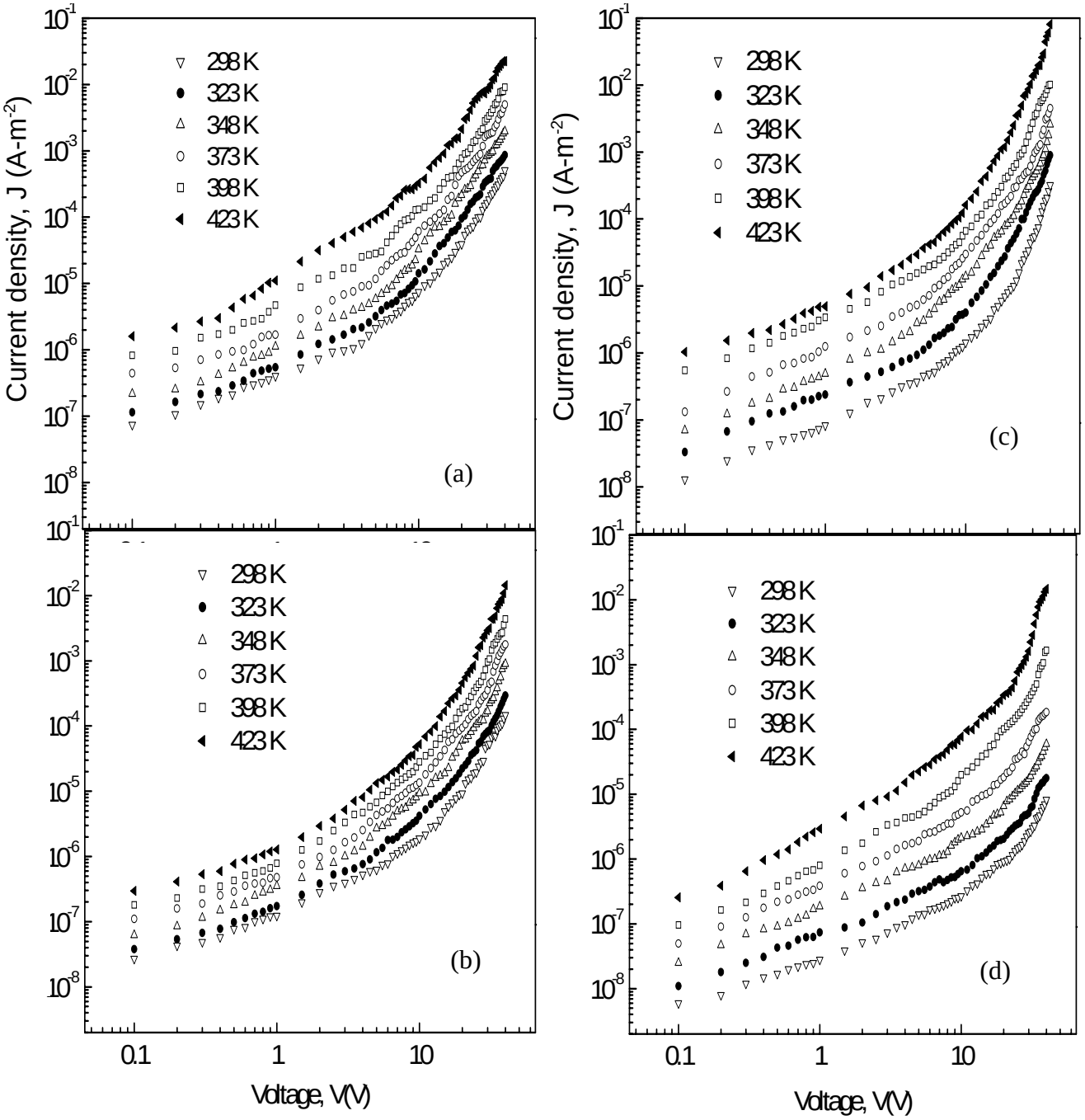

Fig. 5.19 Variation of current density with applied voltage at different temperatures for PPDEAEMA thin film of thickness (a) 100 nm, (b) 200 nm, (c) 250 nm and (d) 300 nm.

Table 5.9 The values of the slopes at low and high voltage regions for samples of different thicknesses at different temperatures.

Thickness (nm)	Temperature T (K)	Values of the slope, n	
		Low voltage region	High voltage region
100	298	0.96	2.78
	323	0.98	2.81
	348	0.97	3.17
	373	0.90	3.27
	398	0.99	3.33
	423	1.06	4.30
200	298	1.08	2.36
	323	0.92	3.59
	348	1.02	5.24
	373	1.10	5.08
	398	1.11	4.81
	423	1.11	5.14
250	298	0.92	4.71
	323	0.95	4.20
	348	0.97	4.36
	373	0.91	4.62
	398	0.95	5.28
	423	0.94	4.89
300	298	0.93	2.26
	323	0.91	2.24
	348	0.96	2.72
	373	0.91	3.25
	398	1.10	2.63
	423	1.11	3.87

Moreover, the current densities at higher temperatures are increased significantly illuminating a temperature dependence of the current density. This type of strong temperature dependence was also reported for PMMA by Shukla and Gaur [24]. It is seen that as the

temperature increases the knee voltage corresponding to the sharp rise in current in PPDEAEMA films increases.

5.7.1 Current density-Thickness characteristics of as deposited PPDEAEMA thin films

At the higher voltage region the dependence of *J* on thickness and voltage recommend that the current may be due to space charge limited conduction, Schottky or PF conduction mechanisms in PPDDEAEMA thin films. To differentiate the type of conduction mechanisms, the dependence of *J* on film thickness, *d*, for the thin films of different thicknesses at a constant voltage (30 V) and at room temperature is depicted in Fig. 5.20. The dependence of the current density upon thickness in the non-ohmic region of applied voltage can be given by $J \alpha d^{m}$, where *m* is a parameter which depends on the distribution of traps. A slope of $m < 3$ suggests the possibility of Schottky or PF mechanism, whereas $m \geq 3$ gives the preference of SCLC mechanism in PPDEAEMA thin films.

Fig. 5.20 shows the variation of *J* with *d* for PPDEAEMA thin films in the non-ohmic region (V= 30 V). The plot exhibits that *J* is inversely proportional to *d* with a slope of - 4.2 which is much higher than that corresponding to the Schottky and PF conduction mechanism and this value is in good agreement to the required value ($m>3$) of *'m'* for SCLC mechanism. Consequently, it can be recommended that SCLC is the most probable mechanism of charge transport in PPDEAEMA thin films. Shukla and Gaur [24] reported that as a polar, amorphous material PMMA provide a large number of trapping centers and trapping of charge carriers in these trapping sites which would result in the build up of a space charge. Thus as a derivative of MMA, PPDEAEMA may also have the same characteristics.

In SCLC the current density in absence of traps can be expressed by the classical Mott-Gurney relation, equ^{n} (5.1).

$$J = \frac{9}{8}\frac{\mu\varepsilon'\varepsilon_0 V^2}{d^3} \qquad (5.1)$$

where μ is the mobility of charge carriers, ε' is the dielectric constant of the material, ε_o is the permittivity of free space, *V* is the applied voltage and *d* is the thickness of the film. Hence, for SCLC current density *J* will depend linearly on V^2 and d^{-3}. So, the slope of the *J*-*V* characteristics should amount to 2. From the slope of log*J*-log*V* curve it is observed that in the

higher voltage region, the slopes are equal to or greater than 2 i.e. current density, *J*, depends quadratically on the voltage, *V*, which recommends the possibility of SCLC in PPDEAEMA thin films.

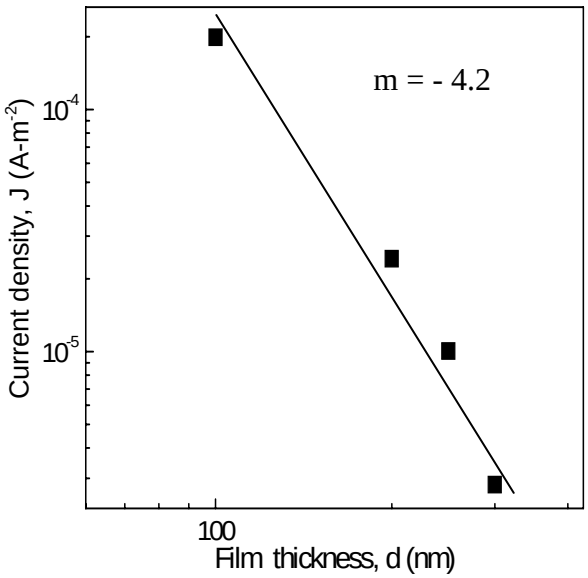

Fig. 5.20 Plot of the current density against different thicknesses for PPDEAEMA thin films in the non-ohmic region (30 V).

In the SCLC region, the carrier mobility μ is calculated for samples of different thicknesses and depicted in Table 5.10. The low mobility arises due to hopping process of carriers from the center to center involving a finite energy jump for each transition in an amorphous material. The interesting features of equ^{n} (5.1) are *J* is directly proportional to V^2 and is inversely proportional to d^{-3} in SCLC. If the insulator contains traps, a large fraction of the injected space charge will condense in that and since the occupancy of traps is a function of temperature, the expression for *J* reduces to

$$J = \frac{9}{8}\frac{\mu\varepsilon'\varepsilon_0\theta V^2}{d^3} \tag{5.2}$$

with $\theta = \frac{N_c}{N_t}\exp(-\frac{E_t}{kT}) < 1$ is the fraction of the total space charge which remains free. Where N_c the effective density of states in the conduction band, N_t the density of trapping levels situated at an energy E_t below the conduction band edge. In general the parameter θ is an increasing function of voltage, so the *J*-*V* characteristics will not essentially be proportional to the square of the voltage, i.e., $n \geq 2$ and be voltage dependent. Lampert [26] mentioned that only when the injected free carrier density n_i exceeds the volume generated

free carrier density n_o space charge effect would occur, when $n_0 > n_i$ the volume (ohmic) conductivity will predominate. From Fig. 5.18, the carrier mobility in the SCLC region was calculated and depicted in Table 5.10. The low mobility arises because of the movement of carriers by a hopping process from the center to center involving a finite energy jump for each transition, in an amorphous material.

Table 5.10 Carrier mobility, μ, free carrier density, n_0, and trap density, N_t for PPDEAEMA thin films of different thicknesses at room temperature.

Thickness d(nm)	Carrier mobility μ ($m^2V^{-1}S^{-1}$)	free carrier density n_0 (m^{-3})	trap density N_t (m^{-3})
100	2.78×10^{-18}	1.78×10^{23}	1.58×10^{24}
200	2.43×10^{-18}	1.84×10^{23}	8.81×10^{23}
250	1.92×10^{-18}	1.97×10^{23}	7.68×10^{23}
300	9.48×10^{-19}	2.10×10^{23}	6.88×10^{23}

From Table 5.10 it is noticed that the PPDEAEMA thin films of smaller thickness, the trap density is high. Conversely, for samples of higher thickness, the values of trap densities are lower than that of lower thickness. The total density of traps may have two origins, one from the surface and the other from the volume or bulk. When the thickness of the PPDEAEMA films increases the interfacial strain may be reduced due to increase in the volume of the samples, that is, surface stress in the interface may be reduced as the volume of the thin films increases. Also due to plasma interaction some fragmentation of the monomer takes place. Owing to the exposure to the atmosphere oxygen is present as carboxyl group. The presence of C=C bonds, unsaturated bonds of carbon and nitrogen, carboxyl groups, etc., are also responsible for the SCLC type of conduction in the material. The higher values of μ and N_t for lower thickness confirm the conductivity of PPDEAEMA thin films of lower thickness is higher than that of the films of higher thickness.

The observed (Fig.5.19) low current densities at low voltages are due to the capture of injected charges in traps. With gradual increase of the bias voltage, the number of injected carriers increases, thereby filling the limited traps. According to Lampert, if sufficient charge is injected into the polymer film, all the traps will become filled reaching the trap filled limit

(TFL) and as a result the current becomes SCLC. Since all the traps are now filled-up, any more carriers injected from the Al electrode go into the conduction band and contribute into the current and consequently the current increases steeply and is proportional to V^n, with n >2. When $V > V_{TFL}$, the J-V characteristics will be described by equ^n (5.1) rather than equ^n (5.2), thus as V just exceeds V_{TFL}, the current rises rapidly by an amount θ^{-1}.

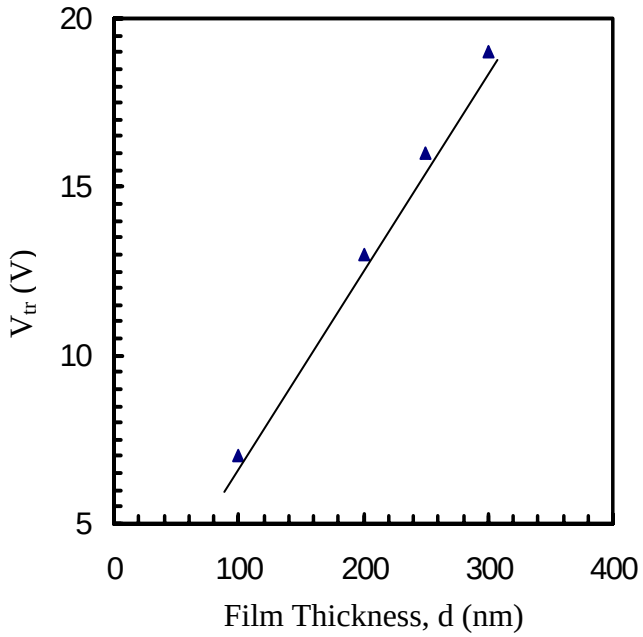

Fig. 5.21 Variation of V_{tr} against different thicknesses for PPDEAEMA thin films in the non-ohmic region.

The voltage V_{TFL} at which filling of all traps occurred is given by

$$V_{TFL} = \frac{eN_t d^2}{2\varepsilon'\varepsilon_0} \qquad (5.3)$$

where ε' is the relative permittivity of the material and N_t is the total concentration of traps. We observe that the current becomes non-ohmic above a certain transition voltage V_{tr} and the system then switches to the SCLC. Equilibrium carrier concentration n_o can be determined from the equ^n

$$n_0 = \frac{9\varepsilon'\varepsilon_0 V_{tr}}{8ed^2} \qquad (5.4)$$

where V_{tr} is the voltage at which the transition from ohmic to SCLC occurs. The value of the dielectric constant ε' is required to calculate both n_o and N_t. The capacitance of the PPDEAEMA thin films were measured at 5 kHz and ε' was determined to be 3.8 -16. By

using the values of V_{tr} and V_{TFL} (Fig. 5.19) the values of n_0 and N_t were estimated using equation (5.3) and (5.4) and are presented in Table 5.10. The dependence of V_{tr} (between ohmic and SCL conduction) with thickness d is shown in Fig. 5.21. It is observed that V_{tr} increases with the increase of thickness, so for higher thickness the V_{tr} is higher i.e. higher V_{tr} is required for higher thickness PPDEAEMA thin films for transition from ohmic to SCLC.

5.7.2 Temperature dependence of current density of as deposited PPDEAEMA thin films

According to Arrhenius law, the variation of current density, *J* with temperature T is given as

$$J = J_0 \exp(-\tfrac{\Delta E}{kT}) \qquad (5.5)$$

where J_0 is a constant, ΔE is the thermal activation energy of electrical conduction and *k* is the Boltzmann constant. The dependence of *J* on inverse absolute temperature, 1/T, for PPDEAEMA thin film of different thicknesses is presented in Fig. 5.22. There are two curves, corresponding to the temperature dependence in the ohmic (V= 2 V) and in the SCLC regions (V= 30 V) respectively. It is observed that the current density increases slowly for temperatures <400 K and above this *J* increases rapidly with temperature.

This increase in *J* with temperature may be due to the increased movement of the adventitious ions and/or electrons. Both of the curves can be characterized by two different slopes in the low and high temperature regions. The curves have varying slope at low temperatures but become almost linear in the high temperature region, corresponding to well-defined activation energy. The activation energies associated with two temperature regions were calculated from the slopes of $J - \frac{1}{T}$ plot for samples of thicknesses 100, 200, 250 and 300 nm and are presented in Table 5.11. When the charge carriers are localized there is no free motion of charge carriers and the conduction proceeds via the phonon- assisted hopping of charge carriers between localized sites. Since the localized states have quantized energies extending over a certain range, activation energy is required for each hop. The activation energies were estimated to be about 0.12 to 0.20 eV and 0.16 to 0.28 eV for 2 V and 30 V of PPDEAEMA thin films of different thicknesses. These small values of the activation energies suggest the existence of the shallow traps levels in PPDEAEMA thin films.

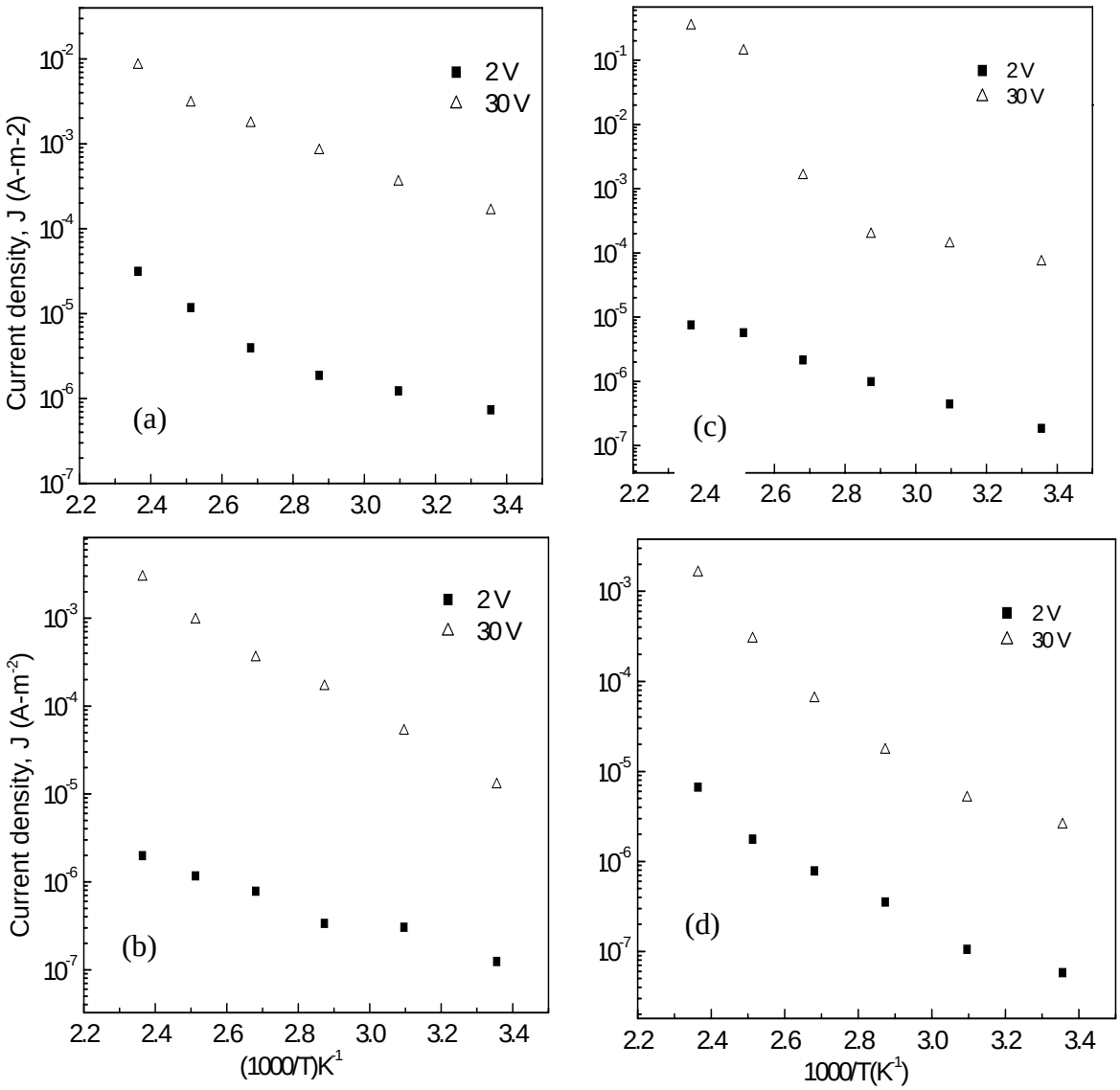

Fig. 5.22 Variation of current density with temperature in the ohmic and non-ohmic regions for PPDEAEMA thin films of of thickness (a) 100 nm, (b) 200 nm, (c) 250 nm and (d) 300 nm.

The low activation energies indicate that the thermally activated hopping conduction is operative in PPDEAEMA thin films. It possibly occur in PPDEAEMA thin films since the existence of ester functional group, with the carbonyl oxygen atom being a basic site, leads to DEAEMA (like PMMA [27]) exhibiting electron-donor ability. So the conduction process takes place by electron hopping between donor atoms and empty sites situated in the energy band gap.

Table 5.11 The values of activation energy ΔE (eV) for PPDEAEMA thin films of different thicknesses.

Thickness	Activation energy, ΔE (eV)	
d (nm)	2 V	30 V
100	0.14 ±0.01	0.16 ±0.01
200	0.12 ± 0.02	0.20 ±0.01
250	0.13 ± 0.01	0.28 ±0.04
300	0.20 ± 0.03	0.25.±0.02

5.7.3 Current-density-Voltage characteristics for iodine doped PPDEAEMA thin films

The J-V characteristics of iodine doped PPDEAEMA thin films of thicknesses 100 and 200 nm were recorded at temperatures of 298, 323, 348, 373, 398 and 423 K within the voltage range from 0.1 to 40 V and depicted in Fig. 5.23 and follow the power law of the form $J \alpha V^n$ with different slopes in the lower and higher voltage regions. The values of slopes are $0.96 < n < 1.1$ and $2.0 < n < 3.29$ in the low and high voltage region respectively and given in Table 5.12. In all these curves there are two distinct voltage regions having slope of about 1 corresponding to ohmic conduction and of 2.0 to 3.29 in the non-ohmic region. The reason behind the nonlinear current-voltage characteristics is the space charge limited conduction (SCLC) [25] which is influenced by traps.

The dependence of *J* on inverse absolute temperature, 1/T, for iodine doped PPDEAEMA thin film of thicknesses 100 and 200 nm are presented in Fig. 5.24. There are two curves, corresponding to the temperature dependence in the ohmic (V= 2 V) and in the SCLC regions (V= 30 V) respectively. It is seen that the current density increases with the increase in temperature. This increase in *J* with temperature may be due to the increased movement of the adventitious ions and/or electrons. The activation energies associated with two temperature regions were calculated from the slopes of $J - \frac{1}{T}$ plot for the iodine doped PPDEAEMA thin films of thicknesses 100 and 200 nm are presented in Table 5.13. The low

activation energies reveal that hopping conduction mechanism is operative in iodine doped PPDEAEMA thin films.

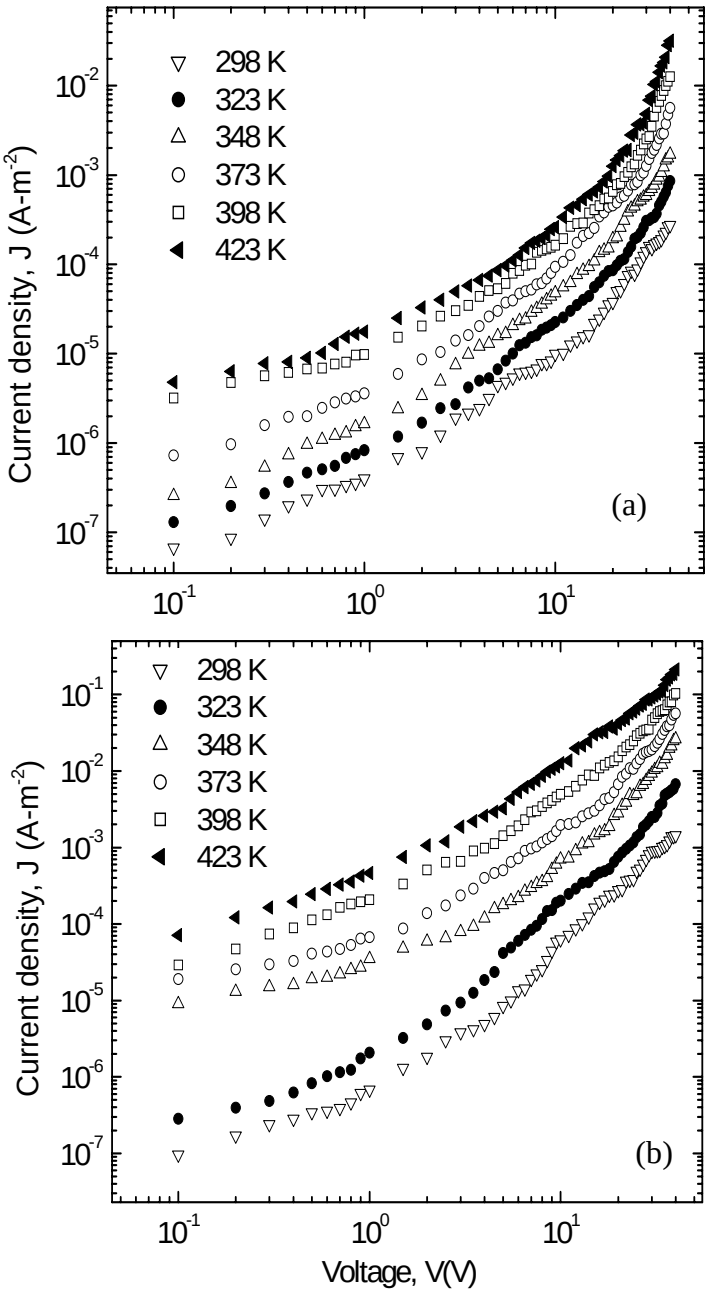

Fig. 5.23 Variation of current density with applied voltage at different temperatures for iodine doped PPDEAEMA thin film of thickness (a) 100 nm and (b) 200 nm.

Table 5.12 The values of the slopes at low and high voltage regions for samples of different thicknesses at different temperatures.

Thickness (nm)	Temperature T (K)	Values of the slope, n	
		Low voltage region	High voltage region
100	298	1.12	2.68
	323	1.16	2.15
	348	0.90	2.43
	373	1.02	2.13
	398	1.09	2.00
	423	1.10	1.79
200	298	1.06	3.01
	323	1.09	2.47
	348	1.08	3.04
	373	0.99	2.49
	398	0.97	2.67
	423	0.96	3.29

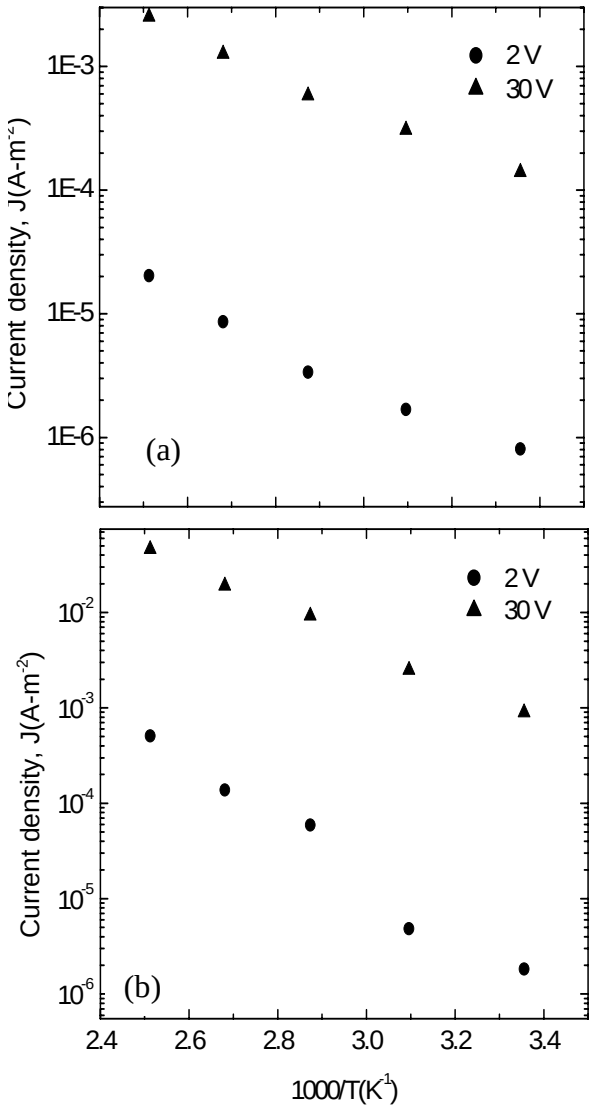

Fig. 5.24 Variation of current density with temperature in the ohmic and non-ohmic regions for iodine doped PPDEAEMA thin films of thicknesses (a) 100 nm and (b) 200 nm.

Table 5.13 The values of activation energy ΔE (eV) for iodine doped PPDEAEMA thin films of different thicknesses.

Thickness	Activation energy, ΔE (eV)	
d (nm)	2 V	30 V
100	0.16 ±0.01	0.21±0.02
200	0.18 ± 0.02	0.25±0.03

5.7.4 Dc electrical conductivity due to iodine doping

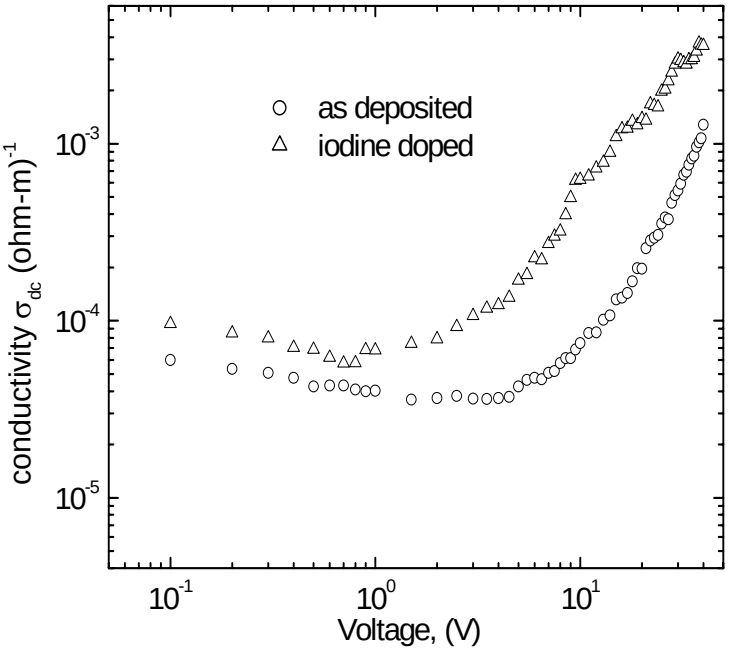

Fig.5.25 Variation of dc electrical conductivity with applied voltage of as deposited and iodine doped (for 45 min) PPDEAEMA thin films of 100 nm.

The variation of dc electrical conductivity with applied voltage (Fig. 5.25) shows a comparative feature between as deposited and iodine doped (for 45 min) PPDEAEMA thin films. It is observed that conductivity increases due to iodine doping. Quamara et al. [28] reported that iodine diffuses preferentially in the less dense volume region of the polymer and is present either interstitially or trapped between the chain configurations and forms a charge transfer complex within the structure; helps in increasing the electron-hole pair concentration thus enhance the conductivity.

5.8 Ac electrical characteristics of as deposited PPDEAEMA thin films

5.8.1 Variation of ac electrical conductivity with frequency and temperature

The ac conductivity σ_{ac} was calculated from the measured values of conductance G(w) by using the formula $\sigma_{ac} = G_p d/A$, where d is the thickness of the sample and A is the cross sectional area of the electrode. The variation of ac conductivity σ_{ac} against frequency from 100Hz to 100 kHz at room temperature for PPDEAEMA thin films of thicknesses 100, 200,

250 and 300 nm are presented in Fig.5.26. It is seen that σ_{ac} increases with the increase in thickness.

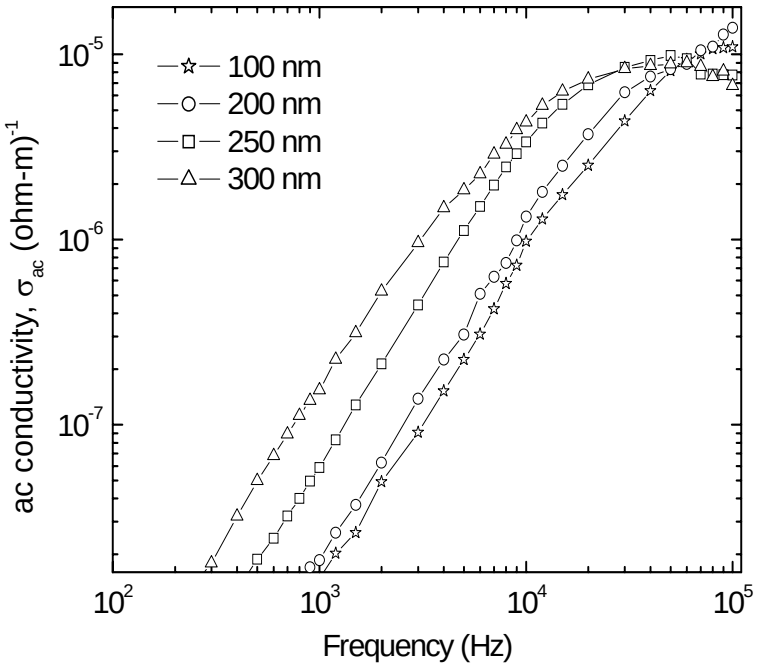

Fig. 5.26 Variation of AC conductivity with frequency for different thicknesses of PPDEAEMA thin films at room temperature.

Figs.5.27 represents the plot of ac conductivity σ_{ac} as a function of frequency from 100Hz to 100 kHz in the temperature range from 298 to 398 K for PPDEAEMA thin films of thicknesses 100, 200, 250 and 300 nm. It is observed that the σ_{ac} increases as frequency increases. There is a little variation of conductivity with thickness. The σ_{ac} increases rapidly up to 10^4 Hz and then the rate of increase become slower. This can be interpreted by the following empirical relation $\sigma_{ac}(\omega) \propto \omega^n$ where ω is the angular frequency and n the index that is used to understand the type of conduction mechanism in amorphous materials and takes the value less than unity for Deby type mechanism. The values of exponent for PPDEAEMA are found to be 0.94-1.3 below 10^3 Hz and 1.4 - 1.88 above 10^3 Hz. The values of the slope n, are found to be around 1 in the lower frequency (f<1kHz) region which corresponds to the Debye type mechanism. The exponent n is the measure of departure from ideal Debye type of relaxation process (n = 0). It has been shown that when n ≤1 the polarization process is of Debye type.

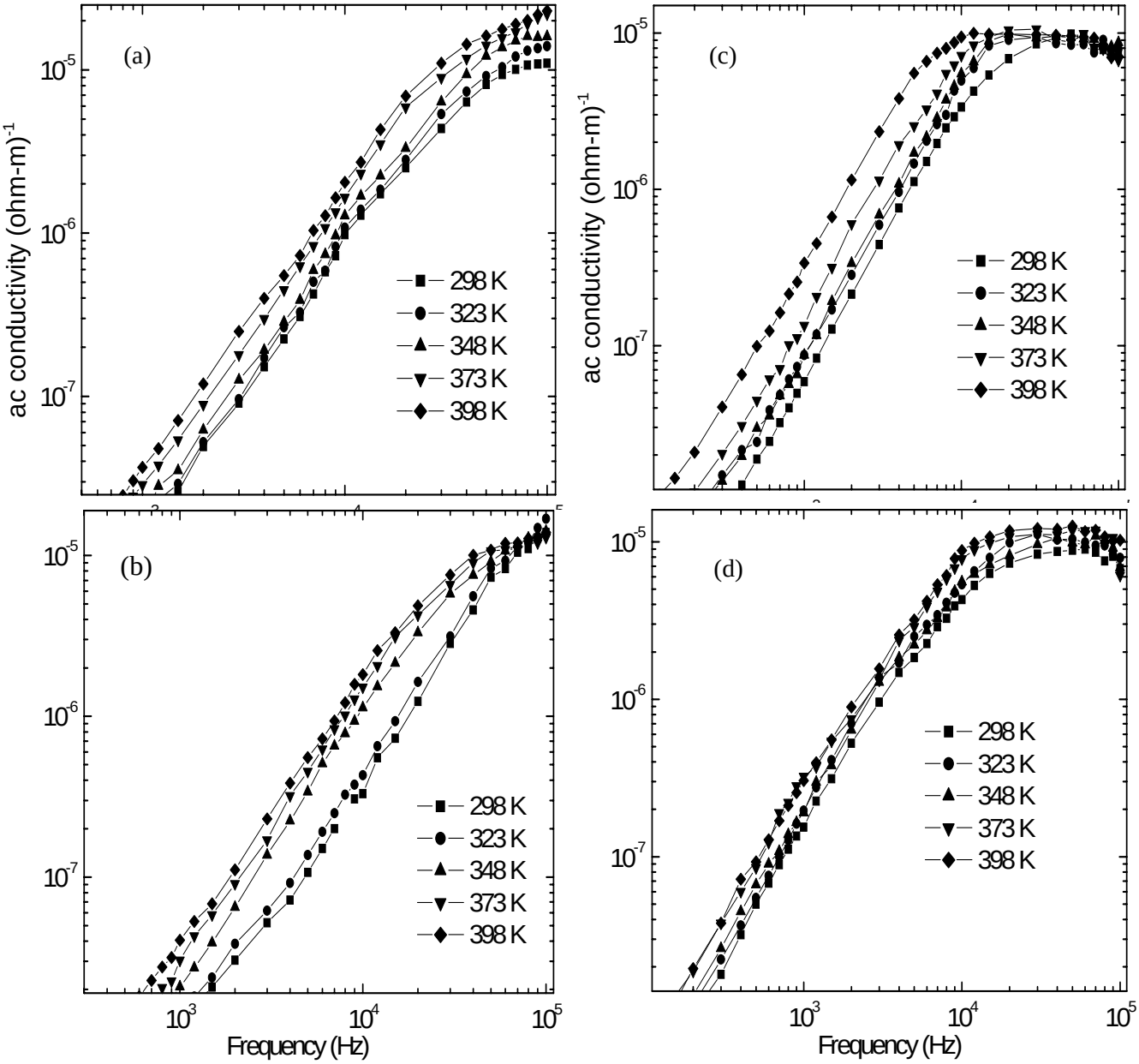

Fig. 5.27 AC conductivity, σ_{ac}, as a function of frequency of PPDEAEMA thin films of thicknesses (a) 100, (b) 200, (c) 250 nm and (d) 300 nm at different temperatures.

The values of n for PPDEAEMA thin films at different temperatures are recorded in Table 5.14. The calculated values of n reveal that Debye type mechanism is operative in the low frequency region and in the high frequency the values of n are high enough that required for Debye type relaxation process.

Table 5.14 The values of n for different temperatures.

PPDEAEMA films with thickness (nm)	Measurement Temperature (K)	Values of " n" in the frequency range	
		10^2-10^3 Hz	>10^3 Hz
		Low	High
100	298	1.19	1.88
	323	1.18	1.70
	348	1.23	1.85
	373	1.17	1.83
	398	1.20	1.71
200	298	0.99	1.59
	323	0.94	1.81
	348	1.02	1.80
	373	1.00	1.50
	398	1.18	1.40
250	298	1.29	1.65
	323	1.27	1.83
	348	1.22	1.77
	373	1.12	1.53
	398	1.24	1.58
300	298	1.54	1.49
	323	1.54	1.51
	348	1.46	1.48
	373	1.59	1.55
	398	1.57	1.47

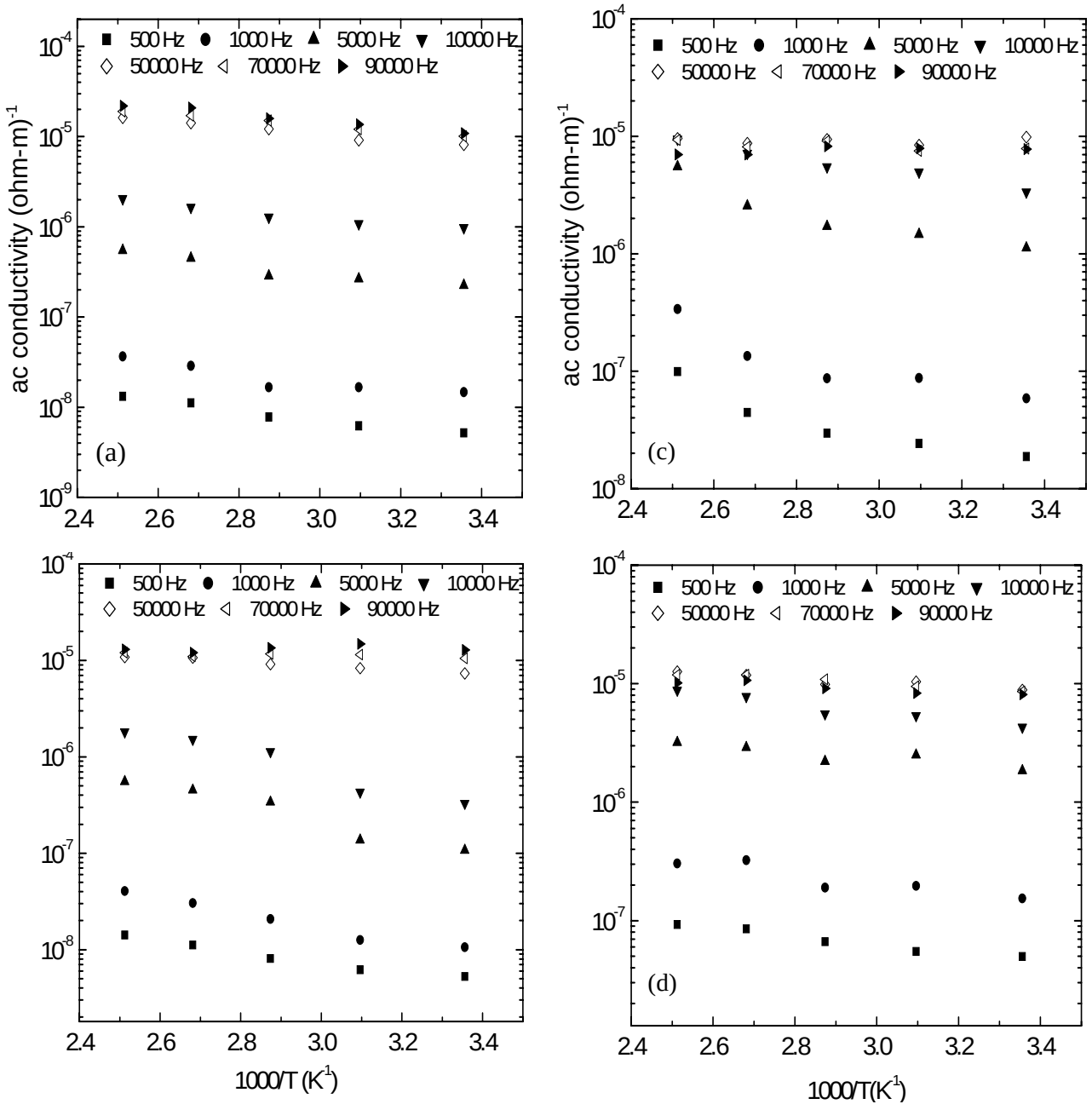

Fig. 5.28 AC conductivity, σ_{ac}, as a function of inverse of absolute temperature of the PPDEAEMA thin films of thickness (a) 100, (b) 200, (c) 250 nm and (d) 300 nm at different frequencies.

Fig. 5.27 exhibits that σ_{ac} increases upto a certain value, say f_{max}, and then become

constant or sometimes decreases. This is due to the fact that if applied frequency is higher than f_{max} it does not affect the hopping conduction mechanism i.e. for $f > f_{max}$ the applied field obstruct the hopping mechanism and consequently the conductivity remains unaffected or decreases with increasing frequency. So, for $f < f_{max}$ the applied field accelerates the charge carriers and the conductivity increases. To reveal the temperature dependence of σ_{ac} behavior at different frequencies and different thicknesses (100 to 300 nm), the data of Fig. 5.28 are plotted as σ_{ac} against inverse of absolute temperature in Figs. 5.28. It is observed that at low frequency i.e. upto 1500 Hz there is no effect of temperature in PPDEAEMA thin films. But above this frequency σ_{ac} gradually increases with the increase with temperature and also with frequency though σ_{ac} is weakly dependent on temperature below about 350 K. El-Shaarawy et al. [28] reported similar type of temperature dependence for PMMA. Activation energy is found about 0.02 eV in the low temperature at low frequencies and throughout the whole temperature range in the higher frequencies. This very low activation energy of the carriers in the low temperature and strong dependence of the σ_{ac} on frequency are indicative of a hopping conduction mechanism. These observations suggest that the conduction may be dominated by hopping of carrier between the localized states at low temperatures and movements of thermally excited carriers from energy levels within the band gap in the high temperature region.

5.8.2 Variation of dielectric constant with frequency and temperature

The variation of dielectric constant with applied frequency for PPDEAEMA thin films of thicknesses 100, 200, 250 and 300 nm, at room temperature are presented in Fig. 5.29 which shows that at low frequency, the dielectric constant for all the samples are almost independent of frequency, but at high frequencies the decrease in ε' is very prominent. The extent of the decrease of dielectric constant is more noteworthy in the high frequency region than in the low-frequency region.

The behavior that dielectric constant of polymer thin films varies with film thickness has been reported by several authors [29-30] and it is found that two factors are responsible for much different electrical properties of polymer thin films than those of bulk materials: (i) the orientation of polymer chains along the substrate and (ii) the interaction of polymer chains with the substrate or the electrode. The reason behind the decrease of ε' with decreasing film

thickness was explained as the restriction of polymer chains by the solid wall of the substrate; or electrode in the interfacial region between the polymer film and the substrate or electrode. This characteristic dependence of the ε' on frequency could be elucidated with space charge accumulation at the structural interface of the PPDEAEMA thin films. The charges present in the PPDEAEMA thin films can migrate under the influence of an electric field. It is possible that they get blocked at the electrode dielectric interface, which leads to space charge polarization. Such distortion causes an increase in ε' of PPDEAEMA thin films at the low frequencies.

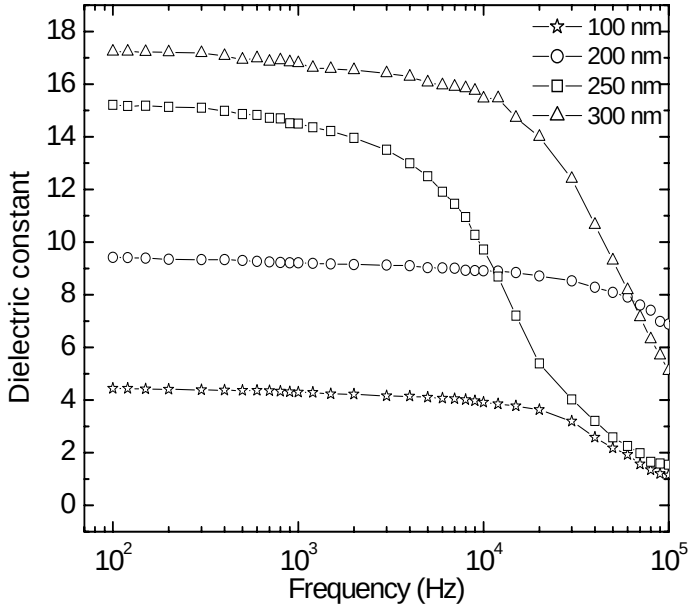

Fig.5.29 Dielectric constant versus applied frequency for PPDEAEMA thin films of different thicknesses at room temperature.

The dielectric behaviour of a material is usually described by using Debye dispersion [31] equation

$$\varepsilon = \varepsilon' - i\varepsilon'' = \varepsilon_\infty + \frac{\varepsilon_0 - \varepsilon_\infty}{1 + (\omega\tau)^2}$$

where ε_0 is the static or relaxed dielectric constant at ($\omega = 0$), ε_∞ is the high frequency or unrelaxed dielectric constant and the quantity τ is a characteristic time constant, usually called the dielectric relaxation time; it refers to a gradual change in the polarization following an abrupt change in applied field. When frequency reaches the characteristic frequency ($\omega = 1/\tau$), the ε' drops means relaxation process. At very high frequency ($\omega \geq 1/\tau$) dipoles

can no longer follow the field, $\varepsilon' \approx \varepsilon_\infty$. Relaxation may be occurred above 1 MHz $(1/\tau \geq 1MHz)$. This is indicating of a fast polarization mechanism and the polarization process will be labeled the γ process. The γ process dominates the behavior of ε' from 100 Hz to 10^5 Hz. The variation of ε' with frequency at different temperatures (298 K-398 K) of all the samples of thicknesses 100, 200, 250 and 300 nm are presented in Figs. 5.30. The ε' decreases slowly with increasing frequency and increase with increasing thicknesses. In Fig. 5.30 (a) the ε' lies from 2.5 to 4.5 up to 10^4 Hz and then decreases in the high frequencies for PPDEAEMA thin films of 100 nm thickness. Similarly Fig. 5.30(b), (c) and (d) shows dielectric constant about 7.2-9.4, 10-15, 13.2-15.2 for thicknesses of 200nm, 250nm and 300 nm respectively and all the values decreases as the frequency increases. So the general trend of ε′ is to decrease slightly with increasing temperature in the lower frequency region. But in the high frequency region (>10^4Hz), ε′ start to decrease rapidly with the increase in frequency. El-Shaarawy et al. [27] found this type of decrease in ε′ for PMMA. It is observed that dielectric constant increases with increasing thickness of the PPDEAEMA films which may be explained as follows. Because of the complex nature of the deposition process of thin films in glow discharge, the presence of dangling bonds may occur in the bulk of the samples as deposition proceeds. In addition to the above fact, the deposition time of the film in plasma may also be one of the factors. In this situation the amount of dangling bonds may not be uniform throughout the sample, which may result an increase of the dielectric constant with thickness.

As the frequency increases, dipoles begin to lag behind the field, and ε' slightly decreases. It could be seen that in the whole frequency region there is a decrease in the ε' with an increase in the frequency. This characteristic dependence of the ε' on frequency could be explained with space charge accumulation at the structural interface of the PPDEAEMA thin films. The charges present in the PPDEAEMA thin films can migrate under the influence of an electric field. It is possible that they get blocked at the electrode dielectric interface, which leads to space charge polarization. Such distortion causes an increase in ε' of PPDEAEMA thin films at the low frequencies. The decrease of ε' with frequency can be attributed to the electrical relaxation processes and multi-component contribution of polarizability of the polar materials, for example, deformational (electronic and ionic) and

relaxation (orientational and interfacial) polarization. The observed frequency dependence is due to the interfacial/space charge polarization, which is usually observed in sandwich type configurations. The interfacial or space charge polarization occurs due to the space charge accumulation at the structural interfaces of an inhomogeneous dielectric material. These charge carriers become mobile under the influence of an applied electric field. The space charge polarization typically occurs at frequency range from 1 to 10^3 Hz.

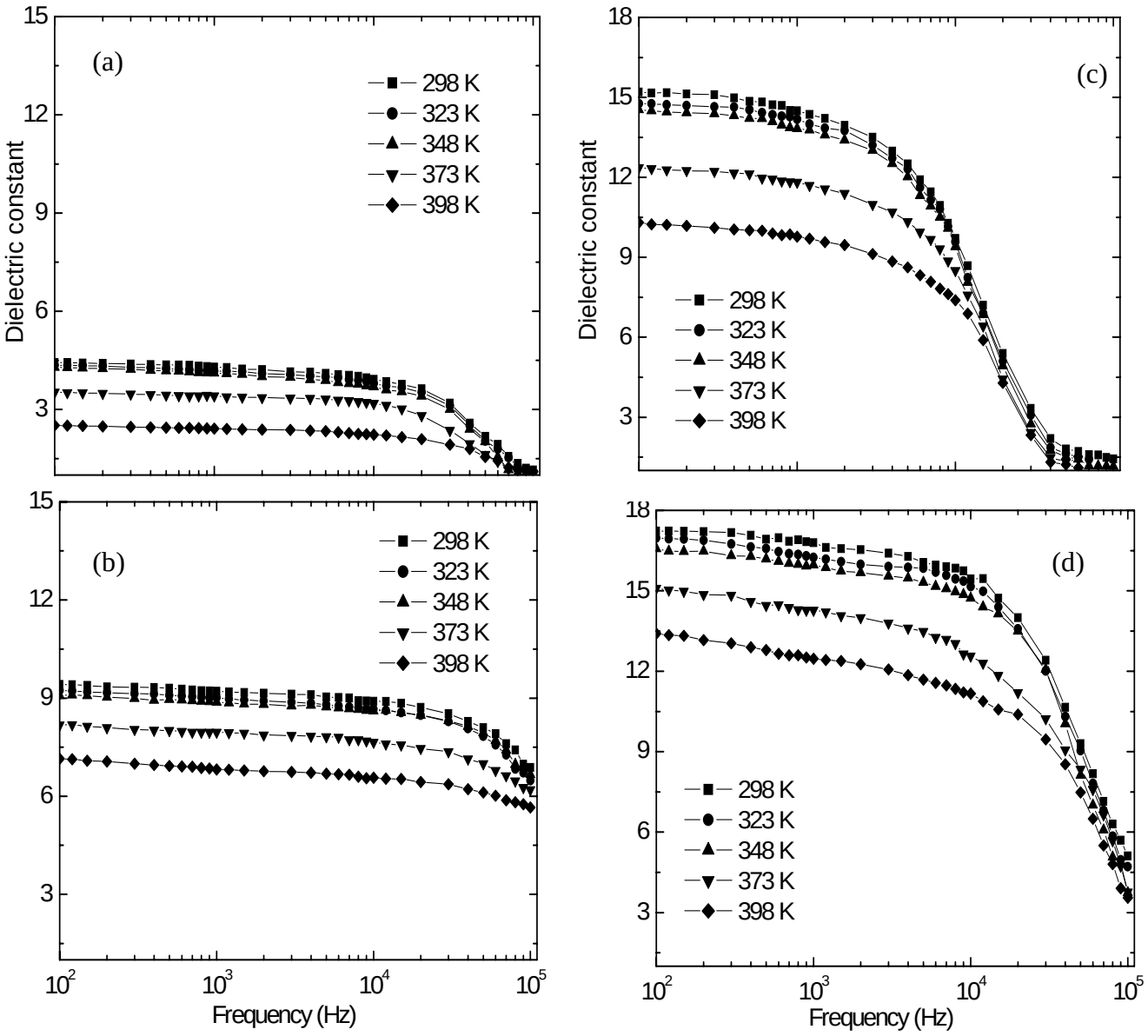

Fig. 5.30 Dielectric constant, ε', as a function of frequency for PPDEAEMA thin films of thickness (a) 100 nn, (b) 200 nm, (c) 250 nm and (d) 300 nm at different temperatures.

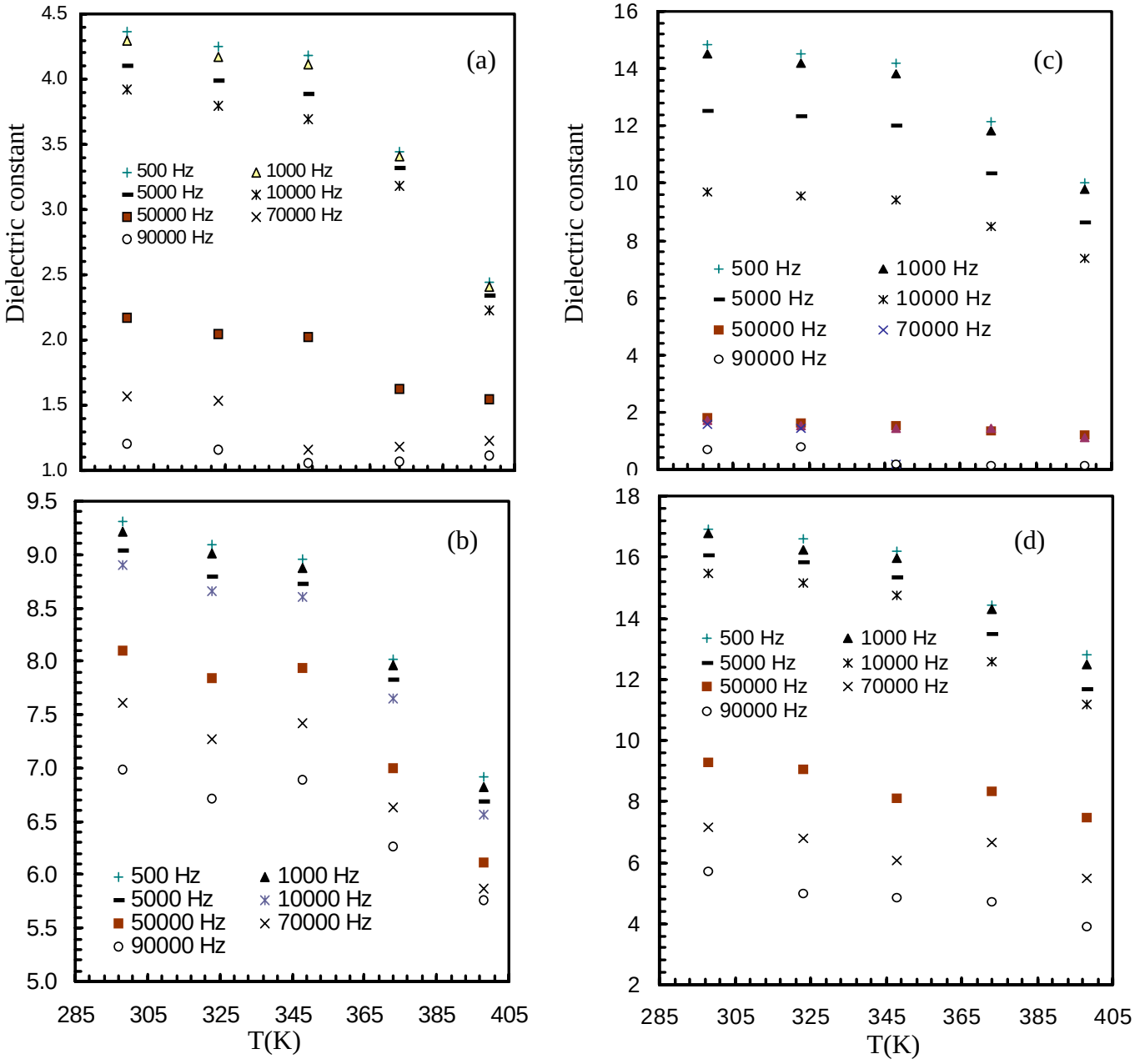

Fig. 5.31 Dielectric constant,ε′, as a function of temperature for PPDEAEMA thin films of thickness (a) 100, (b) 200, (c) 250 nm and (d) 300 nm at different frequencies.

However, since the interfacial polarization is very typical in sandwich type configurations, the other relaxation processes can be superimposed with this polarization. For example, the decrease of ε' with increasing frequency is the expected behavior in most dielectric materials, and could be attributed to the orientation polarization of molecular chains, which is also the cause of anomalous dispersion. Since the orientation polarization depends upon the molecular

arrangement of dielectric and at higher frequencies the rotational motion of the polar molecules of dielectric is not sufficiently rapid for the attainment of equilibrium with the field. The orientation polarization is therefore decreased with increasing frequencies which in turns result in a decrease of dielectric constant with increasing frequency [32]. It is also known that the effect of polarization is to reduce the field inside the medium. Therefore, the dielectric constant of a substance may be decreased substantially as the frequency is increased. The total polarization of the dielectric material can be given as the sum of these four types of polarization [33]. But since the electronic and ionic polarization occurs at very high frequencies (10^{10} ~ 10^{16} Hz) which are beyond of the present measurement, so these two types polarization could not be attributed to the relaxation process of the present system.

The variations of ε' with respect to temperature are illustrated in Fig.5.31 which shows that ε' decrease slightly upto 350 K and then there is comparatively faster decrease in ε' with the increase of temperature. The variation of ε' with temperature is related to the charge carriers, which in most cases cannot orient themselves with respect to the direction of applied field, therefore they posses a weak contribution to the polarization and hence to the ε'. As the temperature increases, the space charge carriers get enough thermal excitation energy to be able to respond to the change in the conductivity. This conductivity change in turn decreases their contribution to the polarization leading to decrease of the ε' due to high dielectric loss.

5.8.3 Variation of dielectric loss tangent with frequency

A real capacitor can be represented with a capacitor and a resistor. The parameters such as angular frequency (ω) of the applied field, the parallel conductance G_p, parallel capacitance C_p are related to $tan\partial$ as $tan\partial = \frac{G_p}{2\pi f C_p}$, where f is the linear frequency in Hz. The dependence of the dielectric loss tangent, tanδ, with frequency at different temperatures (298 to 398 K) for as deposited PPDEAEMA thin films of different thicknesses is shown in Fig. 5.32. It is observed that tanδ increases as the frequency increases and show some relaxation peaks at the high frequency region (>10^4Hz) which is shifted with thickness. An increase in $tan\delta$ with increasing applied frequency is dominated by resistive losses since the mobile charges contained in the film cannot follow high-frequency electric fields. This

loss of energy is associated with the degree of orientation of molecules in addition to the degree of internal friction of the films [34]. At higher frequencies, the very fast periodic reversal of the electric field occurs and no excess ion diffusion would become possible in the direction of the field.

After a certain frequency the polar ionization decreases due to the charge accumulation results to a decrease in the value of the loss tangent since the orientation of

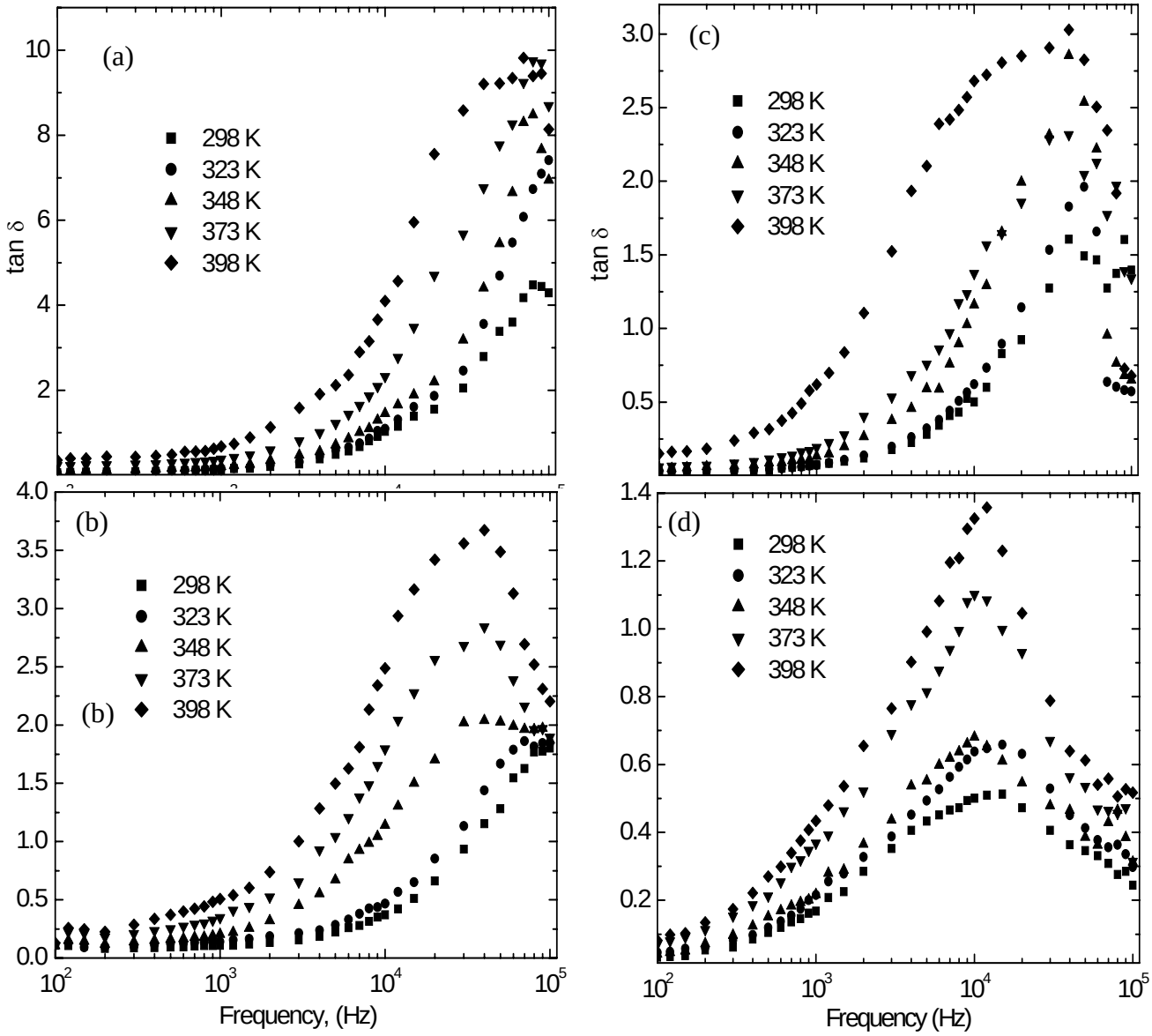

Fig. 5.32 Dielectric loss tangent, as a function of frequency of the PPDEAEMA thin films of thickness (a) 100, (b) 200, (c) 250 nm and (d) 300 nm at different temperature.

dipoles cannot keep up at high frequency. The frequency corresponding to maximum loss was found to shift to lower frequencies with increasing temperature. The loss peaks and their shifts with temperature suggest a dielectric relaxation process. The increase in the maximum value of loss tangent with the increase in temperature indicate the number of charge carriers increases by thermal activation [35]. At higher temperature region, the maximum loss increased with increasing temperature i.e. charge carriers increased by thermal activation at higher temperature.

5.8.4 Dependence of ε″ on ε′ (Cole-Cole plot)

The Cole-Cole curve is useful to understand the degree of the distribution of the relaxation times.

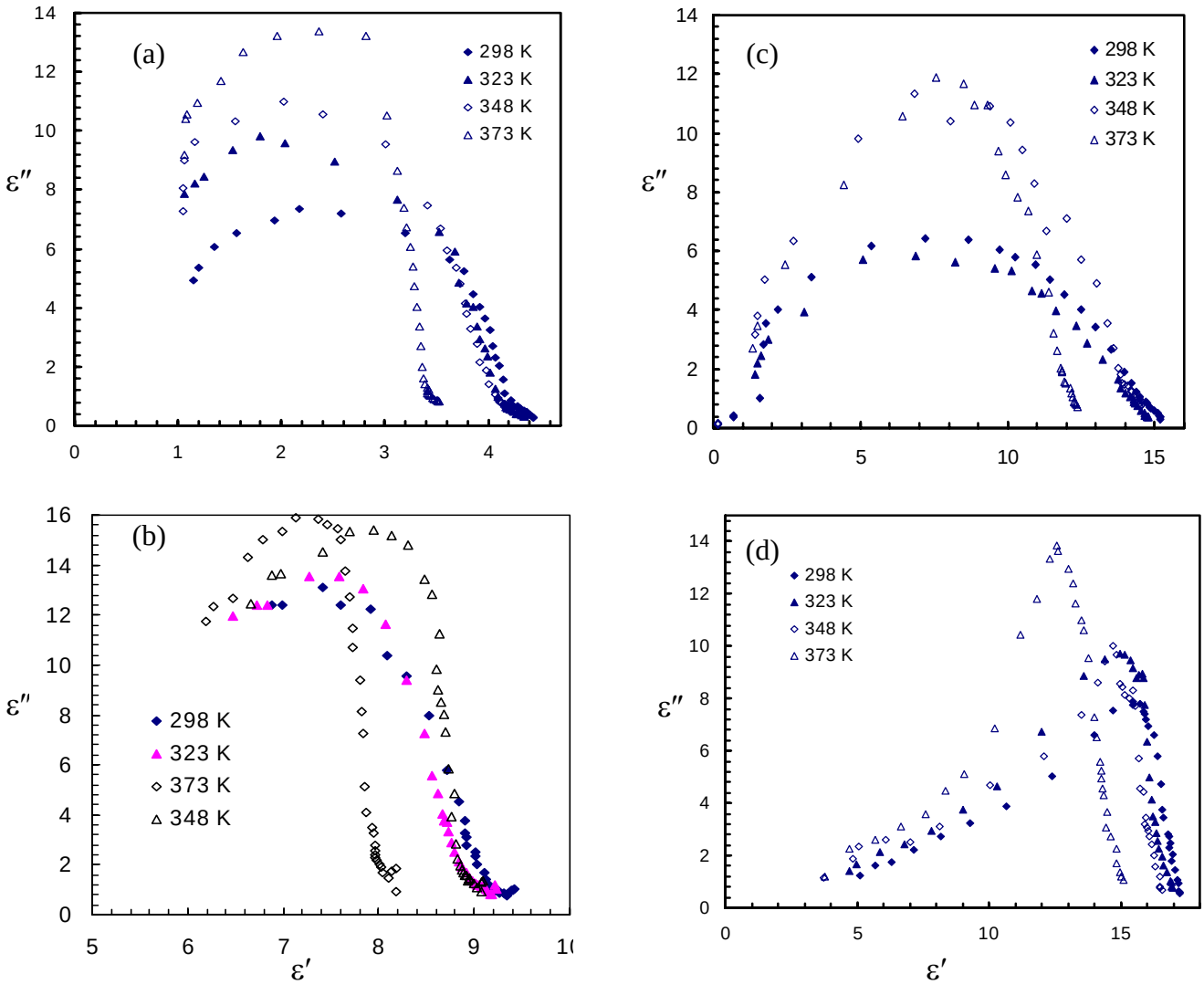

Fig. 5.33 Cole-Cole plots of PPDEAEMA thin films of thickness (a) 100, (b) 200, (c) 250 nm and (d) 300 nm at different frequencies.

Fig.5.33 shows the variation of real and imaginary parts of ε for a PPDEAEMA thin film as functions of temperature and frequency in the form of Cole-Cole plots. In general, a full, or a partial or no arc is observed depending on relaxation strength in the sample within experimentally available frequency range. When the angle between the two radii of the Cole-Cole curve is defined as βπ, the factor β indicates the degree of distribution of the relaxation time. The values of β are presented in Table 5.15. The values of β are thus found to be 0.77-0.91,which are smaller than the value (unity) of the Debye model with a single relaxation, indicating the presence of distribution of relaxation time in PPDEAEMA thin films. The Cole Cole plot reveals that there is a tendency of deformation of the semicircular shape with increase of temperature. This implies that the relaxation time distribution increase with temperature.

Table 5.15 Values of β from Cole –Cole plot.

Temperature (K)	β			
	Sample thickness (nm)			
	100	200	250	300
298	0.85	0.82	0.77	0.88
323	0.91	0.87	0.81	0.88
348	0.90	0.90	0.77	0.87
373	0.88	0.87	0.86	0.88
398	0.91	0.85	0.81	0.81

5.8.5 AC electrical characteristics of iodine doped PPDEAEMA thin films

The variation of ac conductivity σ_{ac} with frequency from 100 Hz to 100 kHz in the temperature range from 298 to 398 K for iodine doped PPDEAEMA thin films of thicknesses 100 and 200, nm are presented in Fig. 5.34 which exhibits that the σ_{ac} increases as frequency increases. A little variation in conductivity is observed with increasing temperature. The σ_{ac} increases rapidly up to 10^4 Hz, after that the rate of increase become slower and then start to decrease slowly. The values of exponent n for iodine doped PPDEAEMA thin films are found to be 0.87-1.1 below 10^3 Hz and that are 1.5 - 1.7 above 10^3 Hz.

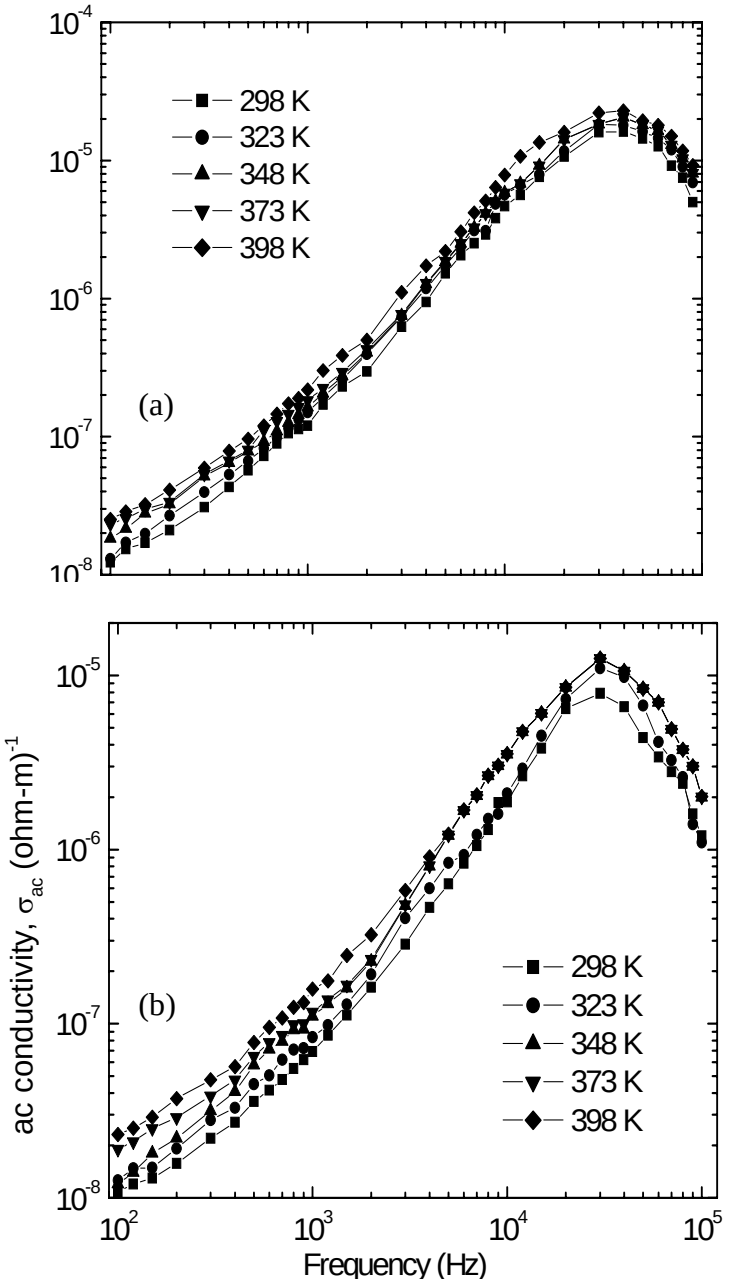

Fig. 5.34 AC conductivity, σ_{ac}, as a function of frequency of iodine doped PPDEAEMA thin films of thicknesses (a) 100 nm and (b) 200 nm at different temperatures.

Table 5.16 shows the values of n for iodine doped PPDEAEMA thin films at different temperatures. The n value suggest that Debye type mechanism is operative in low frequency region. The values obtained in high frequency is not suitable for Debye type mechanism. Fig. 5.35 shows the temperature dependence of σ_{ac} at different frequencies for iodine doped

PPDEAEMA thin films of thickness 100 and 200 nm. It is observed that for the sample of 100 nm there is almost no variation with temperature. But the sample with 200 nm thickness shows that σ_{ac} is weakly dependent on temperature.

Table 5.16 The values of n for different temperatures for iodine doped PPDEAEMA

PPDEAEMA films with thickness (nm)	Measurement Temperature (K)	Values of " n" in the frequency range	
		10^2-10^3 Hz	>10^3 Hz
		Low	High
100	298	1.16	1.65
	323	1.05	1.70
	348	0.98	1.73
	373	1.06	1.71
	398	1.04	1.59
200	298	0.94	1.70
	323	0.93	1.46
	348	0.97	1.68
	373	0.87	1.67
	398	0.93	1.50

Activation energy is calculated from Fig. 5.35 and is found about 0.02 eV in the low temperature at low frequencies and throughout the whole temperature range. This very low activation energy of the carriers in the low temperature and strong dependence of the σ_{ac} on frequency indicates that hopping conduction mechanism is operative in iodine doped PPDEAEMA thin films. In comparison to Fig. 5.27 it can be said that the value of σ_{ac} show an enhancement in the conductivity of doped PPDEAEMA thin films. Since iodine doping associates charge transfer complexes. The addition of iodine may also reduce the insulating capacity due to introduction of localized states. Since the doping of iodine increase the amorphous nature and the enhancement of the irregularities of the polymer thin film.

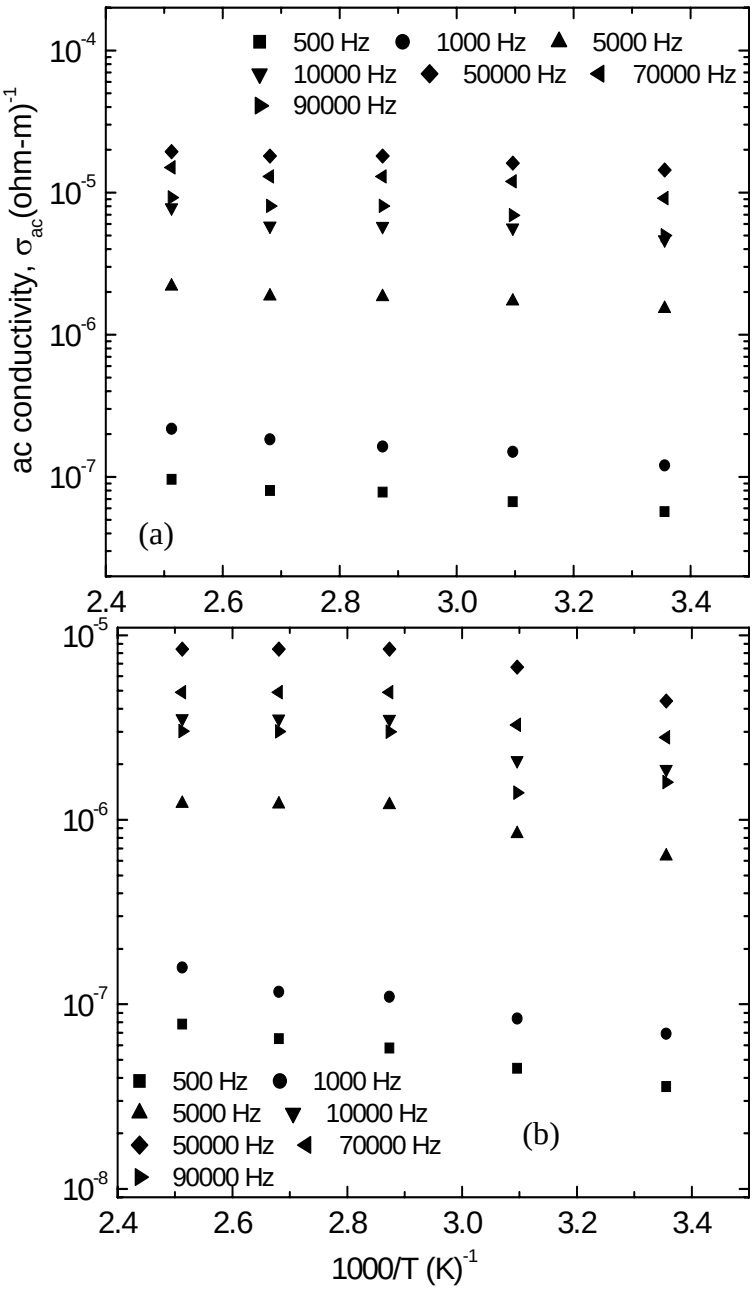

Fig. 5.35 AC conductivity, σ_{ac}, as a function of inverse of absolute temperature of the iodine doped PPDEAEMA thin films of thickness (a) 100 nm and (b) 200 nm at different frequencies.

The plot of dielectric constant as a function of applied frequency for iodine doped PPDEAEMA thin films of thicknesses 100 and 200 nm are presented in Fig. 5.36 which shows that the value of dielectric constant slightly decrease with the increase in frequency. But above 10^4 Hz the decrease is faster for PPDEAEMA thin films of 100 nm though it is not observed for PPDEAEMA thin films of 200 nm.

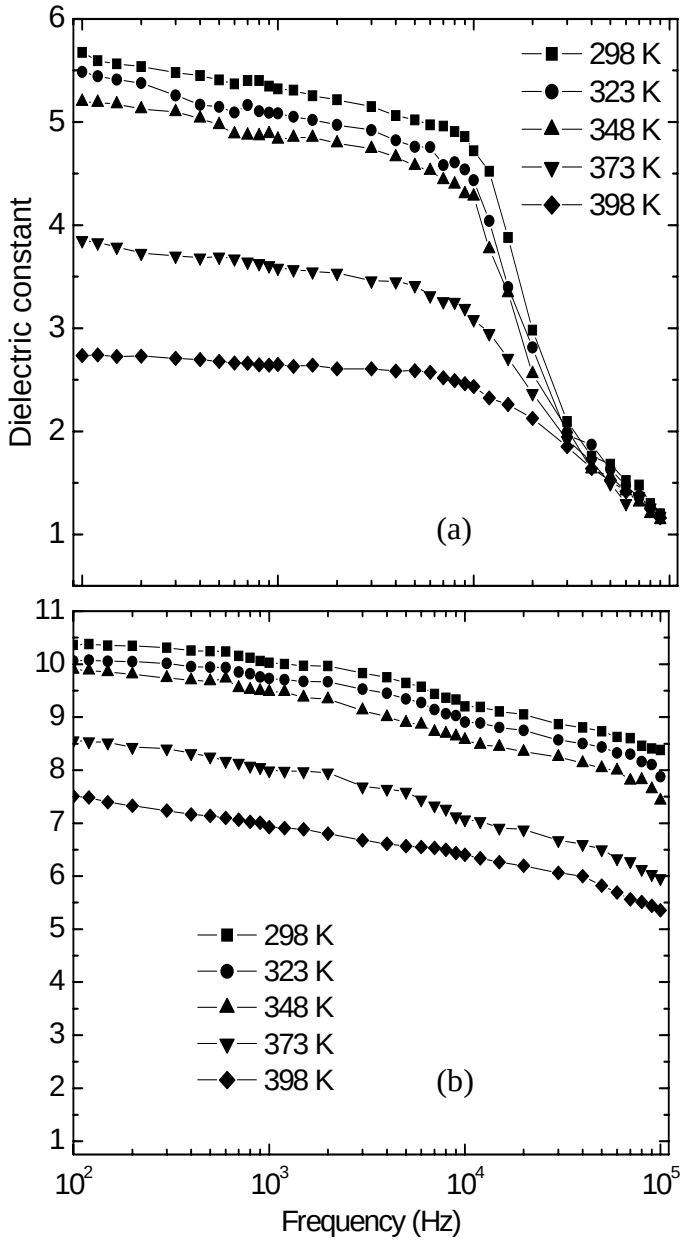

Fig. 5.36 Dielectric constant,ε', as a function of frequency for iodine doped PPDEAEMA thin films of thickness (a) 100 nm and (b) 200 nm at different temperatures.

In comparison to Fig. 5.30 it is noticed that the value of dielectric constant increases due to iodine doping since doping increases the number of dipoles participating in the orientation process, while the frequency of orientation remain unchanged. Fig.5.37 exhibits the variations of ε' with respect to temperature. It is seen that ε' decrease slightly upto 350 K

and then there is comparatively faster decrease in ε' with the increase of temperature as like the as deposited PPDEAEMA thin films.

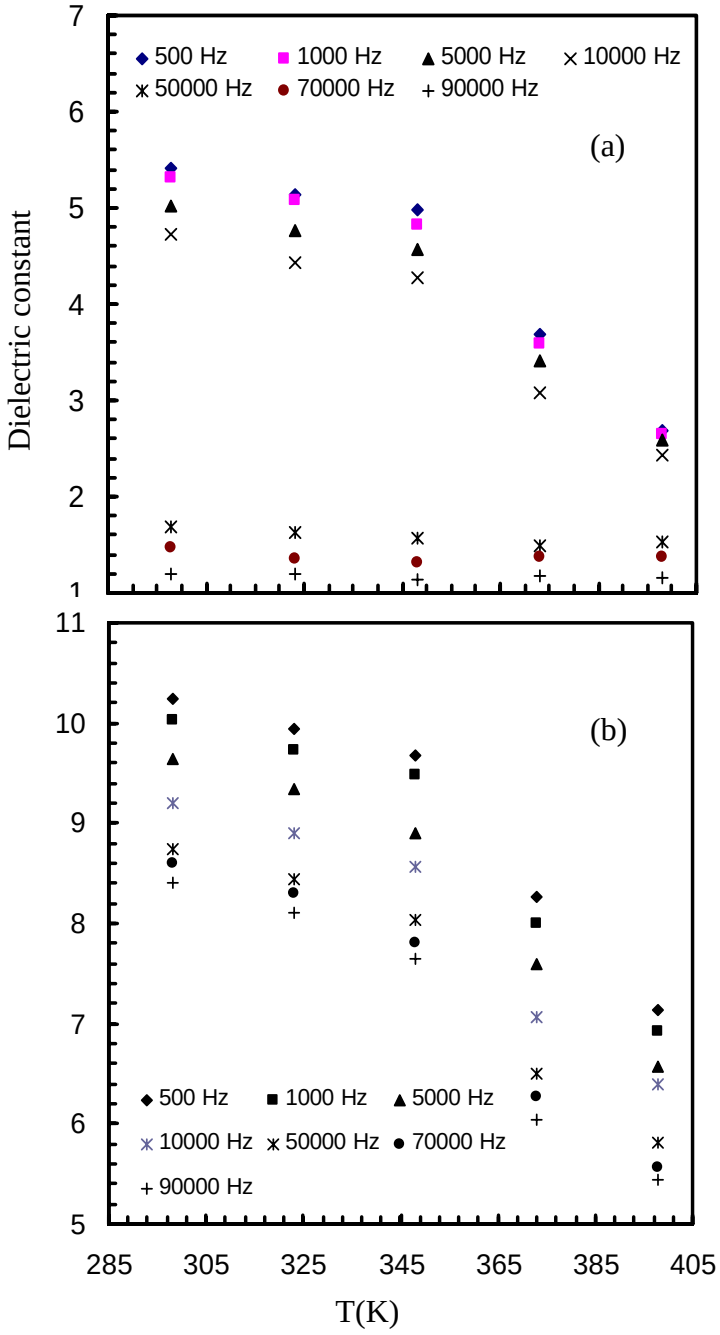

Fig. 5.37 Dielectric constant,ε', as a function of temperature for PPDEAEMA thin films of thickness (a) 100 and (b) 200 nm at different frequencies.

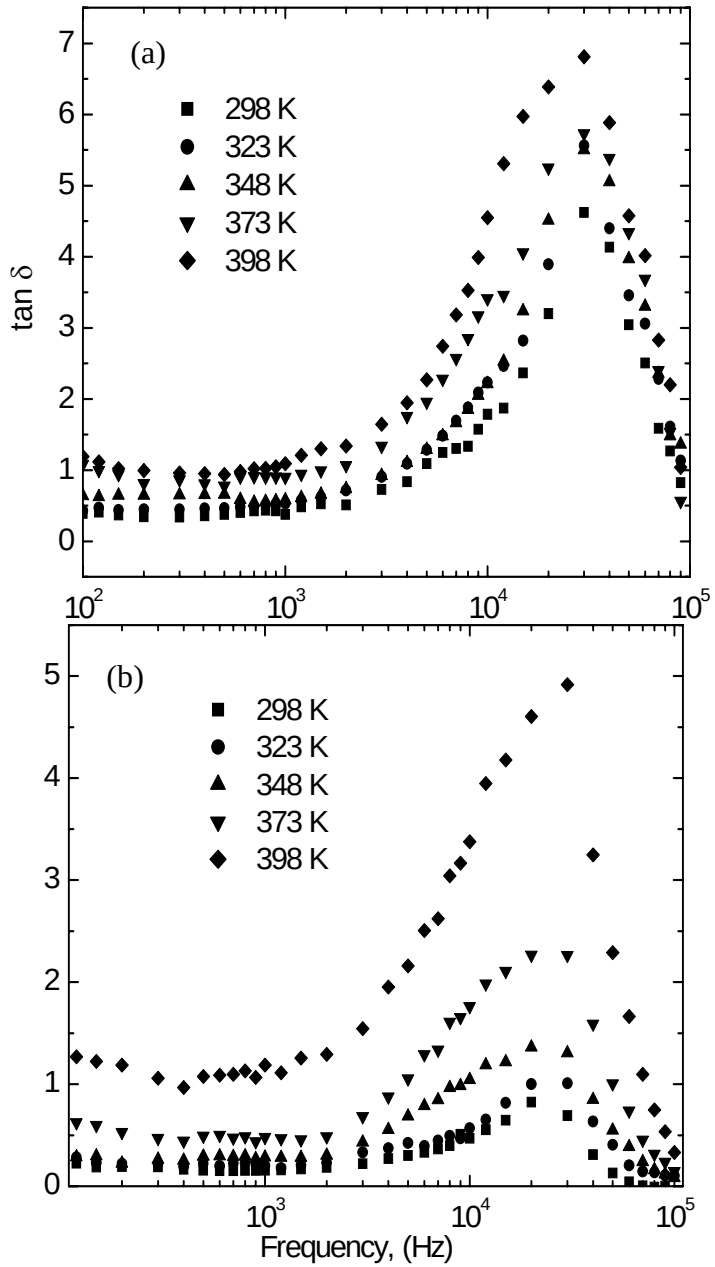

Fig. 5.38 Dielectric loss tangent, as a function of frequency of the iodine doped PPDEAEMA thin films of thickness (a) 100 and (b) 200 nm at different temperature.

Since in most cases, charge carriers cannot orient themselves with respect to the direction of applied field, therefore they posses a weak contribution to the polarization and hence to the ε'. As a consequence, when the temperature increases, the space charge carriers get enough thermal excitation energy to be able to respond to the change in the conductivity. This conductivity change in turn decreases their contribution to the polarization leading to decrease of the ε' due to high dielectric loss.

Fig. 5.38 presents the variation of the dielectric loss tangent, tanδ, with frequency at different temperatures (298 to 398 K) for iodine doped PPDEAEMA thin films of 100 and 200 nm thicknesses. It is observed that tanδ increases as the frequency increases and show some relaxation peaks at the high frequency region (>10^4Hz) which is shifted with temperature and indicates the presence of relaxation in iodine doped PPDEAEMA thin films. From the above observations, it is seen that $\sigma_{ac,}$ ε' and $tan\delta$ increased after iodine doping, which may be due to the formation of charge transfer complexes. Tanwar et al. [36] reported that iodine may undergo substitution into polymer chain at the amorphous region and creates additional hopping sites for the charge carriers and hence σ_{ac} increases. The addition of iodine boost up the polar character of PPDEAEMA thin films hence it becomes more electrically conductive. According to Quamara et al. [28], iodine diffuses preferentially in the less dense volume region of the polymer and is present either interestially or trapped between the chain configurations and forms a charge transfer complex within the structure; iodine assists in increasing the electron-hole pair concentration. Due to the electrostatic interaction between chain and iodine, the intermolecular interactions are reduced facilitating the motion of the molecules thus increasing in their mobility, dielectric constant and the high dielectric loss. Therefore, PPDEAEMA is proficient to form charge transfer complex which proceeds as excess of carriers/electron-hole pairs in PPDEAEMA thin films.

References

[1] Yasuda, H., 'Plasma Polymerization', Academic Press, New York, 1985.

[2] Inagaki, N., 'Plasma Surface Modification and Plasma Polymerization', Technomic Publishing Co. Inc., New York, 1996.

[3] Kaniappan, K. and Latha, S., **'**Certain Investigations on the Formulation and Characterization of Polystyrene /Poly(methyl methacrylate) Blends', Inter. J. Chem. Tech. Resear. 3(2), 708-717, 2011.

[4] Balamurugan, A., Kannan, S., Selvaraj, V. and Rajeswari, S., 'Development and Spectral Characterization of Poly(Methyl Methacrylate) /Hydroxyapatite Composite for Biomedical Applications', Trends Biomater, 18(1), 41-45, 2004.

[5] Choi, H. E., Woo, H. J., Hong, W., Kim, J. K., Lee, S. K., Eum, C. H., 'Structural modification

of poly(methyl methacrylate) by proton irradiation', Appl. Surf. Sci. 169-170, 433-437, 2001.

[6] Robert, T. Conley, 'Infrared spectroscopy', Allyn and Bacon, Inc. Boston, 1975.

[7] Meyers, R. A. (Ed.), 'Interpretation of Infrared Spectra, A Practical Approach', John Coates in Encyclopedia of Analyt Chem; 10815-10837© John Willey & Sons Ltd. Chichester, 2000.

[8] Davis, E.A. and Mott, N.F., 'Electronic Processes in non-crystalline materials', Philos. Mag. 22, 903, 1970.

[9] Urbach, F., 'The Long-Wavelength Edge of Photographic Sensitivity and of the Electronic Absorption of Solids', Phys. Rev. 92, 1324, 1953.

[10] Jeon, H.S., Wyatt, J., Harper- Nixon, D., Weinkauf, D.H., 'Characterization of Thin Polymer-Like Films Formed by Plasma Polymerization of Methylmethacrylate: A Neutron Reflectivity Study', J. Polym. Sci.: Part B: Polym. Phys., 42, 2522–2530, 2004.

[11] Tauc, J., 'Optical Properties of Solids', F. Abeles Ed. North-Holland, Amsterdam, 1972.

[12] Mahr, H., 'Ultraviolet Absorption of KI Diluted in KCl Crystals**',** Phys. Rev. 125, 1510-1516, 1962.

[13] Yakuphanoglu, F., Arslan M., 'The fundamental absorption edge and optical constants of some charge transfer compounds', Optic. Mater. 27, 29–37, 2004.

[14] Hilal Goktas, Dogan Mansuroglu, Betul Atalay, Sinan Bilikmen, Ismet Kaya, 'Polyfluorene Thin Films Synthesized by a Novel Plasma Polymerization Method', Plasma Chem. Plasma Process. 32, 35–44, 2012.

[15] Bilici, A., Kaya, I., Yldrm, M., Eur. Polym. J. 47:1005–1017, 2011.

[16] Elashmawi, I. S., Abdelrazek, E. M., Ragab, H. M., Hakeem, N. A., 'Structural, optical and dielectric behavior of PVDF films filled with different concentrations of iodine', Physica B 405, 94-98, 2010.

[17] Mathai, C. J., Saravanan, S., Anantharaman, M. R., Venkitachalam, S., Jayalekshmi, S. , 'Effect of iodine doping on the bandgap of plasma polymerized aniline thin films**',** Journal of Physics D: Applied Physics 35, 2206-2210, 2002.

[18] Cherian, L.; Radhakrishnan, P. Curr. Sci. 62,423,1992.

[19] Laurs, H.**,** Heiland, G.,'Electrical and optical properties of phthalocyanine films**'**, 149,129-142, 1987.

[20] Kashiwazaki, N., 'Iodized Polymeric Yb-Diphthalocyanine Films Prepared by Plasma Polymerization Method', Jpn. J. Appl. Phys. 31, 1892, 1992.

[21] Coppo P., Schroeder, R., Grell, M., Michel L. Turner, 'Investigation of solution processed poly(4,4-dioctylcyclopentadithiophene) thin films as transparent conductors'**,** Synthetic Metals 143, 203-206, 2004.

[22] John, J., Sivaraman, S., Jaylekshmy, S., Anantharaman, M. R., 'Investigation on the mechanism of carrier transport in plasma polymerized pyrrole thin films', J. of Phys. and Chem. of Solids, 71, 935-939, 2010.

[23] Maisel I. Leon, Glang, R., 'Hand Book of Thin Film Technology', McGraw Hill Book Company: New York, 1970.

[24] Shukla, P., Gaur, M. S., 'Investigation of electrical conduction mechanism in double-layered polymeric system', J. Appl. Polym. Sci., 114, 222-230, 2009.

[25] Lampert, M.A., Mark, P., 'Current Injection in Solids, Academic Press', New York, 1970.

[26] Lampert, M. A., 'Simplified theory of space-charge-limited currents in an insulator with traps', Phys. Rev. 103, 1648, 1956.

[27] El-Shaarawy, M. G., Mansour, A. F., El-Bashir, S. M., El-Mansy, M. K., Hammam, M., **'**Electrical conduction and dielectric properties of poly(methyl methacrylate)/perylene solar concentrators**'** J. Appl. Polym. Sci., 88, 793, 2003.

[28] Quamara, J. K. , Singh, P. J., Kaushika, B. K., 'Dielectric constant and loss investigations of pristine, iodine doped and annealed polyetherimide film', Polym. Int. 698-702, 630, 2011.

[29] Liang, T., Makita, Y., Kimura, S., 'Effect of film thickness on the electrical properties of polymide thin films', Polymer 42, 4867-4872, 2001.

[30] Despotopoulou, A. M., Miller, R. D., Rabolt, J. F., Frank, C. W., 'Polymer chain organization and orientation in ultrathin films: A spectroscopic investigation', J. Polym. Sci. Part B 34 2335-2349, 1996.

[31] Blythe, A. R., 'Electrical Properties of polymers, Cambridge University Press', Cambridge, London, 1979.

[32] Smith C. P., 'Dielectric behavior and structure', McGraw Hill, New York, 1955.

[33] Barsoum M., 'Fundamentals of Ceramics', McGraw Hill, New York, 1977.

[34] Biloiu C., Biloiu I. A., Sakai Y., Sugawara H., Ohta A., 'Amorphous fluorocarbon polymer (*a*-C:F) films obtained by plasma enhanced chemical vapor deposition from perfluoro-octane (C_8F_{18}) vapor. II. Dielectric and insulating properties', J. Vac. Sci. Technol. A 22 1158, 2004.

[35] Vella N., Toureille A., 'Space charge behavior of different pei observed by the coupling of thermal step method and TSDC method', IEEE Annual Report, 1 , 84-87, 1997.

[36] Tanwar A., Gupta K. K., Singh P.J., Vijay Y. K., 'Dielectric parameters and ac conductivity of pure and doped poly(mehyl methacrylate) films at microwave frequencies', Bull. Mater. Sci.., 29, 397-401, 2006.